CHARLES LEE POWELL

STRUCTURAL RESEARCH LABORATORIES

Report No.
SSRP 98/13
FHWA-AK-RD-99-02

FULL-SCALE TEST OF THE ALASKA CAST-IN-PLACE STEEL SHELL THREE COLUMN BRIDGE BENT

By

Pedro F. Silva
Sri Sritharan
Frieder Seible
M.J. Nigel Priestley

Report to Alaska Department of Transportation and Public Facilities, Juneau, Alaska.

February 1999

Division of Structural Engineering
University of California, San Diego
La Jolla, California 92093-0085

CHARLES LEE POWELL

STRUCTURAL RESEARCH LABORATORIES

Report No. SSRP-98/13

FHWA-AK-RD-9902

FULL-SCALE TEST OF THE ALASKA CAST-IN-PLACE STEEL SHELL THREE COLUMN BRIDGE BENT

By

Pedro F. Silva

Post-Doctoral Research Engineer

Sri Sritharan

Assistant Project Scientist

Frieder Seible

Professor of Structural Engineering

M.J. Nigel Priestley

Professor of Structural Engineering

Report to Alaska Department of Transportation and Public Facilities, Juneau, Alaska.

February 1999

Technical Report Documentation Page

1. Report No.	2. Government Accession No.	3. Recipient's Catalog No.
SSRP 98/13 FHWA-AK-RD-99-02		

4. Title and Subtitle	5. Report Date
Full-Scale Test of the Alaska Cast-in-Place Steel Shell Three Column Bridge Bent	February 1999
	6. Performing Organization Code

7. Author(s)	8. Performing Organization Report No.
P. F. Silva, S. Sritharan, F. Seible, M. J. N. Priestley	UCSD SSRP-98/13

9. Performing Organization Name and Address	10. Work Unit No. (TRAIS)
Division of Structural Engineering School of Engineering University of California, San Diego La Jolla, California 92093-0085	11. Contract or Grant No. 53205

12. Sponsoring Agency Name and Address	13. Type of Report and Period Covered
Federal Highway Administration Alaska Department of Transportation and Public Facilities 3132 Channel Drive Juneau, Alaska, 99801-78989	Final 14. Sponsoring Agency Code

15. Supplementary Notes
Prepared in cooperation with the State of Alaska Department of Transportation and Public Facilities.

16. Abstract

This report describes the research investigation of a full-scale bridge bent conducted for the State of Alaska Department of Transportation and Public Facilities. The bent consisted of three cast-in-place steel shell columns and was designed using research findings from recently completed projects at the University of California San Diego (UCSD) to ensure a ductile performance under seismic loading.

Specific tasks investigated in this research project were: (1) column longitudinal reinforcement ratio, (2) straight bar anchorage of the column longitudinal reinforcement into the beam/column joints, (3) termination of the column steel shells below the cap beam, (4) flexural design of the cap beam to sustain maximum feasible input moments from the columns, (5) shear design of the cap beam, and (6) design of the cap beam/column joints. Test results were then used to validate the procedure presented in this research project for the seismic design of reinforced concrete bridge bents with multiple column *Cast-in-Place Steel Shells*.

Following the design of the test unit, the monotonic force-displacement response was predicted using a push-over analysis program, and seismic testing of the full-scale structure was subsequently conducted. Experimental results indicate that the test unit responded in a ductile manner with column moment capacities developing in preselected hinges, and the ultimate displacement capacity was characterized by low cycle fatigue fracture of the columns longitudinal reinforcement, which matched satisfactorily with the theoretically predicted failure mode. In addition, processed test data and test observations confirm that no joint failure occurred, which ensured the development of the column ultimate moment capacities. Consequently, corroborated by experimental investigation, the design procedure was adequate in ensuring a ductile performance of the test unit. In this report are presented: (1) the design details of the test unit, (2) results of the pushover analysis, (3) test observations, (4) reduced test data, and (5) seismic design recommendations.

17. Key Words	18. Distribution Statement
concrete, seismic design, bridges, columns, pile shafts pile cap connections, joint design	Unlimited

19. Security Classification (of this report)	20. Security Classification (of this page)	21. No. of Pages	22. Price
Unclassified	Unclassified	157	

Disclaimer

Opinions, findings, conclusions and recommendations expressed in this report are those of the authors and do not necessarily reflect views of the Federal Highway Administration and the State of Alaska Department of Transportation and Public Facilities.

Acknowledgments

The research project described in this report was funded by the Federal Highway Administration and the State of Alaska Department of Transportation and Public Facilities under project No. 53205.

We greatly appreciate the input and coordination provided by Mr. Richard Pratt and Mr. Elmer Marx from the Alaska Department of Transportation and Public Facilities during the development of this research project.

List of Symbols

A_b Cross sectional area of a reinforcing bar.

A_g Gross sectional area of concrete section.

A_{gl} Effective area.

A_{st} Total longitudinal steel area.

A_{shell} Cross sectional area of the steel shell.

b_j Effective joint width.

c Section neutral axis.

C_c Concrete compression force.

C_s' Reinforcing steel compression force.

C_{shell} Steel shell compression force.

D Column diameter or width.

D_j Steel shell outside diameter.

D_i Steel shell inside diameter.

d_b Diameter of reinforcement bar.

E_c Young's modulus of concrete or initial tangent modulus of elasticity of concrete.

E_s Young's modulus of reinforcing steel.

E_{sec} Secant modulus of elasticity of concrete.

E_{shell} Young's modulus of steel shell.

f_c' Concrete compressive strength.

f_{co}' Unconfined concrete compressive strength.

f_{cc}' Confined concrete compression strength.

f_l' Effective lateral confining pressure.

f_h Horizontal axial stress in the joint region.

f_v Vertical axial stress in the joint region.

f_y Yield strength of steel reinforcement.

f_{yj} Yield strength of steel shell.

f^o_y Reinforcement yield strength at overstrength.

I_{eff} Effective moment of inertia.

h_b Depth of pier cap.

h_{cur} Height of curvature cell.

l_d Development length of reinforcing steel.

$l_{d,shell}$ Distance from the cap beam interface to termination of the connection reinforcement.

L_c Distance from the column inflection point to the underside of the cap beam.

M_C Column moment.

P_C Column axial load.

P_h Horizontal axial force on the joint.

P_v Vertical axial force on the joint.

T_s Reinforcing steel tension force.

T_{shell} Steel shell tension force.

t_j Steel shell thickness.

V_C Column shear force.

V'_y Lateral load at first section yielding.

V_y Lateral load at section yielding.

V_I Lateral load at ideal flexural strength.

V_{jv} Vertical joint shear force.

v_{jv} Vertical joint shear stress.

W_{cur} Length of curvature cell.

α_s Reinforcing steel force participation factor.

α_{sj} Steel shell force participation factor.

Δ Lateral deflection.

Δ_y' First section yield displacement.

Δ_y Yield displacement.

Δ_U Ultimate displacement.

μ_Δ Displacement ductility.

ρ_t Joint principal tensile stress.

ρ_{sj} Volumetric ratio of the steel shell.

φ Section curvature.

φ_{exc} Experimentally determined average curvature.

Table of Contents

Abstract

This report describes the research investigation of a full-scale bridge bent conducted for the State of Alaska Department of Transportation and Public Facilities. The bent consisted of three cast-in-place steel shell columns and was designed using research findings from recently completed projects at the University of California San Diego (UCSD) to ensure a ductile performance under seismic loading.

Specific tasks investigated in this research project were: (1) column longitudinal reinforcement ratio, (2) straight bar anchorage of the column longitudinal reinforcement into the beam/column joints, (3) termination of the column steel shells below the cap beam, (4) flexural design of the cap beam to sustain maximum feasible input moments from the columns, (5) shear design of the cap beam, and (6) design of the cap beam/column joints. Test results were then used to validate the procedure presented in this research project for the seismic design of reinforced concrete bridge bents with multiple column *Cast-in-Place Steel Shells*.

Following the design of the test unit, the monotonic force-displacement response was predicted using a push-over analysis program, and seismic testing of the full-scale structure was subsequently conducted. Experimental results indicate that the test unit responded in a ductile manner with column moment capacities developing in preselected hinges, and the ultimate displacement capacity was characterized by low cycle fatigue fracture of the columns longitudinal reinforcement, which matched satisfactorily with the theoretically predicted failure mode. In addition, processed test data and test observations confirm that no joint failure occurred, which ensured the development of the column ultimate moment capacities. Consequently, corroborated by experimental investigation, the design procedure was adequate in ensuring a ductile performance of the test unit. In this report are presented: (1) the design details of the test unit, (2) results of the pushover analysis, (3) test observations, (4) reduced test data, and (5) seismic design recommendations.

1 Introduction

Over the past thirty years there has been a continuous effort by structural engineers and researchers to develop procedures for the seismic design of reinforced concrete bridge structures with an intension of avoiding structural failures in seismic zones. Seismic design of bridges in the United States and many countries abroad is currently based on a capacity design philosophy [1]. A fundamental basis of this seismic design method relies on carefully selecting and detailing regions where inelastic actions are to occur during seismic events. Furthermore, all other regions are designed to remain elastic under seismic loading according to a strength hierarchy sufficient to cope with potential strain hardening and uncertainties in material properties.

Consistent with the principles of a capacity design philosophy, the ideal approach for the seismic design of reinforced concrete multiple column bridge bents is to conveniently select plastic hinges to form in the top and bottom of columns [1]. As plastic hinges develop in the top and bottom of columns, inspection and repair can be achieved without significant traffic disruption, and a ductile performance is easily achieved by the confining action of steel shells and/or transverse reinforcement. Thus, the earthquake energy is dissipated in the column plastic hinge through hysteretic damping. In addition, cap beams are protected from any significant inelastic actions, as these members are not conveniently used to provide energy dissipation.

1.1 Background

In reviewing reports and publications concerning the seismic performance of bridge structures in recent earthquakes, there are a considerable number of reports that document numerous failures in bridge structures. For example, during the 1971 San Fernando earthquake, anchorage failure of a column longitudinal reinforcement occurred by pull-out of the entire reinforcement cage from the footing. In this footing the top layer reinforcement was not provided, and as a result, a proper transfer of forces did not develop for the anchorage of the column longitudinal reinforcement [1]. Other examples demonstrated the impact of brittle shear failure of columns in the unsatisfactory performance of bridge structures under seismic actions, as documented from the 1987 Whittier and 1994 Northridge earthquakes [1]. These types of failures developed as a result of inadequate transverse reinforcement and lead to rapid strength degradation. Cap beam failures were also documented from previous earthquakes mainly as a result of shear failures, premature curtailment of the negative moment reinforcement (top), and anchorage failure of the cap beam longitudinal reinforcement in the end regions [1]. Moreover, other types of failures were also documented in the connection between the cap beam and the columns. These are some of the documented failures from previous earthquakes, which lead to

a rapid strength degradation, low energy absorption structural systems and must be avoided if a proper ductile response of a bridge structure is desirable.

Following these major earthquakes, extensive experimental and analytical studies were conducted at UCSD to evaluate these failures, provide design guidelines and prevent future catastrophic failures of bridge structures. Assessment of a number of design details of bridge structures built in the State of Alaska [2] was conducted by employing some of the models developed at UCSD. Analyses of these bridges under simulated seismic loads indicated that there is a high propensity for excessive damage to these bridges. Some of the design deficiencies identified during this part of the study were:

(i) Excessive Amounts of Column Longitudinal Reinforcement. For example, a column longitudinal reinforcement ratio as high as 10% was identified in the columns of the Susitna River Bridge [2]. This high level of reinforcement ratio imposes very large shear demands in the joints and consequently, requires impracticable amounts of reinforcement in the joints.

(ii) Potential for Plastic Hinging in the Cap Beam. As an example, a cap beam ultimate flexural strength to column ultimate flexural strength ratio of approximately 0.50 was identified in the Chena River Bridge [2]. Consequently, inadequate longitudinal reinforcement in the cap beam will not prevent inelastic actions from developing in these members under seismic loading.

(iii) Inadequate Joint Shear Reinforcement. Inadequate joint shear reinforcement will not prevent undesirable inelastic actions in the connection of the beam to the column.

(iv) Deficient Cap Beam Shear Strength. Inadequate transverse reinforcement would lead brittle shear failure of the cap beam based on the levels of design forces imposed from column. Inadequate confinement of plastic hinges in the cap beam will result in premature failure.

(v) Embedment of Steel Shells in the Joint Region. A pile shaft/column, commonly employed in the construction of bridges in the State of Alaska, consists of a cast-in-place steel shell section (CISS), which is embedded into the cap beam/column connection. Even at low levels of column rotation, damage to the cap beam bottom surface cover concrete would be inevitable due to the prying action of the embedded portion of the steel shell. This may result in exposure of the cap beam reinforcement to corrosive environments and premature corrosion of this reinforcement, which would be potentially hazardous under seismic actions.

In order to address the above design issues and to ensure a proper ductile response of multiple column bridge bents, findings from recent research studies at UCSD were used to design the test unit. In this context, state-of-the-art seismic design procedures recommended by Priestley et al. **[1]**, testing of bridge joints systems and multi-column bents test units by Sritharan et al. **[3][4][5]**, and seismic testing of pile foundation systems by Silva et al.**[6]**, are relevant to the current investigation.

As a main objective to develop constructable joints with minimal amount of reinforcement, several joint tests were conducted at UCSD, and a joint design methodology is recommended in reference **[5]**. One of the test units consisted of two joints in a multiple column test configuration, as depicted in **Fig. 1-1**. In addition to investigate the joint detailing, seismic design of multiple column bents was verified and appropriate recommendations are provided in reference **[4]**, which were utilized in the design of the test unit presented in **Chapter 4**.

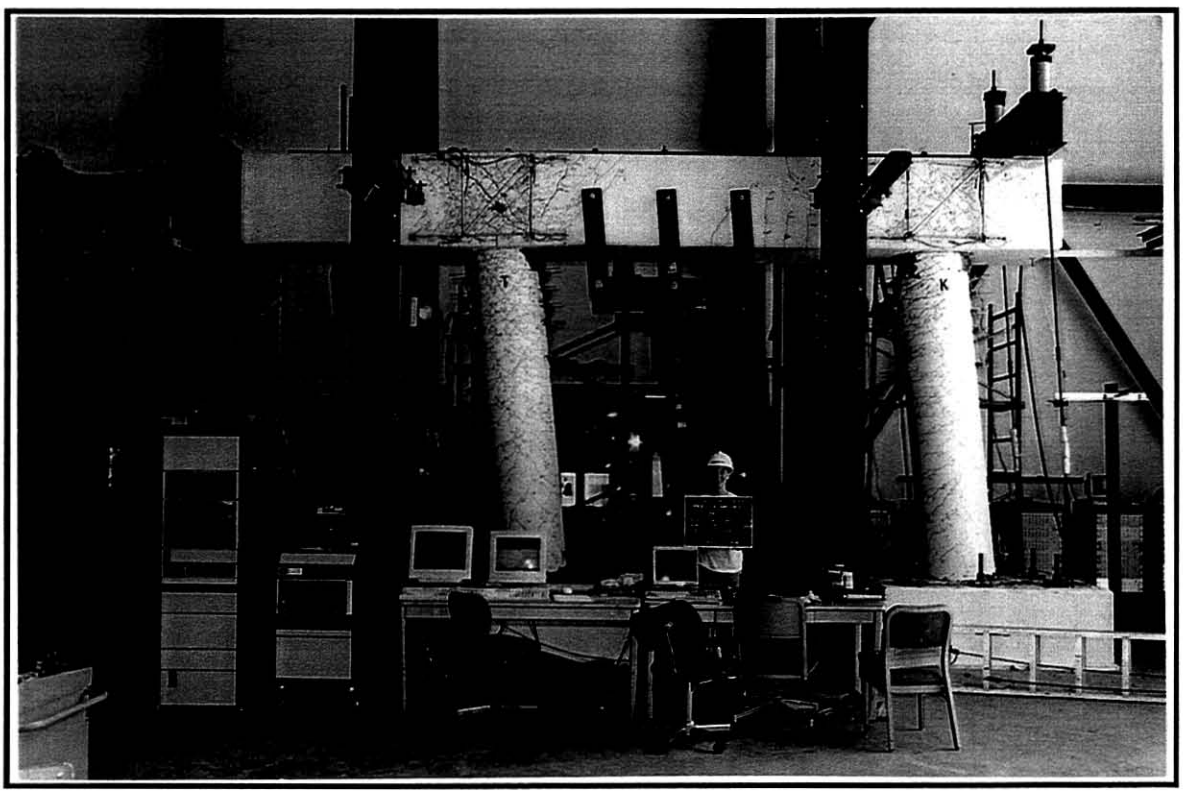

Fig. 1-1 Deformed Shape of a Previous Test Unit
Representative of Multiple Column Bents

In addition, a series of pile to pile cap connection tests were conducted also at UCSD to provide basic information as to the state of damage of pile foundation systems at the connection of piles to the pile cap **[6]**. In these series of tests, two cast-in-place steel shell piles with steel shells embedded into the pile cap were used, reflecting typical Caltrans pile details, which have direct relevance to the seismic performance of CISS pile/cap beam connections. Test results show that the pile cap was severely damaged, as a result of the prying action of the embedded steel shell, as depicted in **Fig. 1-2**

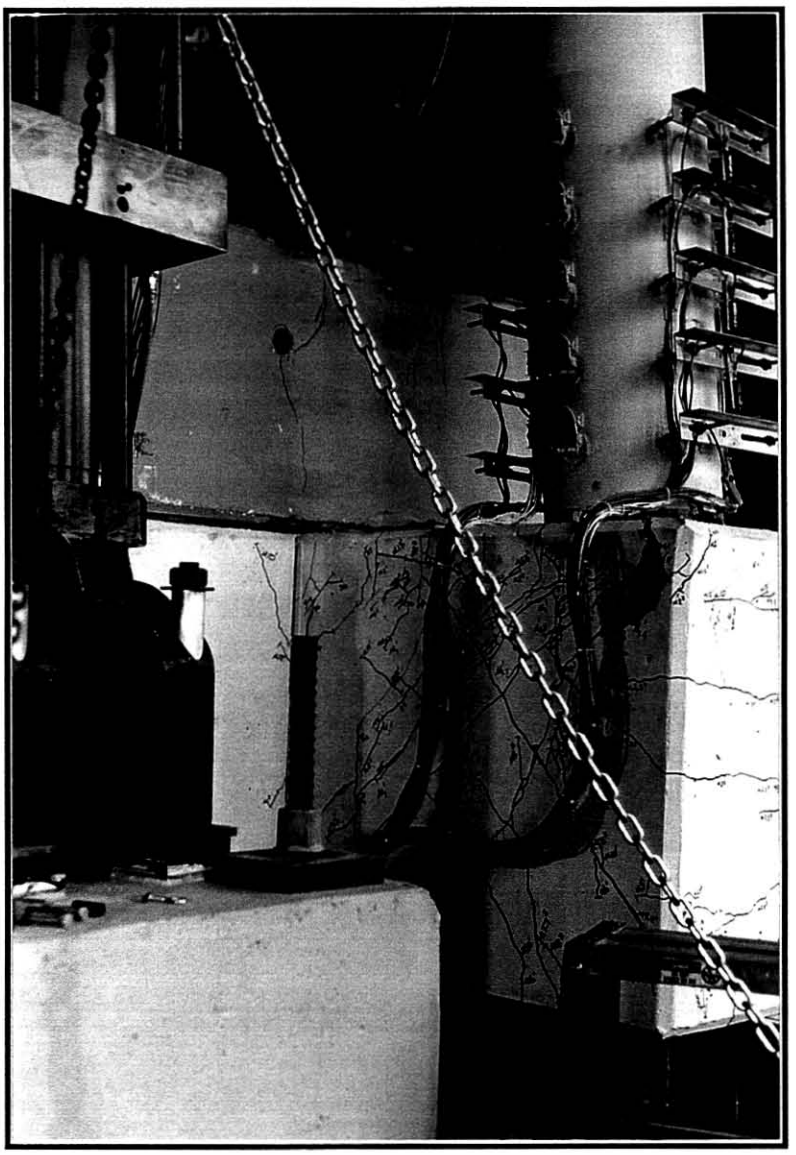

Fig. 1-2 Damage of a Test Unit with a Steel Shell Embedded into the Pile Cap

1.2 Scope of Research

The primary objective of this research project was to experimentally validate the design recommendations developed for the seismic design of reinforced concrete bridge bents with cast-in-place steel shells. Design recommendations presented in this report were developed in accordance with the capacity design philosophy previously described. Specific issues adopted for the design of the Alaska full scale proof test were:

(i) Column Longitudinal Reinforcement. In the United States the upper limit for the longitudinal steel ratio is 8%. However, this limit is uncommonly used in design practice because it leads to design difficulties associated with the confinement of large steel quantities, flexural and shear design of the cap beam, and joint reinforcement design, which are essential for a ductile performance of bridge bents. In reference [1], the recommended upper limit for the column steel ratio is 4%, and ratios below 3% are normally found in the design of bridge columns. Consequently, the longitudinal reinforcement ratio was limited to 2.5% consistent with the design recommendations by Priestley et al.[1].

(ii) Anchorage of Column Longitudinal Reinforcement. In order to improve constructability of the joint regions, the column longitudinal bars were terminated straight into the cap beam.

(iii) Steel Shell Embedment. In order to protect the cap beam from extensive damage due to the prying action of the steel shells, the steel shells were terminated 51 mm below the cap beam.

(iv) Confinement of Plastic Hinges. Confinement of the column plastic hinge at the gap region was ensured by providing adequate transverse reinforcement to constrain buckling of the column longitudinal reinforcement and permit large inelastic rotations.

(v) Cap Beam Design. Design of the cap beam was developed in order to ensure an elastic response of this member under seismic action.

(vi) Joint Design. Design of the connection between the cap beam and the columns was performed to achieve joint constructability and to limit significant damage within the joint region under seismic actions.

Another issue, in the seismic design of pile shaft/columns that deserves special attention is the formation of subgrade hinges. These in-ground hinges were not studied in this research project, but could bear examination in further specialized studies, as illustrated by studies performed by Budek et al.[7].

Competence of the design procedure established for reinforced concrete bridge bents was examined in a proof test, by studying the influence of the design issues described above on the overall seismic response of a full-scale test unit. Based on the seismic performance of the test unit, appropriate design recommendations were made, and in a parallel analytical study an attempt was made to predict the monotonic force-displacement response of the test unit.

1.3 Report Layout

Following an introduction to the seismic design of reinforced concrete bridge bents, and scope of the current study in this chapter, **Chapter 2** describes the prototype structure, the geometry of the test unit, and the reinforcement layout for the test unit. **Chapter 3** presents the design forces used for the design of the test unit. **Chapter 4** describes the design procedure for the test unit, while **Chapter 5** covers the construction, the concrete and steel material properties, instrumentation, and loading sequence of the test unit. In **Chapter 6** the predicted response of the test unit is presented, and in **Chapter 7** experimental results are described. Finally, this report concludes with specific recommendations for the seismic design of reinforced concrete bridge bents with cast-in-place steel shell pile-shaft/columns,as presented in **Chapter 8**.

2 Geometry and Reinforcement Layout of the Test Unit

In this research project, a typical multiple column bent was investigated to assess the seismic performance and capacity of a reinforced concrete bridge bent with integral pile-shaft/columns, as shown schematically in **Fig. 2-1.**

2.1 Laboratory Test Model

In order to achieve the research objectives described in **Section 1.2** it was determined to represent the prototype structure as a test model with columns extending from the cap beam to inflection point *A*, as shown in **Fig. 2-1(b)**. Thus, modeling of the test unit was accomplished by designing the columns as pinned conditions at the base of the footings. Since it was not feasible to provide pin supports with zero moment resistance, reinforced pin connections were provided at the column bases. These pinned connections had small moment resistance, which did not significantly alter the column moment gradients. Design of these pin connections is covered in **Section 4.4.**

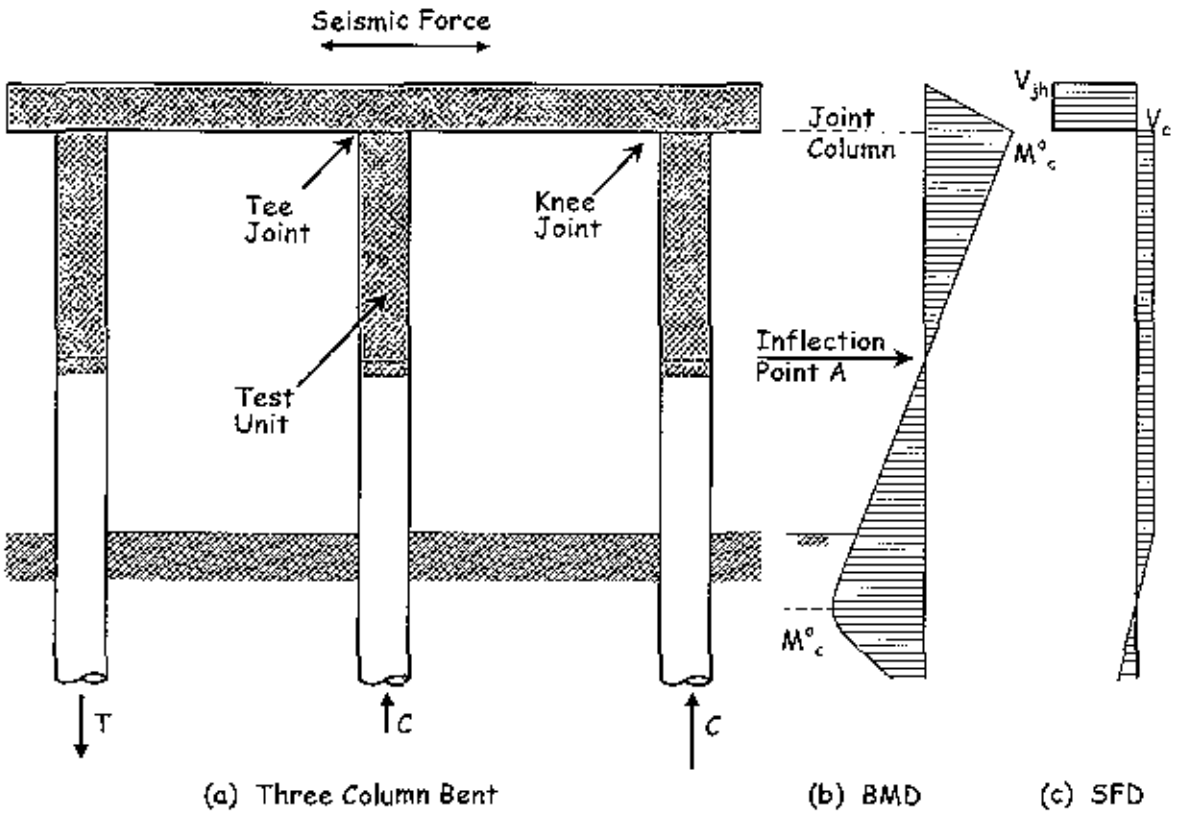

Fig. 2-1 Prototype Structure and its Representative Test Model Using the Concept in Reference [4]

The full-scale test unit geometry is presented in this chapter. As illustrated in **Fig. 2-2** through **Fig. 2-4**, the test unit consisted of three CISS columns with a clear height of 4.34 m and a center line spacing between columns of 4.27 m. The outside diameter of the steel shell was 0.91 m with a thickness of 12.70 mm. The length of the steel shells were shorter than the columns, which terminated 50.8 mm below the cap beam, and 63.5 mm above the footings. The test unit cap beam dimensions were 1.37 m x 1.07 m (W x H). An expansion joint material with a thickness of 63.50 mm was provided in the pin connection of the columns to the footings. Tie-down of the footings to the strong floor consisted of eight 35 mm diameter high strength bars with a stressing force per bar of 534 kN. The dimensions of each footing were 2.29 m x 1.67 m x 0.61 mm reinforced concrete section with the tie-down arrangement illustrated in **Fig. 2-3**.

Gravity loads were simulated at four locations along the cap beam using four loading fixtures, which were positioned at 1.22 m from the column centerlines, as illustrated in **Fig. 2-3**. The total axial load required adjacent to the exterior columns was 1,223 kN per loading fixture, and the total axial load required adjacent to the interior column was 445 kN per loading fixture, which provided a total applied axial load of 3,336 kN. To simulate the seismic lateral forces, two hydraulic actuators were attached to the test specimen on each side of the test unit through load transfer blocks. One of the actuators was connected to the laboratory strong wall while the second actuator was connected to two reaction frames by a transverse steel beam. These two hydraulic actuators have a maximum stroke of 457 mm and a maximum capacity per actuator of 1,397 kN in the pull direction and 2,286 kN in the push direction, which provided a total feasible lateral force of 3,683 kN. The vertical distance from the line of action of the applied lateral force to the center line of the cap beam was 1.52 m and the distance to the laboratory floor was 7.01 m, as illustrated in **Fig. 2-2**. In the remainder of this report columns and joints of the test unit are designated according to the identification presented in **Table 2-1**.

Table 2-1 Column and Joint Identification

Exterior Column	*EC1*
Interior Column	*IC*
Exterior Column	*EC2*
Knee Joint - Exterior	*KJ1*
Tee Joint - Interior	*TC*
Knee Joint - Exterior	*KJ2*

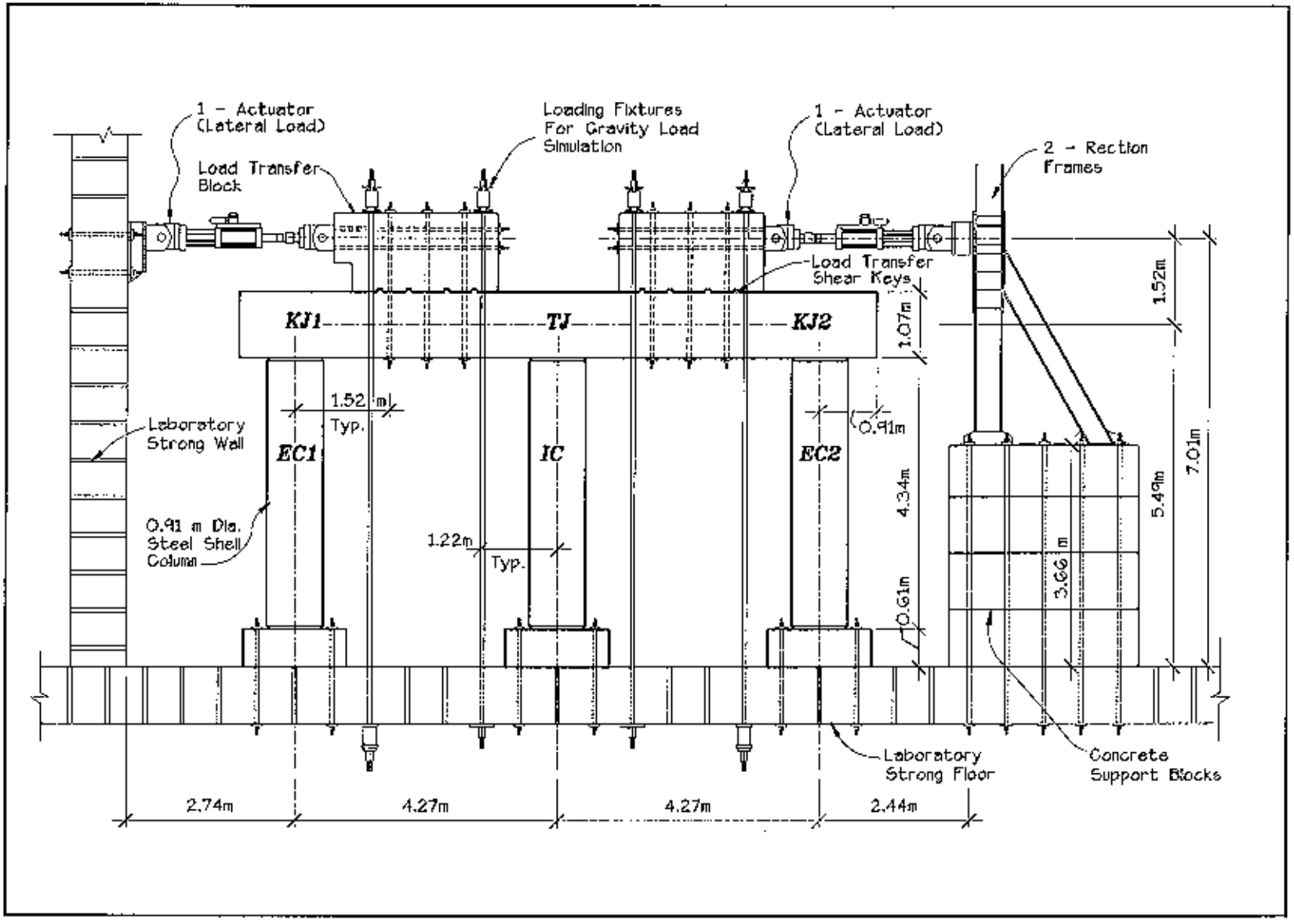

Fig. 2-2 Test Configuration - Front View

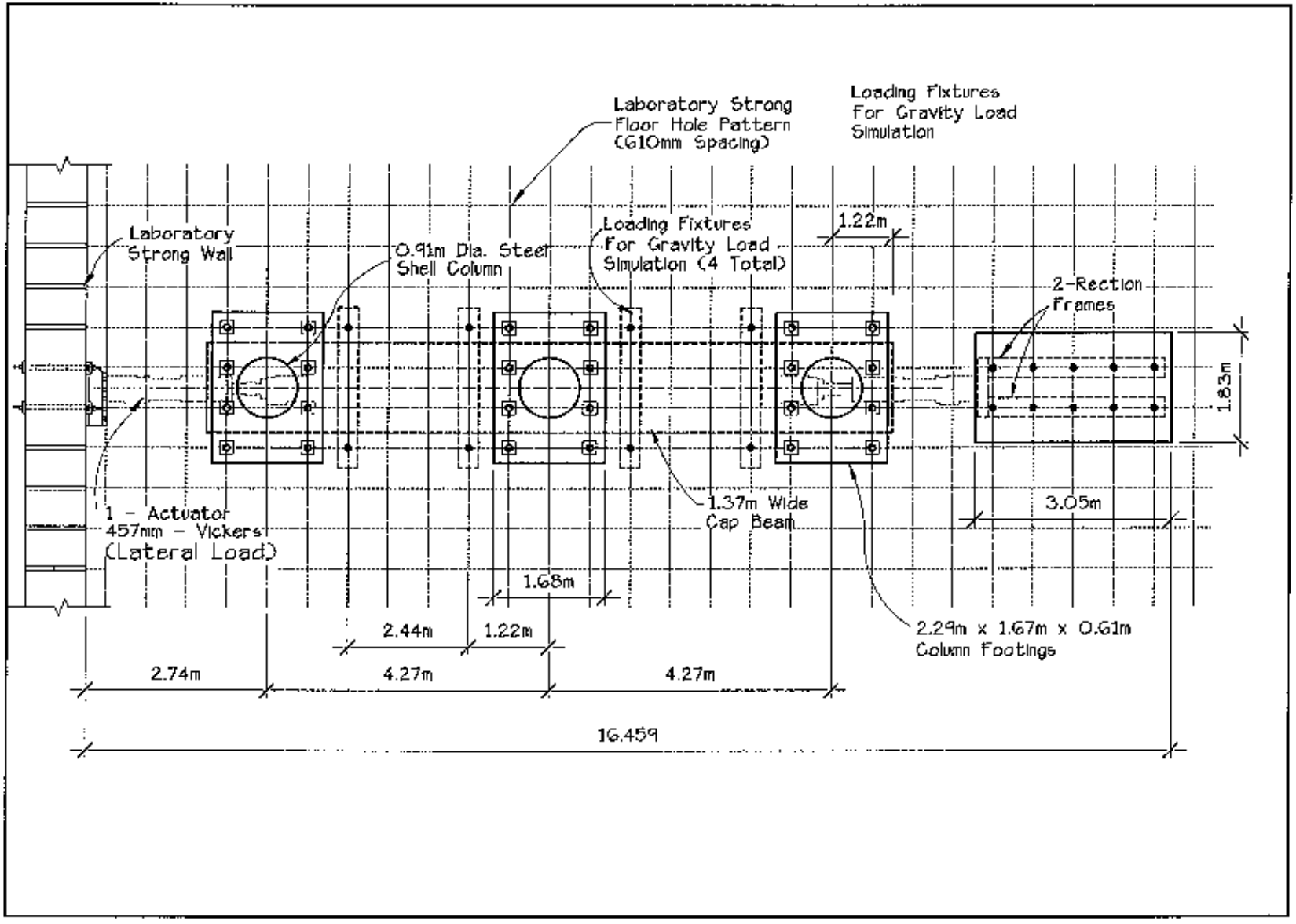

Fig. 2-3 Test Configuration - Top View

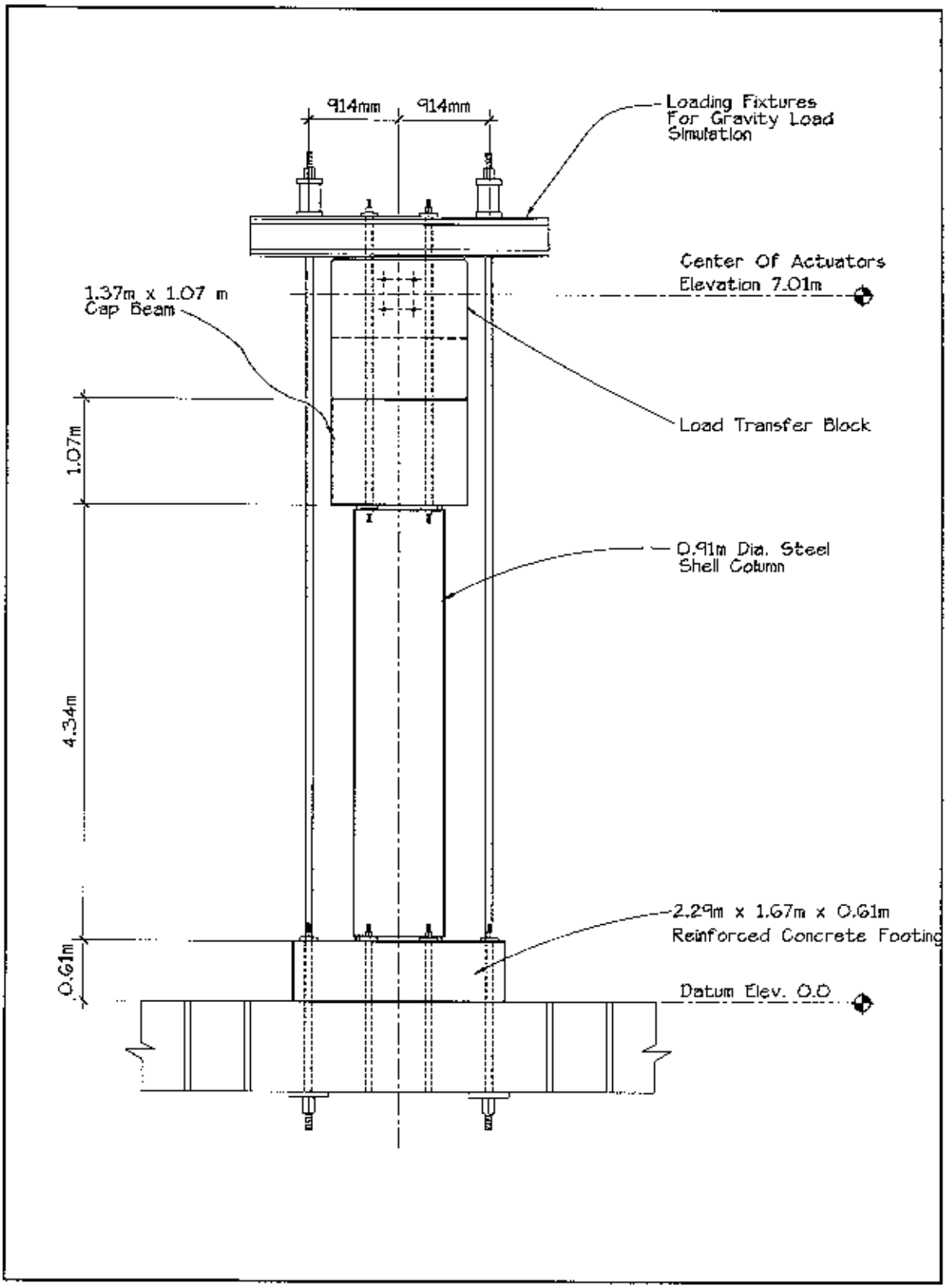

Fig. 2–4 Test Configuration - Side View

2.2 Reinforcement Layout of the Test Unit

The test unit was detailed according to design considerations presented in **Chapter 4**. In this section, a summary of various reinforcement details is presented. A brief description of the reinforcement utilized in the construction of the test specimen columns, cap beam, joints, pin connections and footings are presented. A section depicting the overall reinforcement layout is presented in **Fig. 2-5**.

2.2.1 Column Reinforcement

Design of the test unit was performed in order to model the seismic response of a three column/cap beam bridge substructure system. Column section dimensions and reinforcement are presented in **Table 2-2**. For the design of the column longitudinal reinforcement, a ratio of ρ_l=2.5% was chosen, in order to avoid design problems related to confinement of large amounts of longitudinal reinforcement, cap beam reinforcement for flexural and shear design, and joint shear reinforcement. Furthermore, this steel ratio matches typical values used in bridge design **[1]**. This reinforcement ratio lead to a section with *16 - M36* bars with a total longitudinal reinforcement area of 16,112 mm^2. The gross sectional area was 0.62 m^2, which does not include the steel shell area. The column bars were arranged around the inner circumference of the spiral steel with a cover concrete to the outside of the steel shell of 76.20 mm, as shown in **Fig. 2-6** and **Fig. 2-7**. The column longitudinal reinforcement terminated straight into the cap beam with a development length of 940 mm and a clear distance to the cap beam top surface of 127 mm.

Table 2-2 Column Section Dimensions and Reinforcement

Column Diameter	910 mm Outside Diameter
Steel Shell Thickness	12.70 mm
Inner Core Longitudinal Reinforcement	16 - M36 (ρ_l = 2.5%)
Transverse Reinforcement	Hoops: M16 @ 127 mm o.c. - Inside Joints Spirals: M16 @ 305 mm Pitch - Outside Joints
Steel Shell Gap	Top of Columns: 50.8 mm Bottom of Columns: 63.5 mm
Cover to Longitudinal Reinforcement	76 mm

Because of the presence of the 12.70 mm thick steel shell, the transverse reinforcement consists only of nominal reinforcement of M16 spirals at a pitch of 305 mm below the joint region for assembly of the longitudinal reinforcement steel cage.

2.2.2 Cap beam Reinforcement

Reinforcement of the cap beam was designed based on the design procedure presented in **Section 4.2** and **Section 4.3**, and cap beam section dimensions and reinforcement are presented in **Table 2-3**. The longitudinal reinforcement in the cap beam was determined by ensuring that yielding in this reinforcement did not occurred at the established design moments. Additional longitudinal reinforcement required for joint force transfer mechanism was also provided. With distribution of some longitudinal reinforcement along the sides as recommended in [4], reinforcement of the cap beam top layer consisted of *10 - M29* and *6 - M29* bars in the vicinity of the exterior columns and interior columns respectively, as illustrated in **Fig. 2-8(a)**. In the bottom layer *13 - M29* and *6 - M29* bars are provided in the vicinity of the exterior columns and interior columns, respectively, as illustrated in **Fig. 2-8(b)**. Additional top and bottom longitudinal reinforcement was provided according to the models presented in **Section 4.2**. Additionally *5 - M29* longitudinal bars were provided in the bottom layer reinforcement *and 6-M29* longitudinal bars were provided in the top layer reinforcement in the exterior joints ***KJ1*** and ***KJ2***. Additionally, *6-M29* longitudinal bars were provided in the top and bottom layer reinforcement in interior joint ***TJ***. In addition, *8-M13 horizontal J-hooks* were provided within the joint region and *12 and 10 legs M10* horizontal U-pins were provided in the top and bottom layer, respectively, at the cap beam ends, as illustrated in **Fig. 2-5** and **Fig. 2-9**.

The transverse reinforcement in the cap beam was obtained from shear and joint design considerations (see **Chapter 4**), which resulted in different reinforcement quantities in various regions along the cap beam. In exterior joint ***KJ1***, the column transverse reinforcement in this region consisted of *M16 welded hoops at 127 mm on center*. Inside this joint region, the vertical stirrups reinforcement consisted of *2 sets of 6 legs M13* stirrups equally spaced. Outside of the joint region *5 sets of 6 legs M13* stirrups were provided in the overhang, and *6 sets of 6 legs M13* stirrups were provided within a distance of 533 mm from the column face, equally spaced and designed according to the model presented in **Section 4.3**. In addition, *8-M13 horizontal J-hooks* were provided within the joint region, and *12 and 10 legs M10* horizontal U-pins were provided in the top and bottom layer, respectively, at the cap beam ends, as illustrated in **Fig. 2-6**.

In interior joint ***TJ***, transverse reinforcement in this region consisted of *M16 welded hoops at 127 mm on center*. Inside this joint region vertical stirrup reinforcement consisted of

3 sets of 6 legs M13 stirrups, equally spaced. Outside of the joint region *7 sets of 6 legs M13* stirrups were provided within a distance of 1.07 m from the column face, equally spaced and designed according to the models presented in **Section 4.3**. In addition, *8-M13 horizontal J-hooks* were provided within the joint region, as illustrated in **Fig. 2-7**.

In joint ***KJ2***, vertical stirrup reinforcement consisted of *3 sets of 6 legs M13* stirrups equally spaced, and outside of the joint region *5 sets of 6 legs M13* stirrups were provided in the overhang, and *7 sets of 6 legs M13* stirrups within a distance of 1.07 m. from the column face equally spaced. Reinforcement detail in exterior joint ***KJ2*** is shown in **Fig. 2-6.**

Table 2-3 Cap Beam Section Dimensions and Reinforcement

Cap Beam Width	1.37 m
Cap Beam Depth	1.07 m
Top Layer Longitudinal Reinforcement	Exterior Joints 10 - M29 Interior Joint 6 - M29
Bottom Layer Longitudinal Reinforcement	Exterior Joints 13 - M29 Interior Joints 6 - M29
Side Reinforcement	Exterior Joints 4 - M29 Interior Joints 2 - M29
Minimum Shear Reinforcement	4 legs of M13 @ 241 mm. o.c.
Vertical Stirrups Reinforcement Exterior Joint ***KJ1***	2 Sets 6 Legs M13 Inside Joint 5 Sets 6 Legs M13 in Overhang 7 Sets 6 Legs M13 within533 mm from Column Face
Vertical Stirrups Reinforcement Interior Joint ***TJ***	3 Sets 6 Legs M13 Inside Joint 7 Sets 6 Legs M13 within 1.07 m from Column Face
Vertical Stirrups Reinforcement Exterior Joint ***KJ2***	3 Sets 6 Legs M13 Inside Joint 5 Sets 6 Legs M13 in Overhang 7 Sets 6 Legs M13 within 1.07 m from Column Face
Cover to Top Longitudinal Reinforcement	51 mm
Cover to Bottom Longitudinal Reinforcement	51 mm

2.2.3 Footing Reinforcement

A total of *13 - M22* bars top and bottom with a reinforcement ratio of 0.24% was provided in the longitudinal and transverse direction. Vertical *M13 J-hooks* were provided in the footings at each bar intersection. The connection of the columns to the footings consists of *8 sets (16 legs) M19* bars arranged in a criss-cross pattern, and with a development length of 1.22 m, as previously described, and presented in **Fig. 2-10.**

Table 2-4 Footing Dimensions and Reinforcement

Footing Plan Dimensions	2.29 m x 1.67 m
Footing Height	610 mm
Longitudinal Reinforcement	Top: 13 - M22 Bottom: 13 - M22
Vertical Reinforcement	M13 J-Hooks
Reinforcement in Column/Footing Connection	8 sets (16 Legs) M19 with a Vertical Lap Length of 1.22 m
Cover to Longitudinal Reinforcement	51 mm

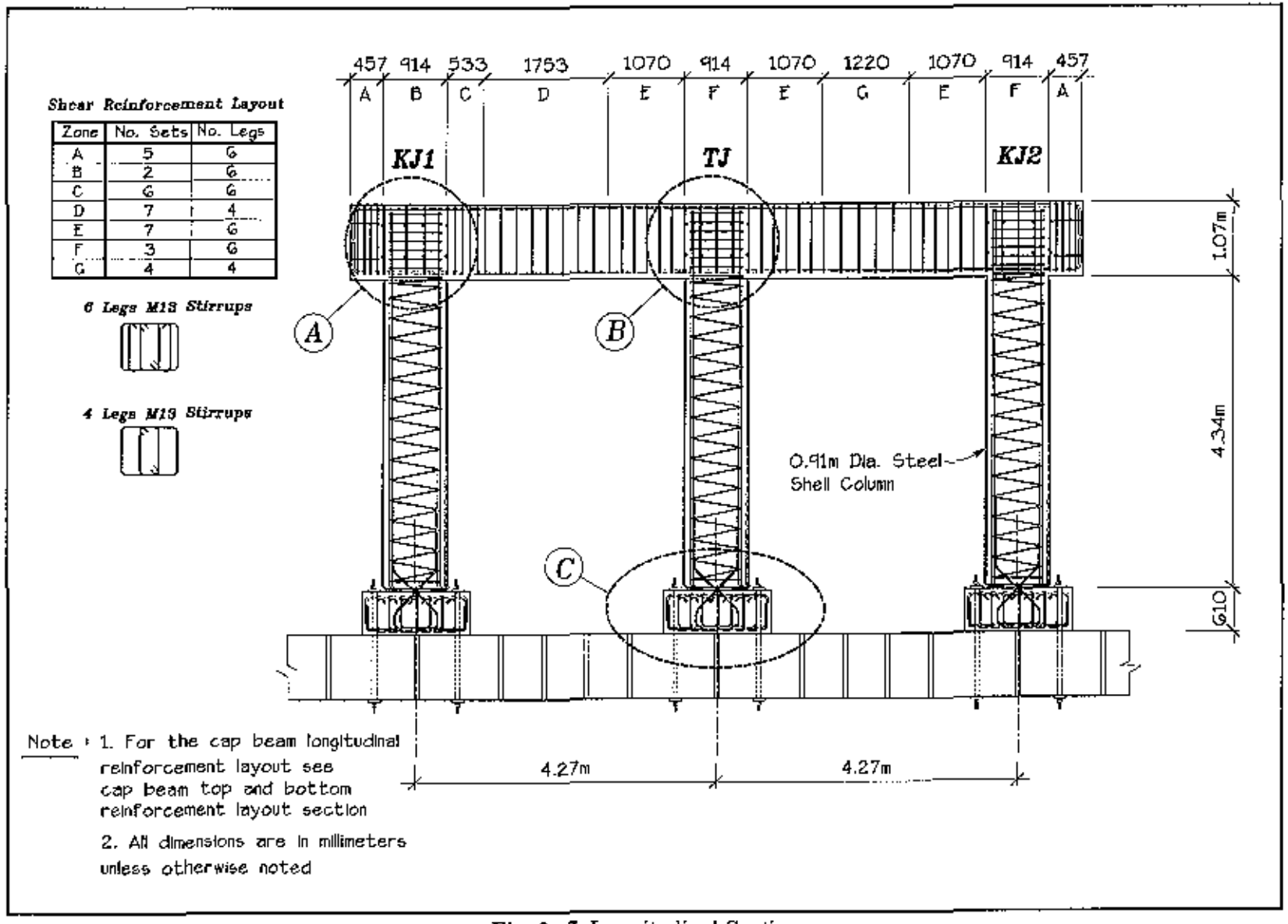

Fig. 2-5 Longitudinal Section

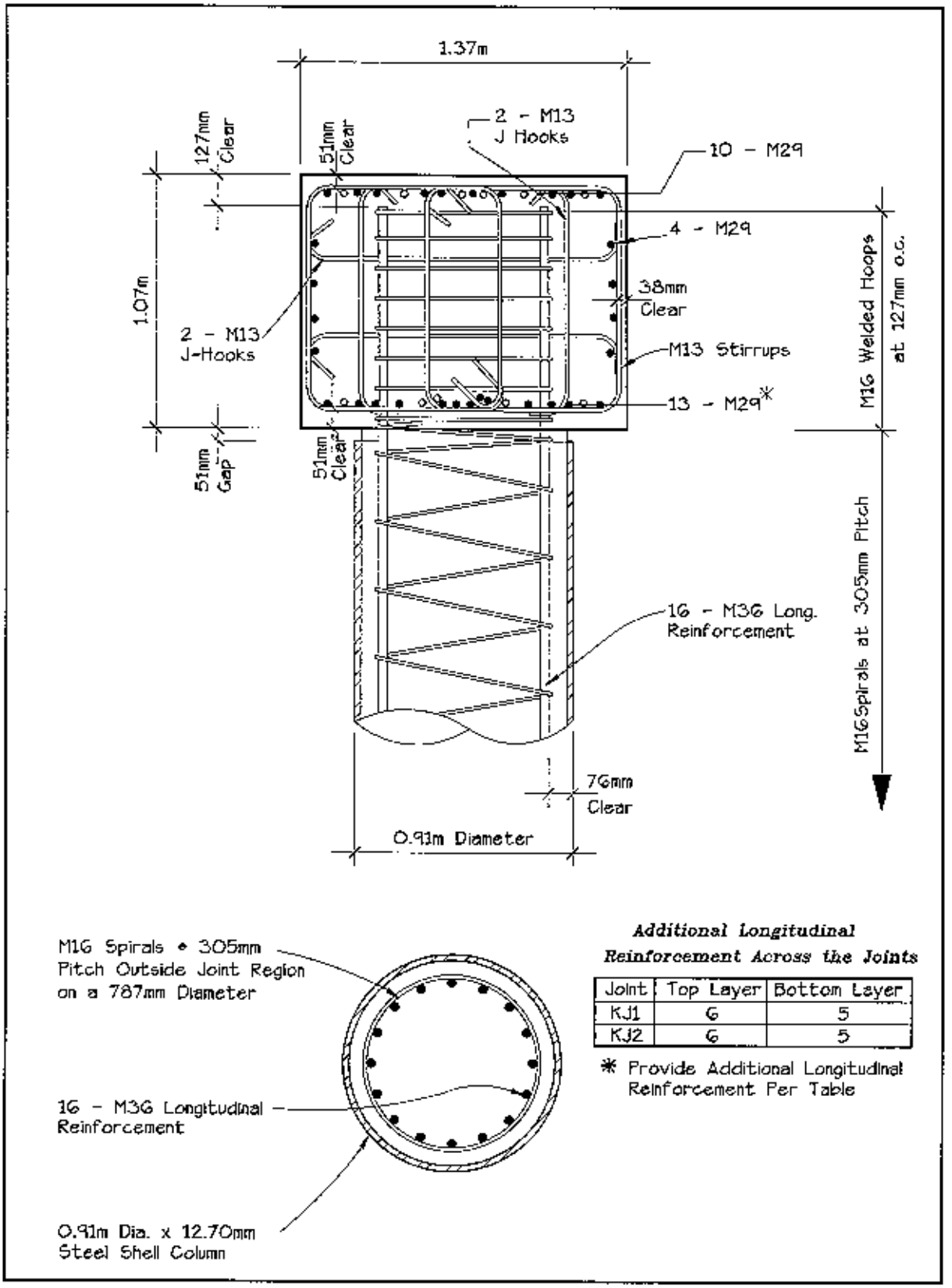

Fig. 2–6 Section *A-A* - Exterior Joint

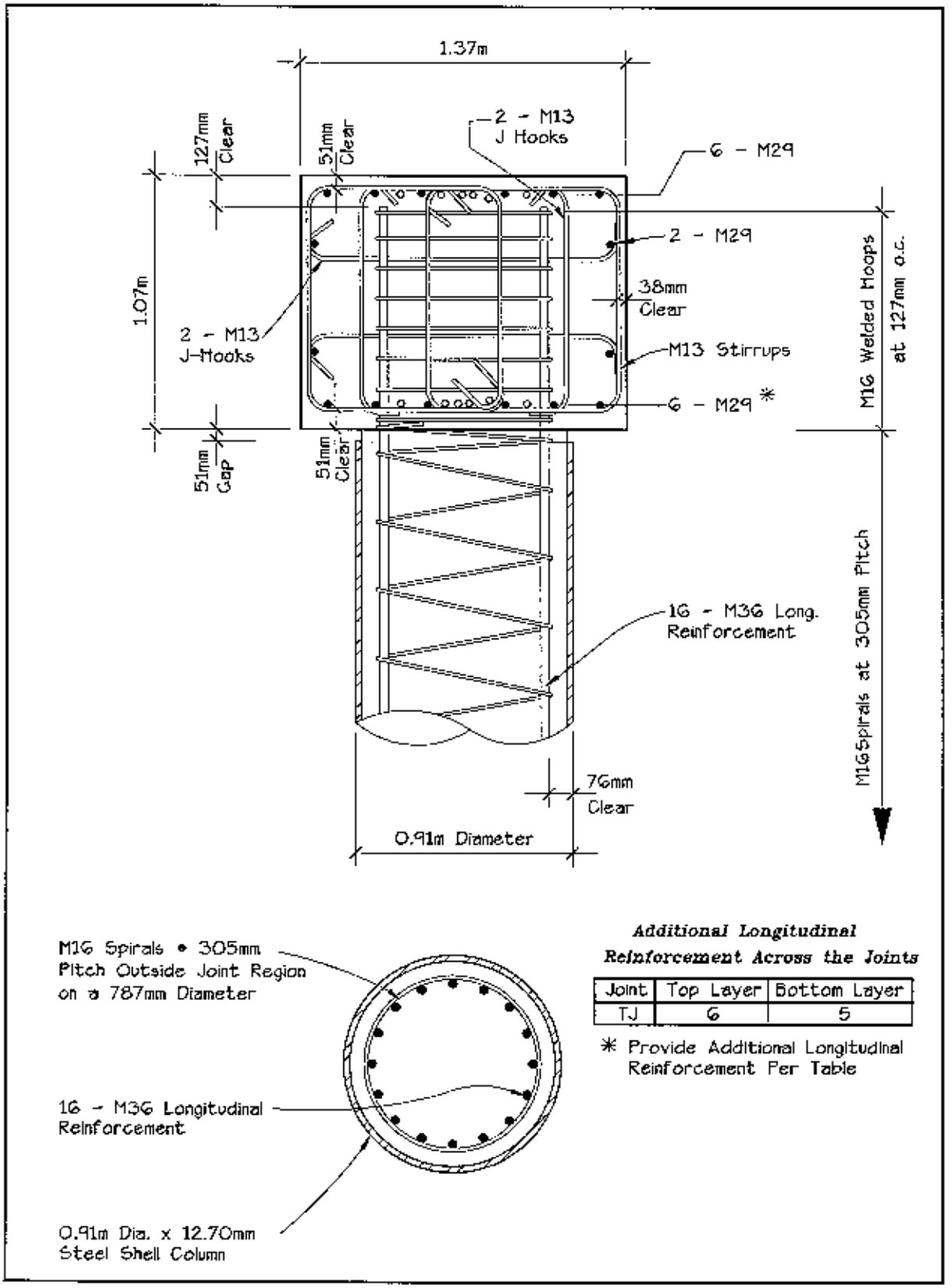

Fig. 2-7 Section ***B-B*** - Interior Joint

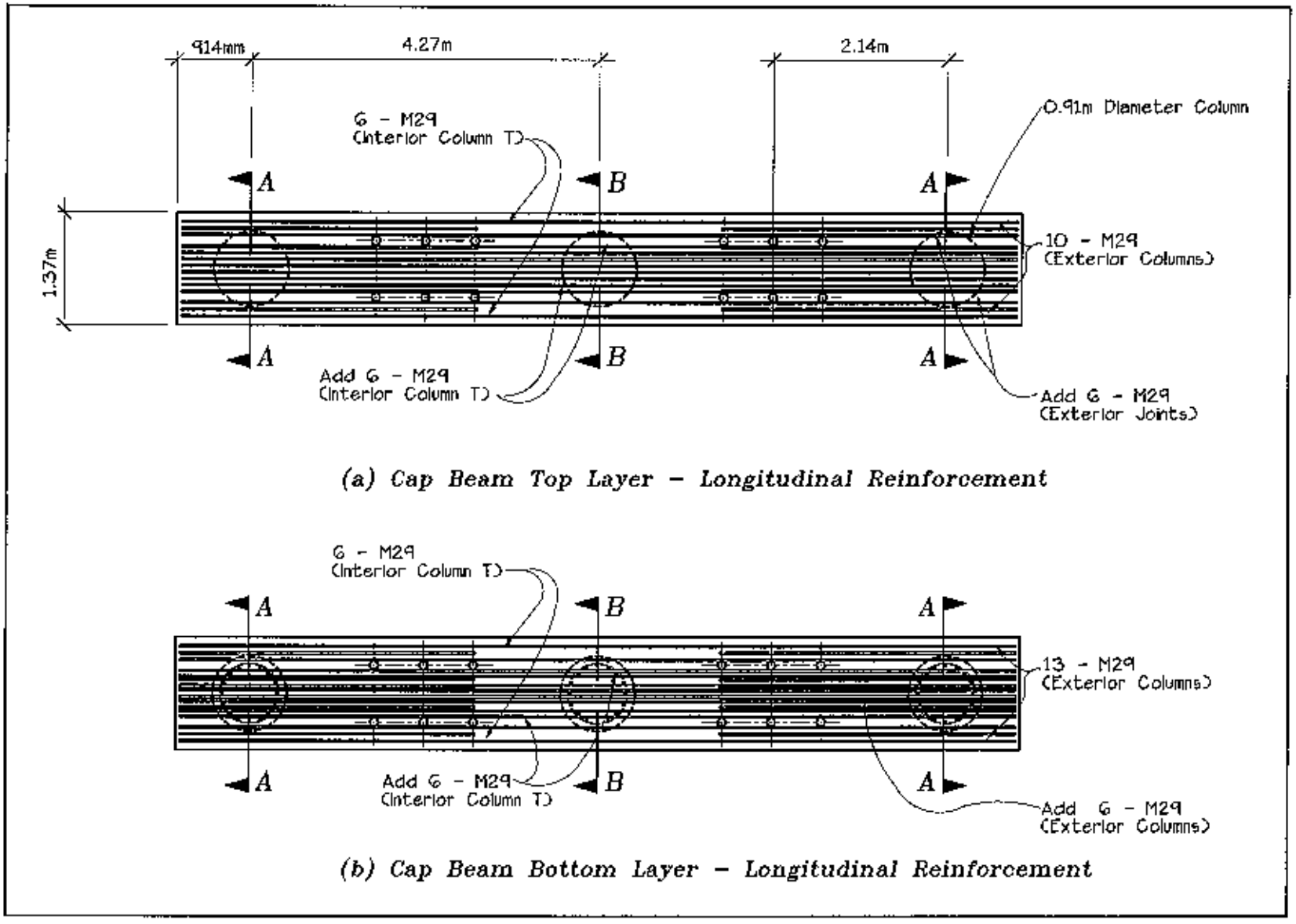

Fig. 2-8 Cap Beam Top and Bottom Layer Longitudinal Reinforcement

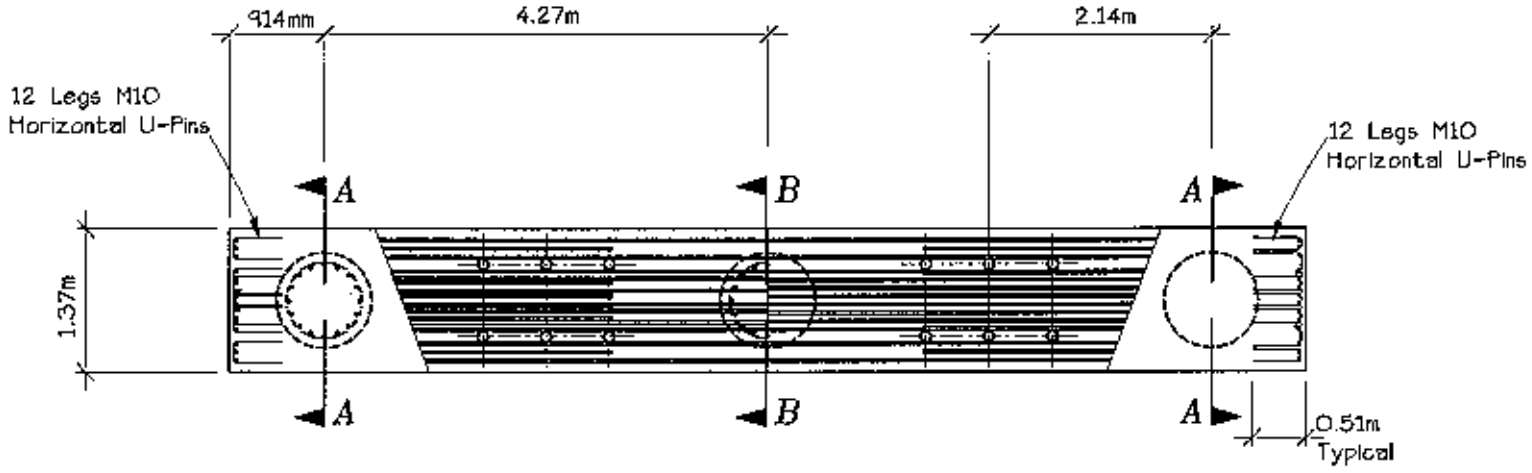

(a) Cap Beam Bottom Layer

(b) Cap Beam Top Layer

Fig. 2-9 Cap Beam Ends Horizontal U-Pins

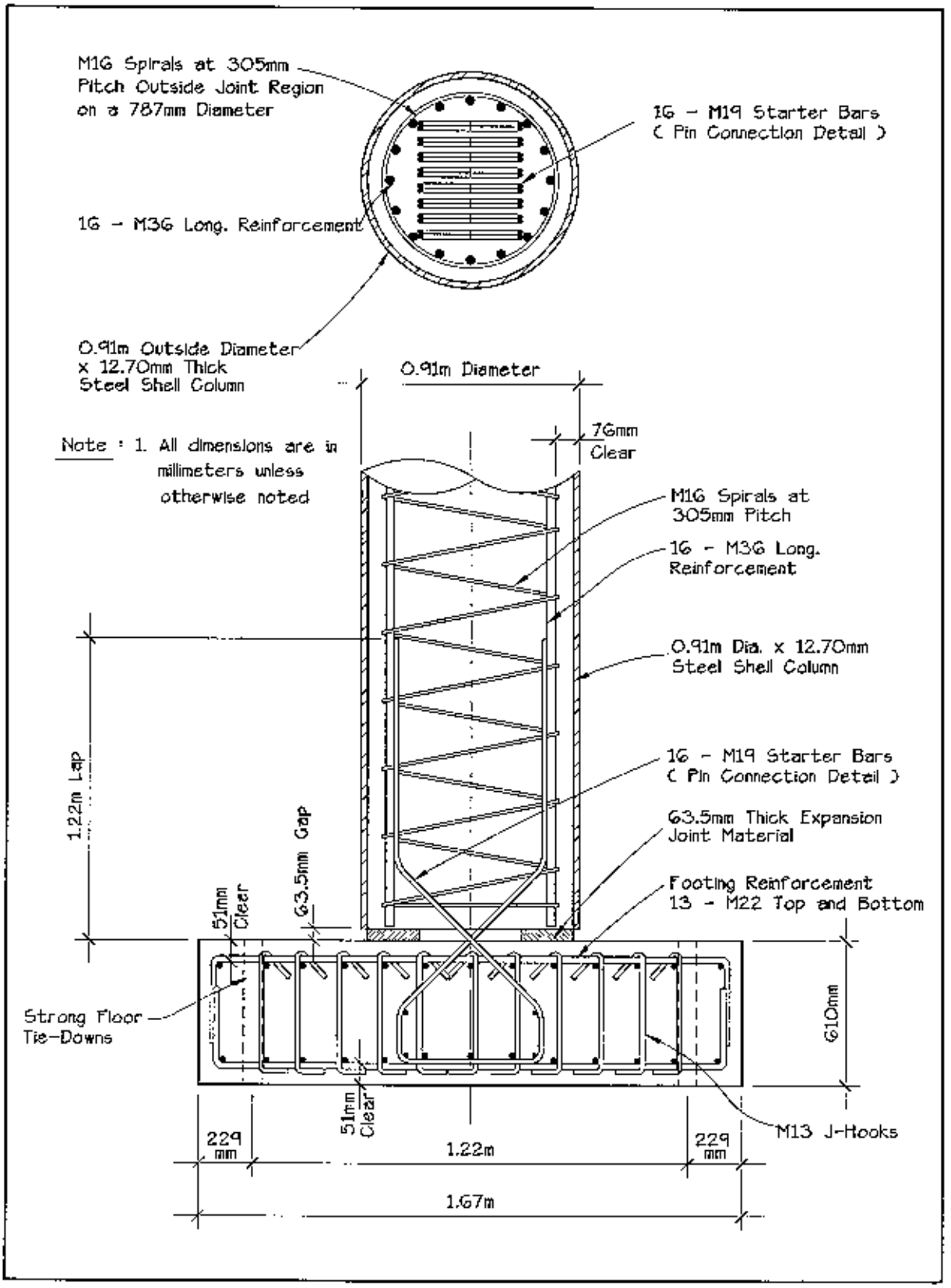

Fig. 2–10 Section *C-C* - Column Base

3 Analysis Considerations

The design forces and theoretical response of the test unit were obtained from a pushover analysis. The procedure followed in this analysis is described in **Section 3.1** and the results are presented in **Section 3.2** and **Section 3.3**. However, it must be emphasized that a similar type of analysis is **not** required to establish design forces for multiple column bents. A simpler approach based on column overstrength moment capacities obtained from a section analysis can be adopted as described in references **[1]** and **[4]**. In this chapter, a brief description of the analytical model is presented, and results that were used to establish the test unit design forces.

3.1 Modeling of the Test Unit

The pushover analysis in this study was conducted through a control program, which interacted with a moment-curvature analysis program **[8]** and a structural analysis program CALSD **[9]**, which were both developed at UCSD. An analytical finite element model was developed to study the seismic response of the test unit. The cap beam and columns were modeled using elements with member lengths to the centerline of the columns and cap beam. During the analysis, each element stiffness was updated based on the tangent stiffness approach illustrated in **Fig. 3-1** and computed according to the following expression:

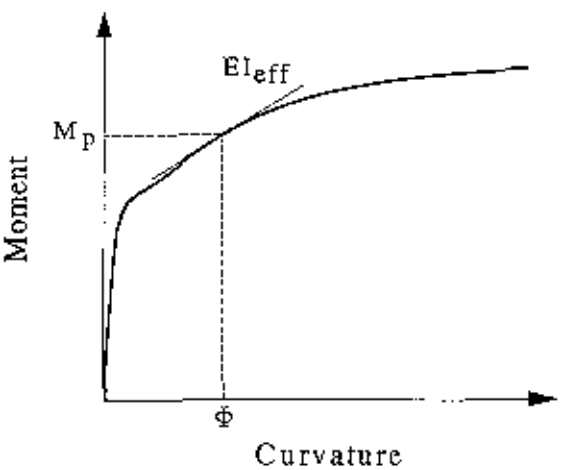

Fig. 3-1 Tangent Stiffness Approach

$$E I_{eff} = \frac{\Delta M_p}{\Delta \varphi} \tag{3.1}$$

where the change in moment ΔMp and change in curvature $\Delta \varphi$ were obtained from the moment curvature analysis at each incremental setup. A moment curvature program, using a model developed by Mander et al. for confined concrete **[10]**, was developed to update the stiffness of each element.

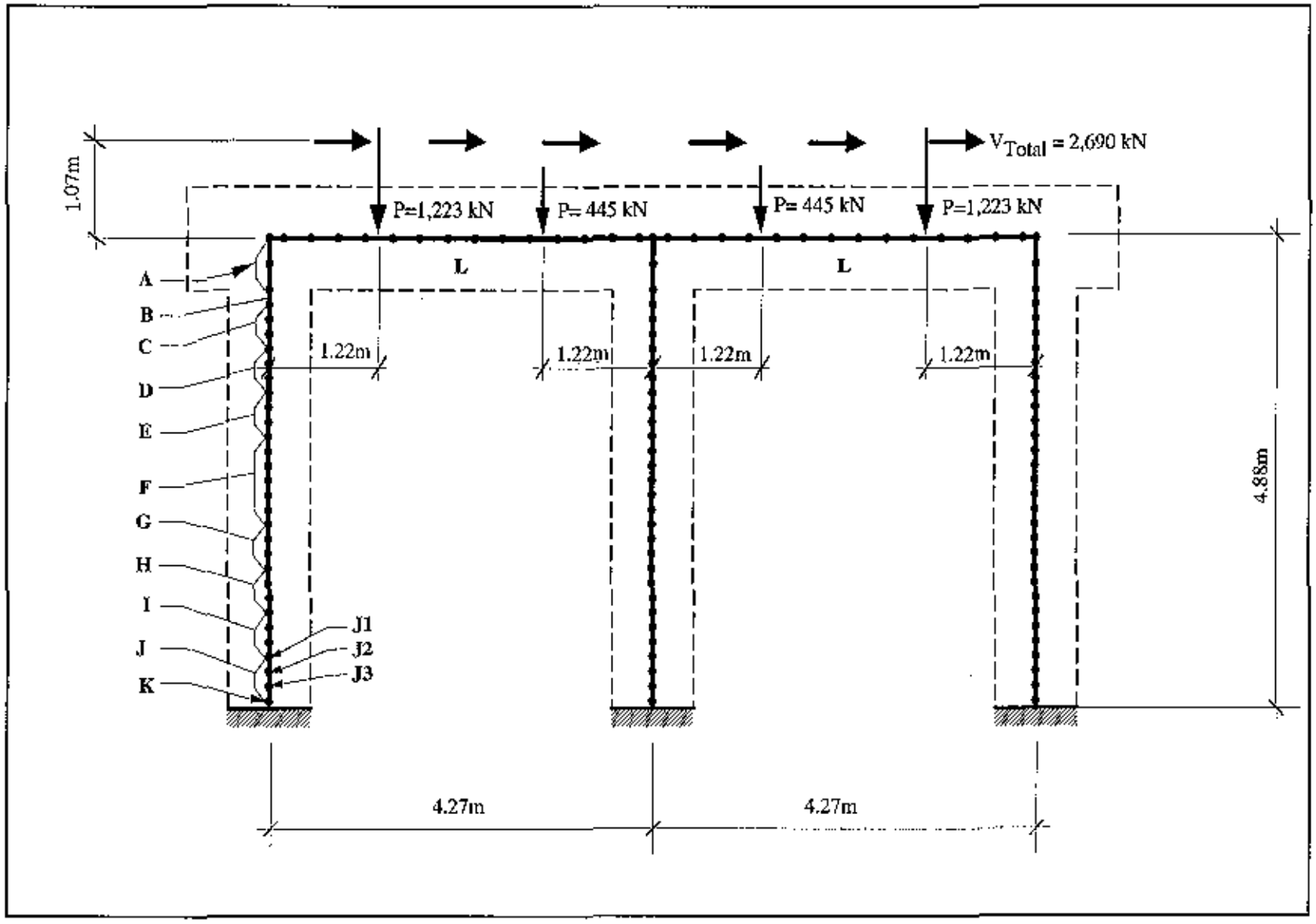

Fig. 3-2 Pushover Analysis Finite Element Model

The moment curvature program allows for modeling of the columns circular section steel shell and longitudinal reinforcement. In these analyses, the development length of the column longitudinal reinforcement at the column bases and the steel shell at the top and bottom of the columns was modeled according to the regions presented in **Fig. 3-2**.

From region ***A*** to region ***J***, the implemented moment curvature program allows modeling of the different regions by considering percentages of contribution of the column longitudinal reinforcement and steel shell to the equilibrium equations according to the expression.

$$\sum C_c + \sum a_s C_s' + \sum a_{sj} C_{shell} = \sum a_s T_s + \sum a_{sj} T_{shell} + P \qquad (3.2)$$

where $\sum C_c$ is the resultant compression force in the confined and/or unconfined concrete section. Confinement of the concrete core was computed from the confining action of the steel shell due to radial confining stresses that develop in the steel shell according to the relationship:

$$f_l' = \frac{1}{2} f_{yj} \rho_{sj} \qquad (3.3)$$

The horizontal volumetric confinement ratio of the steel shell is given by the expression:

$$\rho_{sj} = \frac{4 t_j}{D_j - 2 t_j} \qquad (3.4)$$

where f_{yj} is the steel shell yield strength, t_j is steel shell thickness and D_j is the outside diameter of the steel shell. The confined concrete compressive strength can then be estimated from the confining action of the steel shell according to the expression **[10]**:

$$f_{cc}' = f_c' \left(2.254 \sqrt{1 + \frac{7.94 f_l'}{f_c'}} - \frac{2 f_l'}{f_c'} - 1.254 \right) \qquad (3.5)$$

Chai et al. **[11]** presents a procedure for computing the effects of confinement of concrete by means of a steel jacket.

Additional variables in equation **(3.2)** are the terms $\sum a_s C_s'$ and $\sum a_s T_s$, which represent the resultant compression and tension forces in the reinforcing steel, and a_s defines a percentage contribution of the longitudinal reinforcement in the development length zone at the base of the columns. Similarly, in equation **(3.2)**, the expressions $\sum a_{sj} C_{shell}$ and $\sum a_{sj} T_{shell}$ are respectively the compression and tension resultant forces in the steel shell, and a_{sj} is a variable that defines a percentage contribution of the steel shell at the top and bottom of columns to account for the development of forces in the steel shell. Referring to **Fig. 3-2**, the values of the variables a_s and a_{sj} were defined according to the values depicted in **Table 3-1**.

Table 3-1 Variables α_s and α_{sj} Numerical Values

Region	Member	Region Limit [2]	Longitudinal Reinforcement Contribution Value, α_s	Steel Shell Contribution Value, α_{sj}
A	Column	152	1.00	0.00
B	Column	305	1.00	0.00
C	Column	914	1.00	0.15
D	Column	1,295	1.00	0.30
E	Column	1,676	1.00	0.60
F	Column	2,972	1.00	0.90
G	Column	3,353	1.00	1.00 [1]
H	Column	3,734	1.00	0.60
I	Column	4,145	1.00	0.30
J	Column	4,801	J1 0.85 - J2 0.63 - J3 0.38	0.15
K	Pin	4,880	Pin Connection Detail	Pin Connection Detail
L	Cap Beam	-	Cap Beam Detail	Cap Beam Detail

[1] Full composite action of steel shell and concrete core

[2] Distance in millimeters from cap beam centerline to end of region.

To compute the development length for the column longitudinal reinforcement at the base of the columns, the variable α_s was defined based on an average bond strength of $\mu_{av} = 1.17\sqrt{f_c'}$, which is consistent with values presented in reference **[1]**. An expression to compute the development length is presented in **Section 4.2**. In addition, the variable α_{sj} was defined by assuming that 15% of the steel shell forces are developed at the end of Region *C*. Thus, the average tensile bond strength of the steel shell was 2.08 MPa, which is consistent with values found from test presented in reference **[6]**, and may be computed in this region *C* according to the expression:

$$\mu_{ave} = \frac{0.15\, f_{yj}\, t_j}{L_C} = \frac{0.15 \times 250 \times 12.70}{229} = 2.08\ MPa \qquad (3.6)$$

where L_C is the distance between from top of shell to the node situated in the end of Region *C*.

3.1.1 Pushover Analysis

The following are physical boundary conditions and relevant data that were used to set up the finite element model:

(i) Element Stiffness. As the lateral load was incremented at each step, a moment–curvature analysis for each column and cap beam segment was performed with a varying axial load obtained from the pushover analysis. A column segment refers to all the elements in each column, and a cap beam segment refers to those elements which are situated from the column centerline to the point of inflection in the cap beam. Then, each element stiffness was updated according to equation **(3.1)**, and the input file was revised for re-analysis of the finite element model.

(ii) Column Top Gap. The column top gap, Region ***B***, was modeled with a single element 51 mm long, which corresponds to the length of the steel shell gap in this region. The length of this beam element was updated at each incremental lateral load to account for strain penetrations of the column longitudinal reinforcement into the cap beam according to the following expression [1]:

$$l_{sp} = 0.022\, d_b f_s \quad ; \quad f_s \le f_y \tag{3.7}$$

where l_{sp} is the strain penetration of the columns longitudinal reinforcement, and f_s is the steel stress evaluated at each incremental step, but less than the longitudinal reinforcement yield strength f_y

(iii) Column Base Boundary Conditions. The base of each column was modeled as a fixed end condition. However, upon reaching the ideal moment capacity of the pin connection the boundary conditions at the base of the columns was modified to a pinned end condition.

(iv) Loading Conditions. The lateral load was applied to the finite element model at every node along the cap beam located 610 mm away from the columns centerline. To model the vertical distance between the centerline of the actuator to the center line of the cap beam the nodal loads consisted of horizontal point loads and moments, which were obtained by multiplying the nodal horizontal loads by a lever arm 1.07 m.

The pushover analysis was performed according to the following steps:

(i) Gravity Load. In this stage, only the axial forces and the test specimen selfweight were imposed on the model as described in **Fig. 3-2.**

(ii) Initial Lateral Load. After simulation of the gravity loads, each element stiffness was updated and an initial lateral load was applied, such that at any location, the bending moment was below cracking, either in the columns or cap beam elements.

(iii) Incremental Lateral Load. At each successive iteration and up to the ultimate moment capacity of the columns, while maintaining the imposed lateral load constant, intermediate steps were performed and equilibrium was achieved when the element properties remained constant along the length of the column.

(iv) Analysis in a Descending Branch. To provide an analytical solution for elements that display a descending branch, (i.e. negative stiffness), each element stiffness in a descending branch was set as positive. Then, at each incremental step, increases in deflection, rotations and curvatures were obtained from the pushover analysis results and summed to the respective resultant variables, and moments and shear forces were subtracted from the resultant moments and shear forces.

(v) Ultimate Moment Capacity. The procedure was carried out until ultimate conditions were observed in the top element of one of the columns in region ***B***, which represents the plastic hinge zone.

3.2 Pushover Analysis Results

In this section some results are presented for the pushover analysis, which were then used for the design of the test unit. The design part of the test unit was performed using estimated concrete material properties and average steel material properties obtained from the material properties presented in the **Section 5.2.2.** In the design of the test unit, the estimated unconfined concrete compression strength for the column analysis was f'_c=28 MPa, and for the cap beam analysis the estimated unconfined concrete compression strength was f'_c=34 MPa. In addition, the steel material properties were obtained from three reinforcement tensile strength tests. Reinforcement yield strength for the different bar sizes are presented in **Table 5-2.**

In the finite element model, modeling of the prototype gravity load was accomplished by imposing four vertical point loads along the cap beam such that the end bending moments in the cap beam approximately matched with the bending moment due to application of the prototype gravity loads. As previously described, the simulated gravity loads were positioned at 1.22 m from the centerline of the columns. Adjacent to the exterior columns the point loads were 1,223 kN and adjacent to the interior column the point loads were 445 kN for a total applied axial load of 3,336 kN. Thus, as presented in **Fig. 3-3**, the axial load due to the simulated gravity loads and selfweight in the exterior columns was 1,070 kN and in the interior column was 1,760 kN, whereas the axial loads due to the prototype gravity loads were 1,259 kN and 1,948 kN in the exterior and interior columns, respectively.

In **Fig. 3-3** the bending moment diagram due to gravity loads is shown for the test specimen and for the prototype structure. Referring to **Fig. 3-3**, in the vicinity of the columns the bending moment profile of the model and the prototype were approximately identical, as previously stipulated, except at the cap beam midspans. Bending moment profiles depicted in this figure and subsequent figures are shown on the tension side of the members.

Fig. 3-4 shows the bending moment diagram due to gravity loads and lateral seismic forces at ultimate response of the test unit. At ultimate state, in the push direction, maximum bending moments occur in exterior column ***EC2*** (4,038 kN), followed in the interior column ***IC*** (3907 kN) and next in the exterior column ***EC1*** (3,296 kN).

Referring to **Fig. 3-5**, in the push direction, under gravity loads and lateral seismic load, maximum achieved shear force in the exterior column, ***EC1***, was 790kN. In the interior column, ***IC***, the maximum shear force was 933 kN. In the exterior column, ***EC2***, the shear force was 965 kN. Maximum lateral seismic force estimated was 2,688 kN.

In **Fig. 3-6** maximum achieved axial load in the exterior column, ***EC1***, was -752 kN in tension. In the interior column, ***IC***, the maximum axial load was 1,807 kN in compression. In the exterior column, ***EC2***, the axial load was 2,820 kN. Selfweight of the columns was estimated at 76 kN, pier cap 357 kN, and load transfer blocks that were attached to the cap beam 220 kN. Column and cap beam member end forces were then used for design of the test unit, which are presented in **Section 3.3**.

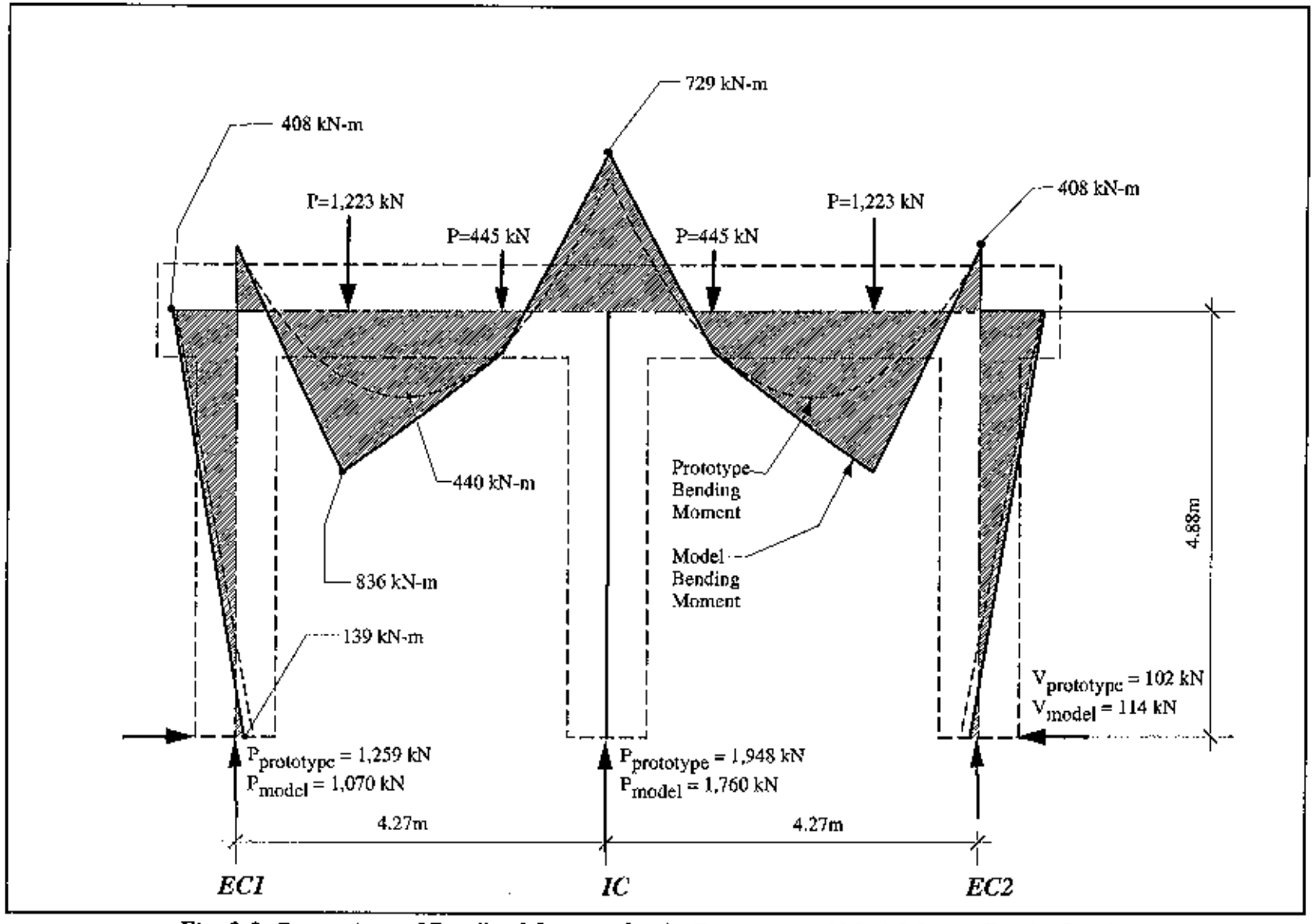

Fig. 3-3 Comparison of Bending Moments for the Prototype and Model due to Gravity Loads

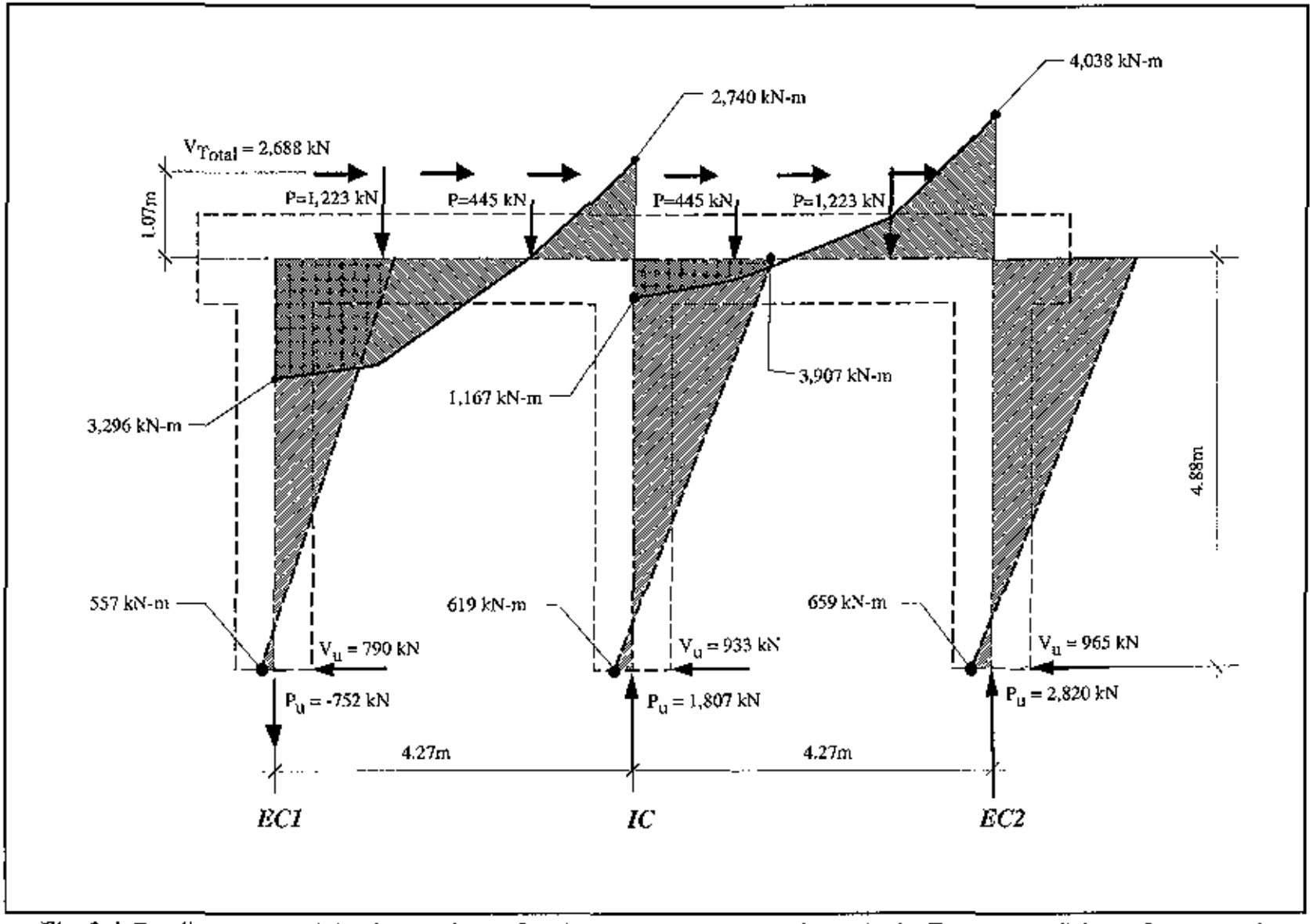

Fig. 3-4 Bending Moment Distribution due to Gravity Loads and Seismic Forces in the Test Unit at Column Overstrength

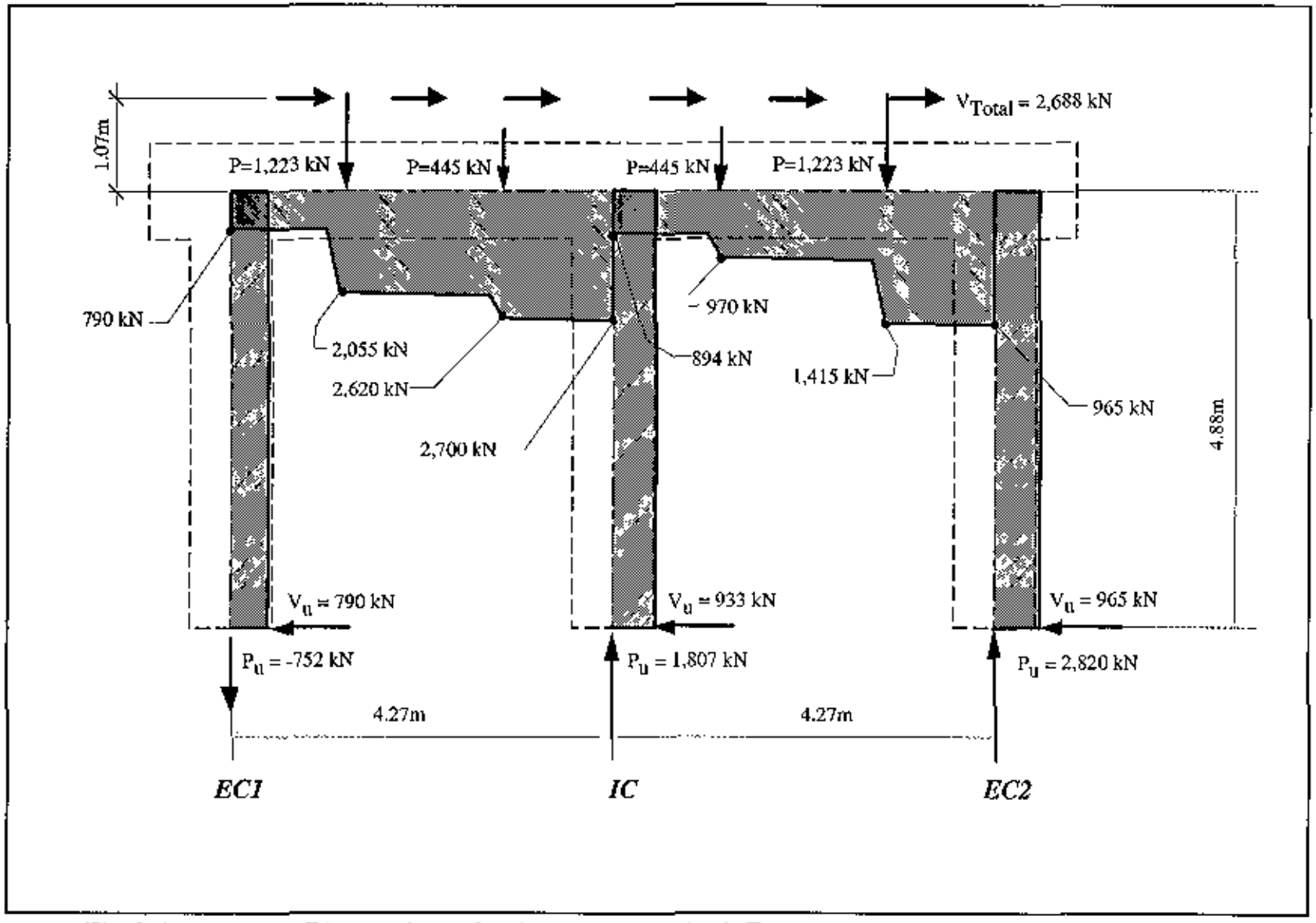

Fig. 3-5 Shear Force Diagram due to Gravity Loads and Seismic Forces in the Test Unit at Column Overstrength

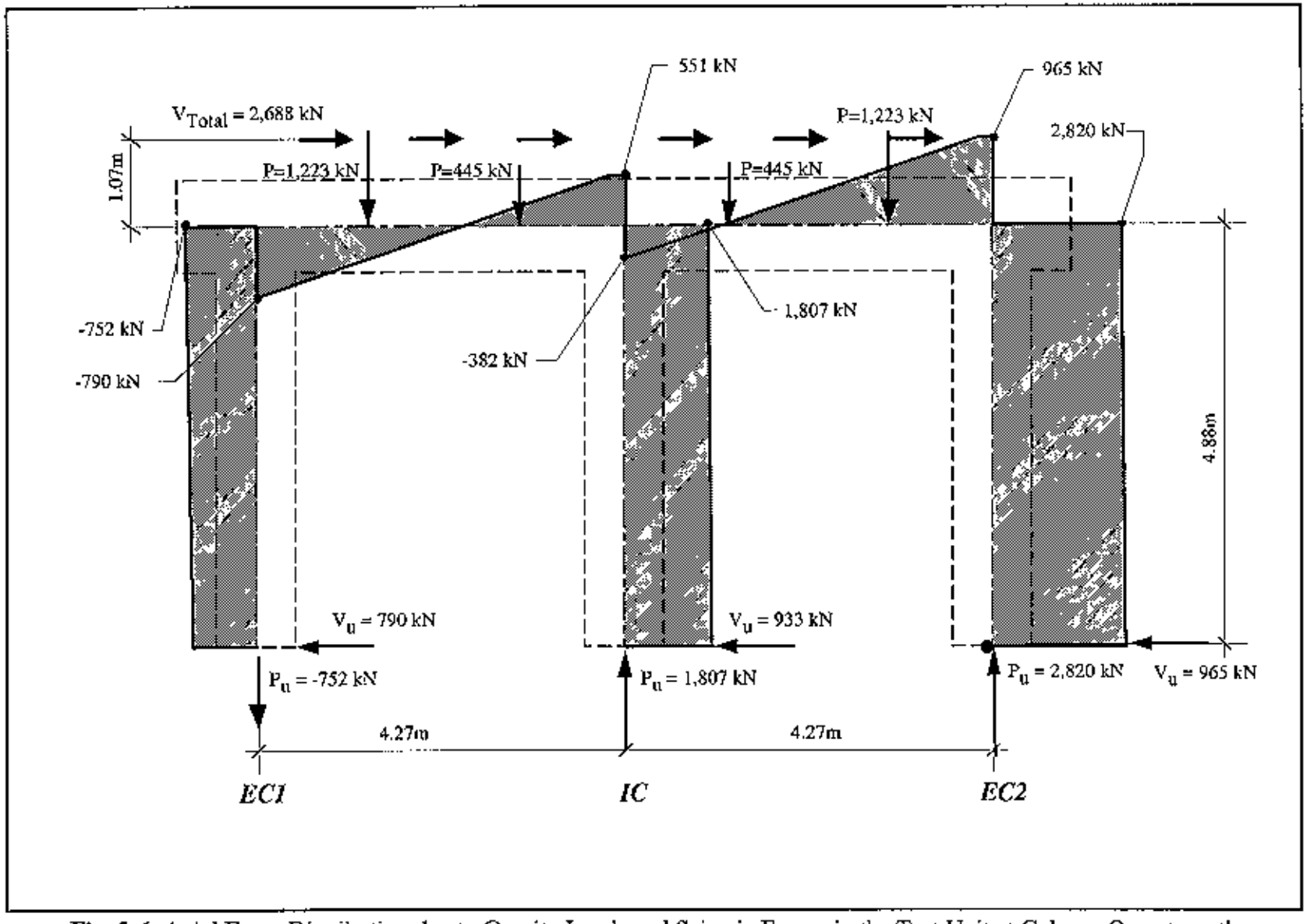

Fig. 3-6 Axial Force Distribution due to Gravity Loads and Seismic Forces in the Test Unit at Column Overstrength

3.3 Cap Beam Design Forces

The column overstrength moments are largely dictated by the stress-strain characteristics of the longitudinal reinforcement. When the column longitudinal steel properties are available from material testing, Sritharan et al.[4] recommend that the column overstrength moment can be approximated to 1.05 times the *theoretical maximum moment*. Furthermore, the gravity loads induced in the columns are small when compared to the moments due to lateral seismic forces, as described in **Section 3.2**. Therefore, the cap beam design bending moment and shear forces were conservatively estimated according to the expressions:

$$\varphi_f M_{D,cap} = 1.05\ M_E + M_D \tag{3.8}$$

where $M_{D,cap}$ is the cap beam design moment at the column face, M_E is the bending moment caused by lateral forces, M_D is the bending moment caused by gravity loads, and φ_f is equal to 0.90 and represents the flexural capacity strength reduction factor. **Fig. 3-7** presents the cap beam design bending moments evaluated at the column faces.

Similar to the design moments, design shear forces were computed at the column faces according to the expression :

$$\varphi_s V_{D,cap} = 1.05\ V_E + V_D \tag{3.9}$$

where $V_{D,cap}$ is the design shear force, V_E is the shear force caused by lateral forces, V_D is the shear force caused by gravity loads, and φ_s is equal to 0.85 and represents the capacity reduction factor for shear. **Fig. 3-8** presents the cap beam design shear forces evaluated at the column faces. Design axial loads were those obtained from the pushover analysis at the ultimate state.

The axial loads appropriate for the cap beam design were obtained by combining the gravity loads and seismic load contributions with considerations to column overstrength. The critical design moments, shear forces and corresponding axial forces are listed in **Table 4-1**.

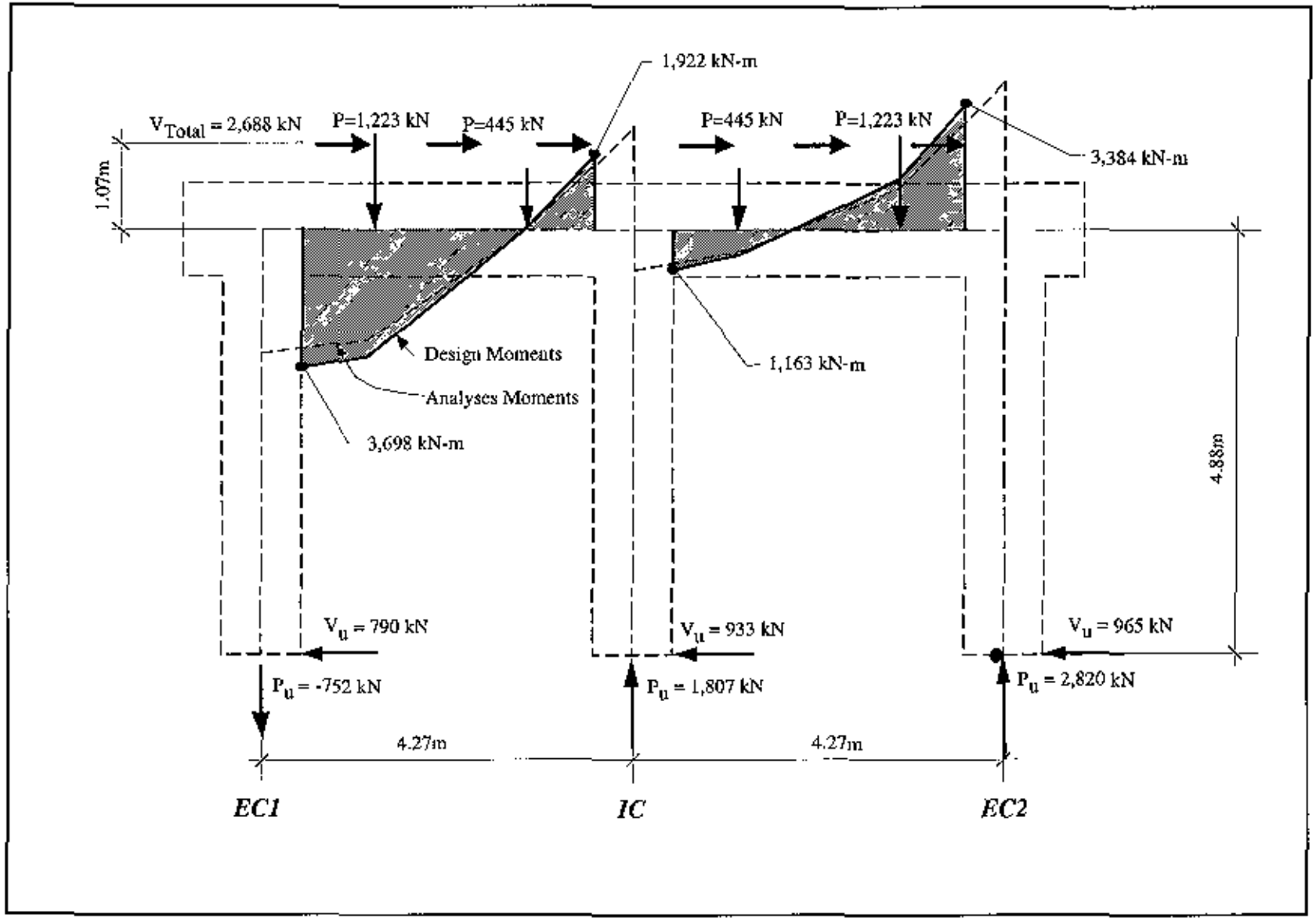

Fig. 3-7 Cap Beam Design Moments for the Test Unit

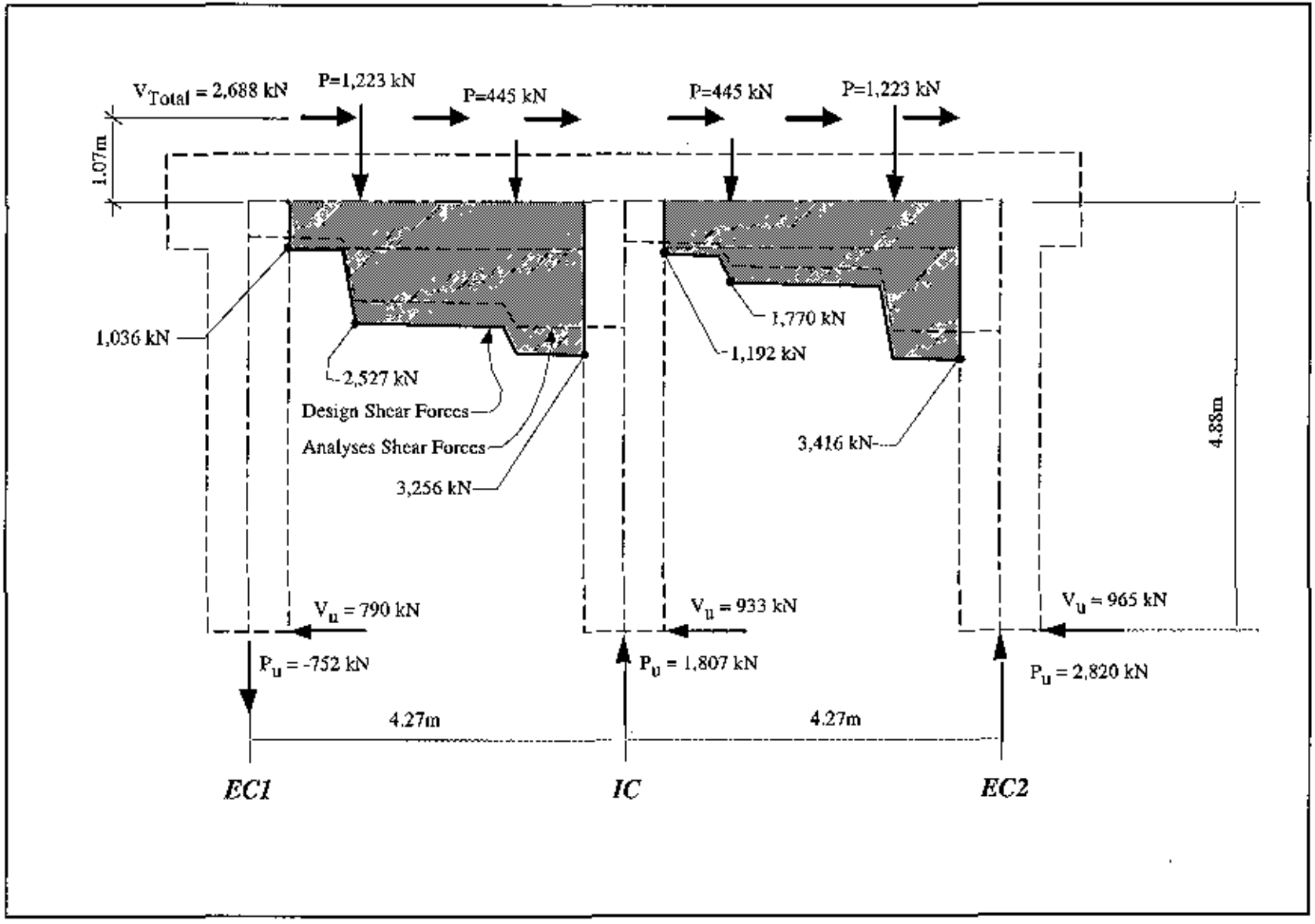

Fig. 3-8 Cap Beam Design Shear Forces for the Test Unit

4 Design Considerations

Design considerations adopted in the detailing of the test unit are presented in this chapter. Design forces used in the design of the test unit are presented in **Section 3.3.**

4.1 Column Design Considerations

According to a capacity design philosophy it is required that undesirable modes of deformation such as shear be inhibited, and the columns must be designed with adequate transverse reinforcement to ensure adequate confinement of the column plastic hinges. In this section, design of the column shear and transverse reinforcement (plastic hinge regions) are presented.

4.1.1 Column Shear Design

The shear strength of test unit columns was computed according to the recommendations given in reference **[1]** for the design of a reinforced cross section. The shear strength of the columns was computed based on the UCSD additive three component model, which is expressed in terms of the following expression **[1]**:

$$V_N = V_c + V_p + V_s \tag{4.1}$$

where V_N is the design shear force, V_c,V_s and V_p are the contributions from concrete, transverse reinforcement and axial load shear resisting mechanisms, respectively.

4.1.1.1 Concrete Component

The strength of the columns concrete shear resisting mechanism was based on the following equation **[1]**:

$$V_c = k\ 0.8\ A_g \sqrt{f_c'} \tag{4.2}$$

where k depends on the curvature ductility, μ_φ, as presented in reference **[1]** and **Fig. 4-1(a).**

4.1.1.2 Axial Load Component

Axial load contribution to the shear resisting mechanism was obtained according to the following expression [1][4]:

$$V_p = k\ P\ \tan\alpha \tag{4.3}$$

where k is equal to 0.85 for axial compression and 1.15 for axial tension, and α is the inclination of the axial strut, as illustrated in **Fig. 4-1(b)**. The value of α can be obtained from a moment-curvature analysis of the section at the column and/or cap beam ends.

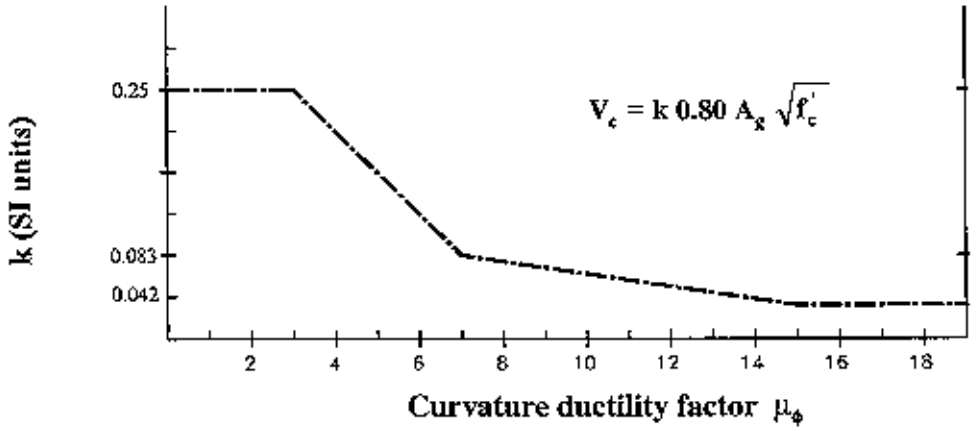

(a) Contribution of Concrete Shear-Resisting Mechanism to Design Shear Strength

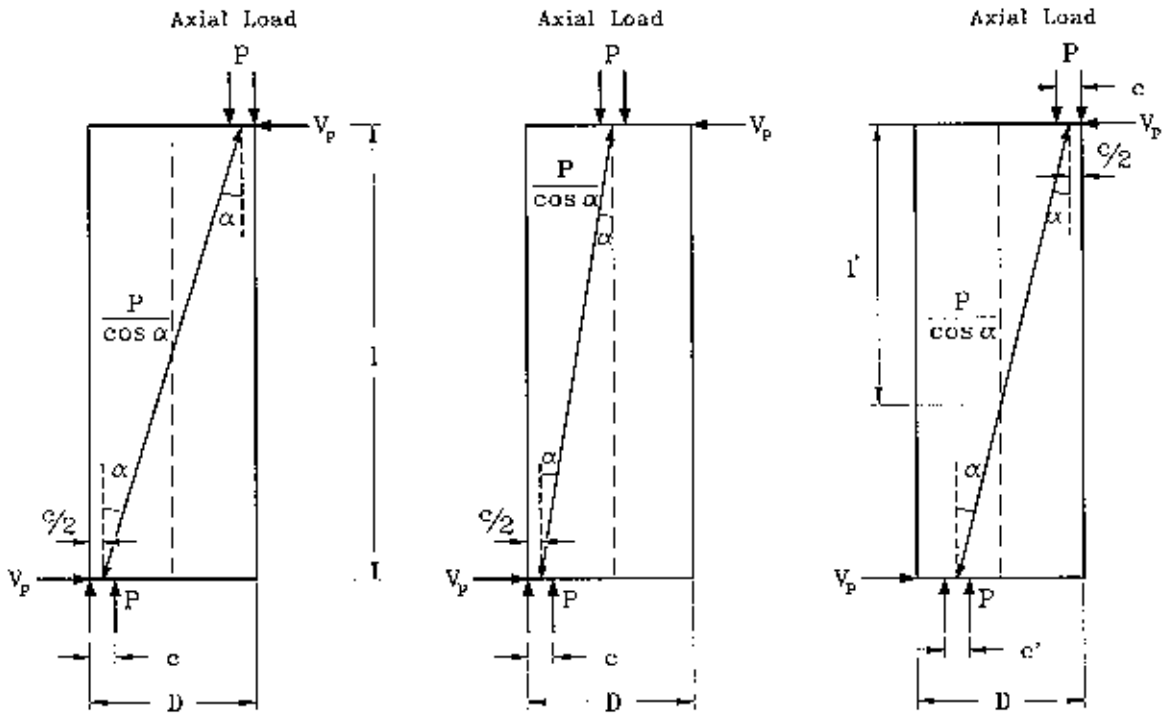

(b) Contribution of Column and/or Cap Beam Axial Force to Shear Strength

Fig. 4–1 Concrete and Axial Load Components of the UCSD Shear Model **[1][4]**

Substituting for tanα in equation (4.3) in terms of the neutral axis, column diameter and effective length, l', the following expression was derived to compute the axial load contribution to shear resistance:

$$V_p = k\ P \frac{D/2 - c/2}{l'} \tag{4.4}$$

where c is the column neutral axis, and l' is the distance from the top of the column to the point of inflection, as depicted in **Fig. 4-1(b)**.

4.1.1.3 Steel Component for Circular Columns

The steel truss component for a reinforced circular section with a steel shell and/or transverse reinforcement was computed based on the following expressions:

(1) Steel Shell Contribution **[11]**:

$$V_s = \frac{\pi}{2} f_{yj}\, t_j\, (D'_j - t_j)\ cot\ \theta \tag{4.5}$$

(2) Transverse Reinforcement Contribution **[12]**:

$$V_s = \frac{\pi}{2} \frac{A_{sp} f_y (D' - NA)}{s}\ cot\ \theta \tag{4.6}$$

where D'_j is the steel shell inside diameter, NA is the section neutral axis, D' is the confined core diameter, A_{sp} is the cross sectional area of the spiral transverse reinforcement, and θ is the crack angle, which was taken as 35° degrees.

Ignoring the concrete and axial load contributions to the shear resisting mechanism, the shear strength of one single column (considering only the steel shell truss mechanism) was estimated at 7,230 kN, which is considerably higher than the expected maximum lateral force (includes the three columns), as described in **Section 6.1**. Thus, the columns had reserved shear capacity to resist the induced shear forces, and the test unit is expected to display a predominant flexural response under the applied seismic loading.

4.1.2 Column Transverse Reinforcement

4.1.2.1 Confinement of Plastic Hinges

Confinement of the column in the plastic hinge region (gap region) was satisfied according to the following requirement **[4]**, in order to ensure a dependable ductile performance

of the structure:

$$\rho_s = 0.16 \frac{f'_{ce}}{f_{ye}} \left[0.5 + \frac{1.25\,P}{f'_{ce} + A_g} \right] + 0.13\,(\rho_l - 0.01) \qquad (4.7)$$

where ρ_s is the volumetric ratio of the transverse reinforcement content, f'_{ce} is the estimated concrete compressive strength, f'_{ye} is the estimated yield strength of the column longitudinal reinforcement, P is the column axial load, A_g is the column gross sectional area, and ρ_l is the column longitudinal reinforcement.

4.1.2.2 Resistance Against Buckling

In order to prevent buckling of the column longitudinal reinforcement, in the gap region at the top of the column, the following design requirement was satisfied [1]:

$$\rho_s = 0.0002\,n \qquad (4.8)$$

where n is the number of column longitudinal reinforcing bars

4.2 Cap Beam Design Considerations

The design of the cap beam was performed considering the column overstrength, to ensure that the cap beam remains essentially elastic and inelastic deformations are concentrated in the column plastic hinges under the imposed gravity and seismic loads. The column overstrengths consider material uncertainties and strain hardening of the column longitudinal reinforcement. Design forces for the cap beam design are presented in **Section 3.3**.

4.2.1 Cap Beam Width

The width of the cap beam was chosen consistent with current seismic design practice [13]. Accordingly, the cap beam width was taken as:

$$W_b = D + 2\,\frac{D}{4} = 914 + 2 \times \frac{914}{4} = 1.37\,m \qquad (4.9)$$

Thus, the width of the cap beam was 1.37 m.

4.2.2 Cap Beam Depth

The cap beam depth was dimensioned to ensure that the column longitudinal bars have sufficient development length into the joint region. The minimum development length was determined using recent recommendations by Priestley et al. [1], and has been experimentally verified by Sritharan et al.[3][4]. The development length of the column longitudinal bars was obtained assuming an average bond stress of $\mu_{av} = 1.17\sqrt{f_c'}$, and development length of a M36 bar was computed based on the expression [1]:

$$l_d = 0.3\, d_b \frac{f_y^o}{\sqrt{f_c'}} = 0.3 \times 36 \times \frac{450}{\sqrt{35}} \approx 822\ mm \qquad (4.10)$$

The cap beam depth was $h_b = 1.07$ m computed based on a development length of 940 mm for the column longitudinal reinforcement and a clear distance from the column bars to the cap beam top surface of 127 mm.

4.2.3 Cap Beam Flexural Design

Computations of design moments, shear forces and axial forces were described in **Section 3.3**, and are presented in **Table 4-1**. Reinforcement layout for the test unit is presented in **Section 2.2**.

Table 4-1 Cap Beam Design Moments, Shear Force and Axial Force

	Design Moment kN-m	Design Shear Force kN	Axial Force kN
Positive Moment at the Exterior Column Face	3,698	1,036	-790 *(T)*
Negative Moment at the Exterior Column Face	3,384	3,416	965 *(C)*
Positive Moment at the Interior Column Face	1,163	1,192	-382 *(T)*
Negative Moment at the Interior Column Face	1,922	3,256	551 *(C)*

Limiting cap beam design moments to the yield moments at the appropriate sections, and allowing distribution of the longitudinal reinforcement in the sides of the cap beam, the following reinforcement quantities were obtained:

(i) Exterior Joint Region. Top bars: 10 - M29, Bottom Bars: 13 - M29, and Side Bars: 4 - M29.

(ii) Interior Joint Region. Top and Bottom Bars: 6 - M29, and Side Bars: 2 - M29.

The adequacy of the amount of cap beam longitudinal reinforcement is illustrated in **Fig. 4-2** through **Fig. 4-5**, where the demand is compared to the yield moment established from section moment-curvature analysis based on the above reinforcement details.

Fig. 4-2 presents the moment-curvature analysis for the cap beam under an axial tension load of 790 kN and under positive moments. In this figure it is shown that the design moment matches approximately with the moment at the first yielding of the cap beam longitudinal reinforcement, which was 3,714 kN-m, and **Fig. 4-3** presents the moment-curvature analysis for the cap beam under an axial compression load of 965 kN and negative moments, which matches approximately with the moment at first yielding of the cap beam longitudinal reinforcement 3,466 kN-m. Shear forces depicted in these figures will be discussed in **Section 4.3.5**.

For the interior joint, **Fig. 4-4** depicts the moment-curvature analysis with an axial tension load of 382 kN and under positive moments. First yield moment of the cap beam longitudinal reinforcement exceeds the design moment. However, a minimum reinforcement limit in the range of ρ_{cc}= ***0.0035*** ? was provided in the design of the cap beam to ensure distribution of flexural cracks in the cap beam. Referring to **Fig. 4-4**, it is shown that the design moment was 1,163 kN-m, and is considerably lower than the moment at first yielding of the cap beam longitudinal reinforcement, which was 1,954 kN-m. **Fig. 4-5** shows the moment-curvature analysis for the cap beam under an axial compression load of 551 kN and negative moments. The section was equally reinforced at the top and bottom, thus, the first yield moment was also 1,954 kN. Shear forces depicted in these figures will be discussed in the next section.

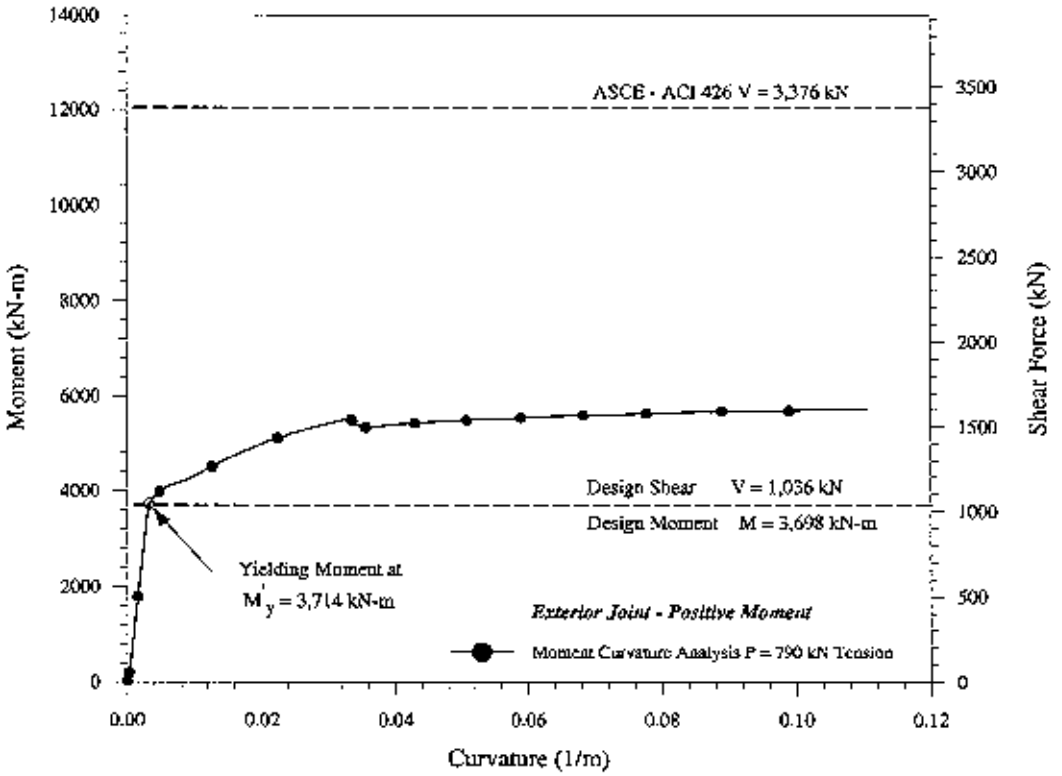

Fig. 4-2 Exterior Joint - Cap Beam Moment-Curvature Analysis for Positive Moments

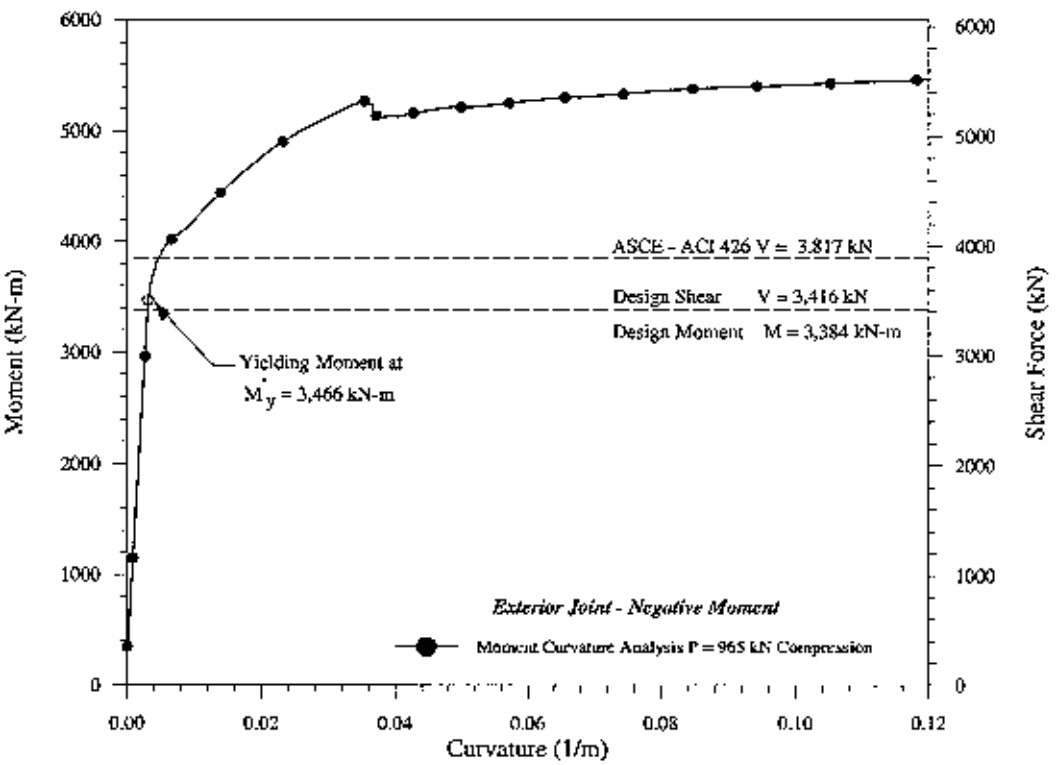

Fig. 4-3 Exterior Joint - Cap Beam Moment-Curvature Analysis for Negative Moments

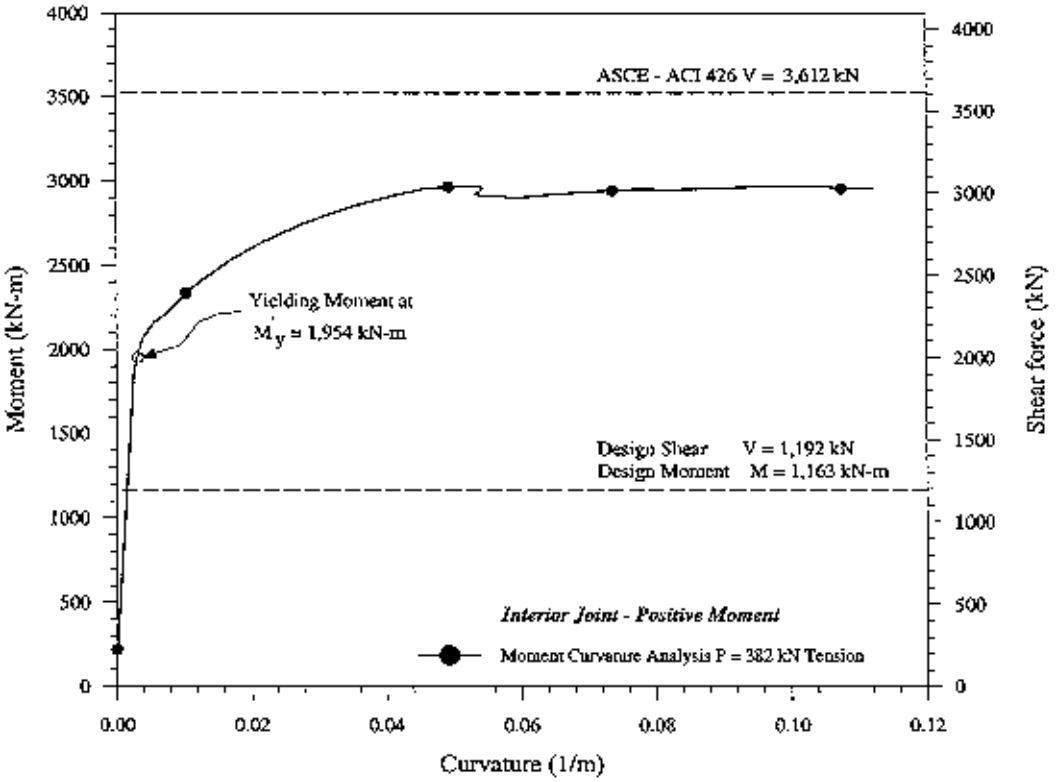

Fig. 4–4 Interior Joint - Cap Beam Moment-Curvature Analysis for Positive Moments

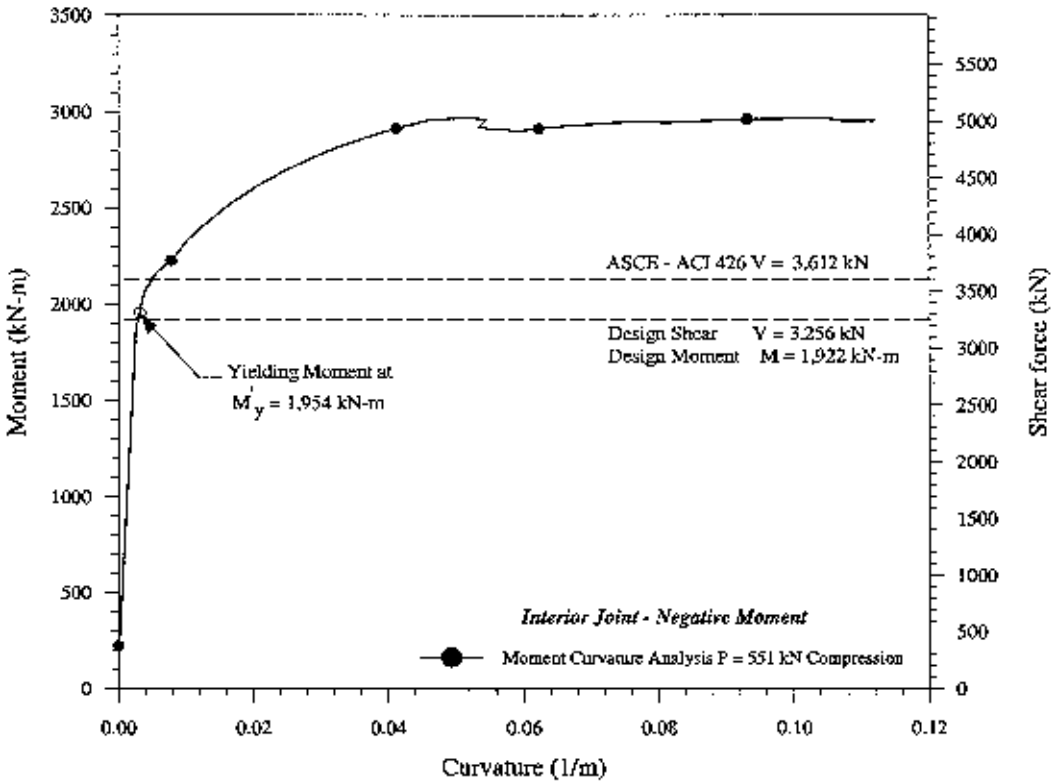

Fig. 4–5 Interior Joint - Cap Beam Moment-Curvature Analysis for Negative Moments

4.2.4 Cap Beam Shear Design

Shear design of the cap beam was performed using the three component shear model developed at UCSD as presented in **Section 4.1.1**.

4.2.4.1 Concrete Contribution

For the cap beam, the concrete shear contribution was obtained from the ASCE-ACI 426 **[14]** design recommendations, which can be described as follows **[1]**:

$$V_c = 0.8\, v_c\, A_g \tag{4.11}$$

In the presence of axial load, the concrete shear strength, v_c, is obtained according to the relation **[1]**:

$$v_c = v_b\left(1 + \frac{3P}{f_c' A_g}\right) \quad (\textit{axial compression}) \qquad \textit{and} \qquad v_c = v_b\left(1 + \frac{P}{500\, A_g}\right) \quad (\textit{axial tension}) \tag{4.12}$$

where P is positive for compression and negative for tension, and v_b is the nominal shear stress computed based on the relation **[1]**:

$$v_b = (0.066 + 10\,\rho_t)\sqrt{f_c'} \le 0.2\sqrt{f_c'} \quad (MPa) \tag{4.13}$$

where ρ_t is the tension steel reinforcement ratio. **Table 4-2** presents the concrete contributions to the shear resistance at various cap beam sections.

Table 4-2 Concrete Contributions to Shear Resistance in the Cap Beam

	Axial Force kN	ρ_t Steel Ratio [1]	v_b kPa	v_c kPa	V_c kN
Positive Moment at the Exterior Joints	-790 *(T)*	0.0065	772	607	627
Negative Moment at the Exterior Joints	965 *(C)*	0.0050	683	683	704
Positive Moment at the Interior Joints	-382 *(T)*	0.0030	565	510	523
Negative Moment at the Interior Joints	551 *C*	0.0030	565	566	583

[1] Reinforcement for the joint mechanism was conservatively excluded.

4.2.4.2 Axial Load Contribution

The axial load contributions to the shear resistance of the cap beam section was previously described in **Section 4.1.1.2**, and are presented in **Fig. 4-1(b)**. Substituting for tanα in equation **(4.3)** in terms of the neutral axis, the cap beam depth and the distance from column face to column face, the following expression was derived to compute the axial load contribution to the shear resistance:

$$V_p = k\,P\,\frac{h_b - \frac{c_1 + c_2}{2}}{l_{cap}} \tag{4.14}$$

where c_1 and c_2 are the neutral axes on either side of the cap beam, and l_{cap} is the cap beam clear distance to the column faces. Axial load contributions to the shear resistance are presented in **Table 4-3**.

Table 4-3 Axial Load Contribution to Shear Resisting Mechanisms Calculations

	Axial Force kN	$(c_1 + c_2)/2$ mm	tan α	k	V_p kN
Positive Moment at the Exterior Joints	-790 *(T)*	248	0.244	-1.15	-165 *(T)*
Negative Moment at the Exterior Joints -	965 *(C)*	279	0.235	0.85	196 *(C)*
Positive Moment at the Interior Joints	-382 *(T)*	178	0.265	-1.15	-80 *(T)*
Negative Moment at the Interior Joints	551 *(C)*	197	0.259	0.85	112 *(C)*

4.2.4.3 Transverse Reinforcement Contribution

Vertical stirrups in the cap beam were designed to satisfy the shear force given by:

$$V_s = V_N - V_c - V_p \tag{4.15}$$

where V_N is the required design shear force presented in **Table 4-1**. The vertical reinforcement contribution to the shear resisting mechanism for rectangular sections is given by [1]:

$$V_s = \frac{A_{sp}\,f_y\,(h_b' - c)}{s}\,cot\,\theta \tag{4.16}$$

where h_b' is the confined section depth, A_{sp} is the cross sectional area of the vertical reinforcement, and θ is the crack angle taken at 35°.

4.2.4.4 Maximum Spacing of Shear Reinforcement

Maximum spacing of shear reinforcement in the cap beam was provided according to the following expression **[14]**:

$$s_{max} \leq 0.50\ h_b' = 533\ mm \leq 610\ mm \qquad \textbf{(4.17)}$$

This expression leads to a maximum spacing of 533 mm.

4.2.4.5 Minimum Shear Reinforcement

Minimum shear reinforcement in the cap beam was provided according to the following equation **[14]**:

$$A_v = (0.35\ h'_b\ s) / f_{ye} \quad [MPa] \qquad \textbf{(4.18)}$$

This expression leads to a minimum shear reinforcement of 440 mm^2. Shear reinforcement provided in the joint region and within a distance of h_b from the column face was 6 legs of M13 stirrups at approximately 356mm, and outside of the joint region *4 legs of M13* at 250mm were provided, as shown in the design drawings presented in **Section 2.2**, which are within the spacing limits and minimum shear reinforcement. Based on the calculations presented in **Table 4-4** shear reinforcement provided in the vicinity of the joint region was *6 legs M13 vertical stirrups* at 356 mm on centers.

Table 4-4 Cap Beam Shear Reinforcement Design

	V_s= $V_U - V_c - V_p$ kN	Provided Shear Reinforcement	Spacing mm	V_s kN	Shear Reinforc.
Positive Moment at the Exterior Joints	574	Minimum	375	2,914	6-M13 @ 356 mm o.c.
Negative Moment at the Exterior Joints	2,516	Steel Truss Component	368	2,914	6-M13 @ 356 mm o.c.
Positive Moment at the Interior Joints	749	Minimum	375	2,914	6-M13 @ 356 mm o.c.
Negative Moment at the Interior Joints	2,561	Steel Truss Component	375	2,914	6-M13 @ 356 mm o.c.

4.3 Cap Beam / Column Joint Design Considerations

Forces acting upon a typical bridge pier tee and knee joint, are depicted in **Fig. 4-6**. Due to large shear forces that develop in bridge joints, as illustrated in **Fig. 4-6(d)**, conventional design methods, which are based directly on joint shear forces, typically demand considerable amount of joint reinforcement **[3][5]**. This results in steel congestion within the joint regions creating difficulties in construction of concrete bridge joints. Therefore, the joints in the test unit were designed using a rational procedure based on force transfer models **[1][5]**. In this study, the modified external strut force transfer model proposed by Sritharan **[5]** was employed because it required the least amount of reinforcement when compared to other possible models **[1]**.

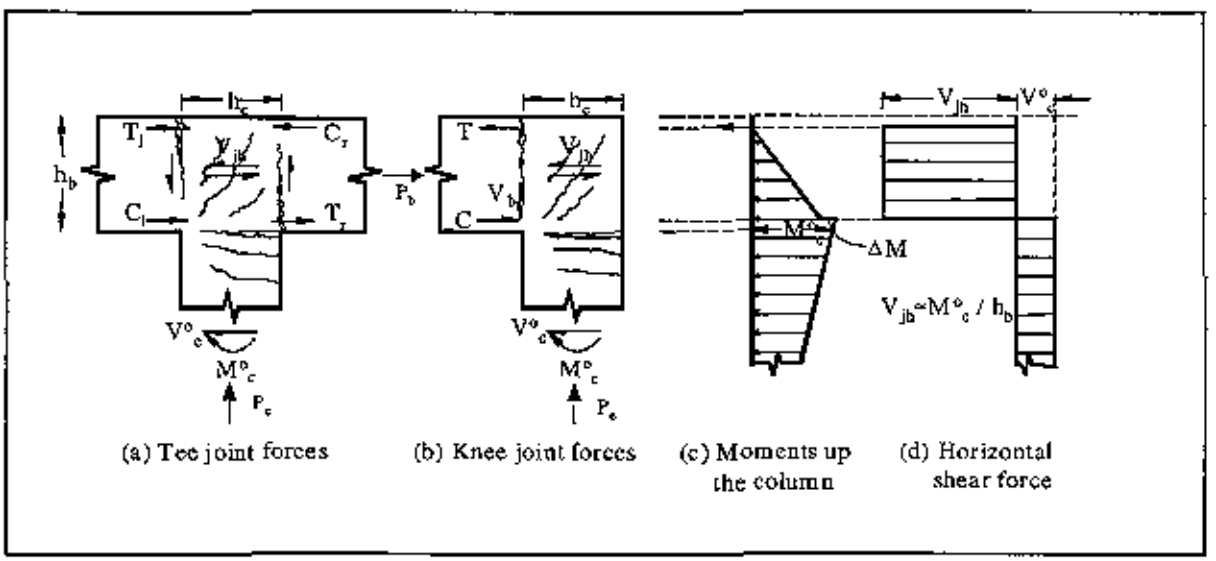

Fig. 4-6 Average Horizontal Joint Shear Forces in Bridge Tee and Knee Joints **[1]**

In this procedure it is suggested that only nominal reinforcement is adequate if the joint principal tensile stresses $p_t \leq 0.29\sqrt{f'_c}$. The principal tensile stresses, presented in **Section 6.3**, indicate higher stress levels, and the reinforcement for the joints was provided as suggested in **[5]**. This procedure is included in the design recommendations presented in **Section 8.3.** The principal tensile stresses were calculated from:

$$p_t = \left(\frac{f_h + f_v}{2}\right) - \sqrt{\left(\frac{f_h - f_v}{2}\right)^2 + v_j^2} \qquad \textbf{(4.19)}$$

where p_t is the principal tension stress, f_h is the axial stress on the joint in the horizontal direction, f_v is the axial stress on the joint in the vertical direction, and v_j is the joint shear stress. Joint axial stresses and joint shear stress are calculated in the following sections.

4.3.1 Joint Axial Stresses

The average joint axial stress in the vertical direction was obtained assuming a 45° dispersion of forces as shown in **Fig. 4-7(a)[4]**. For calculating the joint axial stress in the horizontal direction, the axial force was averaged over the entire beam cross sectional area according to the effective area shown in **Fig. 4-7(b)**.

Joint axial stresses were computed as follows **[4]**:

$$f_h = \frac{P_h}{w_b\, h_b} \quad ; \quad f_v = \frac{P_v}{(D + h_b)\, b_j} \tag{4.20}$$

where P_h is the axial force in the horizontal direction, b_j is the effective joint width assuming a 45° spread in all directions **[1]**, D is the pile section width and h_b is the cap beam section depth.

4.3.2 Joint Shear Stresses

The joint shear force can be approximated to the column overstrength moment at the joint interface, as suggested in reference **[1]**. Hence:

$$V_{jh} = \frac{M_c^o}{h_b} \tag{4.21}$$

where V_{jh} is the horizontal joint shear force. Vertical or horizontal joint shear stresses are computed from the effective area identified in **Fig. 4-7(b)**, and computed according to the following expression **[15]**:

$$v_{jv} = \frac{V_{jv}}{b_j\, h_b} = \frac{V_{jh}}{b_j\, h_c} = v_{jh} \tag{4.22}$$

Computed average principal tensile stresses in the joint region are presented in **Section 6.3**. At ultimate limit state average principal tensile stresses were estimated to be $p_t = 0.56\sqrt{f_c'}$, $p_t = 0.48\sqrt{f_c'}$ and $p_t = 0.42\sqrt{f_c'}$, in exterior joint ***KJ1***, interior joint ***TJ*** and exterior joint ***KJ2***, respectively. Thus, joint shear reinforcement was found consistent with the modified external strut model, as illustrated in **Fig. 4-8**. According to this model the joint reinforcement was provided to develop two mechanisms, namely: the *clamping mechanism*, at Node ***C*** in **Fig. 4-8**, and the *splice transfer mechanism*, at Node ***D*** in **Fig. 4-8**. In the following procedure the total reinforcement required for the two mechanisms are found using the recommendations provided in reference **[5]**.

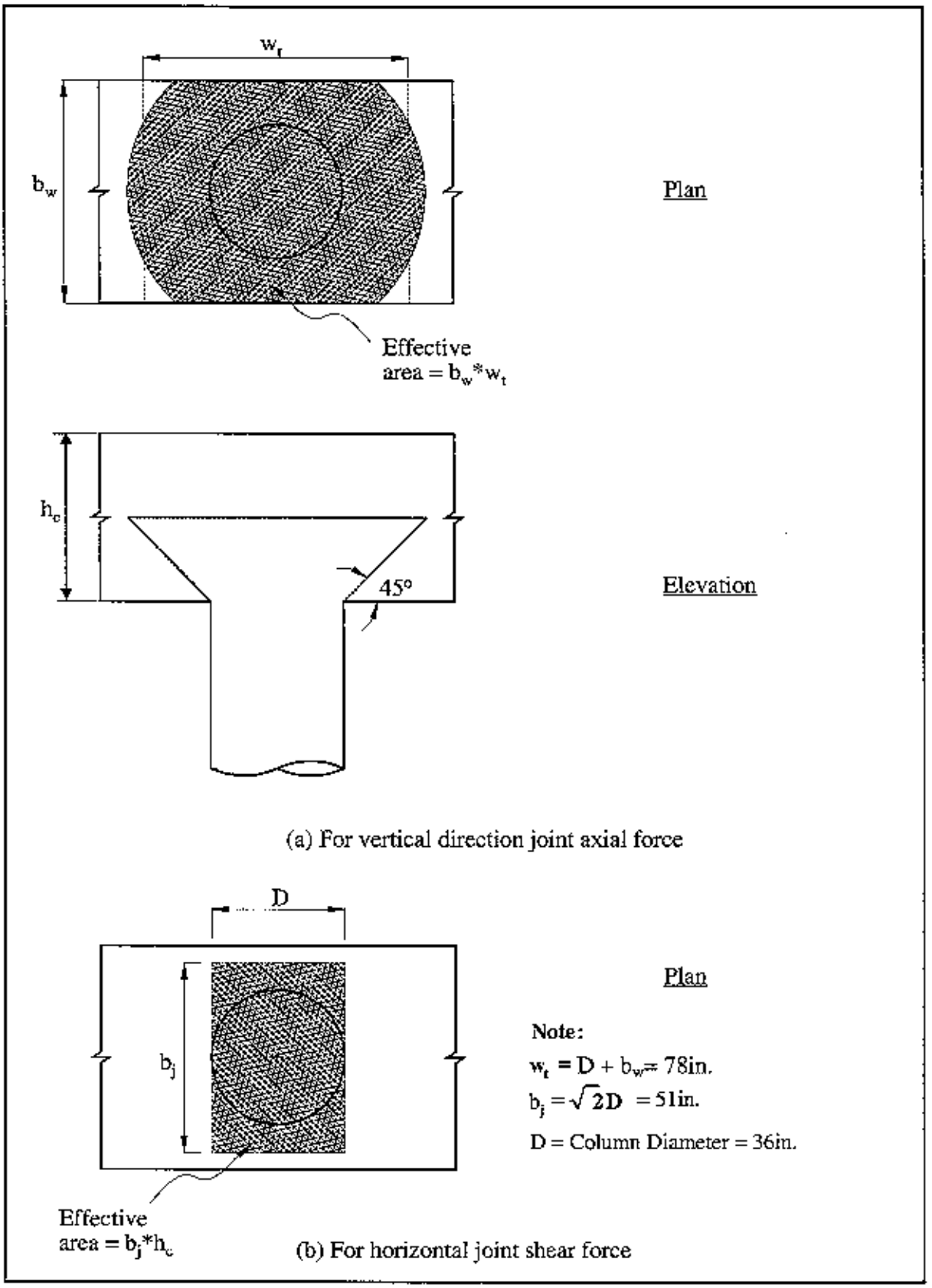

Fig. 4-7 Effective Joint Area For Calculating Principal Tensile Stresses [4]

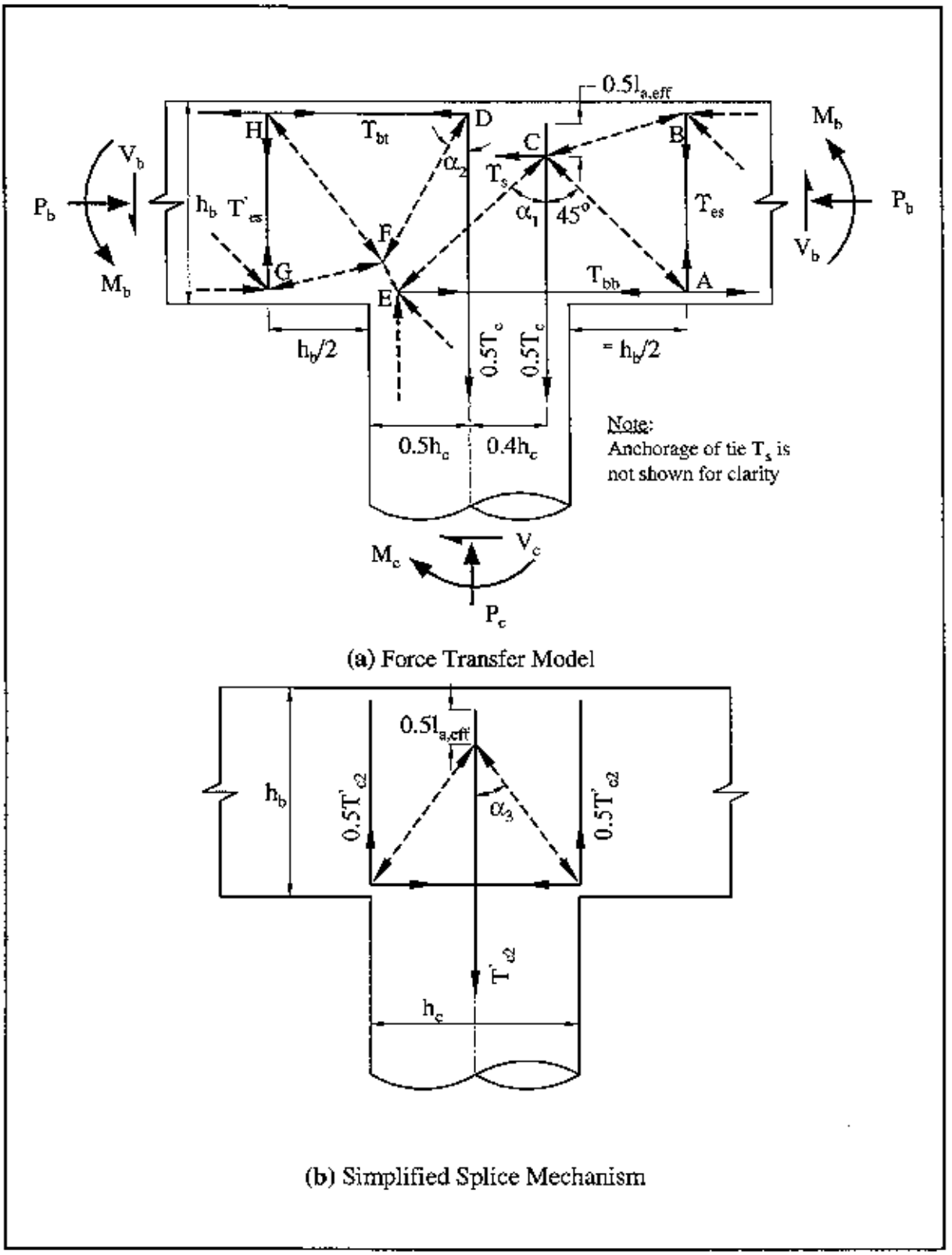

Fig. 4-8 Modified External Strut Joint Force Transfer Model for Seismic Design of Bridge Tee Joints [5]

4.3.3 Interior Joint Design

The joint design model assumes the force transfer for in-plane loading as described in **Fig. 4-8**. As a result, vertical stirrups outside and inside of the joint, joint horizontal hoops, additional top and bottom longitudinal reinforcement in the cap beam, and joint cross-ties were provided as described in this section.

(i) External Joint Vertical Stirrups. Area of external vertical stirrups, A_{jv}, required outside the joint within a distance of h_b from the column face was given by:

$$A_{jv} = 0.125\,\lambda_o\,A_{sc}\frac{f_{y,c}}{f_{y,v}} = 0.125 \times 1.40 \times 16{,}129 \times \frac{448}{414} = 3{,}055\ mm^2 \qquad (4.23)$$

where λ_o is the material overstrength, A_{sc} is the total area of the column longitudinal reinforcement, $f_{y,c}$ is the column bar yield strength, and $f_{y,v}$ is the yield strength of the vertical stirrups. Thus, *4 sets of 6 legs M13 stirrups* were provided within 1.07 m from the column face, which were added to the shear reinforcement requirements described in **Section 4.2.4.3**.

(ii) Internal Joint Vertical Stirrups. Area of internal vertical stirrups, A_{jv} required inside the joint was given by:

$$A_{jv} = 0.095\,\lambda_o\,A_{sc}\frac{f_{y,c}}{f_{y,v}} = 0.095 \times 1.40 \times 16{,}129 \times \frac{448}{414} = 2{,}321\ mm^2 \qquad (4.24)$$

To satisfy the above requirement *3 sets of 6 legs M13 stirrups* were provided within the joint regions.

(iii) Joint Horizontal Hoops. Volumetric ratio of the joint horizontal reinforcement, ρ_s, was designed according to the following expression [1]:

$$\rho_s = \frac{0.30\,\lambda_o\,A_{sc}}{l_a^2}\frac{f_{y,c}}{f_{y,h}} = \frac{0.30 \times 1.40 \times 16{,}129}{940^2}\frac{448}{414} = 0.83\,\% \qquad (4.25)$$

where $f_{y,h}$ is the yield strength of the joint horizontal hoops, and l_a is the anchorage length of the column longitudinal reinforcement. A minimum value for ρ_s was established to ensure some tensile resistance after cracking develops in the joint region according to the expression [4]:

$$\rho_s \geq 0.29\,\frac{\sqrt{f_c'}}{f_{yh}} = 0.29\,\frac{\sqrt{35}}{414} = 0.41\,\% < 0.83\,\% \qquad (4.26)$$

Therefore, joint horizontal reinforcement of ρ_s equal to 0.83% should be satisfied. Using

M16 welded hoops in the joint region, spacing of horizontal reinforcement is obtained according to the expression :

$$s = \frac{4\,A_h}{D'\,\rho_s} = \frac{4 \times 198}{762 \times 0.0083} \approx 125\,mm \qquad (4.27)$$

Thus, *M16 welded hoops at 127 mm on centers* were provided in the joint regions.

(iv) Additional Cap Beam Longitudinal Reinforcement. Additional top longitudinal beam reinforcement equivalent to:

$$\Delta A_{tb} = 0.17\,\lambda_a\,A_{sc}\frac{f_{y,c}}{f_{y,b}} = 0.17 \times 1.40 \times 16{,}129 \times \frac{448}{414} = 4{,}153\ mm^2 \qquad (4.28)$$

was provided in the top layer. This reinforcement was extended h_b from the column face.

Additional bottom longitudinal beam reinforcement equivalent to:

$$\Delta A_{bb} = 0.15\,\lambda_a\,A_{sc}\frac{f_{y,c}}{f_{y,b}} = 0.15 \times 1.40 \times 16{,}129 \times \frac{448}{414} = 3{,}665\ mm^2 \qquad (4.29)$$

was provided in the bottom layer. Consequently, additional *6 - M29 bars* were provided in the top and bottom layers reinforcement. This reinforcement is developed at a distance of h_b from the joint faces.

(v) Joint Cross-Ties. Consistent with previous experimental studies at UCSD [4], 2 - M13 horizontal cross ties were provided for each vertical stirrup within the joint region.

4.3.4 Design of Exterior Knee Joint *KJ2*

The design of exterior knee joint *KJ2* was also based on the modified external strut model, and the corresponding mechanism is described in **Fig. 4–9**. As a result, the amounts of vertical stirrups outside and inside of the joint, joint horizontal hoops, additional top and bottom longitudinal reinforcement in the cap beam, and joint cross-ties were provided as described in the previous section while describing the design procedure for the interior tee joint ***TJ.***

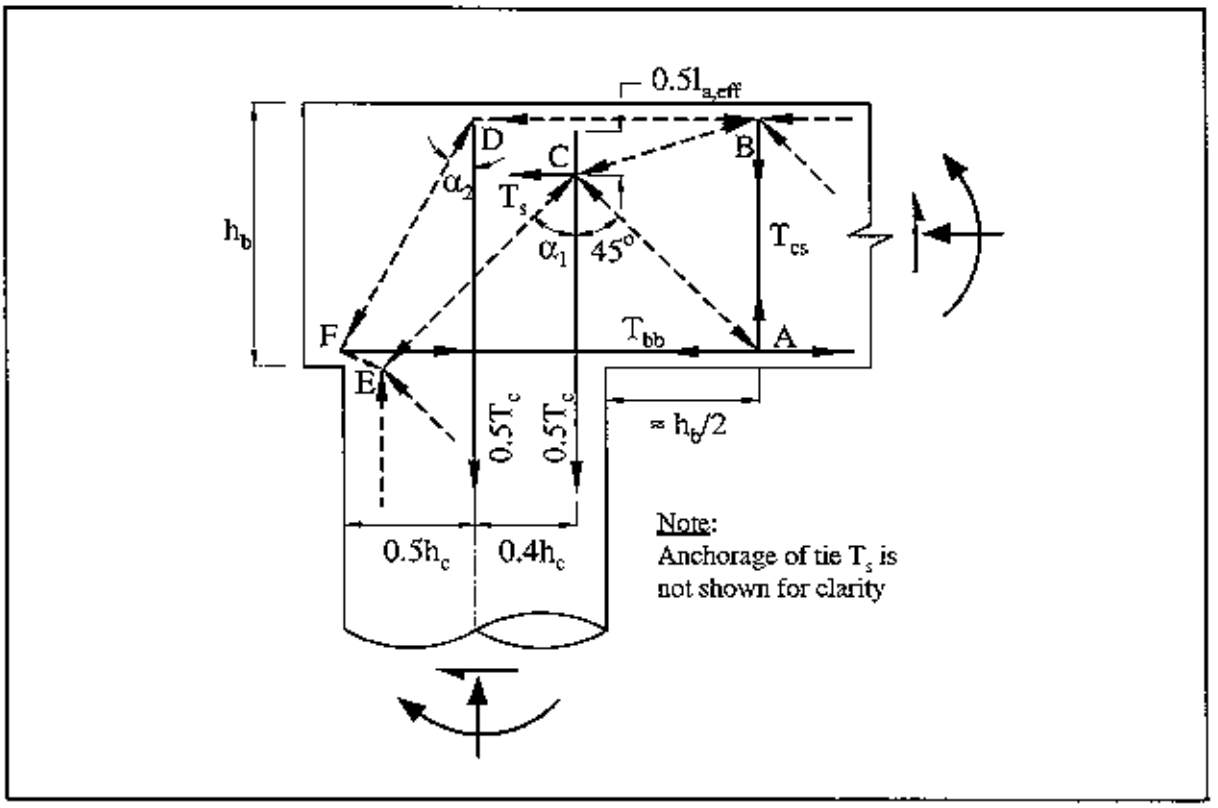

Fig. 4–9 Modified External Strut Joint Force Transfer Model For Seismic Design of Bridge Knee Joints Subjected to Opening Moments **[5]**

If the cap beam top and bottom longitudinal reinforcing bars are provided as continuous reinforcement, there is no additional reinforcement required in the knee joints. However, in the test unit, the beam bars were not continuous and the following reinforcement was added, as recommended in reference **[5]**, primarily to ensure sufficient joint response under closing moments.

The external strut D_2 illustrated in **Fig. 4–10** requires that horizontal U-pins be provided at the bar hooks in order to anchor the bar bents back into the joint regions. This reinforcement is not be required when the overhang dimension is greater than $\mathbf{h_b/2}$. Area of the horizontal U-pins reinforcement were estimated according to the following expression:

$$T_r = 0.085\ T_c \frac{3\,d_b}{6\,d_b} \qquad \textbf{(4.30)}$$

Thus, *12 legs M10* were provided, and an equal amount was provided for the top beam bars.

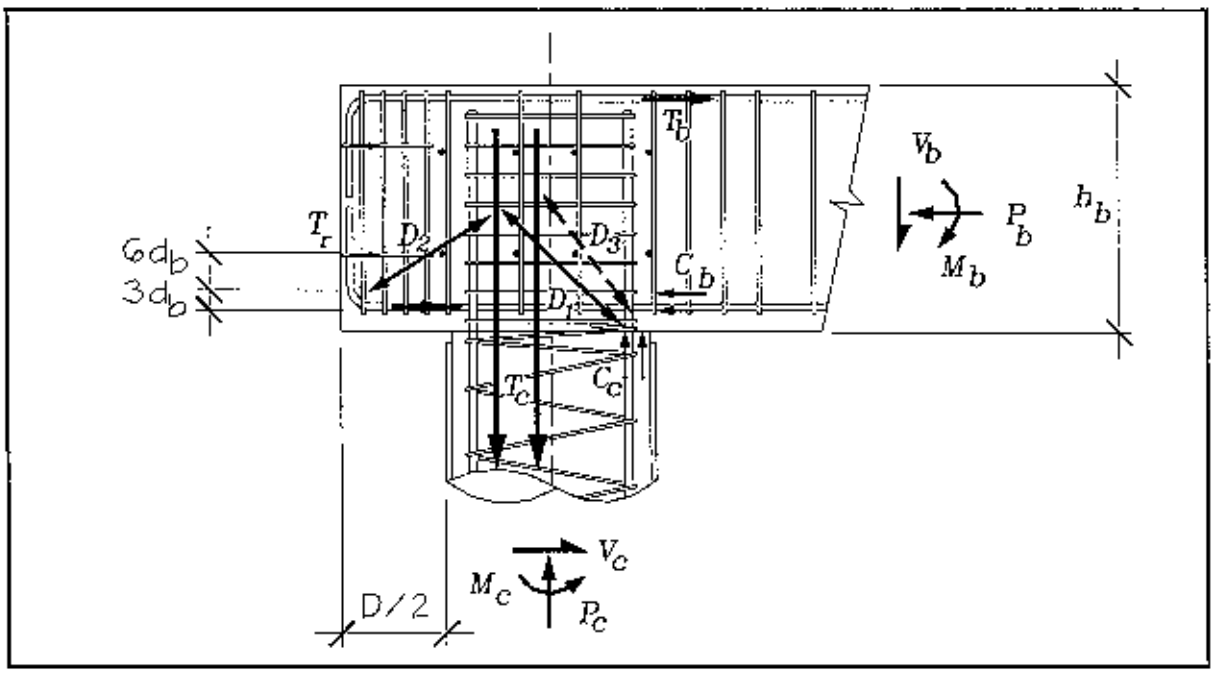

Fig. 4–10 Forces Acting Upon a Bridge Knee Joint and its Idealized Joint Strut

4.3.5 Design of Exterior Knee Joint *KJ1*

Since the force conditions of exterior knee joints ***KJ1*** and ***KJ2*** are similar under reversed cyclic loading, the reinforcement details derived for exterior knee joint ***KJ2*** could have been used for the design of exterior knee joint ***KJ1***. However, slightly different reinforcement details were adopted for the design of exterior joint ***KJ1***. The changes for the design of exterior knee joint ***KJ1*** with respect to details of exterior knee joint ***KJ2*** were as follows:

(i) External Vertical Stirrups. The amount of external vertical stirrups was identical to that provided in the interior joint ***TJ***, but was distributed over a distance of $h_y/2$

(ii) Internal Vertical Stirrups. The amount of internal vertical stirrups was reduced to *2 sets of 6 legs M13 stirrups*.

These changes adopted for the design of the exterior joint ***KJ1*** were experimental in nature and the details adopted for the design of exterior joint ***KJ2*** are recommended for the design of bridge joints. Hence, the design details adopted for exterior joint ***KJ1*** are not included in the design recommendations presented in **Section 8.3**. Further to the above changes, the joint J-hooks cross ties were replaced with headed reinforcement in the exterior knee joint ***KJ1*** to validate the use of headed bars in the joint regions. Test data indicates that the headed reinforcement perform adequately.

4.4 Pin Connection Design Considerations

The pin connections at the column bases were established based on the recommendations presented in reference [4]. All of the column longitudinal reinforcement was terminated 64mm above the footings and the area of the column concrete section was reduced at the column/footing interface. Adequate reinforcement at the center of each column was provided to ensure axial and shear force transfer through the pin connection.

As shown in **Fig. 4-11** the concrete area at the column base was reduced to 406 mm in the loading direction, which corresponded to a 45% reduction in the gross sectional area of the column. The pin longitudinal reinforcement consisted of 8 pairs of single bars arranged in a criss-cross pattern detail, as shown in **Fig. 2-10**. This special detailing was to ensure a pin connection at the column base in the loading direction with increased moment resistance in the orthogonal direction to provide out-of-plane stability to the test unit during testing.

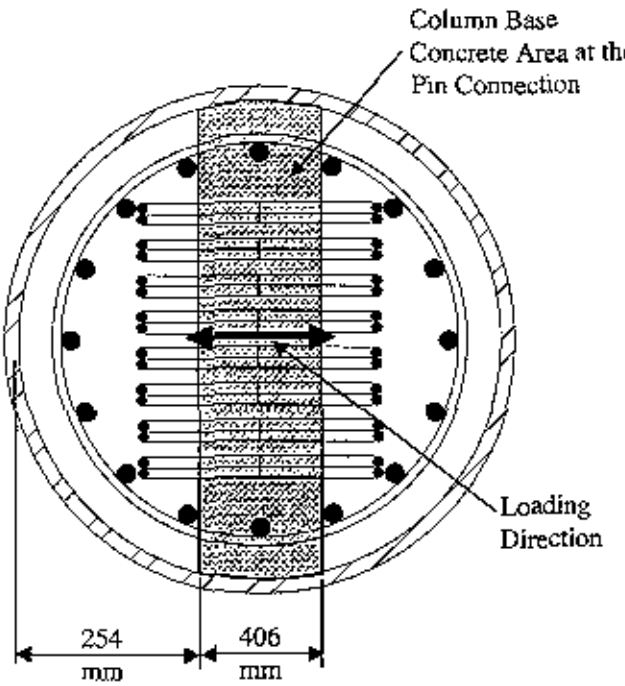

Fig. 4-11 Pin Connection Concrete Area

The area of the concrete section was reduced at the column base using pads made out of expansion joint material, as shown in **Fig. 2-10**. For the maximum expected lateral displacement of 330 mm the corresponding base rotation of 0.08 was conservatively estimated. Allowing a compression in the pads of up to 60% [4] a pad thickness of 63.50 mm was used. Limiting compression in the pads will ensure no significant force transfer through the expansion joint material.

4.4.1 Axial Compression Stress in the Concrete Key

Assuming a uniform stress transfer through the key, the maximum average concrete stress was estimated as follows [4]:

$$\sigma = \frac{P_U}{A_{pin}} = \frac{2.82}{0.339} = 8.32\ MPa \qquad (4.31)$$

A uniform stress across the concrete key is unrealistic and higher stresses should be expected in the extreme compression fiber of the pins. A compressive strength as high as $2f'_c$ is expected for the key. On this basis, it was concluded that crushing of concrete at the key would not occur due to axial force transfer.

4.4.2 Axial Tension Force Transfer

The axial tension force from the column to the pin was transferred by the starter reinforcing bars placed at the center of the column. A maximum axial tension force of 752 kN was estimated in the exterior column, *EC1*, which could be transferred by approximately 8 - M19 bars considering the 45° of the starter bars.

4.4.3 Shear Transfer

A shear friction mechanism was relied upon for shear transfer between the columns and footings. Assuming a friction coefficient of $\mu=1.0$ consistent with the recommendation of ACI [14], the maximum shear force, V_{SF}, that can be transferred across the column/footing interface was significantly greater than the maximum shear force, V_U, expected to develop in the columns. The design shear strength at the column/footing interface was estimated according to the following expression [4]:

$$V_{SF} = \mu \ (P + A_{sv} f_{ye}) \qquad (4.32)$$

where A_{sv} and f_{ye} are the total area and the expected yield strength of the footing starter bars respectively. Hence:

$$V_{SF} = 1.0 (-752 + 4,560 \times 445 / 1,000) = 1,277\ kN < 790\ kN\ ;\ Column\ EC1$$

$$V_{SF} = 1.0 (+1,807 + 4,560 \times 445 / 1,000) = 3,836\ kN < 933\ kN\ ;\ Column\ IC \qquad (4.33)$$

$$V_{SF} = 1.0 (+2,820 + 4,560 \times 445 / 1000) = 4,850\ kN < 965\ kN\ ;\ Column\ EC2$$

A further check on the shear force transfer is necessary since the maximum value of V_{SF} is also dependent on the maximum shear stress that can be developed in the concrete contact area between the column and footing. As recommended by Paulay et al. **[16]**, a maximum V_{SF} corresponding to shear sliding was found by considering an allowable concrete shear stress of $0.25f'_c$ and dowel action of the pin longitudinal reinforcement. The value of V_{SF} corresponding shear sliding was relatively small for exterior column *EC1* subjected to axial tension. This shear force transfer was found as follows:

$$\begin{aligned} V_{SF} &= A_c\ 0.25\,f'_c + A_s\ 0.25\,f_y = \\ &\quad 51 \times 866 \times 0.25 \times 38.7 + \\ &\quad (2 \times 8 \times 284 \times \cos 45) \times 0.25 \times 445 = \\ &\quad 784{,}000\ N = 784\ kN \end{aligned} \tag{4.34}$$

Although the above value appears critical, a shear sliding failure would not be possible since there would be additional resistance from the criss-cross starter bars. The horizontal component of the tension force developed in the starter bars would participate directly in the shear transfer. Therefore, shear transfer across the column-footing interface should not be a problem in all the three pin connections.

In the above calculations, it was assumed that the yield strength was developed in all 16 - M19 starter bars.

Footing starter bars were extended by a distance l_t above the footing. The minimum value of l_t was determined based on the expression **[1],[4]**:

$$l_t = 0.167\,l_c + D_{pin} + l_d = 0.167 \times 610 + 457 + 439 = 1.00\ m \tag{4.35}$$

where l_c is the distance from the base of the column to the point of contraflexure, D_{pin} is the diameter of the pin and l_d is the development length of the starter bars obtained according to equation **(4.10)**. For a M19 bar, l_d was 439 mm Pushover analysis indicates that at the exterior column *EC2* the point of contraflexure is at approximately l_c = 610 mm above the footing. With D_{pin} = 457 mm a minimum value of l_t = 1.00m was obtained from equation **(4.34)**. In the test unit the starter bars were terminated 1.22 m above the footing.

5. Construction, Material Properties, Instrumentation and Testing Procedure

A detailed description of the test unit construction sequence, instrumentation, and testing procedure are presented in this chapter.

5.1 Construction of the Test Unit

A brief description of the construction of the footings, columns, cap beam and load transfer blocks are described in this section.

5.1.1 Column Footings

The column footings were constructed first. **Fig.5-1** shows the reinforcement cage assembly of a column footing where the pin longitudinal reinforcement detail can be seen. **Fig.5-2** shows the column footings positioned on the laboratory floor ready for the installation of the column steel shells. The concrete shear key area at the top of the footing, as identified in **Fig.5-2**, was roughened with a wire brush to expose the aggregate so that a friction coefficient of **1** or greater could be obtained. In addition, to create the pin connection, a 63.50 mm thick expansion joint material was then placed on the footings to form a smaller 381mm wide contact surface with the columns.

5.1.2 Composite Steel Shell Columns

Construction of the composite steel shell columns was accomplished in the next stage. The columns inner core reinforcement cages were assembled and strain gages were placed on the longitudinal and transverse reinforcement, as detailed in **Section 5.3.2**. The first step in this stage consisted of placing a scaffolding assembly around the footing bases in order to install the steel shells and to serve as a working platform for the construction of the test unit cap beam. Next, the steel shells were positioned in contact with the footings expansion joint material. Then, the column inner core reinforcement cages were placed on 6 mm pads above the expansion joint material. Casting of the concrete columns was accomplished with an industrial pump. In order to prevent rotation of the column reinforcement cages during casting, at the column base, the cages were tied to the footing starter bars, and on top a wooden template was attached to the working platform.

5.1.3 Cap Beam

As construction of the columns was progressing, assembly of the cap beam reinforcement cage was simultaneously taking place on the strong floor in order to expedite construction of the test unit. Then, after casting of the columns, the cap beam reinforcement cage was dropped in place. In a typical construction sequence the cap beam cage most likely will be tied in place, however, as it will be shown in future figures, congestion of the cap beam reinforcement was not a concern, and fitting of the cap beam reinforcement cage through the three column starter bars, in the joint region, was accomplished with minimum effort.

In this stage, construction of the cap beam reinforcement cage consisted of first positioning the cap beam bottom longitudinal reinforcement on a temporary wooden beam raised 305mm above the laboratory strong floor. In order to ensure that the cap beam reinforcement cage would fit through the columns inner core longitudinal reinforcement, in the joint region, a template of the column bars was used during construction of the cap beam cage. A secondary wood beam was raised above the strong floor to achieve the required height for construction of the cap beam top longitudinal reinforcement. Before completion of the cap beam reinforcement cage the column horizontal hoops were positioned in the joint regions.

Next, the cap beam vertical stirrups were inserted through the cap beam top and bottom longitudinal reinforcement and tied to the required spacing. Finally the cap beam side bars were tied to the vertical stirrups. **Fig.5-3**, **Fig.5-4** and **Fig.5-5** depict the cap beam reinforcement layout in the vicinity of the joints ***KJ1***, ***TJ*** and ***KJ2***, respectively, illustrating the temporary wooden beams used to support the cap beam top and bottom longitudinal reinforcement, the cap beam vertical stirrups, and the column horizontal hoops in the joint regions.**Fig.5-5** depicts the cap beam reinforcement cage end detail in the vicinity of the exterior joint ***KJ2***. At this stage of construction, the cap beam horizontal J-hooks and end horizontal U-pins were not yet installed. Next, the scaffolding platform top surface was made ready for installation of the cap beam reinforcement cage, and the cap beam reinforcement cage was installed through the column bars, as illustrated in **Fig.5-6**.

Following this stage, the column horizontal hoops in the joint regions were field welded, as illustrated in **Fig.5-7**. During welding of the hoops, the strain gages were protected with asbestos blankets from the torch flames. After welding, the joint horizontal hoops were tied to the columns longitudinal reinforcement to the correct spacing by alternating the welded joints in the direction of loading, to ensure that the welded hoop joints were not cutting through the

direction of shear planes that may develop in the joint regions.

Next, the horizontal J-hooks were positioned in the joint regions. In **Fig.5-8** and **Fig.5-9** is shown the reinforcement cage near the vicinity of column ***EC1***, depicting the horizontal J-hooks in the joint region and the position of the column joint horizontal hoops. The cap beam cage was then completed by positioning horizontal U-pins at the ends of the cage with the reinforcement layout depicted in **Fig.5-10**.

Shear keys were then assembled in the top surface of the cap beam cage to ensure a proper load transfer between the cap beam and the load transfer blocks, as illustrated in **Fig.5-11**. Finally, as illustrated in **Fig.5-12**, an industrial concrete pump was used in the concrete casting of the cap beam.

5.1.4 Cap Beam Load Transfer Blocks

The top surface of the cap beam, which is in contact with the horizontal actuators load transfer blocks, was roughened with a wire brush in order to improve the friction resistance mechanism at this interface. In **Fig.5-13** is shown the load transfer blocks ready for casting. Casting of these load transfer blocks was accomplished, as before, with an industrial concrete pump. **Fig.5-14** illustrate the completion of the test unit before testing. In **Fig.5-14** is shown that close to exterior column ***EC2*** the horizontal actuator was attached to a mounting plate and connected to two steel frames. These steel frames were mounted over an assembly of support blocks to form the correct height for the installation of the horizontal actuator. Close to the exterior column ***EC1*** the horizontal actuator was attached to a mounting plate and connected to the strong wall.

Fig.5-1 A Completed Footing Reinforcement Cage Prior to Casting

Fig.5-2 Footings in Place Prior to Construction of Columns

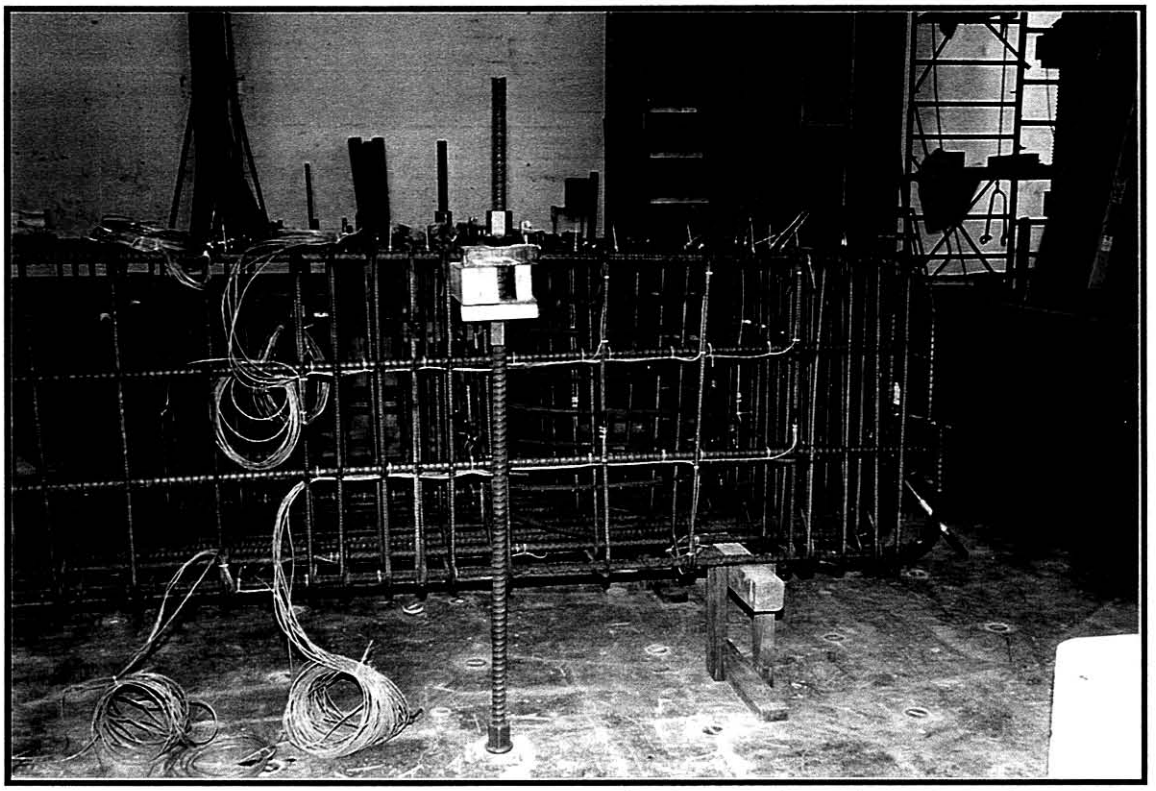

Fig.5-3 Cap Beam Reinforcement Cage in the Exterior Joint ***KJ1*** Region

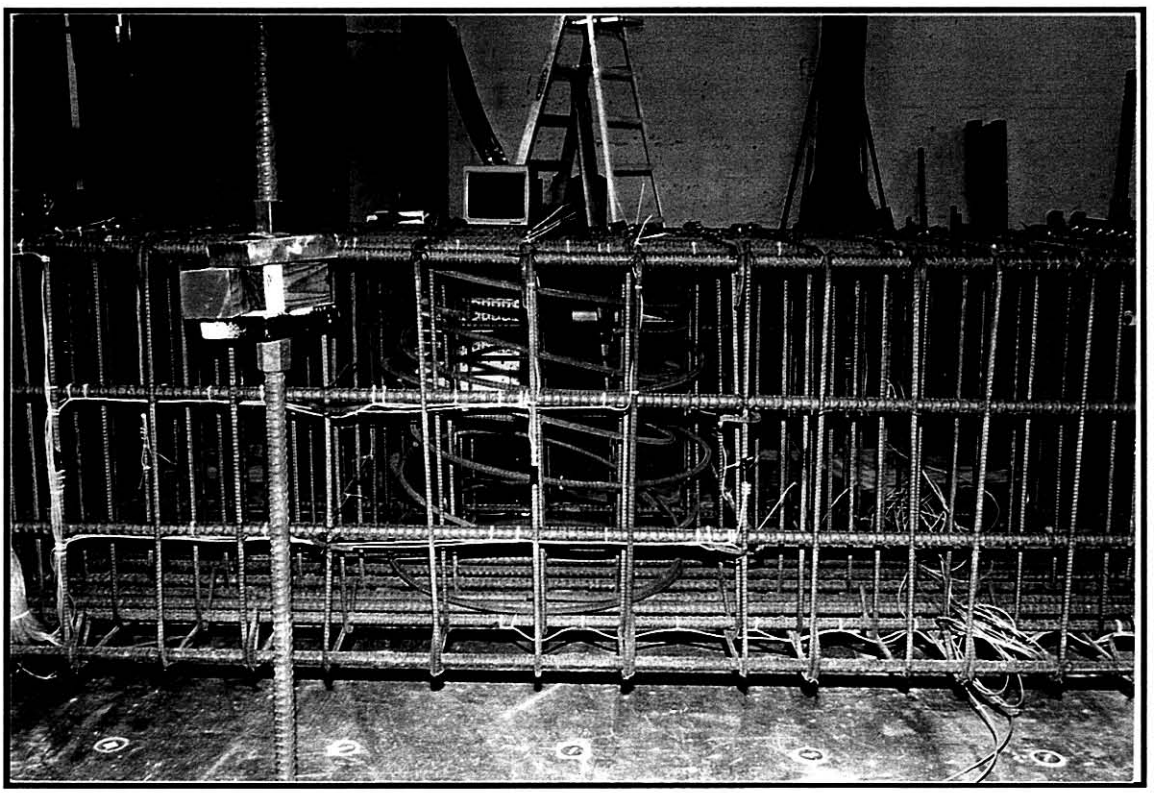

Fig.5-4 Cap Beam Reinforcement Cage the Interior Joint ***TJ*** Region

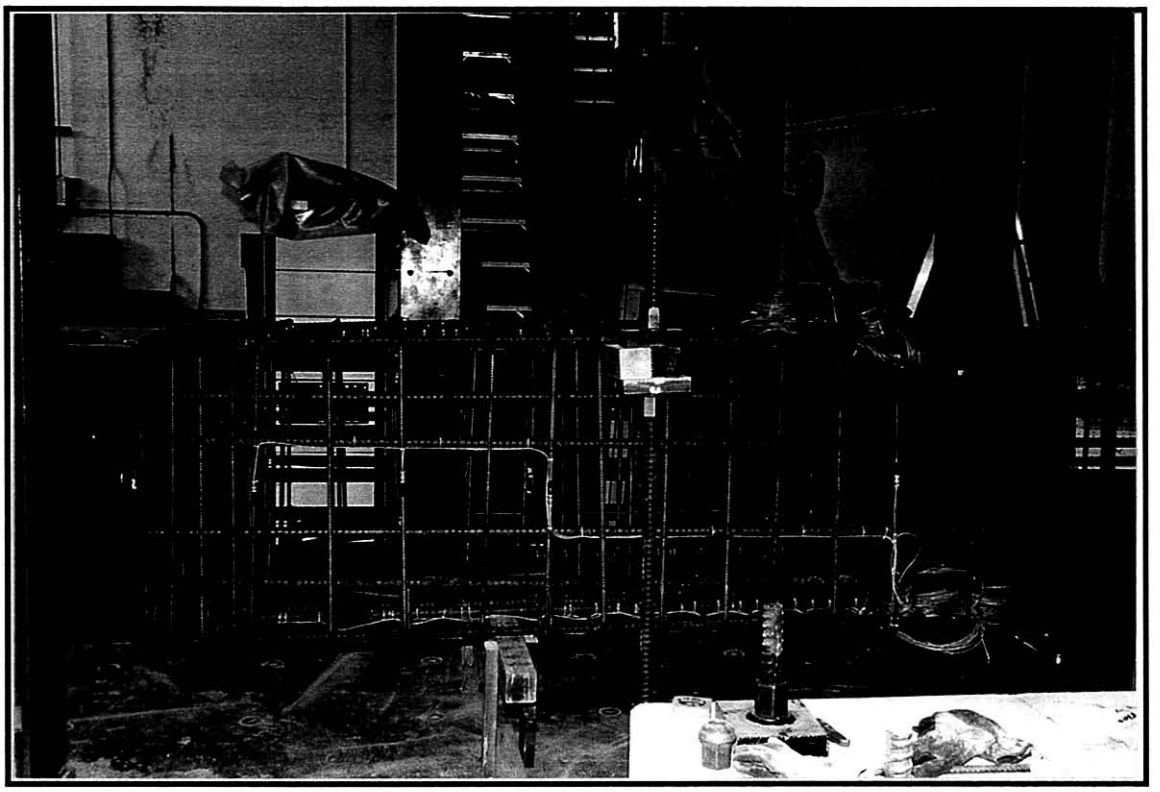

Fig.5-5 Cap Beam Reinforcement Cage in the Exterior Joint ***KJ2*** Region

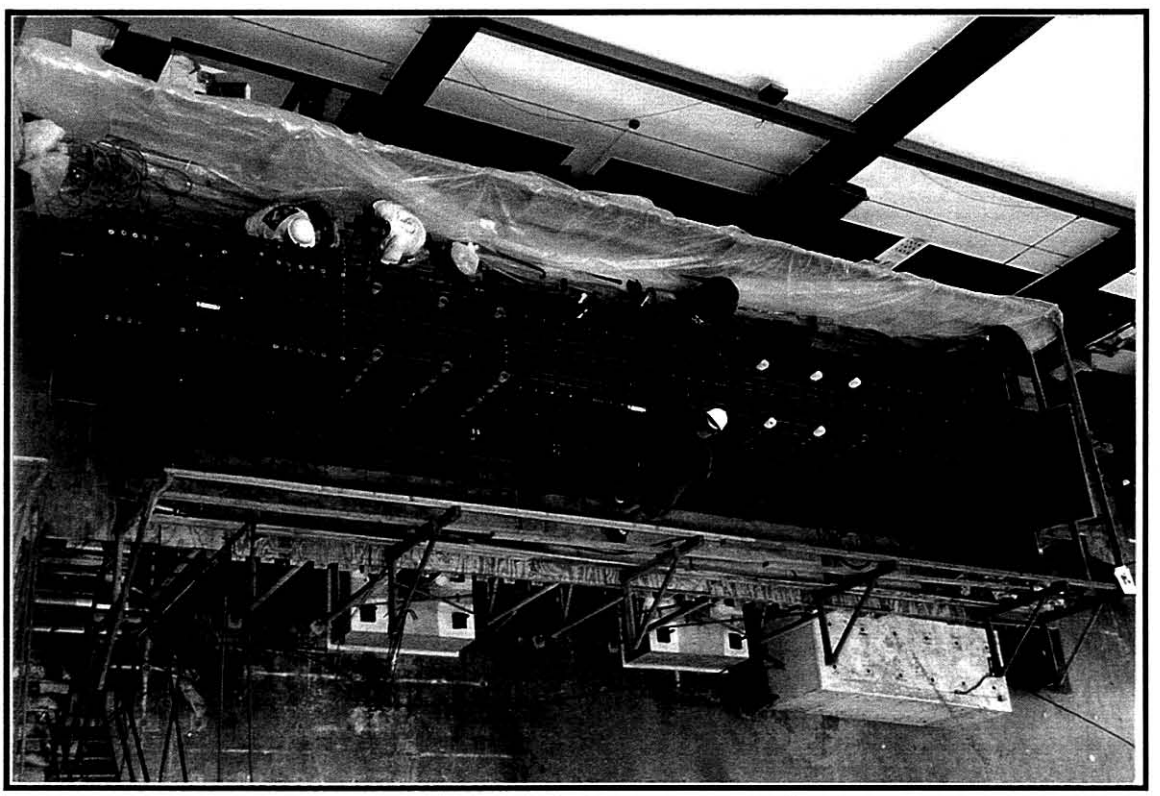

Fig.5-6 Cap Beam Reinforcement Cage in Place

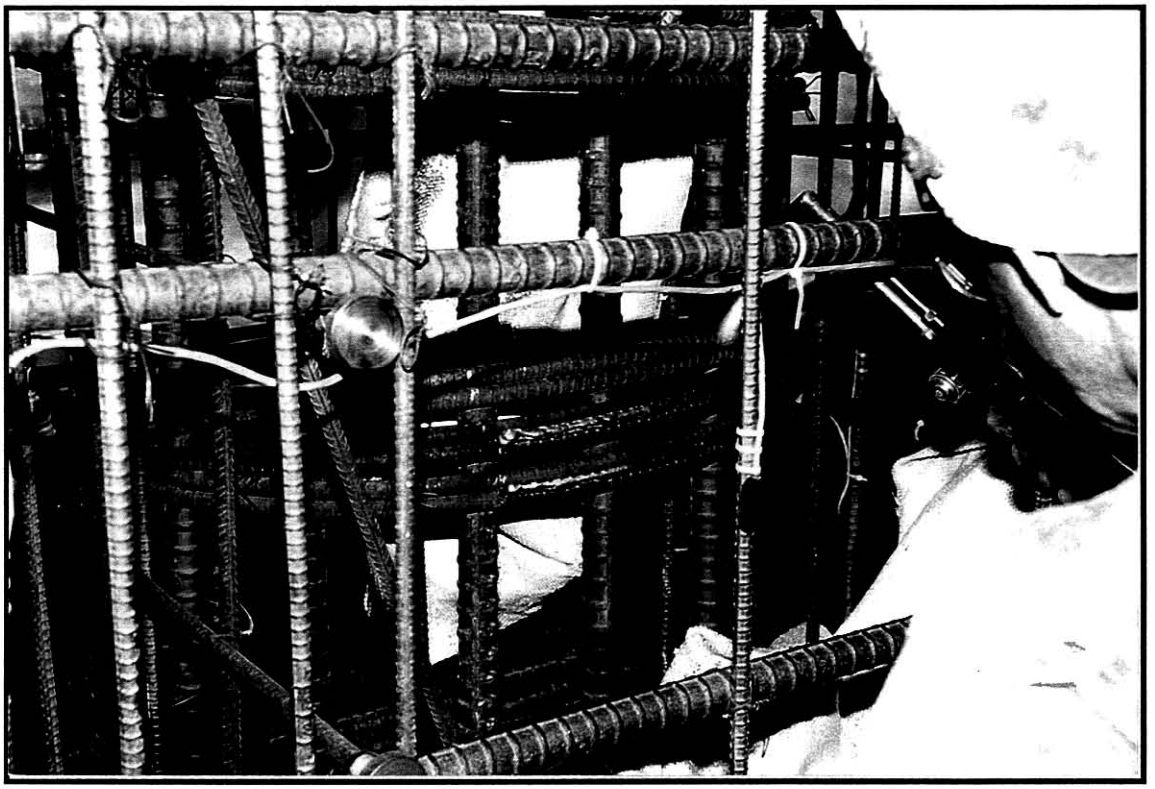

Fig.5-7 After Placing the Cross Ties Joint Hoops were Field Welded

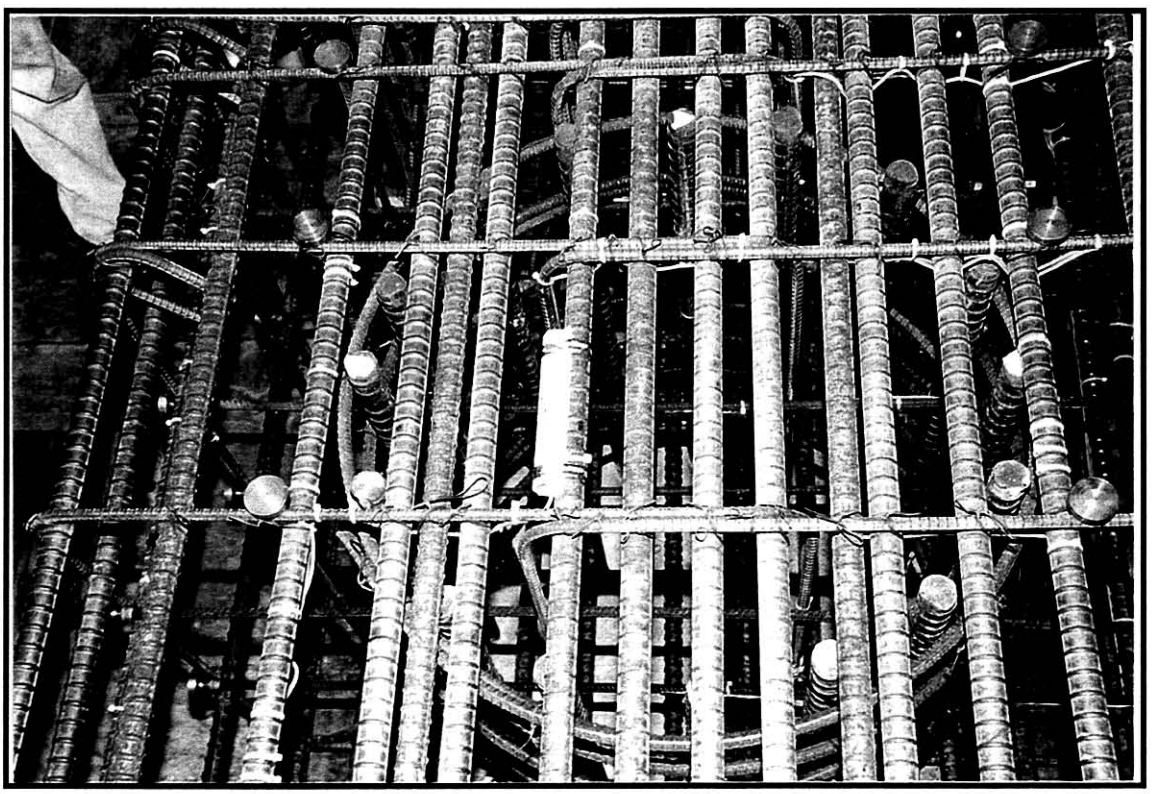

Fig.5-8 Top View of the Completed Reinforcement Detail Near Exterior Joint ***KJ1***

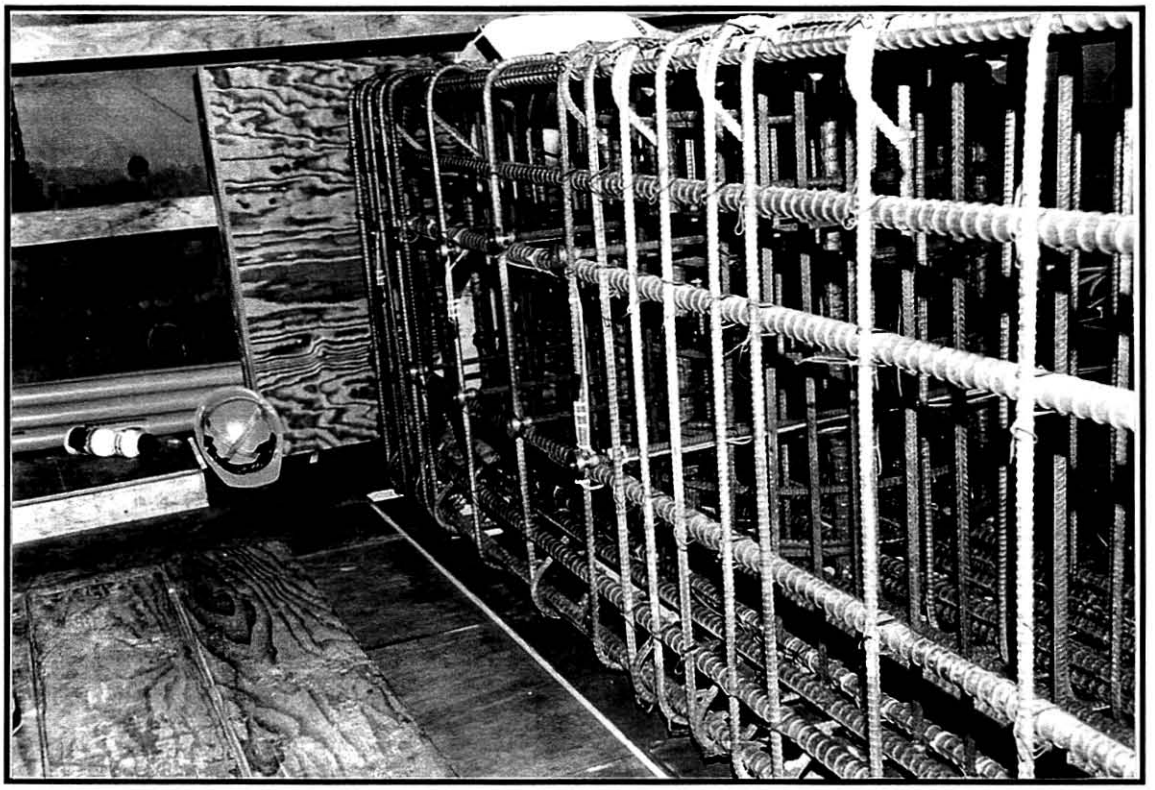

Fig.5-9 Side View of the Completed Reinforcement Detail Near Exterior Joint ***KJ1***

Fig.5-10 Reinforcement Detail at End of Cap Beam With Horizontal U-Pins in Place

Fig.5-12 Casting of the Cap Beam

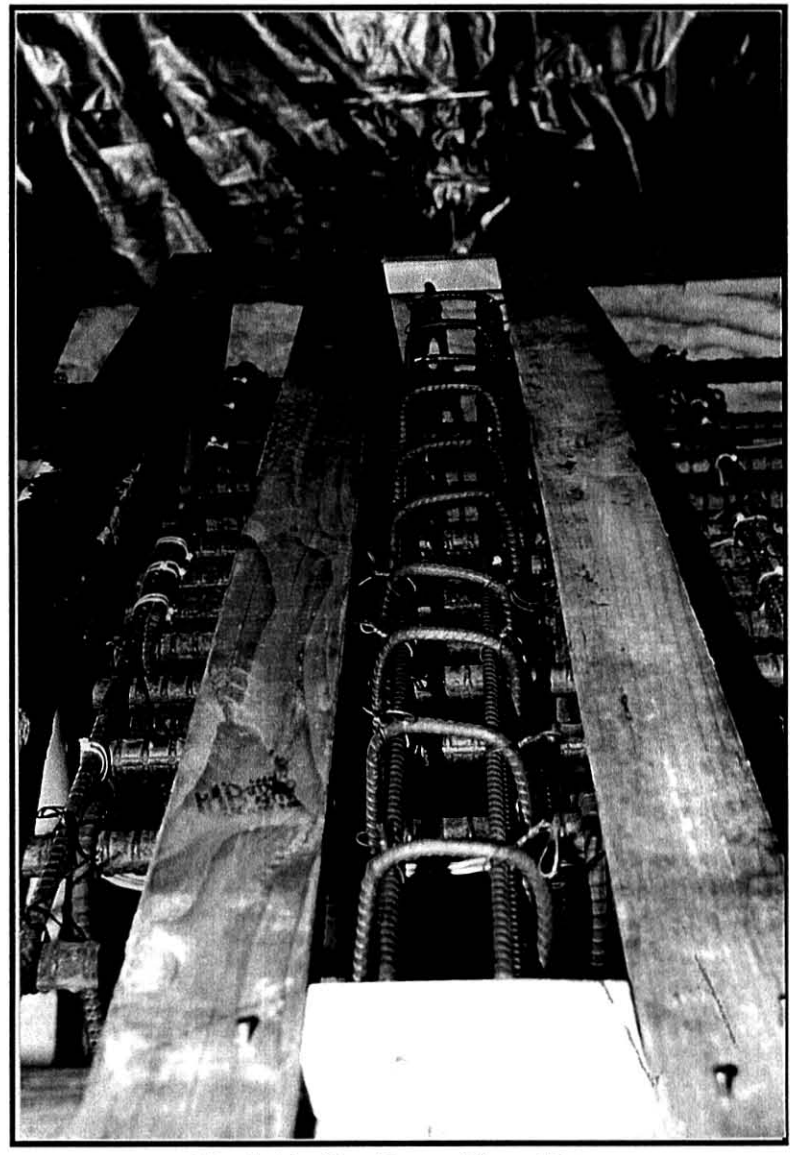

Fig.5-11 Cap Beam Shear Keys

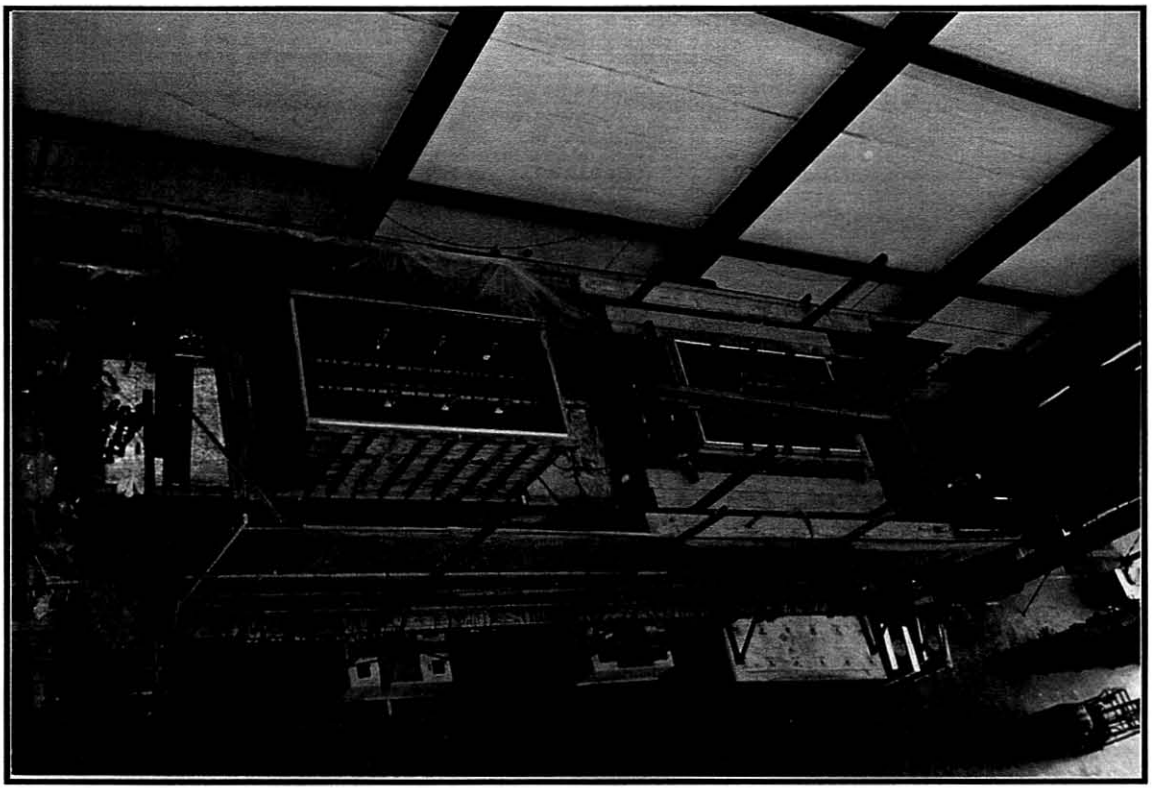

Fig.5-13 Construction of the Load Transfer Blocks After Casting of the Cap Beam

Fig.5-14 Completed Test Unit Prior to Testing

5.2 Material Properties

Concrete and steel material properties were obtained from sample testing on a Satec® material testing machine at the UCSD Charles Lee Powell Laboratory.

5.2.1 Concrete Material Properties

Fig.5-15 shows the concrete casting sequence and concrete batch number. Standard compression cylinder tests for the different concrete batches were performed at 7 days, 28 days and on day-of-testing (d.o.t.). Nine samples were taken from each batch and the measured concrete compression strength for each batch are presented in **Table 5-1**. Each concrete compression strength value presented in **Table 5-1** represents an average from three unconfined concrete cylinders (152.4mm diameter x 304.8mm height), which were cast during each batch pouring. For Batches No. 1, 7 and 8 no concrete compression strength tests were performed at the 7 days mark.

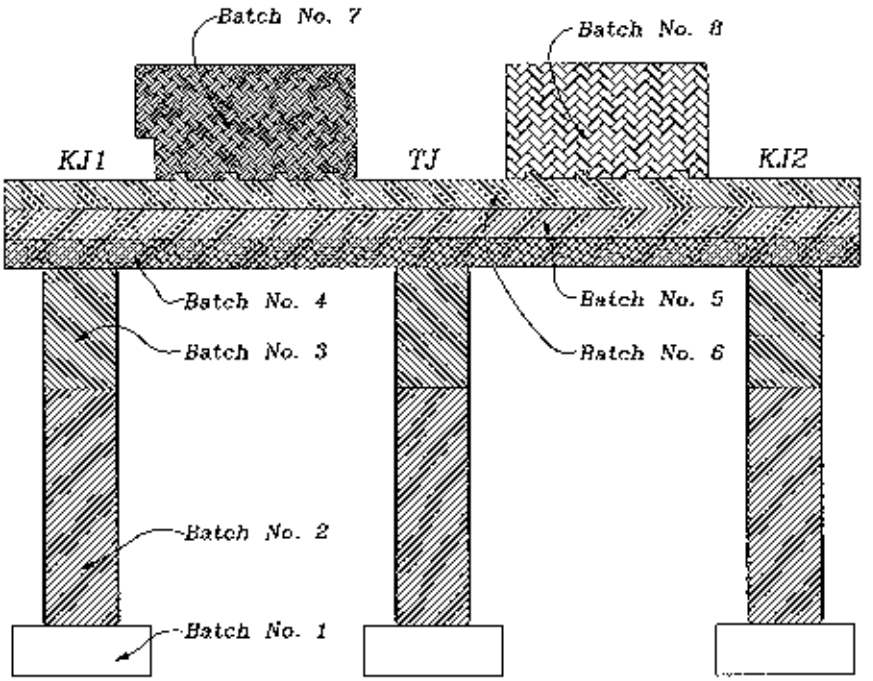

Fig.5-15 Identification of Various Concrete Batches

Table 5-1 Concrete Material Properties

Batch No. [1]	7 - Day f'_c [MPa]	28 - Day f'_c [MPa]	Day-of-Test f'_c [MPa]	Slump [mm]
1 [3,6]	-	30.44	43.92	143
2 [4,5]	23.4	32.0	38.7	118
3 [4,5]	20.2	28.9	34.8	171
4 [4,6]	27.9	35.4	37.9	156
5 [4,6]	29.8	36.6	39.4	121
6 [4,6]	26.8	34.3	35.9	70 [7]
7 [2,6]	-	38.4	41.5	140
8 [2,6]	-	39.3	40.7	133

[1] Concrete strength was determined from 3 cylinders for each batch.

[2] Maximum aggregate is specified as 13mm.

[3] Maximum aggregate is specified as 19mm.

[4] Maximum aggregate is specified as 25mm.

[5] Specified f'_c = 28Mpa.

[6] Specified f'_c = 34Mpa.

[7] 38 litters of water were added to concrete mix before casting.

5.2.2 Steel Material Properties

Three samples of each reinforcement type were tested to determine the stress-strain characteristics of each bar type and the results are summarized in **Table 5-2**. The properties illustrated in **Table 5-2** were obtained by testing three 914 mm long samples from the same group of each bar size, except for the steel shells of which no sample was tested.

Table 5-2 Steel Material Properties

Bar Size [1]	Location	Yield Strength f_y [MPa]	Ultimate Strength f_u [MPa]
M22	Footing Top and Bottom Longitudinal Reinforcing Bars	520	878
M13	Footing Vertical Stirrups	430	706
M36	Column Longitudinal Reinforcing Bars	448	745
M19	Pin Longitudinal Reinforcing Bars	445	731
M16	Column Spirals and Joint Hoops	405	750
M29	Cap Beam Top and Bottom Longitudinal Reinforcing Bars	455	772
M13	Cap Beam Vertical Stirrups and Horizontal J-Hooks	425	716
M13	Cap Beam Cross Ties Headed Reinforcing Bars	450	545
M10	U-Bras in Cap Beam Ends	520	821
12.70mm [2] Steel Shells	Column Steel Shells	Grade 250	-

[1] Average yield stress determined from 3 coupons.

[2] Not tested.

Since, samples from the column spirals and joint hoops did not have a clearly defined yield point, as illustrated in **Fig.5-16**, yield strength of these bars was established at a strain of 0.5% consistent with ASTM specifications. The stress–strain curves obtained from the uniaxial tensile strength tests of the column longitudinal reinforcing bars are presented in **Fig.5-17** with the respective stress-strain curve used for the column section moment-curvature analysis.

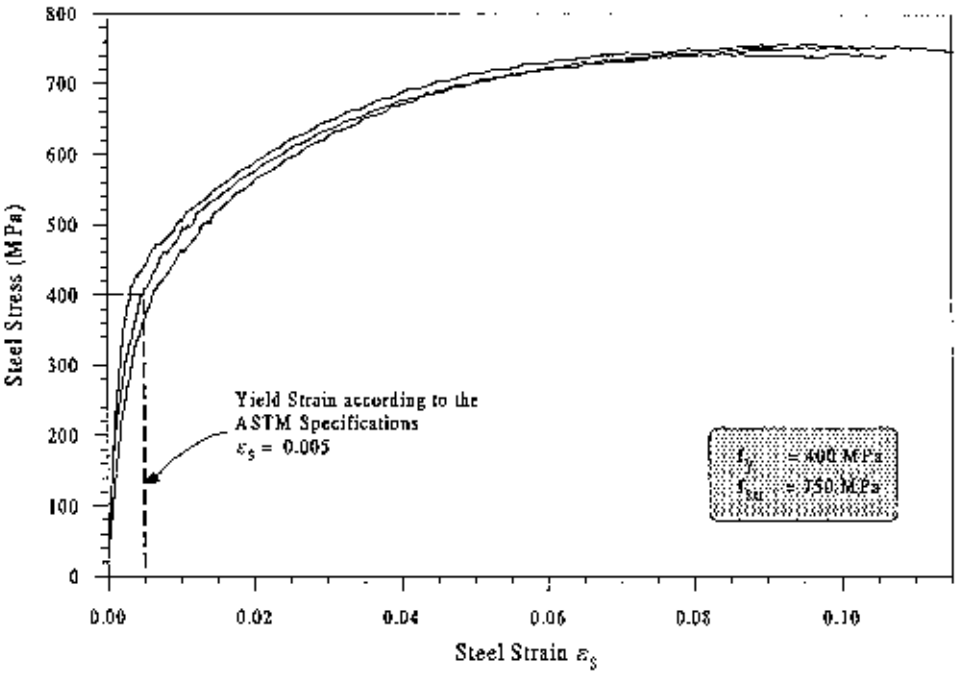

Fig.5-16 Column Spirals and Joint Hoops Steel Stress-Strain Curve

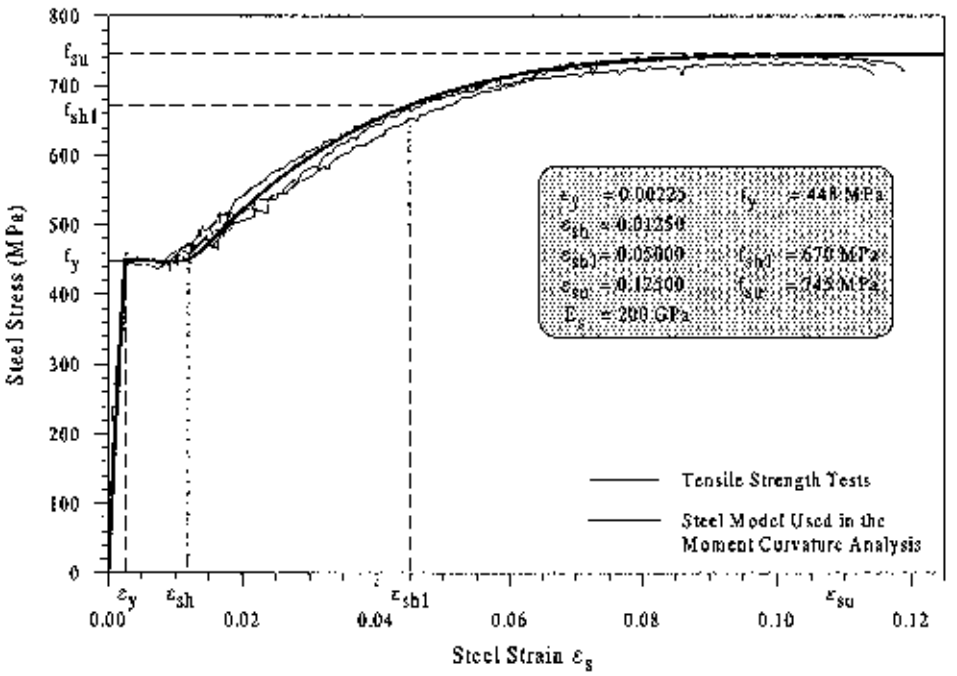

Fig.5-17 Column Longitudinal Reinforcing Bar Stress-Strain Curves

5.3 Instrumentation of the Test Unit

The test unit was instrumented with 46 linear potentiometer devices, 264 electric resistance strain gages, 6 load cells and 1 pressure transducer. Details of the instrumentation are given in this section according to the summary presented in **Table 5-3**. During testing, all the instrumentation was connected to a high-speed data acquisition system, and the test data was recorded at preset trigger intervals.

5.3.1 Linear Potentiometer Devices

Flexural curvatures at the column critical regions were experimentally determined using two linear potentiometers positioned on either side of the column in the loading plane, as shown in **Fig.5-18**, **Fig.5-19** and **Fig.5-20**. **Fig.5-20** shows a linear potentiometer device as installed in the steel shells. From the displacement measurements in the linear potentiometers the curvature was computed as follows:

$$\varphi_{ave} = \frac{\Delta_N - \Delta_S}{W_{cur}\, H_{cur}} \tag{5.1}$$

where φ_{ave} represent the average computed curvature, Δ_N and Δ_S are experimentally measured by the linear potentiometers and represent the vertical displacements between adjacent curvature rods in the extreme faces on opposite sides of the column section, W_{cur} is the width of the curvature cell (or horizontal distance between the pair of linear potentiometers) and H_{cur} is the height of the curvature cell (or vertical between the threaded rods and the bottom surface of the cap). Computation of curvatures was adjusted for the tensile strain penetration component in the height of the curvature cell adjacent to the cap beam, H_{cur}, as follows **[4]**:

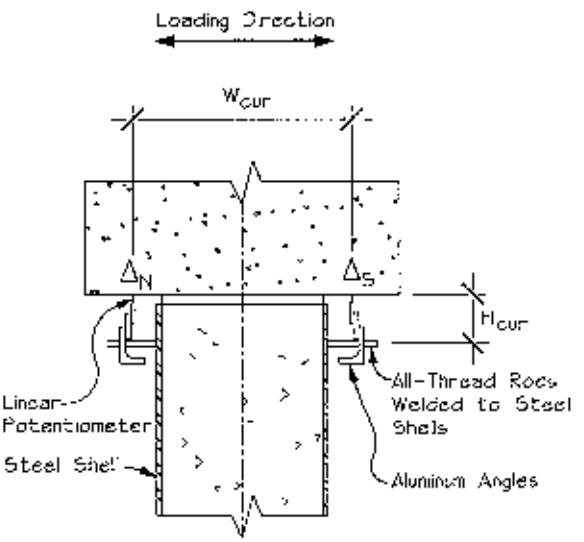

Fig.5-18 Curvature Measurement

$$H^{*}_{cur} = H_{cur}\left(1 - 1.67\frac{H_{cur}}{L_c}\right) + 0.022\, d_b f_y \tag{5.2}$$

where L_c is the distance from the column inflection point to the underside of the cap beam, d_b is the column bar diameter and f_y is the bar yield strength. This, modification accounts for the

rotation at the cap beam interface resulting from strain penetration. At the top of columns W_{cur} was 1.06m, H_{cur} was 153mm, and at maximum response L_c was 3.78m.

Rotations of the column base at the pin connections were measured from linear potentiometers positioned at the columns ends (see **Fig.5-19** and **Fig.5-21**). Assuming displacements in these linear potentiometers were due to rotations at the column ends, base rotations were estimated as follows:

$$\theta_{base} = (\Delta_N - \Delta_S)/W_{cur} \tag{5.3}$$

Cap beam curvature adjacent to the joint was obtained using a similar procedure to that adopted at the column top. However, curvature calculations were performed ignoring the penetration effect, since strains in the cap beam longitudinal bars were not expected to develop beyond yielding. Therefore, cap beam curvatures were computed according to the following equation:

$$\varphi_{ave} = \frac{\Delta_T - \Delta_B}{W_{cur}\, H_{cur}} \tag{5.4}$$

where Δ_T and Δ_B are the linear potentiometers readings. The measured length of the curvature cells, W_{cur}, was 813mm, and the height of the curvature cells, H_{cur}, was 203mm.

Other external instrumentation consisted of 15 linear potentiometers installed on the sides of the cap beam in the joint regions, according to the layout depicted in **Fig.5-19**. **Fig.5-22** shows the arrangement of these devices at joint *TJ*, to estimate joint panel deformations. At each of the joint faces five linear potentiometers were used to measure the joint panel deformation. Joint deformations consists of five independent deformations modes, which are pure shear, extension in the x and y direction , and flexural deformations about the x and y directions, as shown in **Fig.5-23**, and equations to compute these deformations are presented in reference **[4]**.

One linear potentiometer was installed between the two load transfer blocks, to which the horizontal actuators were connected, to measure the relative displacement between these two blocks, as illustrated in **Fig.5-19**. Moreover, **Fig.5-19** shows two linear potentiometers connected at the base of these load transfer blocks to measure horizontal slip of these blocks, and four linear potentiometers were similarly connected to these blocks in order to record uplift of these blocks during application of the lateral loads.

Out-of-Plane deflection of the test unit was monitored at the center of the load transfer blocks with two linear potentiometers connected to two reference columns, as illustrated in **Fig.5-19**. The specimen lateral deflection was recorded by two linear string type potentiometers positioned at the ends of the cap beam near exterior joint ***KJ2***, as shown in **Fig.5-19**. These linear potentiometers had a stroke of ±20in. and were used to control the loading sequence during the displacement control load cycles, as described in **Section 5.4**.

Table 5-3 Summary of Instrumentation

Displacement Transducers	Column Top Curvature	6	
	Column Bottom Rotation	6	
	Cap Beam End-Members Curvature	8	
	Shear Panel Deformation	15	
	Load Transfer Block Horizontal Slip	2	
	Load Transfer Block Uplift	4	
	Interior Joint Deflection	1	
	Test Unit Out-Plane Deflection	2	
	Specimen Lateral Deflection	2	
	Total		46
Strain Gages	Column Longitudinal Reinforcement	32	
	Footing Starter Bars	6	
	Steel Shell Vertical Strain Gages	24	
	Column Transverse Reinforcement	42	
	Steel Shell Horizontal Strain Gages	36	
	Cap Beam Top and Bottom Reinforcement	52	
	Cap Beam Vertical Stirrup Reinforcement	50	
	Cap Beam Horizontal J-Hooks	6	
	Cap Beam Ends Horizontal U-Pins	16	
	Total		264
Load Cells and Pressure Transducers	Horizontal Actuators	2	
	Axial Load Exterior Fixtures	4	
	Axial Load Interior Fixtures	1	
	Total		7
	TOTAL INSTRUMENTATION		317

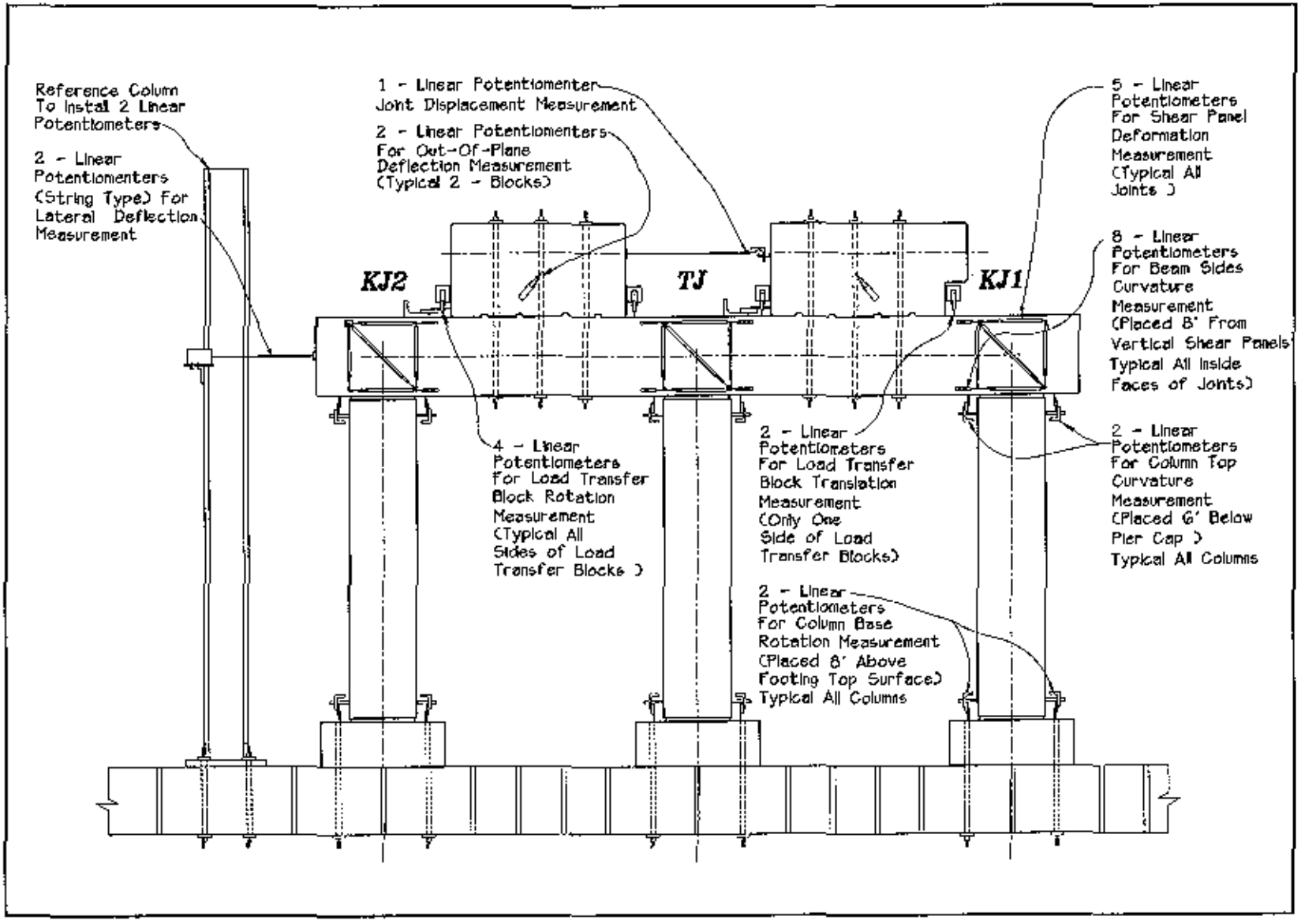

Fig.5-19 Instrumentation Setup

Fig.5-20 Top of Column External Instrumentation

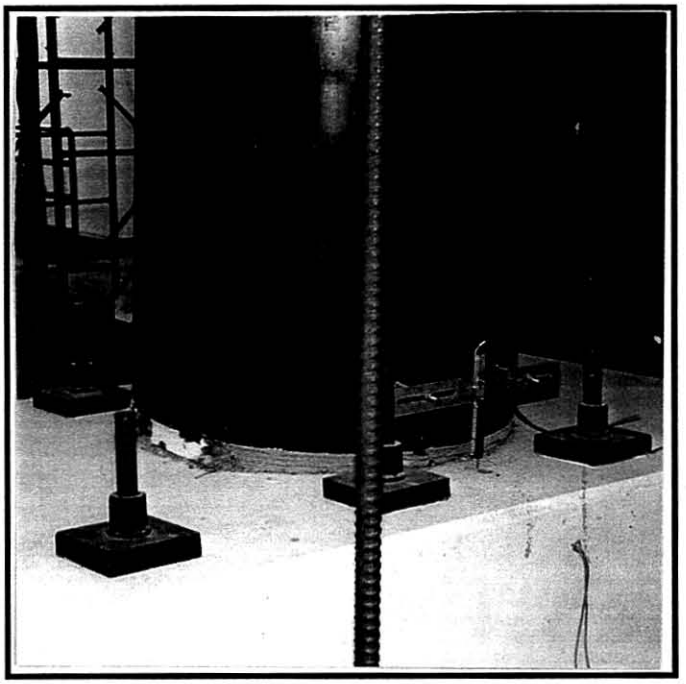

Fig.5-21 Bottom of Column External Instrumentation

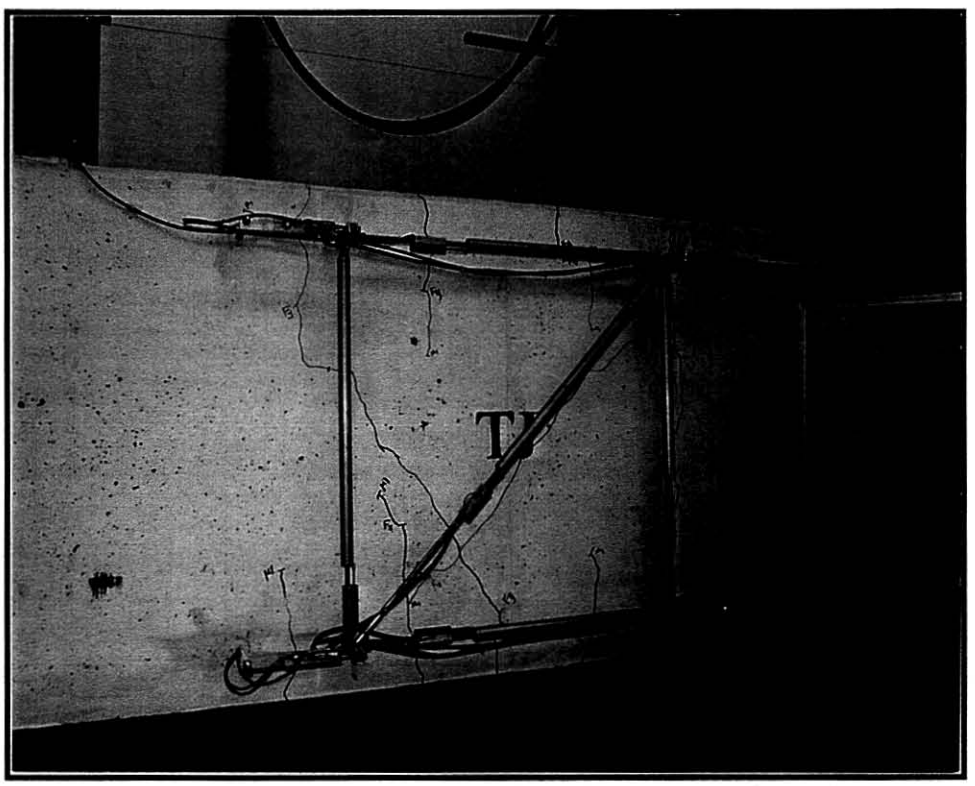

Fig.5-22 External Instrumentation for Joint Panel Deformations at Interior Joint ***TJ***

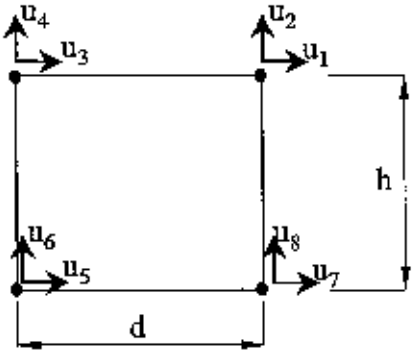

(a) Joint panel nodal displacements

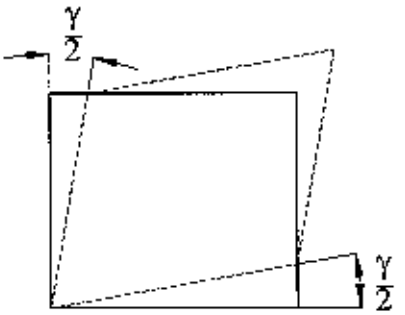

(b) Mode 1 - pure shear

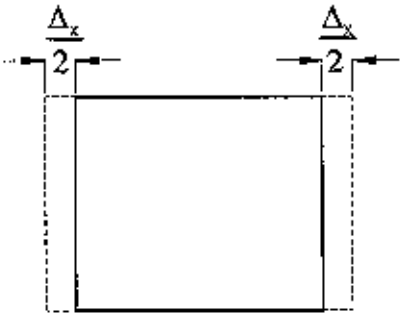

(c) Mode 2 - extension in x direction

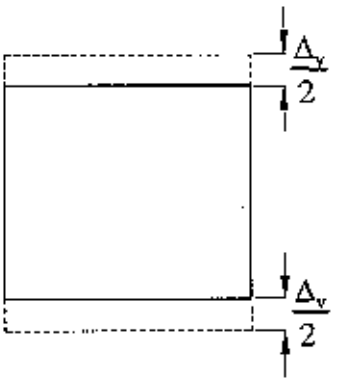

(d) Mode 3 - extension in y direction

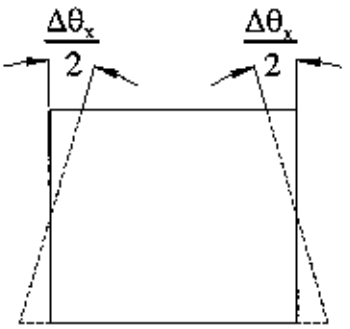

(e) Mode 4 - curvature about x axis

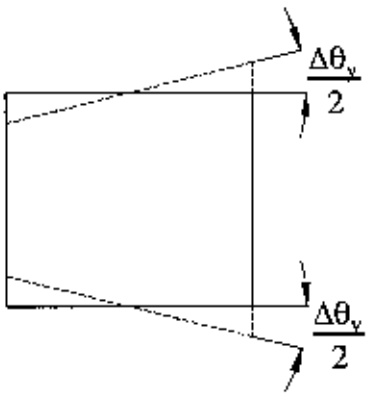

(f) Mode 5 - curvature about y axis

Fig.5-23 Decomposition of Joint Panel Deformation into Five Independent Modes [4]

5.3.2 Electrical Resistant Strain Gages

A summary of the strain gages mounted on the reinforcement of the test unit is presented in **Table 5-3**. Instrumentation of the reinforcement consisted of electric resistance strain gages produced by Tokyo Sokki Kenkyujo Co., Ltd. These strain gages have a gage length of 5mm and a gage resistance of 120±0.3Ω with a scale factor of 2.13. A total of 32 electric resistance strain gages were applied on the column longitudinal reinforcement, and 24 strain gages were positioned vertically in the steel shells according to the gage layout depicted in **Fig.5-24**. In addition, two strain gages were applied in the extreme starter bars at each footing as indicated in **Fig.5-24**. The column transverse reinforcement inside and outside of the joint was instrumented with 42 strain gages according to the layout depicted in **Fig.5-25**. In addition, 36 strain gages were positioned horizontally in the steel shells, as illustrated in **Fig.5-25**.

A total of 52 strain gages were applied on the pier cap top and bottom longitudinal reinforcement, as depicted in **Fig.5-26**. In addition, 50 strain gages were applied on the pier cap vertical stirrups reinforcement, and 6 strain gages were applied on the horizontal J-Hooks according to **Fig.5-27**. Strain gages were also applied to the cap beam end horizontal U-pins, as described in **Fig.5-28**

5.3.3 Load Cells and Pressure Transducer

A total of six load cells were used during testing to monitor the vertical and lateral forces applied to the test specimen. Each of the two horizontal actuators, previously defined in **Chapter 2**, and used for applying the simulated lateral seismic forces, contained a calibrated load cell. In addition, axial load of the test unit consisted of four axial loading fixtures with the layout depicted in **Fig.5-29**. Each loading fixture consisted of a steel cross beam, two high-strength 35mm diameter bars inserted through 50.8mm diameter holes in the steel cross beams and tie downs, as described in **Section 2.1**. As depicted in **Fig.5-29**, the axial loads were applied at positions ***1***, ***2*** ,***3*** and ***4*** with a single hydraulic pump which distributed equal pressure to each position, and was monitored with four individual load cells connected to each high-strength bar, at the tie down end, below the laboratory strong floor. Similarly, at positions ***A***, ***B*** ,***C*** and ***D*** the axial load was applied with a single hydraulic pump, which distributed evenly pressure to each position, but the axial load at these positions was monitored with a single pressure transducer.

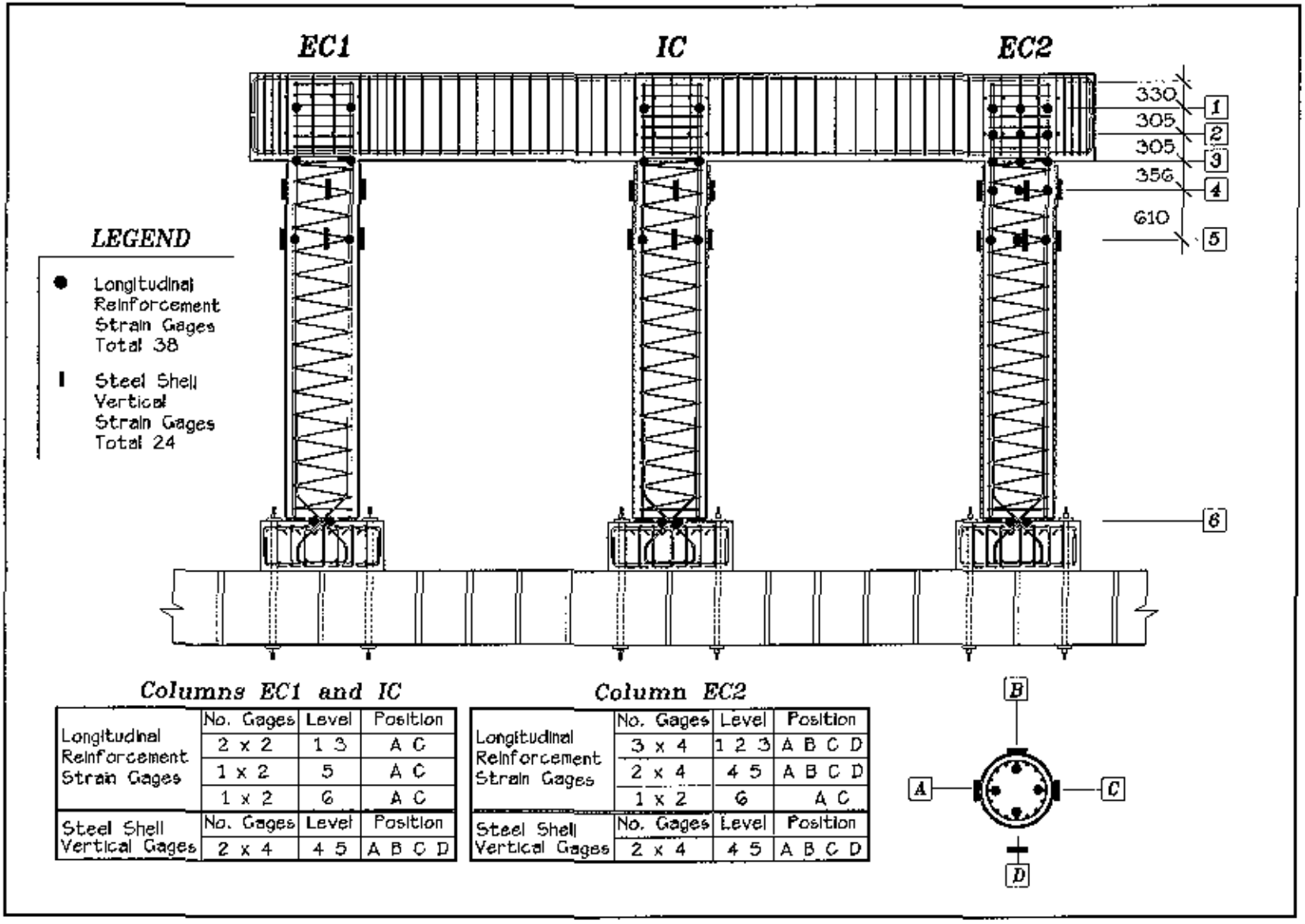

Columns EC1 and IC

	No. Gages	Level	Position
Longitudinal Reinforcement Strain Gages	2 x 2	1 3	A C
	1 x 2	5	A C
	1 x 2	6	A C
Steel Shell Vertical Gages	2 x 4	4 5	A B C D

Column EC2

	No. Gages	Level	Position
Longitudinal Reinforcement Strain Gages	3 x 4	1 2 3	A B C D
	2 x 4	4 5	A B C D
	1 x 2	6	A C
Steel Shell Vertical Gages	2 x 4	4 5	A B C D

Fig.5-24 Steel Shell and Longitudinal Reinforcement Vertical Strain Gage Layout

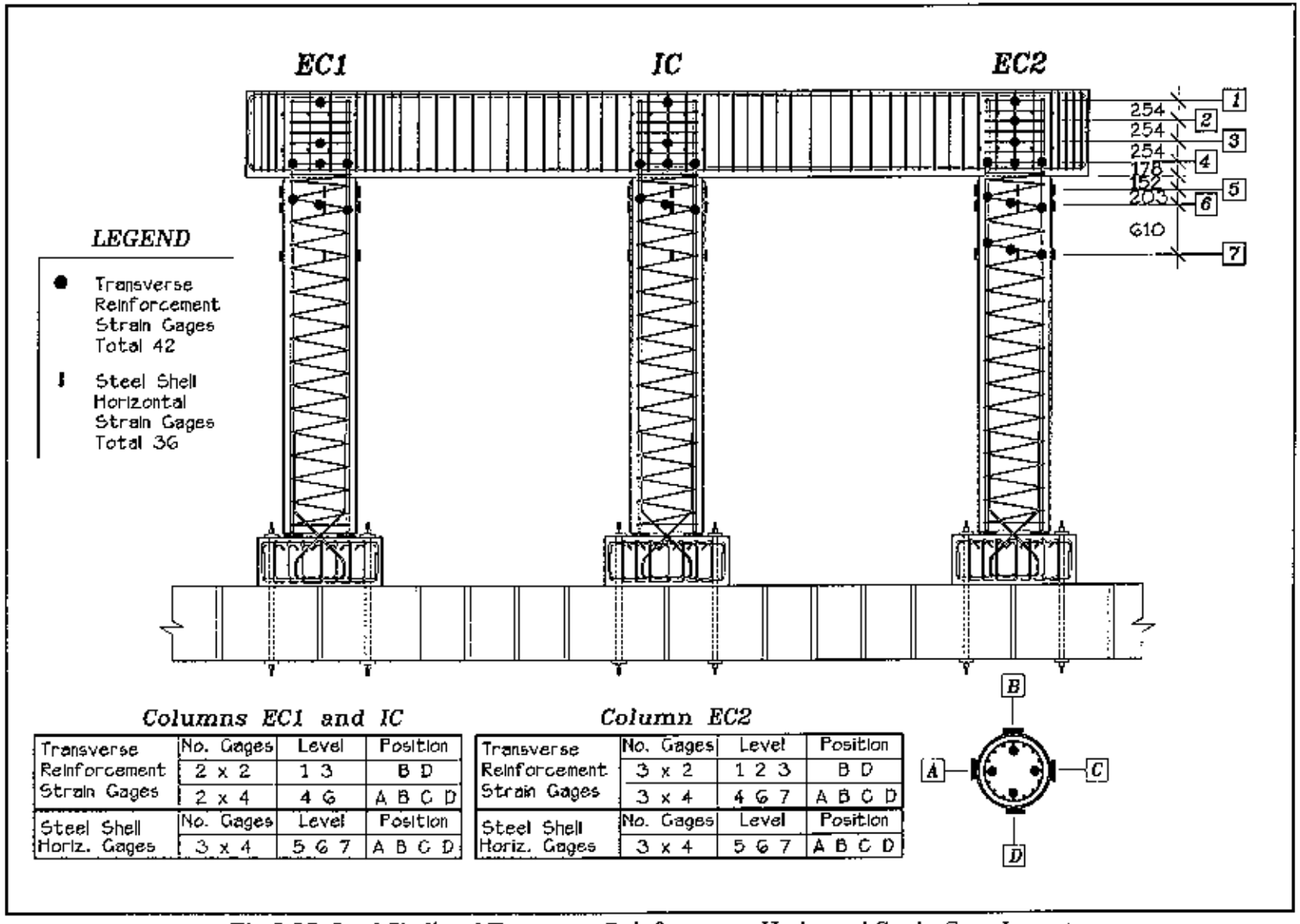

Columns EC1 and IC

	No. Gages	Level	Position
Transverse Reinforcement Strain Gages	2 x 2	1 3	B D
	2 x 4	4 6	A B C D
Steel Shell Horiz. Gages	3 x 4	5 6 7	A B C D

Column EC2

	No. Gages	Level	Position
Transverse Reinforcement Strain Gages	3 x 2	1 2 3	B D
	3 x 4	4 6 7	A B C D
Steel Shell Horiz. Gages	3 x 4	5 6 7	A B C D

Fig.5-25 Steel Shell and Transverse Reinforcement Horizontal Strain Gage Layout

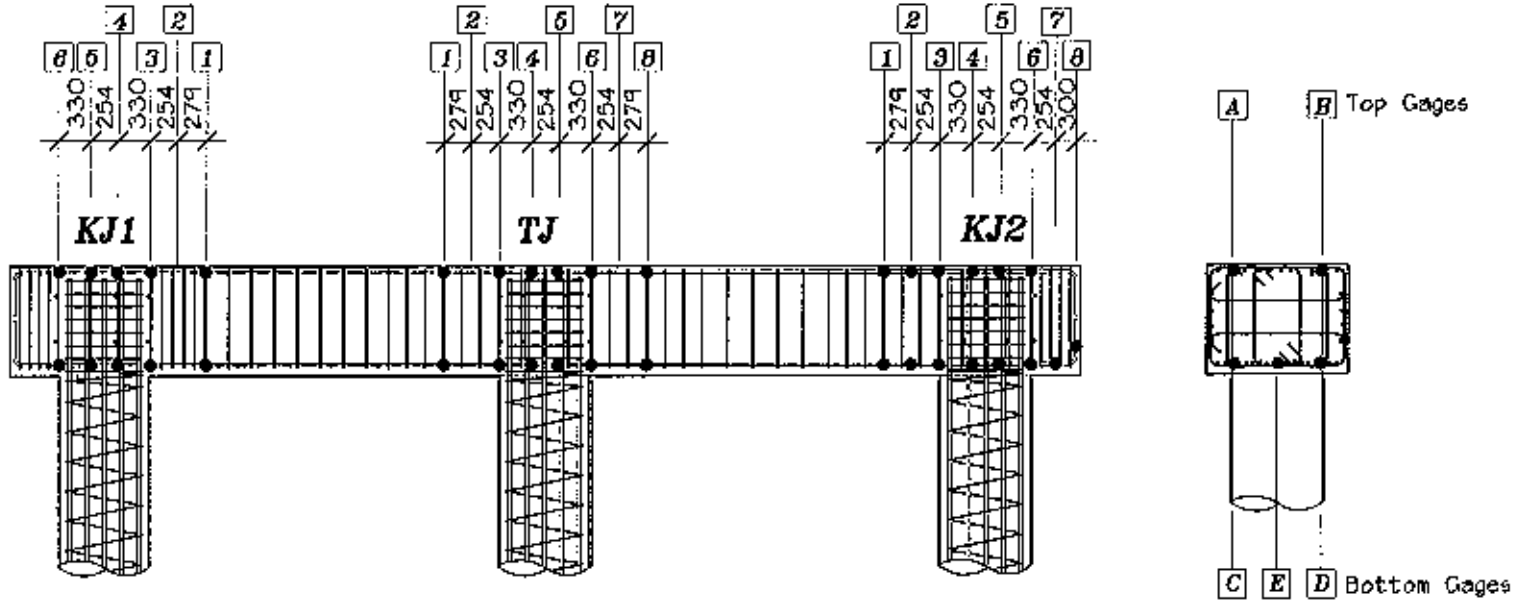

Joint KJ1

Pier Cap Reinforcement Strain Gages	No. Gages	Level	Position
	3 x 2	1 3 5	A D
	2 x 2	4 6	B C

Joint KJ2

Pier Cap Reinforcement Strain Gages	No. Gages	Level	Position
	2 x 4	1 2	A B C D
	4 x 4	3 - 6	A B C D
	2 x 3	7 8	C D E

LEGEND

● Pier Cap Beam Top + Bottom Reinforcement Strain Gages – Total 52

Joint TJ

Pier Cap Reinforcement Strain Gages	No. Gages	Level	Position
	3 x 2	1 3 5	A D
	3 x 2	4 6 8	B C

Fig.5-26 Cap Beam Top and Bottom Longitudinal Reinforcement Strain Gage Layout

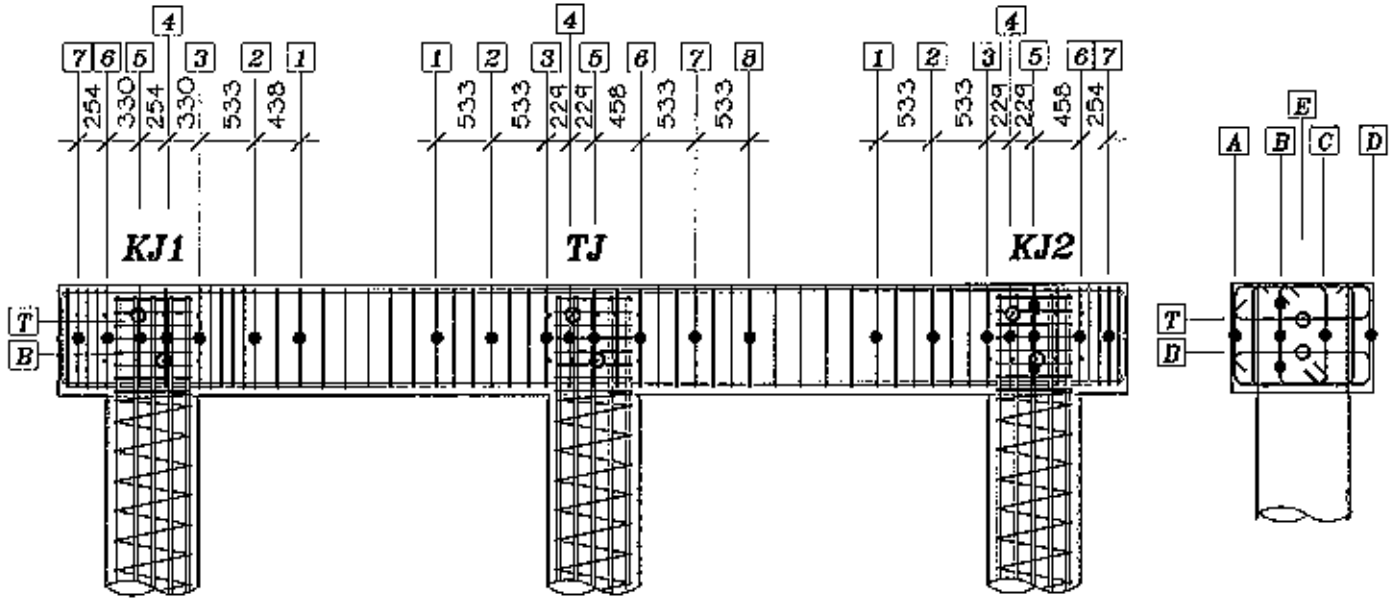

Joint KJ1

Vert. Stirrups Reinforcement Strain Gages	No. Gages	Level	Position
	4 x 2	1 3 5 7	A C
	4 x 2	2 4 5 6	B D
Horiz. J-Hooks Strain Gages	No. Gages	Level	Position
	2 x 1	4 5	E

Joint KJ2

Vert. Stirrups Reinforcement Strain Gages	No. Gages	Level	Position
	4 x 2	1 3 5 7	A C
	4 x 2	2 4 5 6	B D
Horiz. J-Hooks Strain Gages	No. Gages	Level	Position
	2 x 1	4 5	E

Joint TJ

Vert. Stirrups Reinforcement Strain Gages	No. Gages	Level	Position
	4 x 2	1 3 5 7	A C
	5 x 2	2 4 5 6 8	B D
Horiz. J-Hooks Strain Gages	No. Gages	Level	Position
	2 x 1	4 5	E

LEGEND

- ● Cap Beam Vertical Stirrups Reinforcement Strain Gages Total 50
- ○ Cap Beam Horizontal J-Hooks Reinforcement Strain Gages Total 6

Fig.5-27 Cap Beam Stirrups Strain Gage Layout

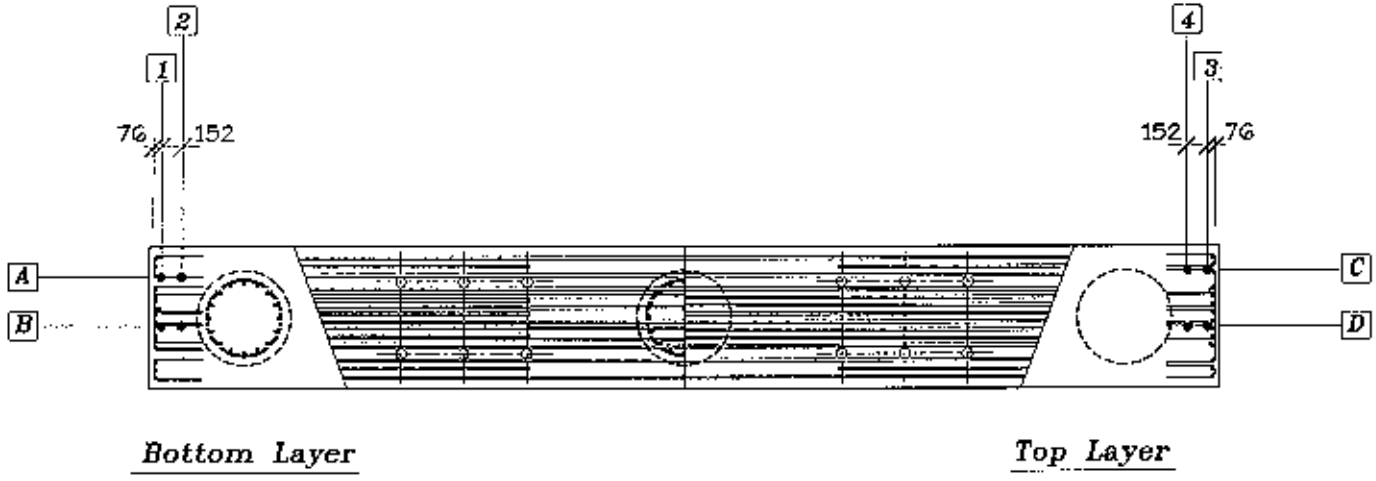

Cap Beam Longitudinal Reinforcement

Joints KJ1 and KJ2

Cap Beam Ends U - Pins Bars Strain Gages	No. Gages	Level	Position
	2 x 2	1 2	A B
	2 x 2	3 4	C D

LEGEND

● Cap Beam Ends Horizontal U-Pins Reinforcing Bars Total 16

Fig.5-28 Cap Beam Ends Horizontal U-Pins Reinforcing Bars Strain Gage Layout

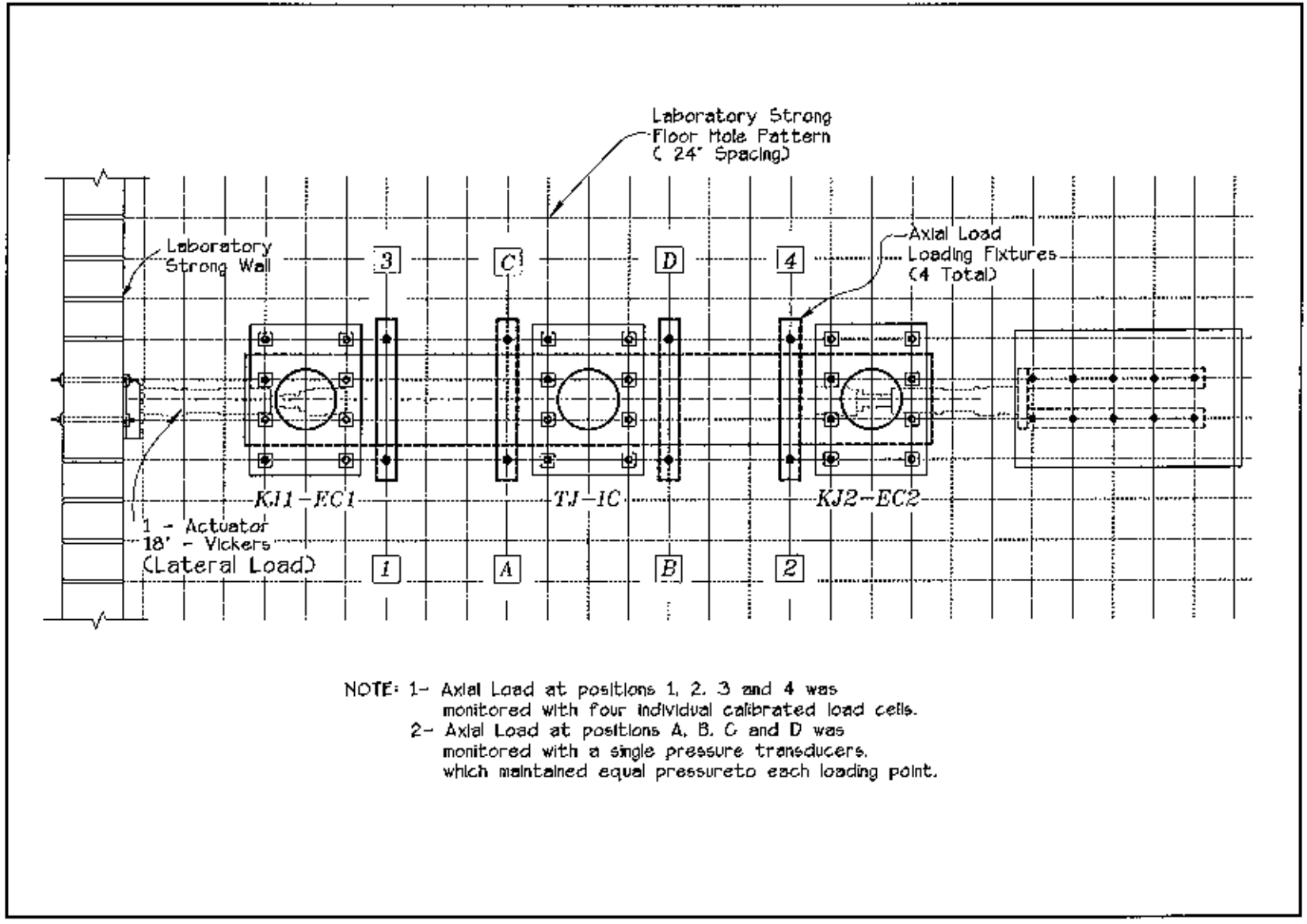

Fig.5-29 Axial Load - Loading Fixtures Layout

5.4 Loading Sequence of the Test Unit

Loading of the test unit was performed according to the loading sequence presented in **Fig.5-30.** The first step in the testing procedure consisted of applying the vertical loads for ***gravity load simulation***. Following the application of the initial axial loads the test unit was first subjected to single cycles under ***force control*** at 25%, 50%, 75% and 100% of the theoretical first yield lateral force, V'_y, of 1,681 kN. First yield of the test specimen was obtained from the predictive analysis presented in **Chapter 6**, and corresponded to the tension yielding of the interior column, ***IC,*** longitudinal reinforcement. The structure was then loaded under ***displacement control*** with three cycles applied at each specified displacement ductility level of μ_1, $\mu_{1.5}$, μ_2, μ_3, μ_4, μ_6, and μ_8. At the displacement ductility μ_{10} only two cycles were performed because of fracture in the column longitudinal reinforcing bars, indicating that the test unit had reached its ultimate limit state.

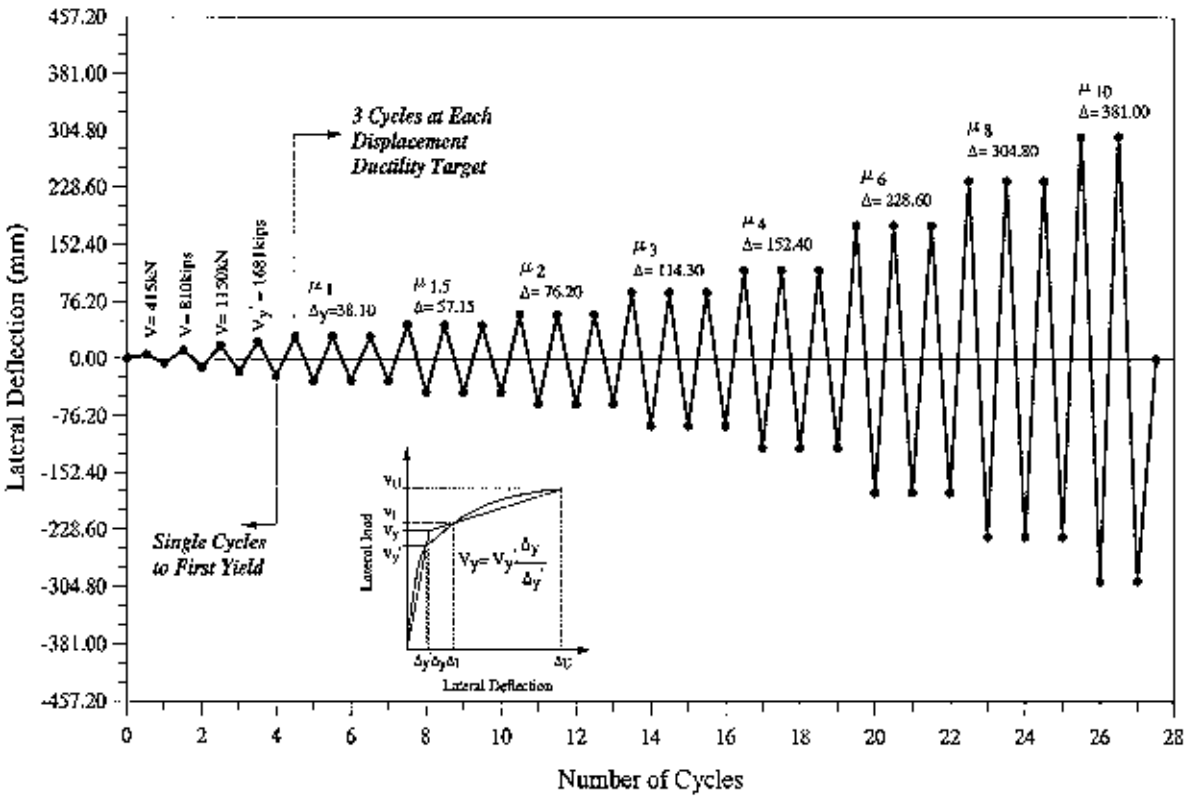

Fig.5-30 Lateral Load Sequence Applied to the Test Unit

Incremental displacement ductility levels were obtained based on the recorded lateral deflections at first yield in both loading directions based on the expression :

$$\Delta_{\mu I} = \frac{\left(|\Delta'_{y1}| + |\Delta'_{y2}| \right)}{2} \frac{V_I}{V'_y} \tag{5.5}$$

where V_I is the total lateral force at the ideal capacity of the specimen. The ideal capacity of the test unit was 2,122 kN, as obtained from analysis corresponding to the concrete compression strain in the interior column, *IC*, when it reached the value of 0.005. The variable $\Delta_{\mu I}$ is the lateral displacement at $\mu_\Delta = 1$, and Δ'_{y1} and Δ'_{y2} are, respectively, the experimental lateral deflections recorded at first yield in the push and pull directions of loading. In the push and pull directions these lateral deflections were 30.92mm and 29.44mm, respectively. Bilinear approximation of the test unit seismic response is presented in **Fig.5-31**. Based on the values previously described the specimen's ideal displacement (38.10mm) was used to calculate the specified displacement ductility levels. Thus, the lateral displacement of the test unit at the displacement ductility level of μ_Δ =1 was 38.10mm.

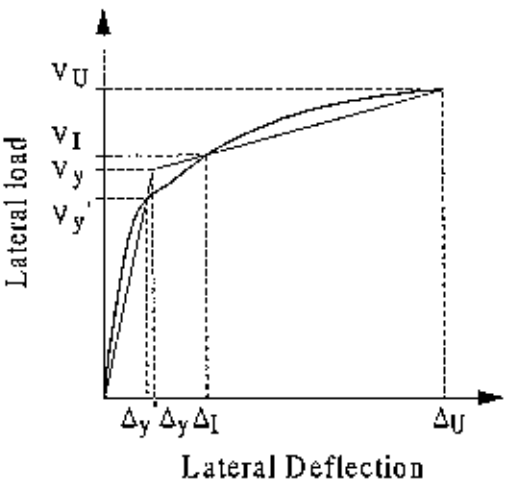

Fig.5-31 Test Unit Bilinear Approximation

6 Predicted Response

The response of the test unit was predicted using a pushover analysis, as described in **Chapter 3**. Since the joints were adequately detailed and the cap beam was protected from any significant inelastic actions, the plastic hinges were modeled at the top of the columns. The predicted force-displacement response, column member end forces, joint shear stresses, and prediction of cover concrete spalling in columns are some of the theoretical results presented in this chapter.

6.1 Force-Displacement Response

The corresponding predicted force-displacement response of the test unit is presented in **Fig. 6-1**. The pre-test analysis for the test unit was performed using average material properties obtained from the material properties presented in the **Section 5.2**. Concrete compression strength at 28 days was used in the analysis with the different batch properties indicated in **Table 5-1**, and the reinforcement yield strength for the different bar types are presented in **Table 5-2**. Because different batches were used in the construction of the columns and cap beam the concrete compression strength used in the pre-test analysis was obtained from the average of the different batches. Thus, for the column analysis the concrete compression strength was f'_c=31 MPa and for the cap beam analysis the concrete compression strength was f'_c=35 MPa.

A list of the expected events determined from analysis is presented **Fig. 6-1**. Events ***1-3*** correspond to response of the test unit at yielding of the pin connection reinforcing bars at the footing interface and in columns ***IC***, ***EC1*** and ***EC2***, respectively. Events ***4-6*** correspond to yielding of the columns longitudinal reinforcement at the cap beam interface in columns ***IC***, ***EC1*** and ***EC2***, respectively. Events ***7-9*** identify the development of the ideal moment strength at the critical section in the plastic hinge regions, which corresponded to the gap region in the top of the columns ***IC***, ***EC1*** and ***EC2***, respectively. The ideal capacity of each column was defined at the moment that develops a strain of ε_c=**0.005** in the extreme compression fibers in the top of columns. Allowing for low cycle fatigue of the column longitudinal reinforcement due to cyclic loading and recognizing that adequate resistance to prevent buckling of the column longitudinal reinforcement by the steel shell, rupture of these bars was predicted at a strain of 7%, which was based on previous laboratory tests. This is also identified in the predicted force-displacement enveloped presented in **Fig. 6-1** as Event **10**.

Theoretical first yielding of the test unit, V_y', was taken as the lateral load that induces yielding in the longitudinal reinforcement of the interior column ***IC***. The theoretical first yielding of the test unit was developed at the lateral load of 1,682 kN and the lateral displacement, Δ_y', of 31.5mm. Ideal capacity of the test unit, V_I, was taken as the theoretical lateral load that induces a concrete strain of ε_c=**0.005** in the interior column ***IC***. Ideal capacity of the test unit was developed at the lateral load of 2,122 kN and a lateral displacement, Δ_I, of 67.8 mm. Finally, the ultimate capacity of the test unit, V_U, corresponded to the response of the test unit at event ***10***, and was developed at the lateral load of 2,692 kN and a lateral displacement of, Δ_U, 330.2 mm.

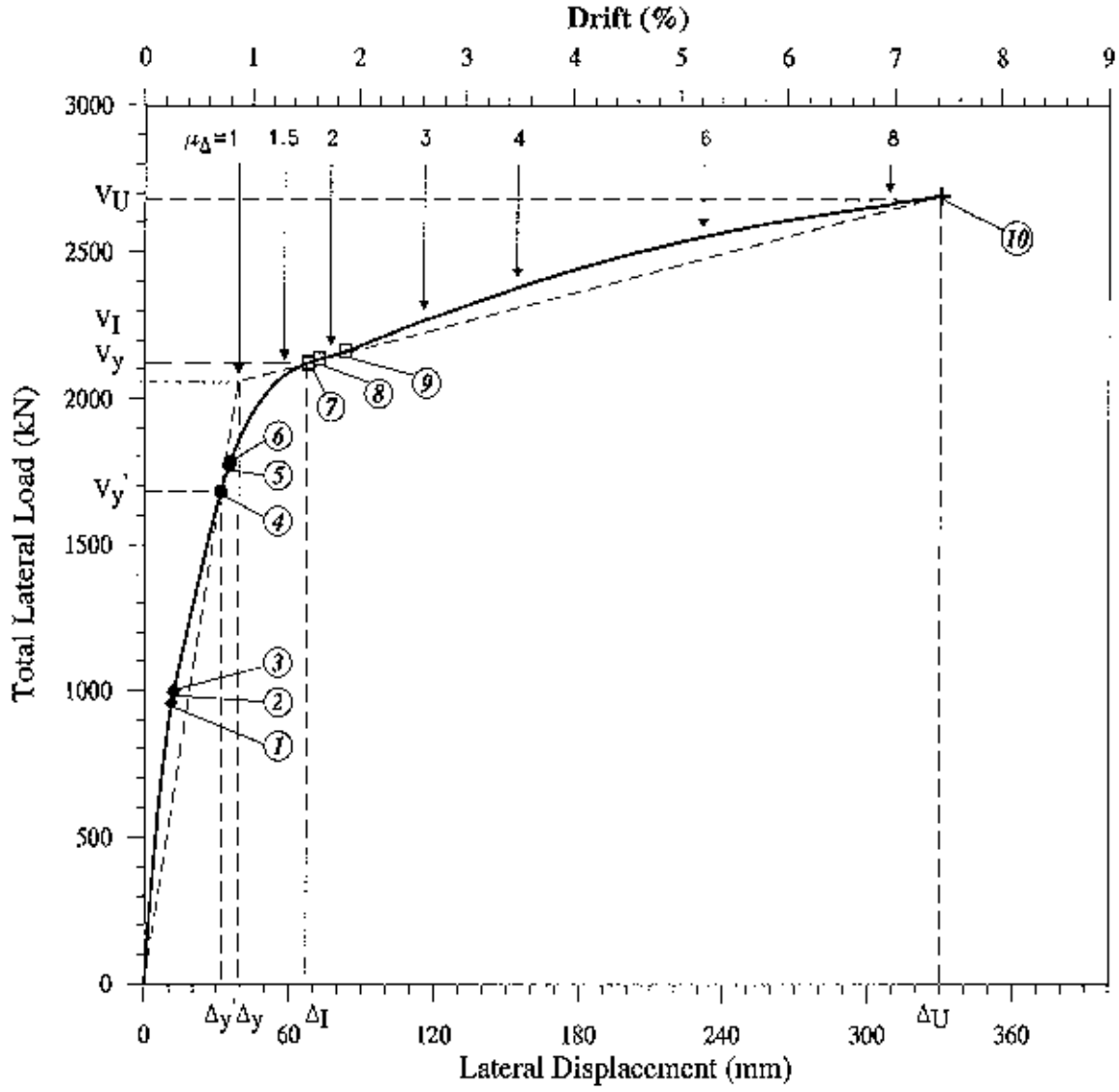

List of Events

Yielding of the Starter Bars in the Pin Connection Region:

1 - Interior Column IC
2 - Exterior Column EC2
3 - Exterior Column EC1

Yielding of the Inner Core Longitudinal Reinforcement at the Cap Beam Interface:

4 - Interior Column IC
5 - Exterior Column EC2
6 - Exterior Column EC1

Concrete Compression Strains of $\varepsilon_c = 0.005$ at the Cap Beam Interface:

7 - Interior Column IC
8 - Exterior Column EC2
9 - Exterior Column EC1

10 - Steel Strain of $\varepsilon_s = 0.07$ at the Cap Beam Interface in the Interior Column IC

$\Delta_y' = 31.5$ mm $\quad V_y' = 1681$ kN

$\Delta_y = 38.6$ mm $\quad V_y = 2060$ kN

$\Delta_I = 67.8$ mm $\quad V_I = 2122$ kN

$\Delta_U = 330.2$ mm $\quad V_U = 2692$ kN

Fig. 6-1 Predicted Force-Displacement Response of the Test Unit

Referring to **Fig. 6-1**, the predicted yield displacement of the test unit, Δ_y, was computed based on the bilinear elasto-plastic approximation of the force-displacement curve according to the expression:

$$\Delta_y = \frac{(V_U \Delta_I - V_I \Delta_U)\, \Delta_y'}{V_y' (\Delta_I - \Delta_U) + \Delta_Y' (V_U - V_I)} = 38.6\ mm \qquad (7.1)$$

and the lateral load at the first yielding, V_y, was computed according to the following expression:

$$V_y = V_y' \frac{\Delta_y}{\Delta_y'} = 2{,}060\ kN \qquad (7.2)$$

Displacement ductility capacity computed at ultimate response, μ_Δ, was obtained based on the following expression:

$$\mu_\Delta = \frac{\Delta_U}{\Delta_y} = \frac{330.2}{38.6} \approx 8.5 \qquad (7.3)$$

Displacement ductility levels computed at different levels of lateral deflection are also shown in **Fig. 6-1**.

6.2 Column Member End Forces

Predicted axial load versus shear force and bending moments at the cap beam interface, for each column, are presented in **Fig. 6-2** and **Fig. 6-3**, respectively. Due to gravity loads and selfweight, the axial load in the exterior columns ***EC1*** and ***EC2*** was 1,070 kN and in the interior column ***IC*** the initial axial was 1,760 kN. Under gravity loads and lateral load maximum achieved axial load, shear force and bending moment in the exterior column ***EC1***, were -756 kN (tension), 792 kN and 3,078 kN-m, respectively. In interior column ***IC***, these loads were 1,830 kN (compression), 929 kN and 3,623 kN-m, respectively. In exterior column ***EC2***, these loads were 2,840 kN (compression), 966 kN and 3,734 kN, respectively. Selfweight of the columns was estimated at 76 kN, cap beam at 357 kN and load transfer blocks at 220 kN.

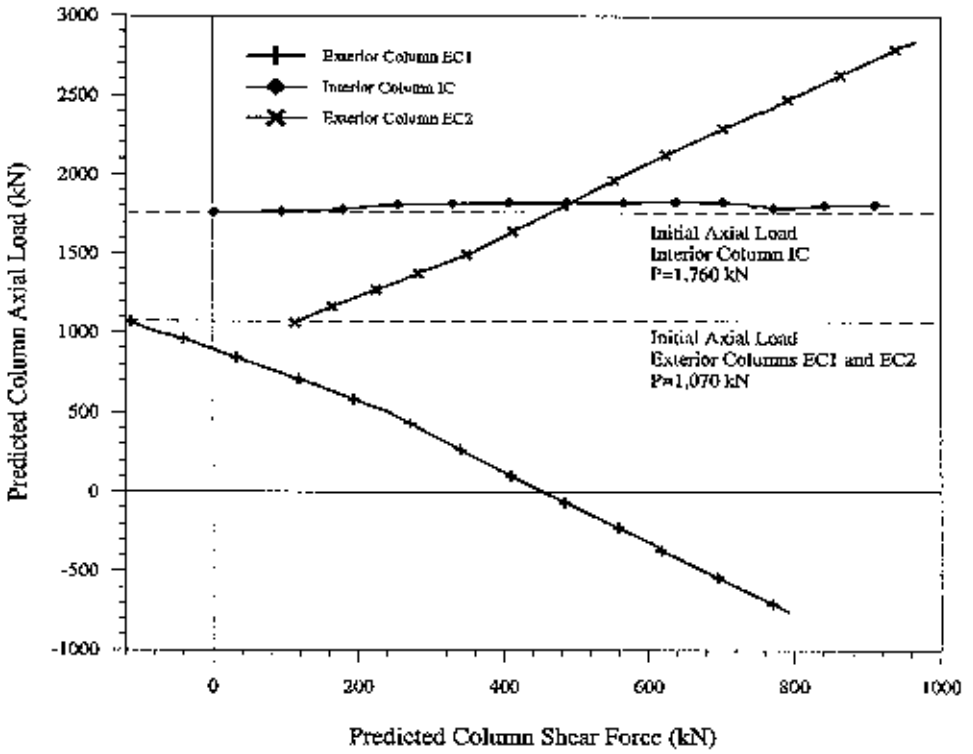

Fig. 6-2 Predicted Column Axial Load versus Shear Force

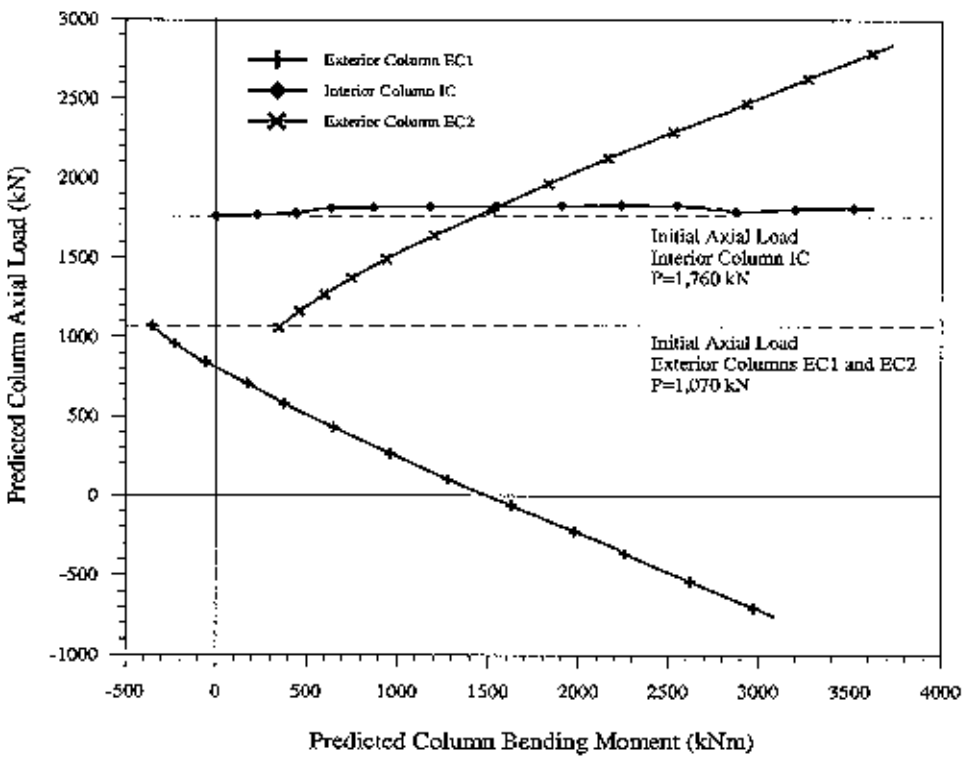

Fig. 6-3 Predicted Column Axial Load versus Bending Moment at the Cap Beam Interface

6.3 Joint Principal Tensile Stresses

Column member end forces (presented in the previous section) were used to estimate the joint principal tensile stresses. The joints of the test unit were designed using efficient force transfer models so that the amount of joint shear reinforcement could be minimized. A joint mechanism, requiring development of strut and ties outside the joint, was chosen for detailing of the joints. This mechanism, which requires the least amount of reinforcement within the joint, has been studied experimentally at UCSD **[3][4][5]**. An extensive treatment on detailing joints using force transfer mechanisms and experimental verification of joints detailed with external strut mechanisms may be found in references **[1]**, **[3]**, **[4]** and **[5]**.

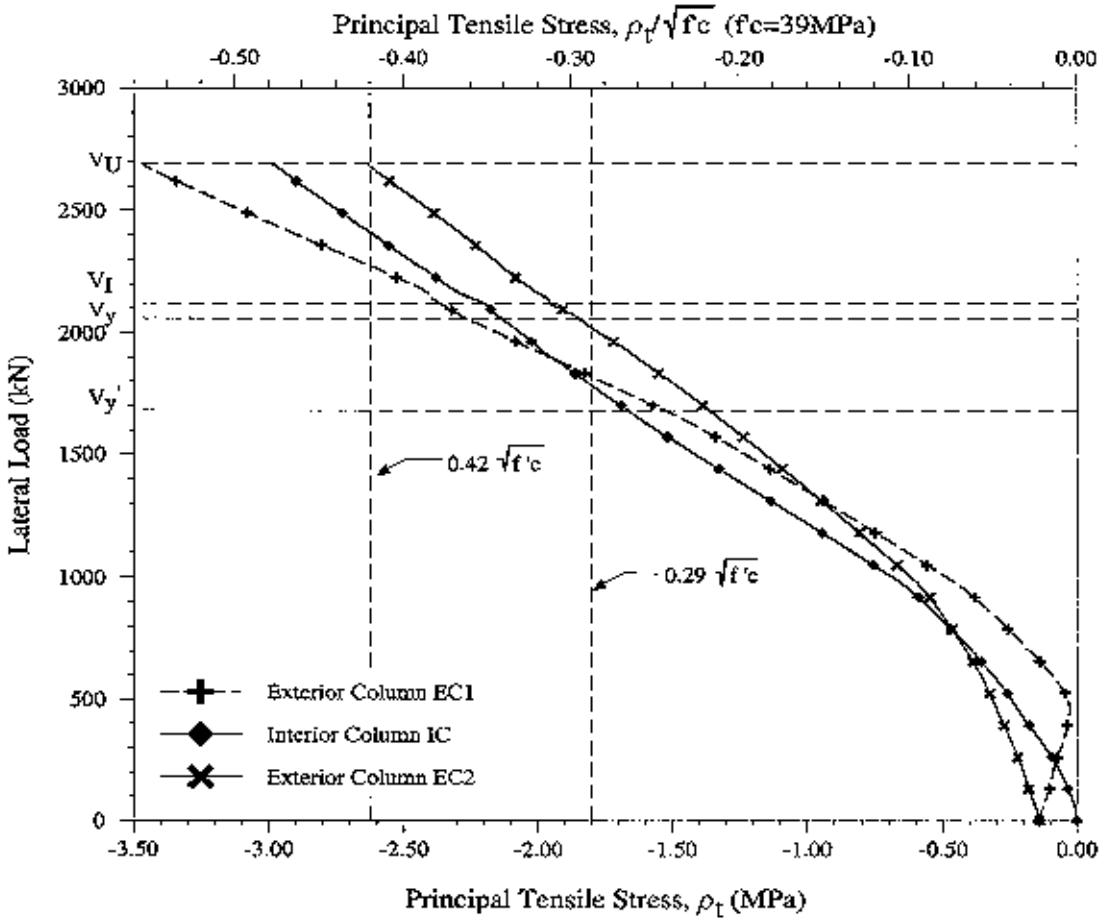

Fig. 6-4 Predicted Principal Tensile Stresses in the Joint Region

Referring to **Fig. 6-4**, average principal tensile stresses in the joint region at the ultimate limit state were estimated to be $p_t = 0.56\sqrt{f'_c}$, $p_t = 0.48\sqrt{f'_c}$ and $p_t = 0.42\sqrt{f'_c}$ in the joint regions at the exterior joint ***KJ1***, interior joint ***TJ*** and exterior joint ***KJ2***, respectively. Consequently, all joints were detailed according to the design models described in **Section 4.3**. Estimated principal tensile stresses of $p_t > 0.29\sqrt{f'_c}$ were achieved in the three joint regions between the theoretical first yield, V_y', and theoretical yield of the specimen, V_y, which indicate that joint shear cracking is most likely to develop in this load range. Estimated principal tensile stresses of $\rho_t \geq 0.42\sqrt{f'_c}$ were developed in the three joints beyond the theoretical ideal capacity of the test unit, V_I.

6.4 Columns Cover Concrete Spalling

Fig. 6-5 depicts the concrete model used in the modeling of the cover and the core concrete. Upper and lower bounds were investigated for spiral spacings that varied from concrete fully confined by the steel shell to a spiral spacing of 304.8 mm, which corresponds to the column spiral spacing below the cap beam interface. The gap at the interface with the cap beam was 50.8 mm. Modeling of the concrete core according to this spiral spacing would seem reasonable, however for design and analysis proposes a shorter spiral spacing should be used in order to avoid increased demands in the cap beam and joint regions. Because of the uncertainties in predicting the effective confinement provided by the steel shell in the gap region at the interface with cap beam, a spiral spacing of 25.4 mm was used in the model of the core concrete, and the cover concrete in this region was assumed unconfined.

Based on the concrete model presented in **Fig. 6-5**, the estimated cover concrete compression stresses in this gap region are presented in **Fig. 6-6**. Referring to **Fig. 6-6**, onset of spalling of the cover concrete was expected between displacement ductility $\mu_{1.5}$ and μ_2, and significant spalling at the displacement ductility of μ_6 was expected. These values matched with observations recorded during testing. In addition, **Fig. 6-7** depicts the expected forces that develop in the cover concrete to the contribution of the flexural strength of the column sections. Referring to **Fig. 6-7**, maximum forces that develop in the cover concrete are expected to occur between the displacement ductility $\mu_{1.5}$ and μ_2 and a rapid decrease in the contribution of these forces to the flexural strength are expected with significant decrease expected at the displacement ductility μ_6, which correlate with observations described in **Fig. 6-6** and during testing.

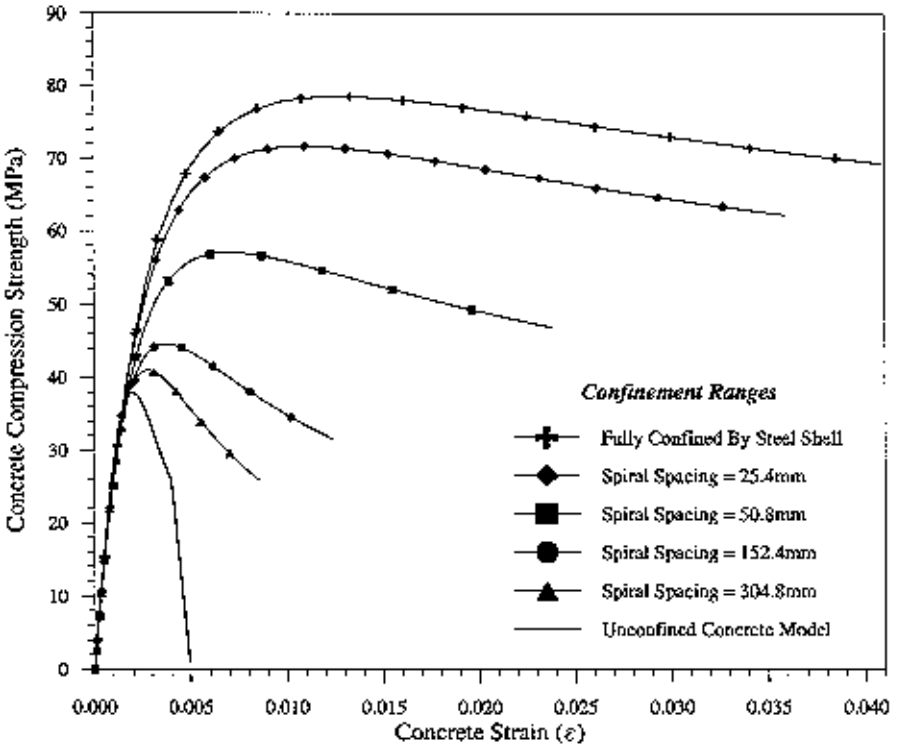

Fig. 6-5 Confined and Unconfined Pre-Test Analysis Concrete Models

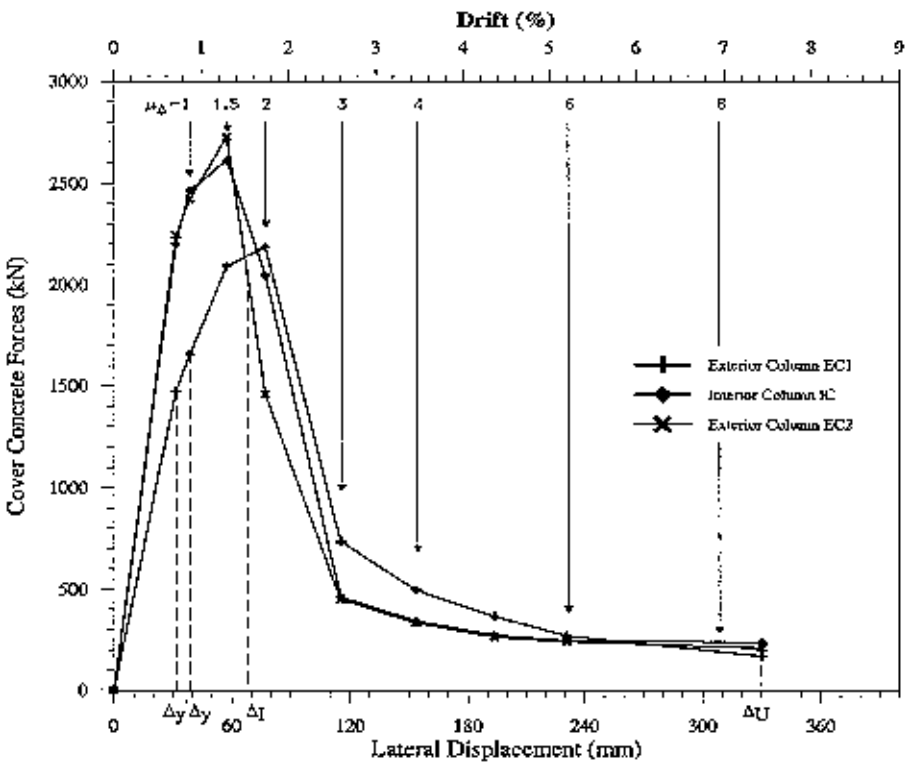

Fig. 6-6 Cover Concrete Forces

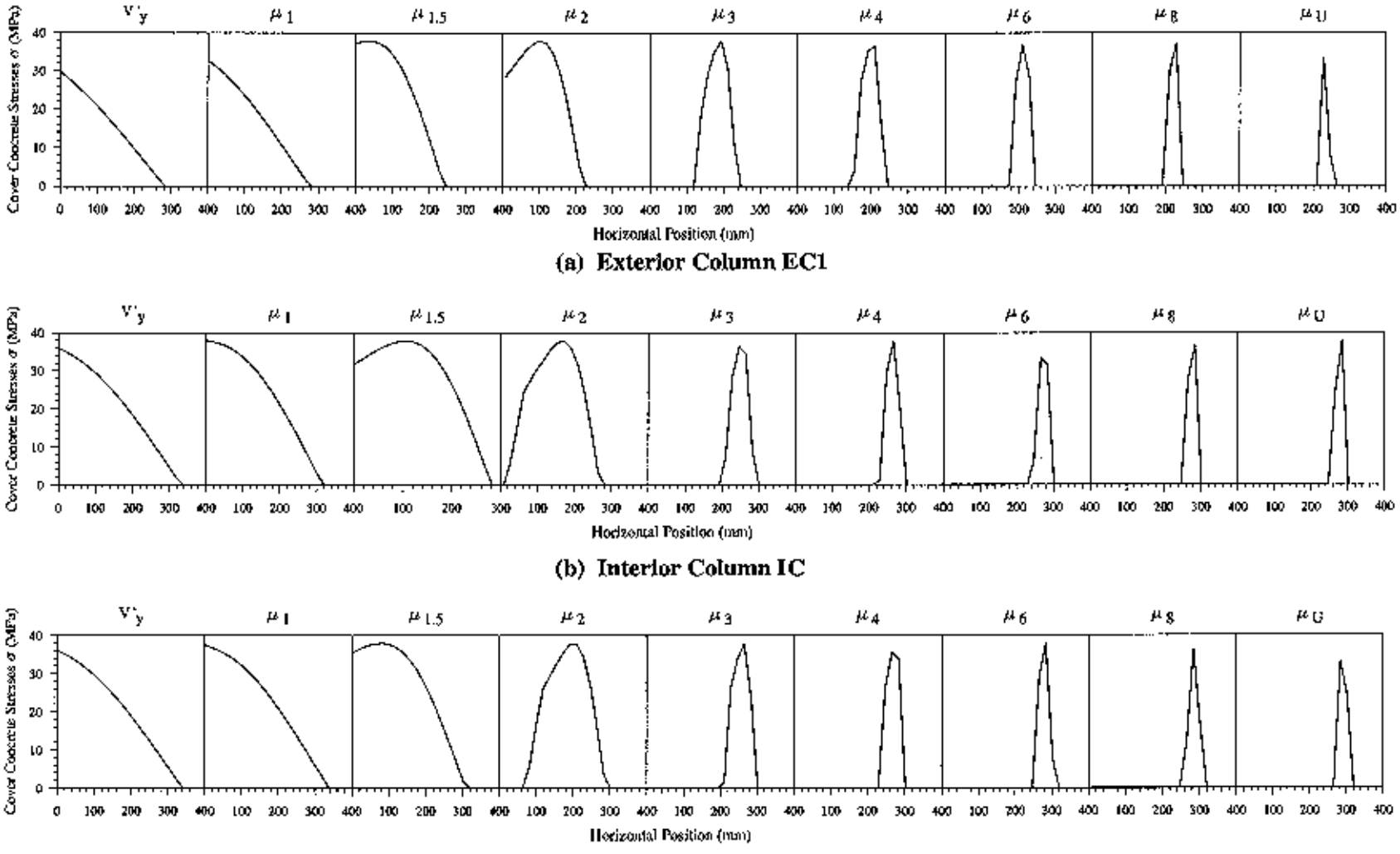

(a) Exterior Column EC1

(b) Interior Column IC

(c) Exterior Column EC2

Fig. 6-7 Cover Concrete Stresses Along Column Section at Different Loading Stages

7. Experimental Results

This chapter presents test observations recorded during seismic testing, and summarizes key experimental results, including force-deformation and reinforcement strain profiles for the columns and cap beam.

Seismic response of the test unit was simulated using a lateral load sequence with fully reversed cycles, as previously described in **Section 5.4**. In the push direction, the lateral load was designated as positive and in the pull direction the lateral load was designated as negative, as illustrated in **Fig.7-1**. The complete test setup of the multiple column unit is shown in **Fig.5-14.**

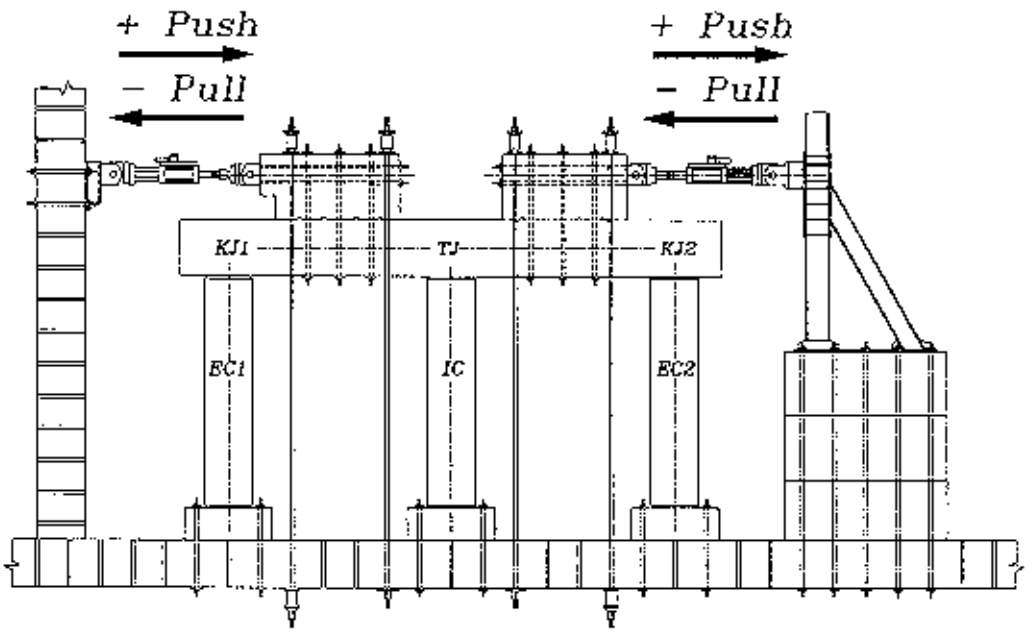

Fig.7-1 Loading Scheme Designation

7.1 Test Observations

General test observations that were recorded during the test (i. e. gravity load, and force and displacement controlled lateral cycles) are summarized in the next sections.

7.1.1 Simulation of Gravity Load

The first stage in the testing procedure consisted of applying the axial load to simulate gravity loads effects. The axial load was applied in three stages. Application of the gravity load is presented in this section.

In the first stage, a 306 kN force was applied to each bar present in the axial loading fixtures at positions *1, 2 ,3* and *4*, (see **Fig.5-35**). This axial load corresponded to 50% of the total axial load to be applied at each of these exterior bars. Next, an axial load of 223 kN was applied to the interior bars at positions ***A***, ***B***, ***C*** and ***D***, (see **Fig.5-35**). This axial load corresponded to 100% of the final axial load to be applied at each of these interior bars. Finally, an additional 306 kN of force was applied at positions *1, 2 ,3* and *4*, for a total axial load of 612 kN per bar. At this stage, the test unit displayed no signs of distress and the first cycles under force control were applied to the test unit.

Although the axial load was to remain constant throughout the test, some variations were encountered in the recorded axial load due to the application of the reversed lateral cyclic loading. **Fig.7-2(a)** through **Fig.7-2(d)** depict the gravity load response for load cells *1, 2 ,3* and *4* during the testing procedure. It can be seen that the axial load recorded in load cells *3* and *4* were slightly below the target gravity load, beyond the displacement ductility of μ_4, while load cells *1* and *2* recorded axial loads closer to the target load even at large lateral displacements. In the pre test analysis, the target gravity load of 612 kN was assumed in each of the bars at positions *1, 2 ,3* and *4*.

Fig.7-3 depicts the axial load measured by the pressure transducer at positions ***A, B, C*** and ***D*** during the testing procedure. Minimum changes were observed in the axial load at these positions.

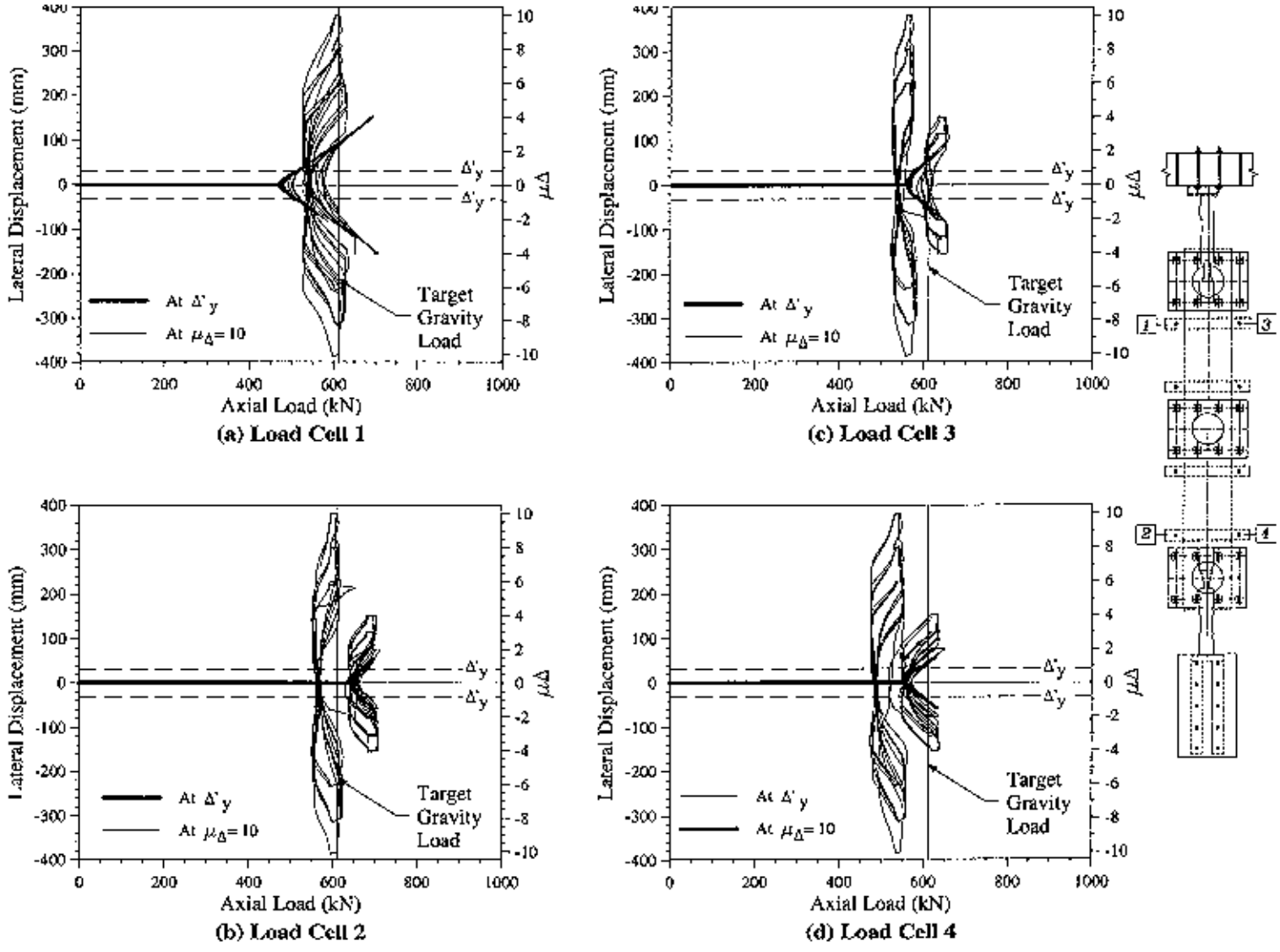

Fig.7-2 Gravity Load Response for Load Cells at Positions *1* , *2*, *3* and *4*

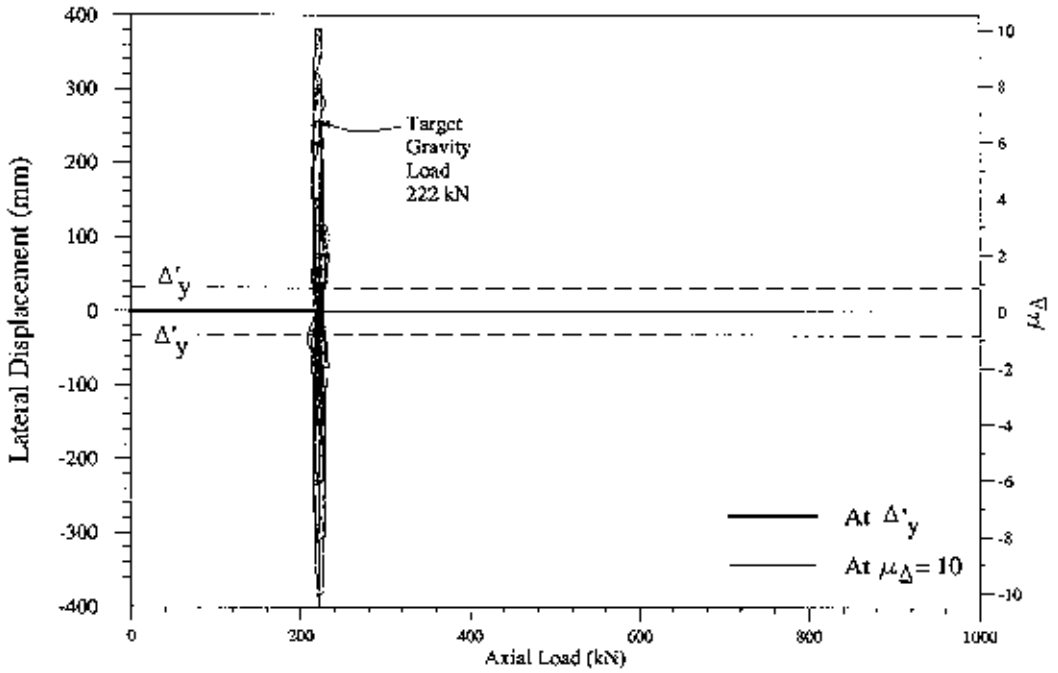

Fig.7-3 Axial Load Measured by Pressure Transducer at Positions ***A***, ***B***, ***C*** and ***D***

7.1.2 Force Controlled Load Cycles

After application of gravity loads, the first lateral load four cycles were performed under force control. At each successive cycle, the test unit was subjected to equal lateral load increments that corresponded to 25%, 50%, 75% and 100% of the theoretical first yield lateral force estimated in the pretest analysis. In each cycle, when the lateral load reached the peak values in the push and pull directions, the test was stopped in order to assess the damage to the test unit. Observations recorded during these first four cycles are described below.

At $\pm 0.25V_y$ (V_{max} = +414 kN, V_{min} = -445 kN)

During this cycle no signs of physical distress were observed to the test unit, and the recorded lateral deflection was ±2.17 mm.

At $\pm 0.50V_y$ (V_{max} = +829 kN, V_{min} = -827 kN)

In this cycle a lateral displacement of ±8.22 mm was obtained. When the lateral load reached its peak value in the push direction, loss of hydraulics to the horizontal actuators caused a sudden drop in the lateral load. Loading of the test unit was immediately restarted to the pull direction. In this cycle, flexural cracking was first observed in all three columns in both loading directions. In exterior column ***EC1*** a single horizontal crack was observed approximately at the center of the gap, as seen in **Fig.7-4**. In interior column ***IC*** a single horizontal crack was observed immediately above the steel shell. In column ***EC2*** a single horizontal crack was observed at the cap beam / column interface, as depicted in **Fig.7-5**. However, at this stage flexural cracking in the cap beam was only observed in the vicinity of the exterior columns ***EC1*** (*Push* direction) and ***EC2*** (*Pull* direction), as illustrated in **Fig.7-4** and **Fig.7-6**, and no signs of physical distress were observed in the vicinity of the interior column ***IC***.

At $\pm 0.75V_y$ (V_{max} = +1,148 kN, V_{min} = -1,152 kN)

At peak lateral loads the lateral displacement was ±14.83 mm. Separation of expansion joint filler pads, at the pin connection, was observed in all three columns, as depicted in **Fig.7-7**. Extension of previous cracks was observed and no damage to the joints had occurred at this stage.

At $\pm V_y$ (V_{max} = +1,682 kN, V_{min} = -1,670 kN)
First Yield

The measured lateral displacement in this cycle was ±30.92 mm. First diagonal shear cracking in the joint regions was observed in the three joints in both loading directions. **Fig.7-8**, **Fig.7-9** and **Fig.7-10** depict the cracking pattern in joint regions ***KJ1***, ***TJ*** and ***KJ2***, respectively. In addition, cap beam flexural cracking in the top surface at exterior joint ***KJ2*** was first observed in this cycle, as illustrated in **Fig.7-11**.

Fig.7-4 Flexural Cracking at $+0.50V_y$ - Exterior Column ***EC1***

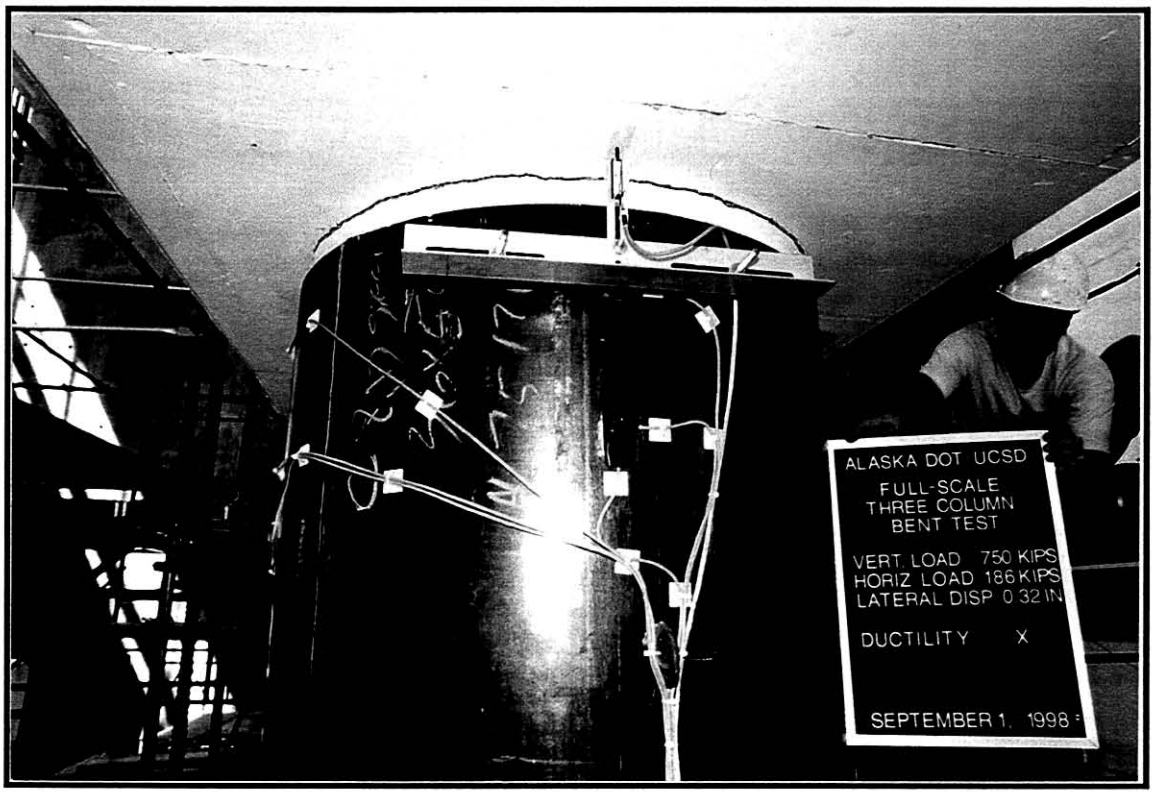

Fig.7-5 Flexural Cracking at $+0.50V_y$ - Exterior Column ***EC2***

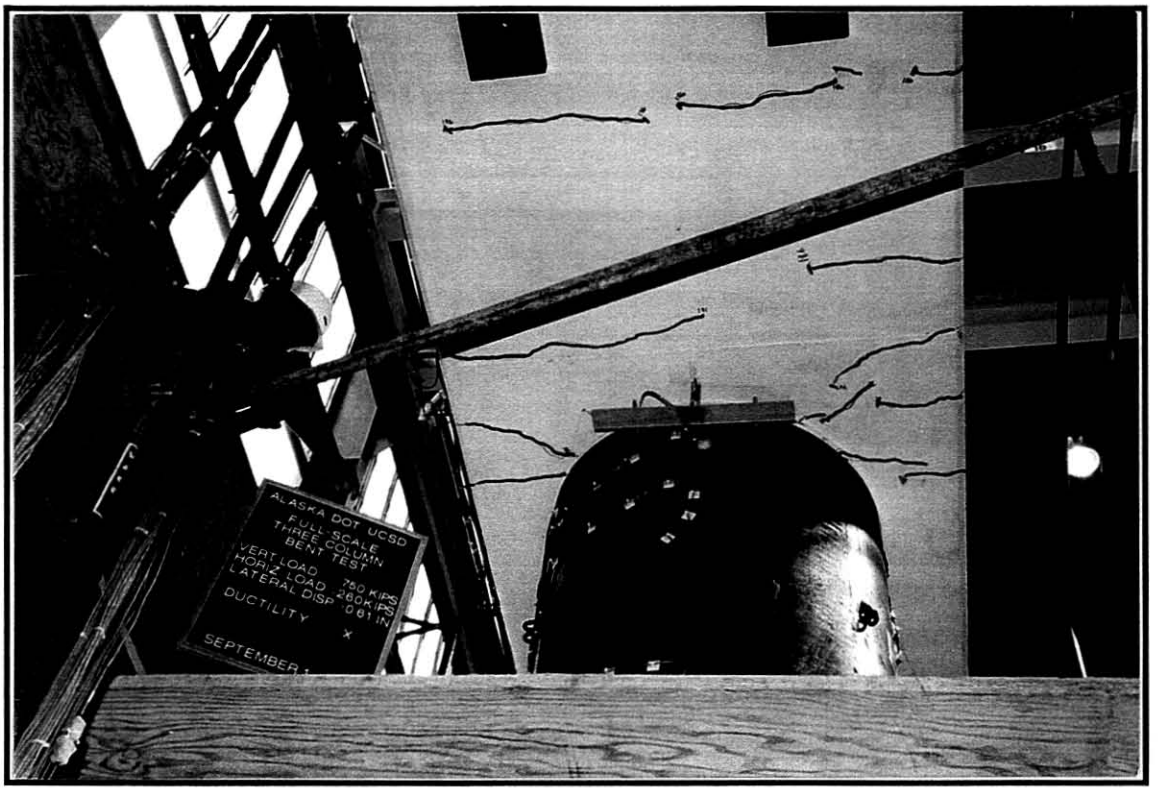

Fig.7-6 Flexural Cracking at $-0.50V_y$ - Exterior Column ***EC2***

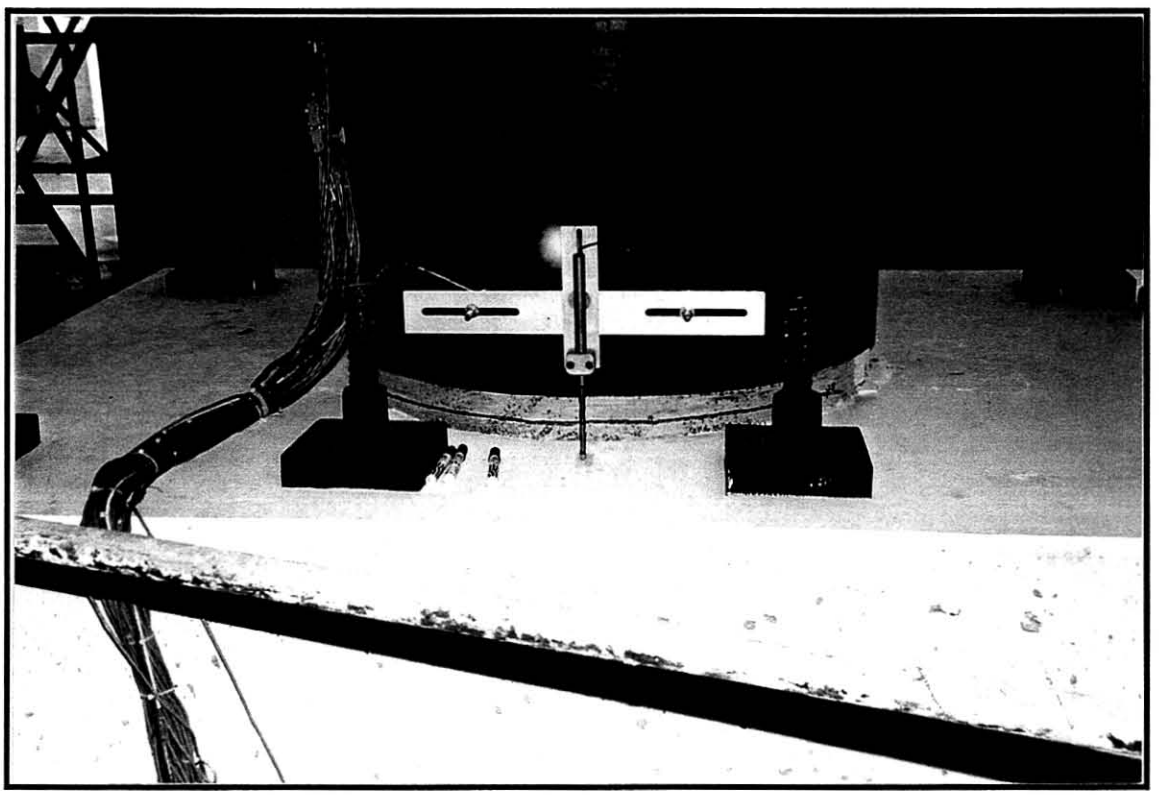

Fig.7-7 Separation of Expansion Joint Filler Pads at $\pm 0.75V_y$

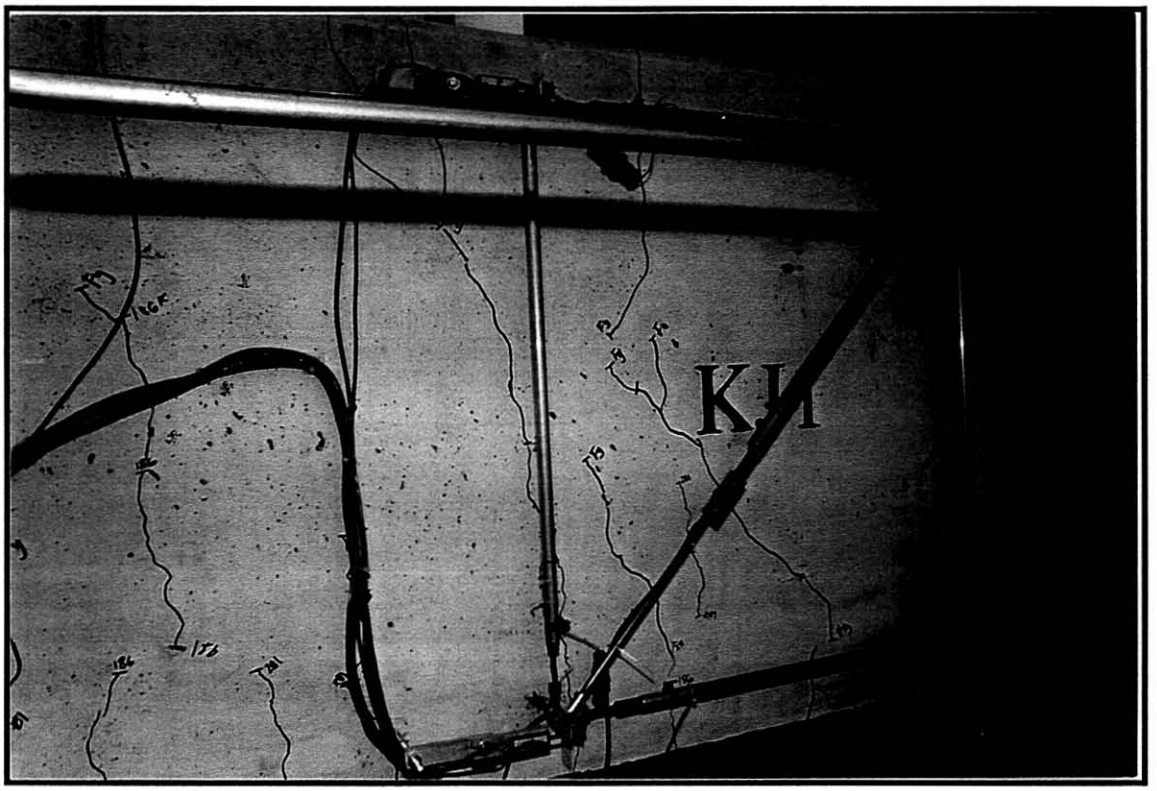

Fig.7-8 Joint Shear Cracking at $\pm V_y$ - Exterior Joint ***KJ1***

Fig.7-9 Joint Shear Cracking at $\pm V_y$ - Interior Joint ***TJ***

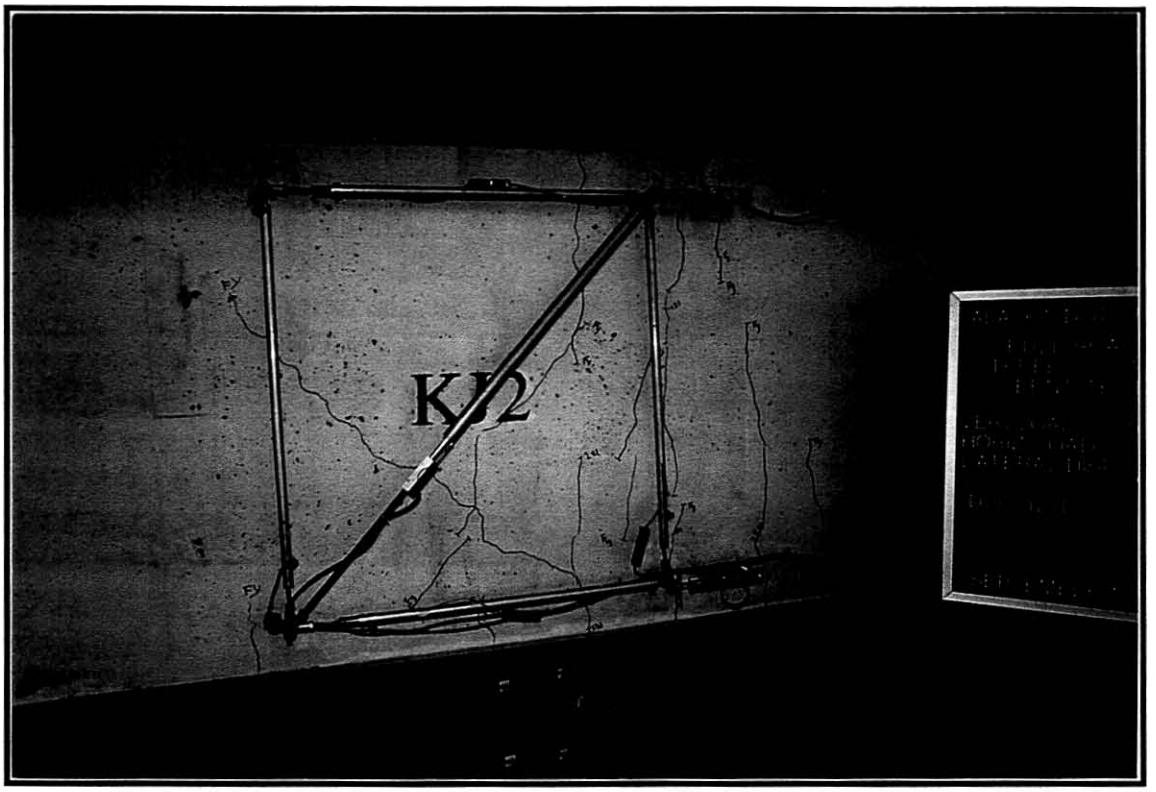

Fig.7-10 Joint Shear Cracking at $\pm V_y$ - Exterior Joint ***KJ2***

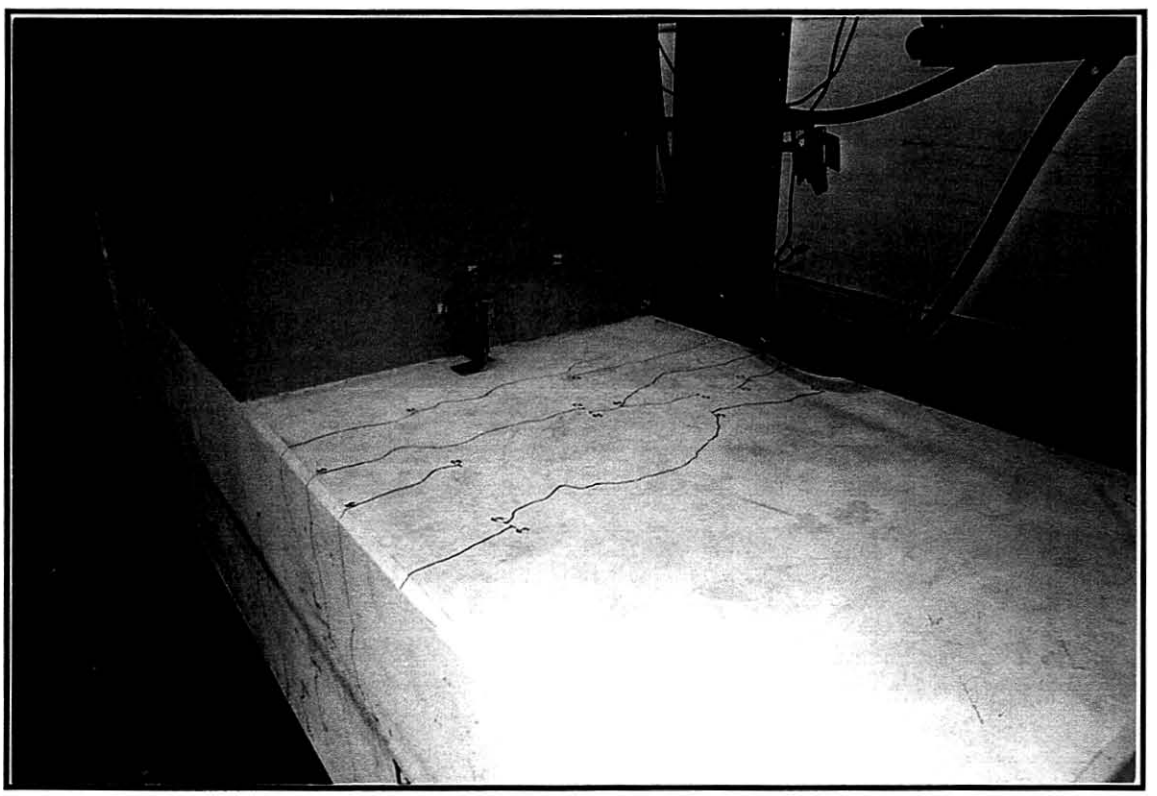

Fig.7-11 Cap Beam Flexural Cracking at $\pm V_y$ - Exterior Joint ***KJ2***

7.1.3 Displacement Controlled Load Cycles

After the force controlled load cycle up to 100% of the theoretical first yield lateral load, the loading pattern was changed from single cycles in force control to three cycles in displacement control according to the displacement ductility levels outlined in **Section 6.3**. In the displacement control cycles, the test was temporarily stopped in the first and third cycles in the push and pull direction in order to assess the damage occurred to the test unit.

3 cycles at μ_Δ= ±1 (Column drift = 0.9%, V_{max} = +1,914 kN, V_{min} = -1,812 kN)

Extension of previous joint cracks was observed, as shown in **Fig.7-12**. Flexural cracking was first observed to the top surface of the cap beam at exterior column ***EC1***, as illustrated in **Fig.7-13**. In addition, in this cycle, spalling of the cover concrete in the gap at the column top occurred at the interior column ***IC***, as visible in **Fig.7-14**. **Fig.7-14** shows radial cracks that propagate outwards from the interior column ***IC***, which is a characteristic of strain penetrations in the column longitudinal reinforcement. Similar observations were also recorded in the vicinity of the exterior columns ***EC1*** and ***EC2***, as depicted in **Fig.7-15**.

At the end of the third cycle at this displacement ductility level, the test was stopped and the testing was continued on the following day after applying the initial axial load as previously.

3 cycles at μ_Δ= ±1.5 (Column drift = 1.3%, V_{max} = +2,229 kN, V_{min} = -2,064 kN)

Extension of previous cracks through the joint regions was recorded at this stage. During the first cycle at this displacement ductility level, onset of spalling of the cover concrete was observed at the column top in exterior columns ***EC1*** and ***EC2***. At the end of the third cycle it was noted that previous column flexural cracks were noticeably widened in all the three columns in the cracks that initially developed in the columns interface at the cap beam.

3 cycles at μ_Δ= ±2 (Column drift = 1.8%, V_{max} = +2,304 kN, V_{min} = -2,136 kN)

No further significant damage was recorded in either of the cycles at this displacement ductility level, and minor spalling of the cover concrete that occurred in columns ***EC1*** is shown in **Fig.7-16**

3 cycles at $\mu_\Delta = \pm 3$ (Column drift = 2.6%, $V_{max} = +2{,}532$ kN, $V_{min} = -1{,}944$ kN)

Radial cracking at the bottom surface of the beam around the perimeter of all three columns was noticeably widened, as illustrated in **Fig.7-17**. Crack pattern on bottom surface of the cap beam in the vicinity of exterior columns ***EC1*** and ***EC2*** include similar radial cracking, as shown in **Fig.7-17**. Based on the pre test analysis it was estimated that at this stage significant spalling in the cover concrete would have occurred, as discussed in **Section 6.4**. However, based on **Fig.7-17** it is clear that spalling of the cover concrete was significantly less than predicted. No significant increase in damage in the joint regions was observed in this ductility level.

3 cycles at $\mu_\Delta = \pm 4$ (Column drift = 3.4%, $V_{max} = +2{,}572$ kN, $V_{min} = -2{,}404$ kN)

No significant changes to the crack pattern in the joint regions were observed at this ductility level, as shown in **Fig.7-18**. Extent of damage to the cap beam bottom surface near the interior column ***IC*** is depicted in **Fig.7-19**, which shows development of further radial cracks. In addition, it can be seen, in **Fig.7-19**, that spalling of the cover concrete had not occurred to the extent that the longitudinal reinforcement would be visible, as predicted from the results presented in **Section 6.4**.

3 cycles at $\mu_\Delta = \pm 6$ (Column drift = 5.2%, $V_{max} = +2{,}756$ kN, $V_{min} = -2{,}410$ kN)

The maximum lateral force resistance of the test unit was recorded during the first cycle in the push direction at this loading stage. Significant damage to the cap beam bottom surface concrete was observed near the vicinity of the columns (see **Fig.7-20** and **Fig.7-21**). In the first cycle to this ductility level the linear potentiometers measuring rotations at the top of the columns were disconnected because of excessive damage in the underside faces of the cap beam where these linear potentiometers were connected. In addition, **Fig.7-20** depicts the cover concrete in the gap region had not yet completely spalled off, which was not sufficiently predicted in the pretest analysis, as previously described in **Section 6.4**.

3 cycles at $\mu_\Delta = \pm 8$ (Column drift = 6.9%, $V_{max} = +2{,}716$ kN, $V_{min} = -2{,}360$ kN)

No new joint cracks were observed, which indicated that column input forces into the joint regions did not increase from previous cycles. However, increase in damage in the cap beam concrete bottom surface was accentuated in the vicinity of interior column ***IC*** and exterior column ***EC2*** (see **Fig.7-22** and **Fig.7-23**). Slight drop in the lateral force was recorded in the first cycle at $\mu_\Delta = +8x1$ when compared to that in the first cycle at $\mu_\Delta = +6x1$.

3 cycles at $\mu_\Delta = \pm 10$ (Column drift = 8.6%, V_{max} = +2,486 kN, V_{min} = -1,934 kN)
End of the Test

Fracture of column longitudinal reinforcement occurred in all three columns at this ductility level, which implied the ultimate flexural strength of the columns was achieved. The fracture first occurred in the column longitudinal reinforcement in the first cycle to displacement ductility μ_{10}, which correlated well with the analytical prediction that fracture of the longitudinal reinforcement should occur beyond the displacement ductility μ_8, as described by event ***10*** in **Fig. 6-1**. Post-test investigations conferred that a total of four bars fractured in the column longitudinal reinforcement. One each in column ***EC1*** and ***IC***, and two in column ***EC2***. **Fig.7-24** depicts the displaced shape of exterior column ***EC1***. The damage to joint region ***KJ1*** at the end of the test is shown in **Fig.7-25**. Comparable damage limited to only distributed cracking was also observed for the other two joints. This confirmed that the seismic behavior of the test unit was not significant influenced by the joint response and the details adopted for the joints were satisfactory despite the provided reinforcement was less than that required by a procedure based directly on shear forces. **Fig.7-26** (Push) and **Fig.7-27** (Pull) show the crack pattern on the bottom surface of the cap beam in the vicinity of exterior columns ***EC1*** and ***EC2***. As would be expected from symmetry of the specimen and load pattern the two crack patterns are similar. Similar observations may also be deduced from **Fig.7-28** (Pull) and **Fig.7-29** (Push). **Fig.7-30** and **Fig.7-31** depict the crack pattern on the cap beam bottom surface in the vicinity of interior column ***IC*** in the Push and Pull directions, respectively. The extent of damage that occurred o the top and bottom of the columns are comparable in all the three columns and is shown in **Fig.7-32** and **Fig.7-33**.

In conclusion, test observations confirm that failure did not occur in the joints, which allowed the test specimen to develop its ultimate moment capacity. Moreover, response of the test unit illustrates that the models developed at UCSD for joint design were adequate for the seismic design of the joints. Ultimate displacement capacity of the test specimen was characterized by low cycle fatigue fracture of the column longitudinal reinforcement and matched satisfactorily with the theoretically predicted failure mode. Condition of the test unit at the peak maximum displacement are depicted in **Fig.7-34** and **Fig.7-35**.

Fig.7-12 Joint Shear Cracking at $\mu_\Delta = \pm 1x1$ - Exterior Joint ***KJ1***

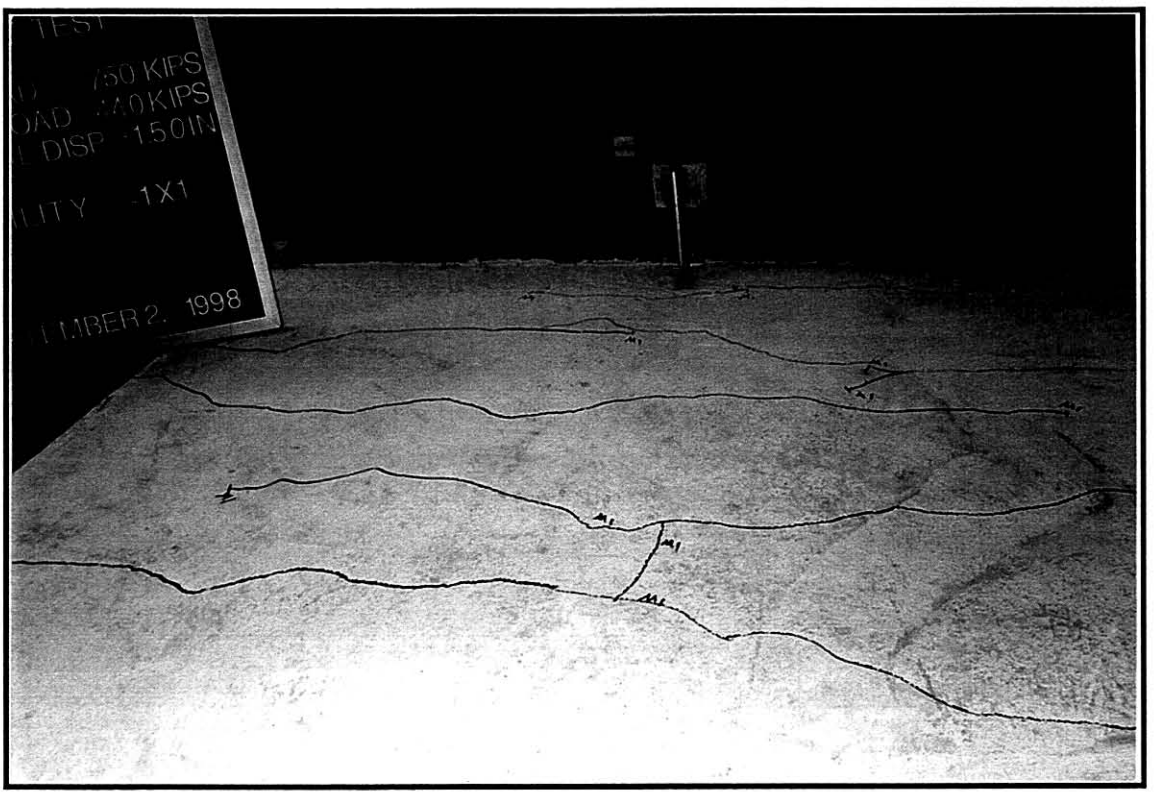

Fig.7-13 Flexural Cracks on Top of the Cap Beam - Exterior Joint ***KJ1***

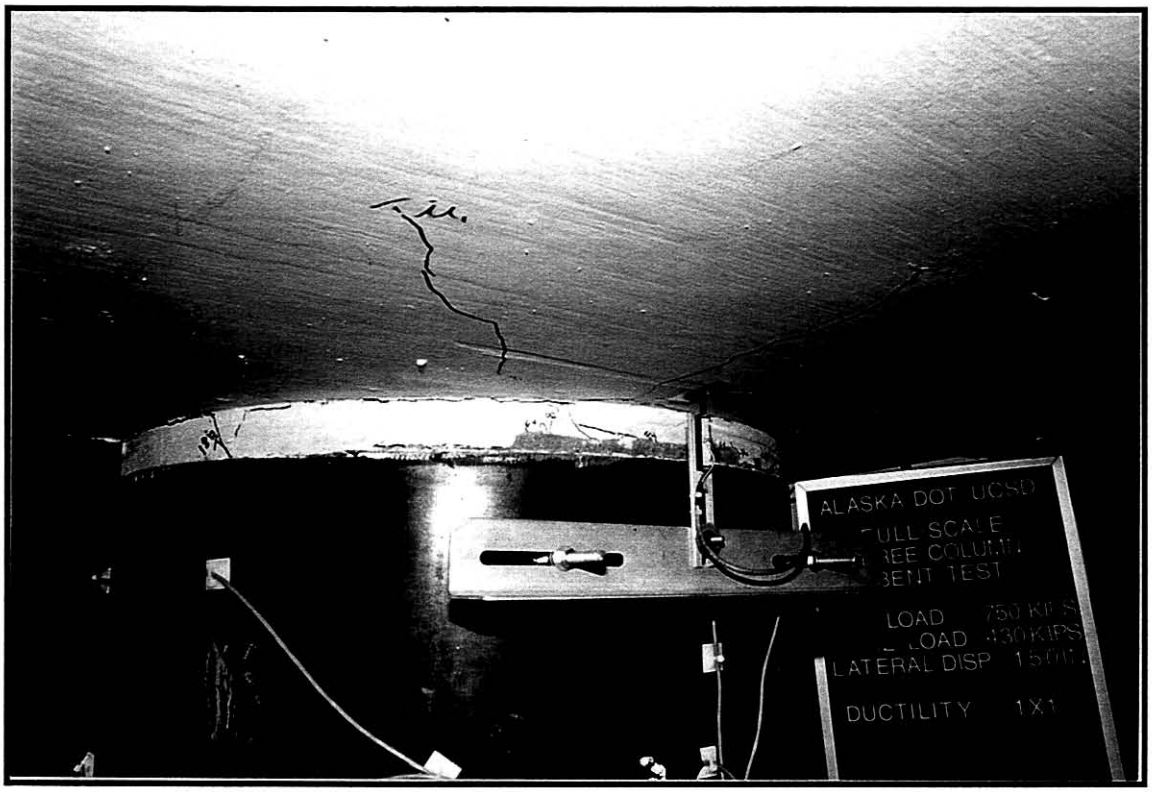

Fig.7-14 Spalling of Cover Concrete and Initiation of Radial Cracks on the Bottom Beam Surface - Interior Column ***IC***

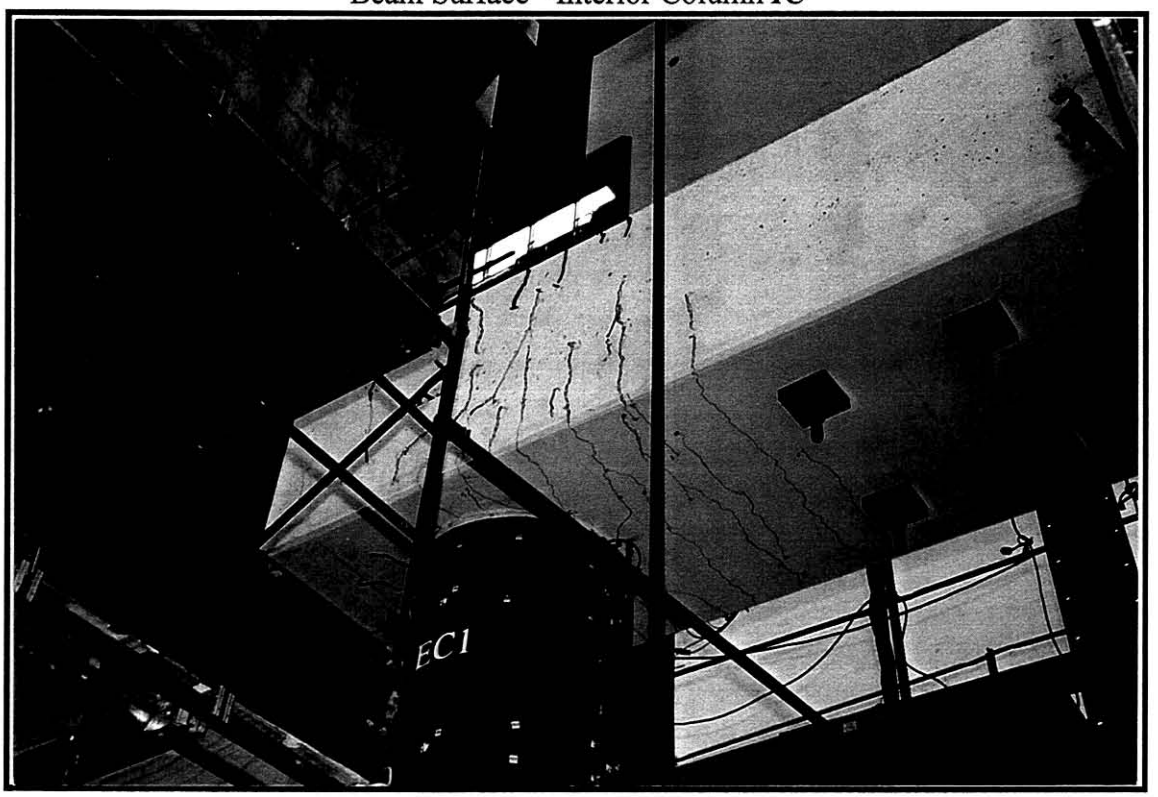

Fig.7-15 Cap Beam Cracking at $\mu_\Delta = \pm 1x1$ - Exterior Joint ***KJ1***

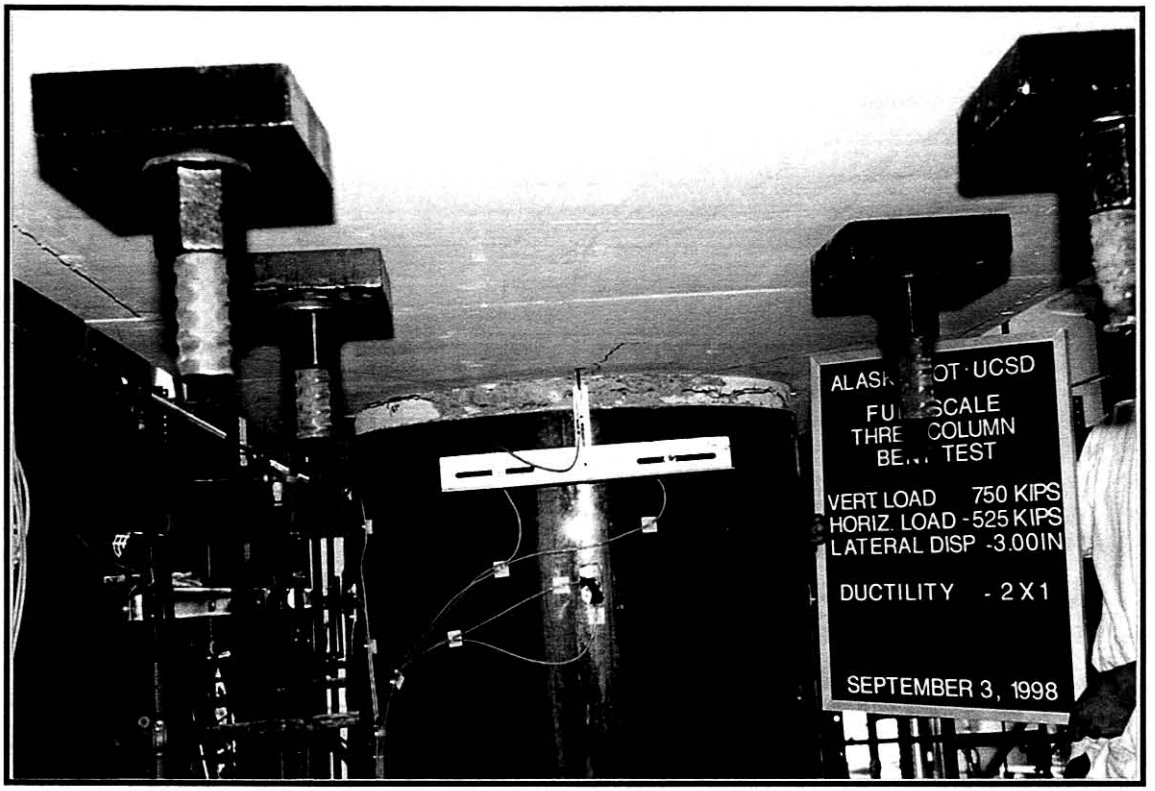

Fig.7-16 Extent of Spalling of Cover Concrete at $\mu_\Delta = \pm 2x1$ - Interior Column ***IC***

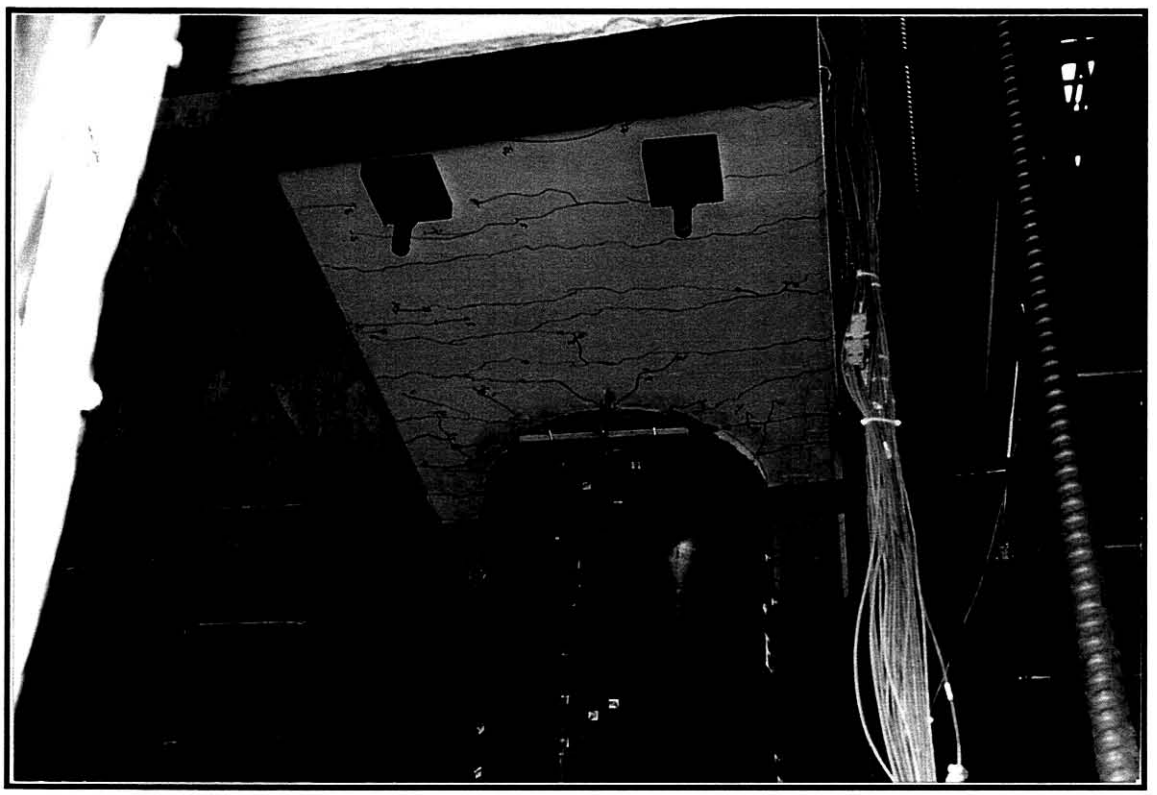

Fig.7-17 Cap Beam Cracking at $\mu_\Delta = \pm 3x3$ - Exterior Column ***EC1***

Fig.7-18 Joint Region Cracking at $\mu_\Delta = \pm 4x3$ - Interior Joint ***TJ***

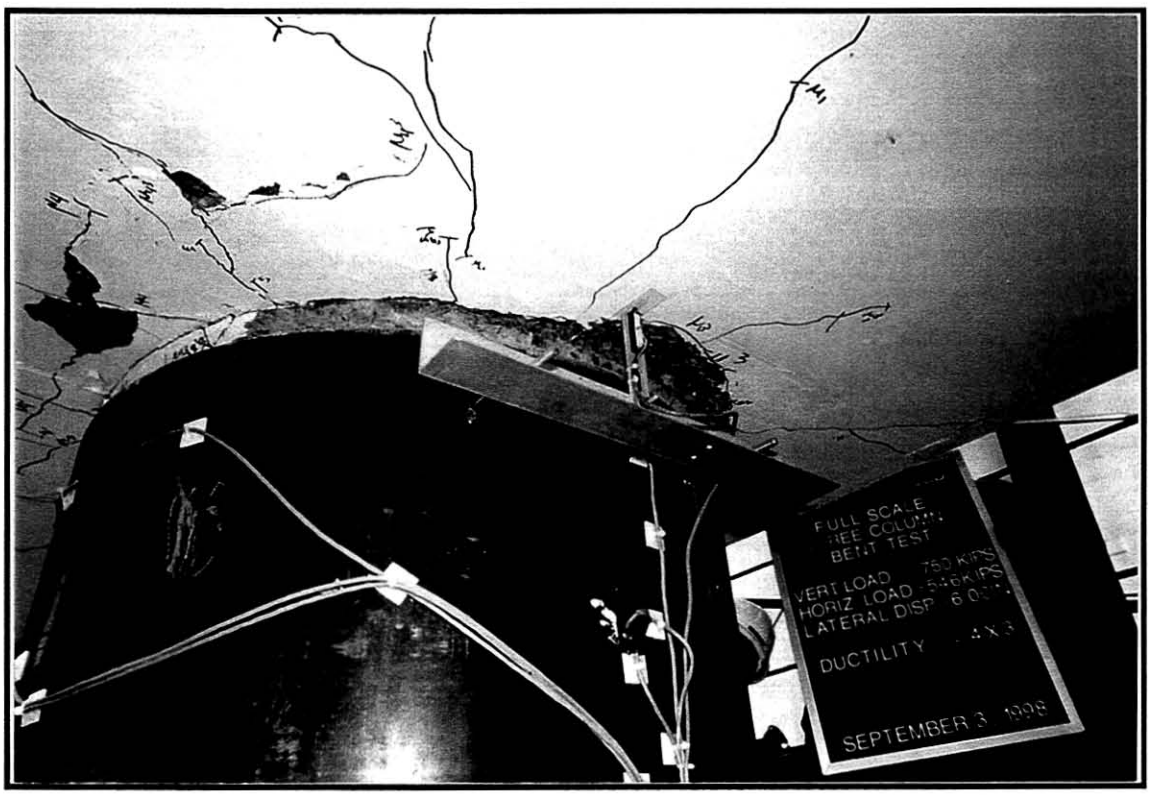

Fig.7-19 Cap Beam Cracking at $\mu_\Delta = \pm 4x3$ - Interior Column ***IC***

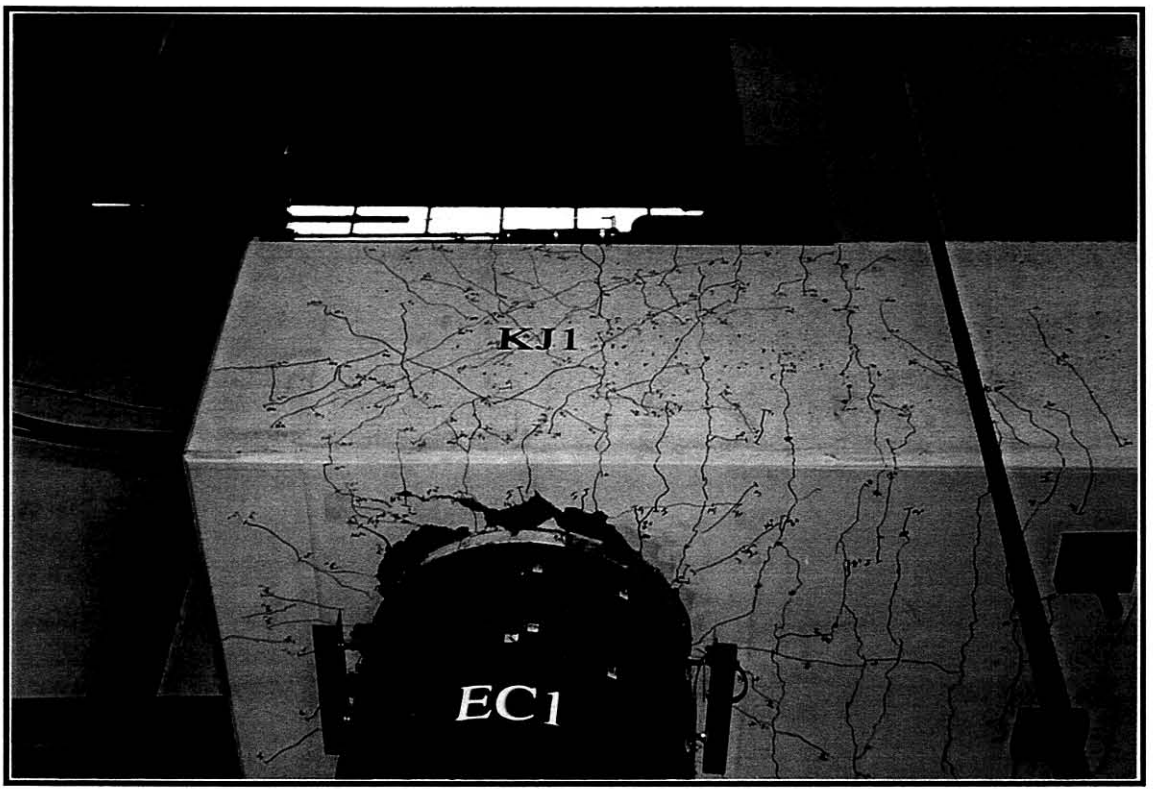

Fig.7-20 Joint Region Cracking at $\mu_\Delta = \pm 6x3$ - Exterior Joint ***KJ1***

Fig.7-21 Joint Region Cracking at $\mu_\Delta = \pm 6x3$ - Interior Joint ***TJ***

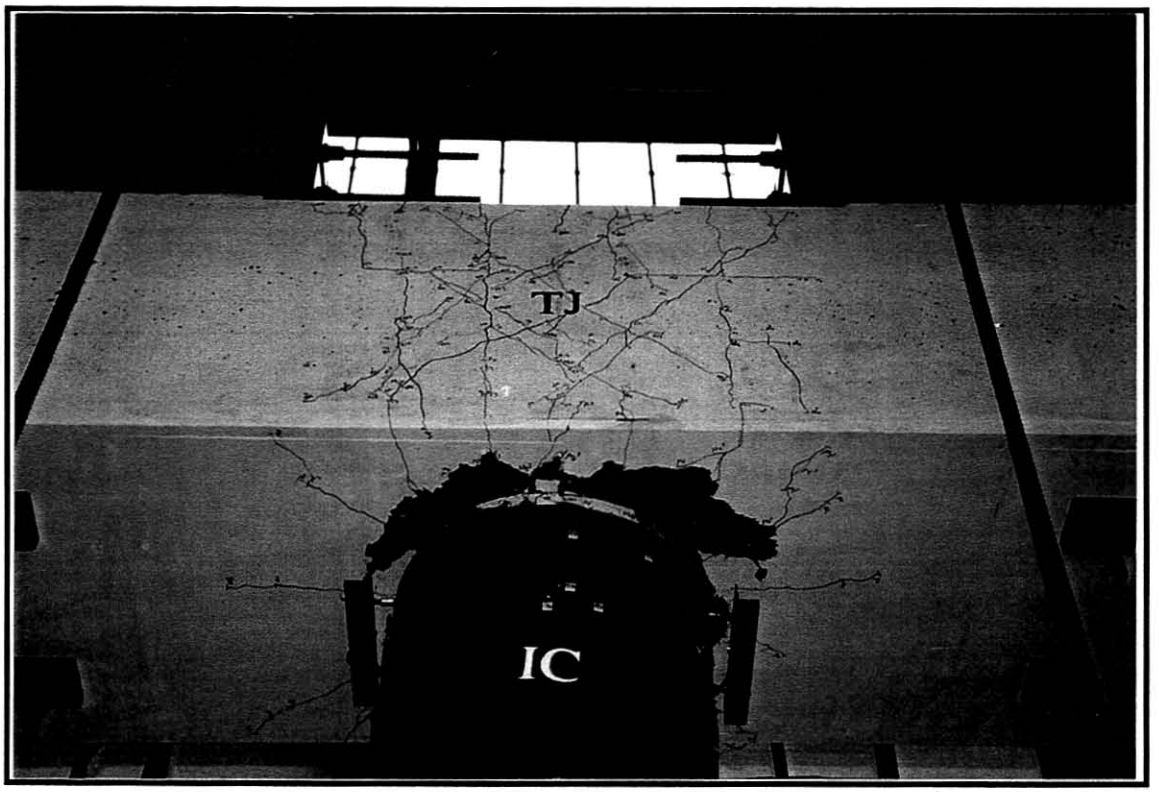

Fig.7-22 Damage to Joint Region at $\mu_\Delta = \pm 8x3$ - Interior Joint ***TJ***

Fig.7-23 Damage to Joint Region at $\mu_\Delta = \pm 8x3$ - Exterior Joint ***KJ2***

Fig.7-25 Column Deformation at $\mu_\Delta = \pm 10x3$
Exterior Column ***EC1***

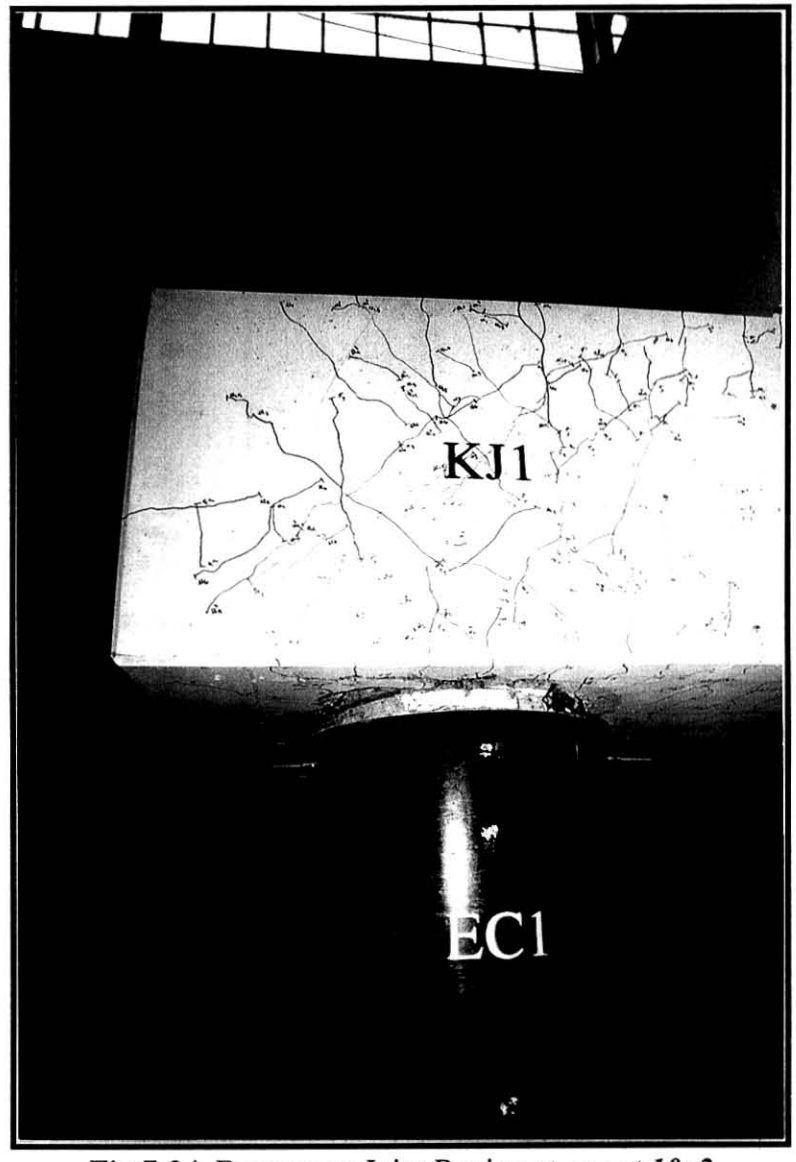

Fig.7-24 Damage to Joint Region at $\mu_\Delta = \pm 10x2$
Exterior Joint ***KJ1***

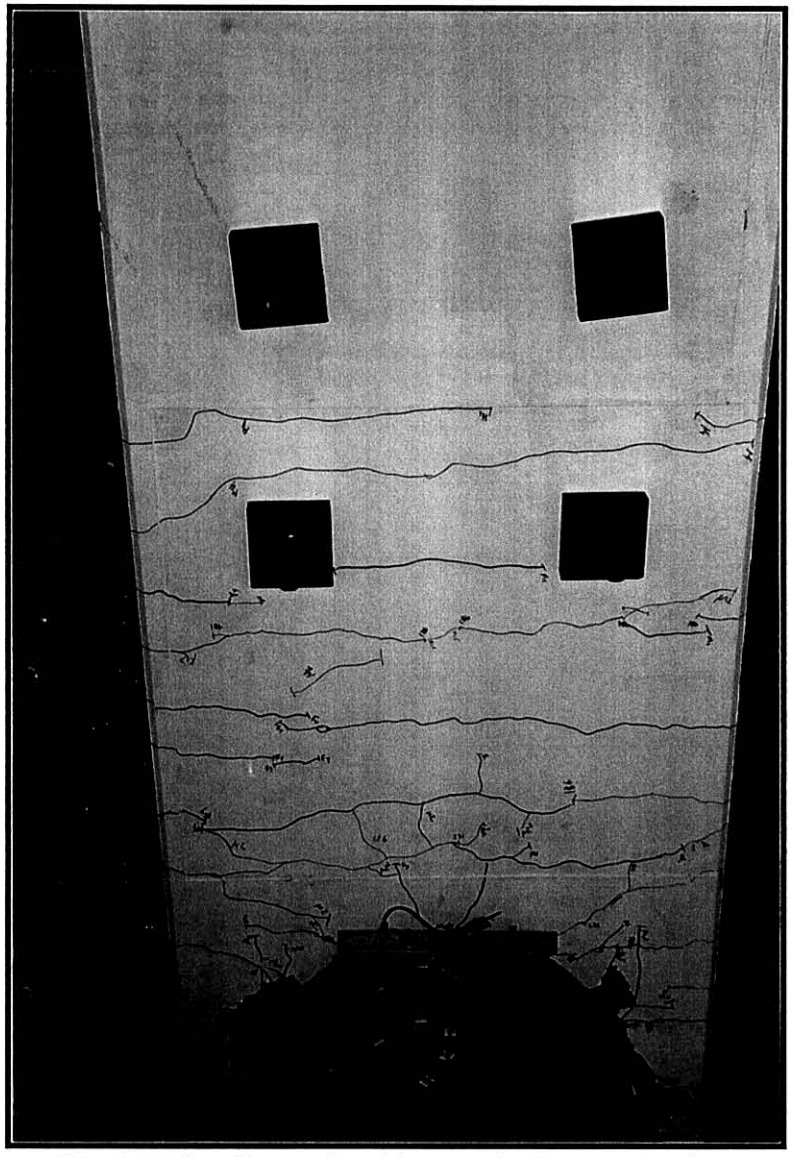

Fig.7-27 Cap Beam Cracking on the Bottom Surface
at μ_Δ= *-10x2 (Pull)* - Exterior Joint ***KJ2***

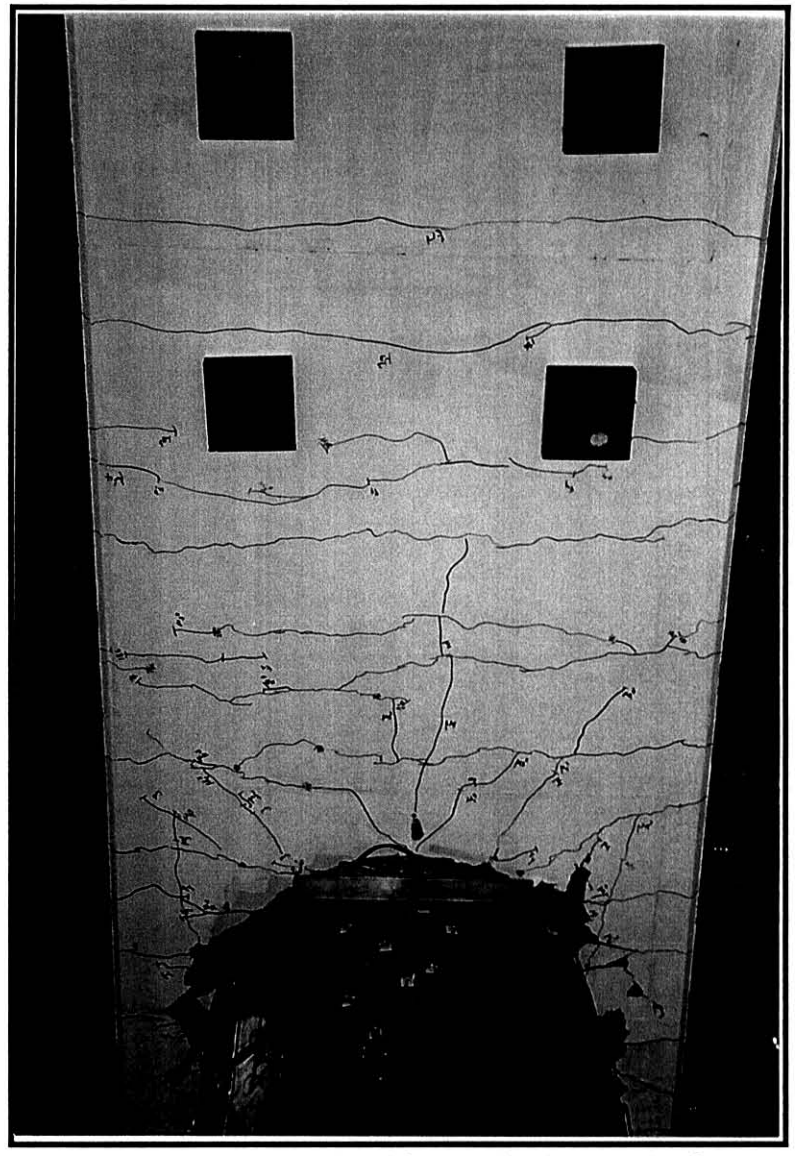

Fig.7-26 Cap Beam Cracking on the Bottom Surface
at μ_Δ= *±10x2 (Push)* - Exterior Joint ***KJ1***

Fig.7-28 Strain Penetration Damage at μ_Δ= ***-10x2 (Pull)*** - Exterior Joint ***KJ1***

Fig.7-29 Strain Penetration Damage at μ_Δ= ***+10x2 (Push)*** - Exterior Joint ***KJ2***

Fig.7-30 Strain Penetration Damage at μ_Δ= ***+10x2 (Push)*** - Interior Joint ***TJ***

Fig.7-31 Strain Penetration Damage at μ_Δ= ***-10x2 (Pull)*** - Interior Joint ***TJ***

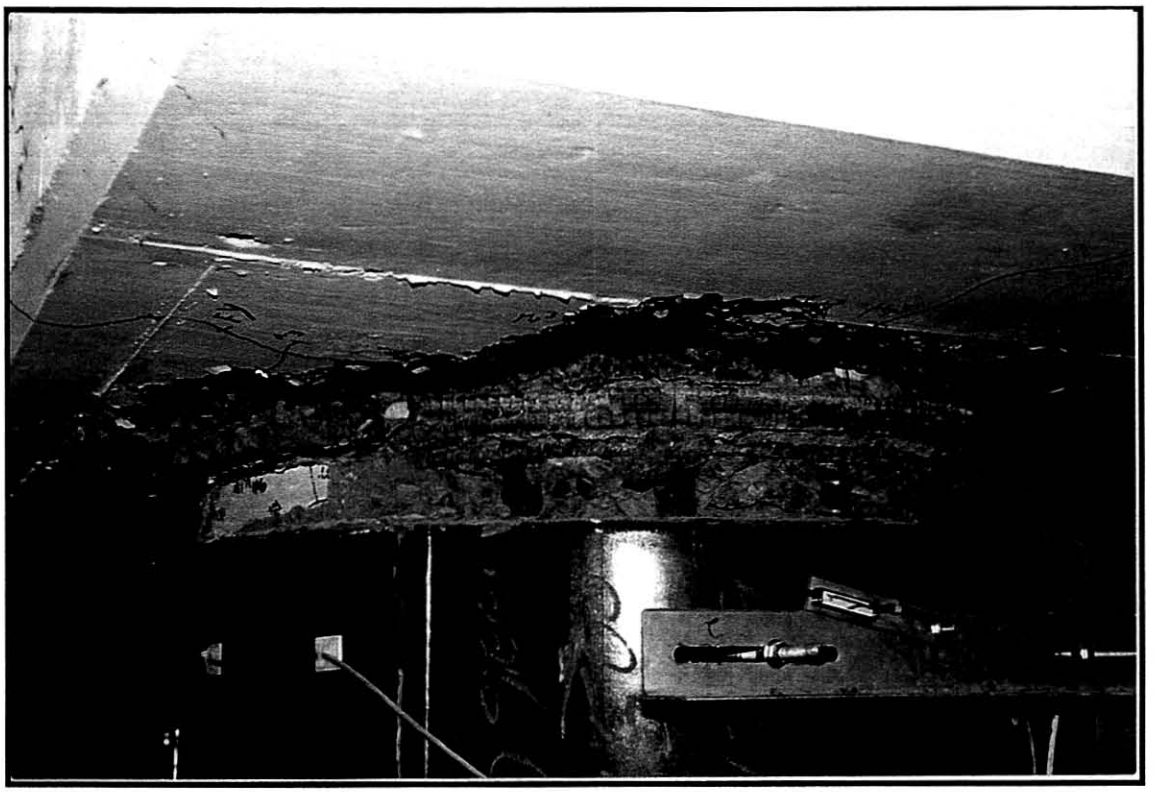

Fig.7-32 Extent of Spalling - Typical at Top of All Three Columns

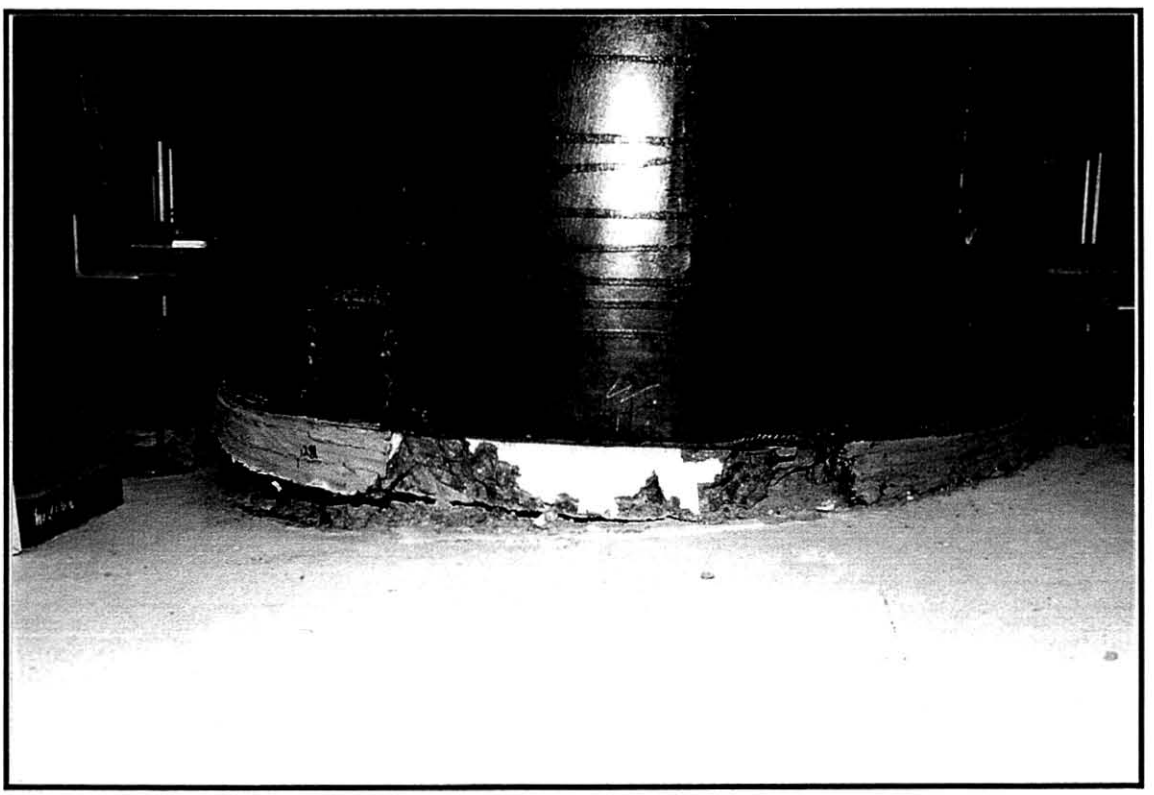

Fig.7-33 Extent of Spalling - Typical at Base of All Three Columns

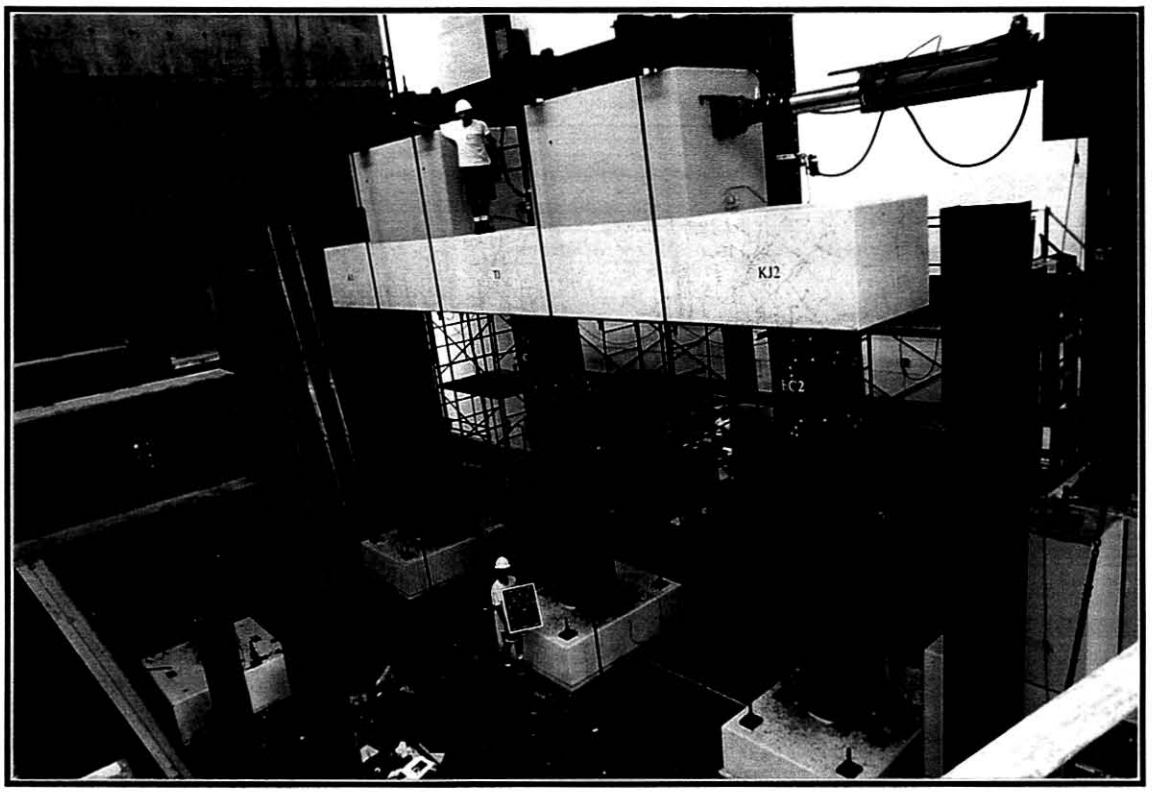

Fig.7-34 Test Unit at μ_{Δ}= *-10x2*

Fig.7-35 Test Unit at μ_{Δ}= *-10x2*

7.2 Force Displacement Response

Fig.7-36 shows the measured total lateral force versus the lateral displacement response of the test unit along with the predicted response established in **Section 6.1**. Response of the test unit shows that the ultimate flexural strength of the columns was achieved, as characterized by fracture in four of the columns longitudinal bars due to low cycle fatigue. The test unit displayed considerable energy absorption capacity with stable hysteretic behavior, as indicated by the area inside the experimental force-deformation hysteresis loops.

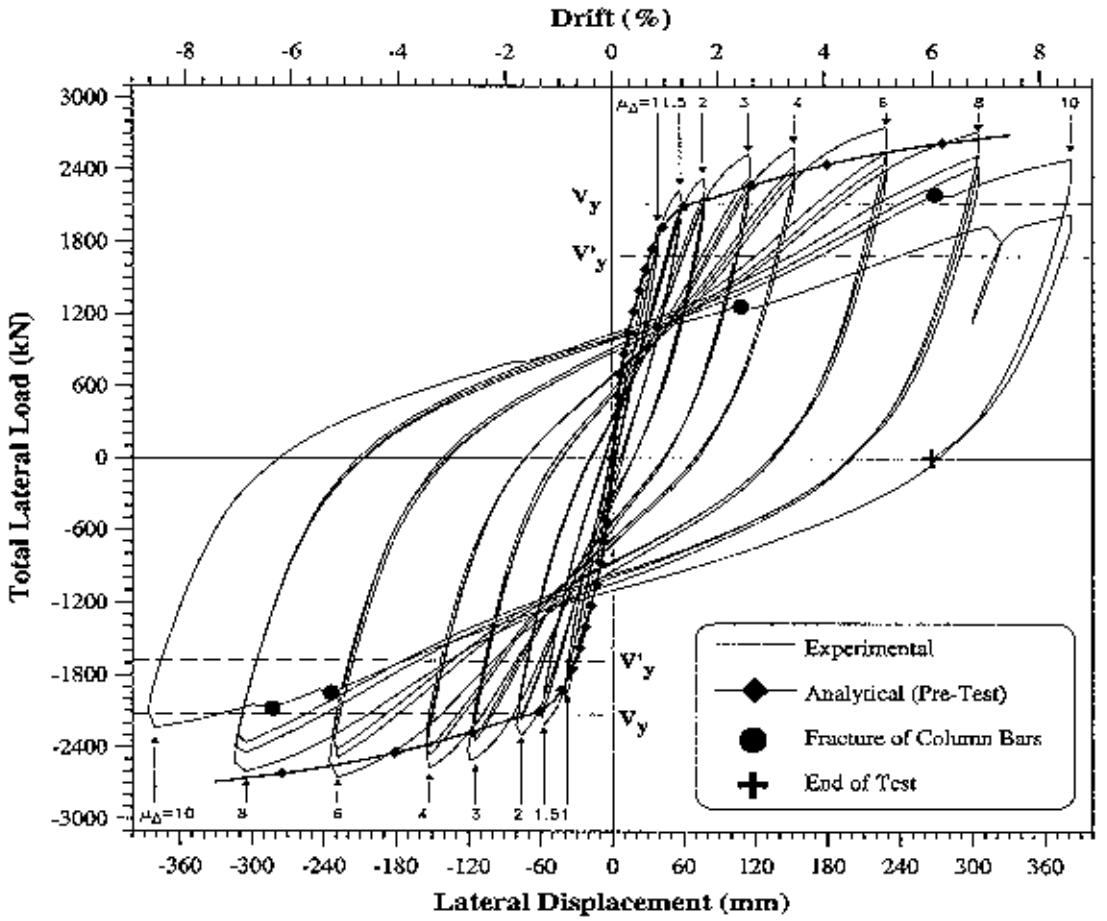

Fig.7-36 Force Displacement Response of the Test Unit

The maximum lateral force applied to the test unit was recorded during the first cycle at the displacement ductility level μ_6. At this cycle, in the push and pull directions the lateral forces were +2,756 kN and -2,654 kN, respectively. During the second and third cycles, in the push direction, a drop in the lateral force of approximately 8% and 11%, respectively, was recorded compared to the forces obtained in the first cycle. During the first cycle, in the push direction, and at the displacement ductility level μ_{10}, the lateral force was 2,486 kN, which corresponds to a reduction of approximately 10% from the maximum observed lateral force. This slight reduction in capacity can be attributed to spalling of the cover concrete in the gap regions at the column top. In addition, before failure of the column longitudinal bars, the maximum achieved displacement ductility was μ_8, and failure of the column longitudinal bars was observed at the displacement ductility was μ_{10}.

Referring to **Fig.7-36**, the pre-test analysis response curve is in good agreement with the test results in the early and later stages of testing. However, between the displacement ductility μ_3 and μ_4 there is a slight deviation from the observed response, which is believed to be due to delayed spalling of the cover concrete in the test unit when compared to the analytical model.

7.3 Column Longitudinal Reinforcement Strains

Strains presented in this section and subsequent sections are indicated as negative when the bar is subjected to compressive strains and positive when subjected to tensile strains. Yielding of the column longitudinal reinforcement occurred at ±2250με, as determined from uniaxial tensile testing of these bars.

Strain histories of four column longitudinal reinforcement gages are presented in **Fig.7-37** and **Fig.7-38**. **Fig.7-37(a)** depicts the strain history for longitudinal bar ***A*** of exterior column ***EC2*** at the interface with the cap beam. This bar is in compression in the push direction, and in tension in the pull direction. Complete strain history is shown only up to displacement ductility μ_4, because the strain gage began malfunctioning at μ_4. **Fig.7-37(a)** reveals that this bar yielded in tension during the first cycle to $-\mu_1$ in the pull direction, and yielded in compression during the third cycle at $+\mu_1$ in the push direction.

Fig.7-37(b) depicts the strain history for longitudinal bar ***C*** of exterior column ***EC2*** at the cap beam interface. This bar is in compression in the pull direction, and in tension in the push direction. As in bar ***A***, complete strain history is shown until failure of the gage at μ_1. **Fig.7-37(b)** reveals that this bar yielded in tension during the first cycle to $-\mu_1$ in the pull direction. This

strain gage began malfunctioning before it reached yielding in compression. Data presented for bars *A* and *C* indicate a good correlation with the theoretical first yield.

Fig.7-38(a) depicts the strain history for longitudinal bar *C* of exterior column *EC2* in the joint region (610 mm above the cap beam interface). Complete strain history is shown only up to displacement ductility μ_1, because the strain gage failed beyond μ_1. On the other, **Fig.7-37(b)** presents the strain history for longitudinal bar *C* of exterior column *EC2* at 965 mm below the cap beam interface. This strain gage was functioning properly during the full testing procedure. Recorded strains indicate that this bar was close to yielding in tension, which indicates the active participation of the longitudinal reinforcement at this location.

7.4 Footing Starter Reinforcing Bars Strains

In **Chapter 6** it was shown that yielding of the starter reinforcing bars in the pin connections was expected at approximately 50% of theoretical first yield, V_y', according to events *1*, *2* and *3*. On the other hand, **Fig.7-39** reveals that these bars yielded at approximately 100% of theoretical first yield and they were generally subjected to tension. Such a discrepancy is not expected to alter the predicted overall response of the test unit.

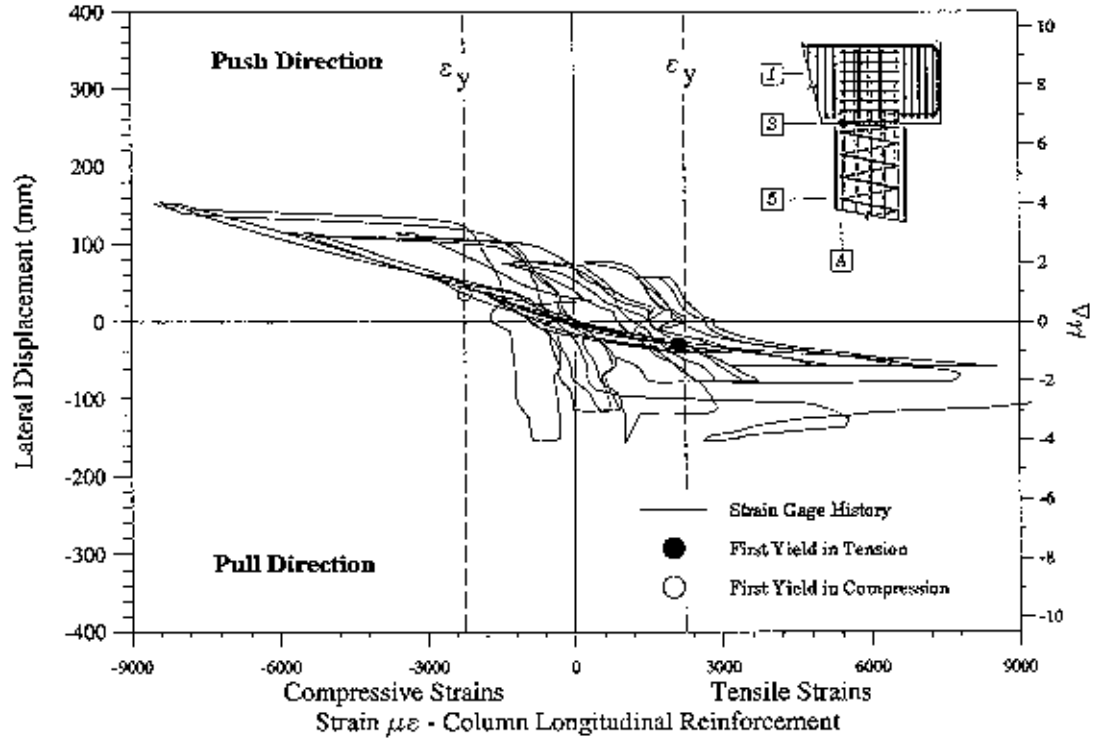

(a) Column EC2 Level A3

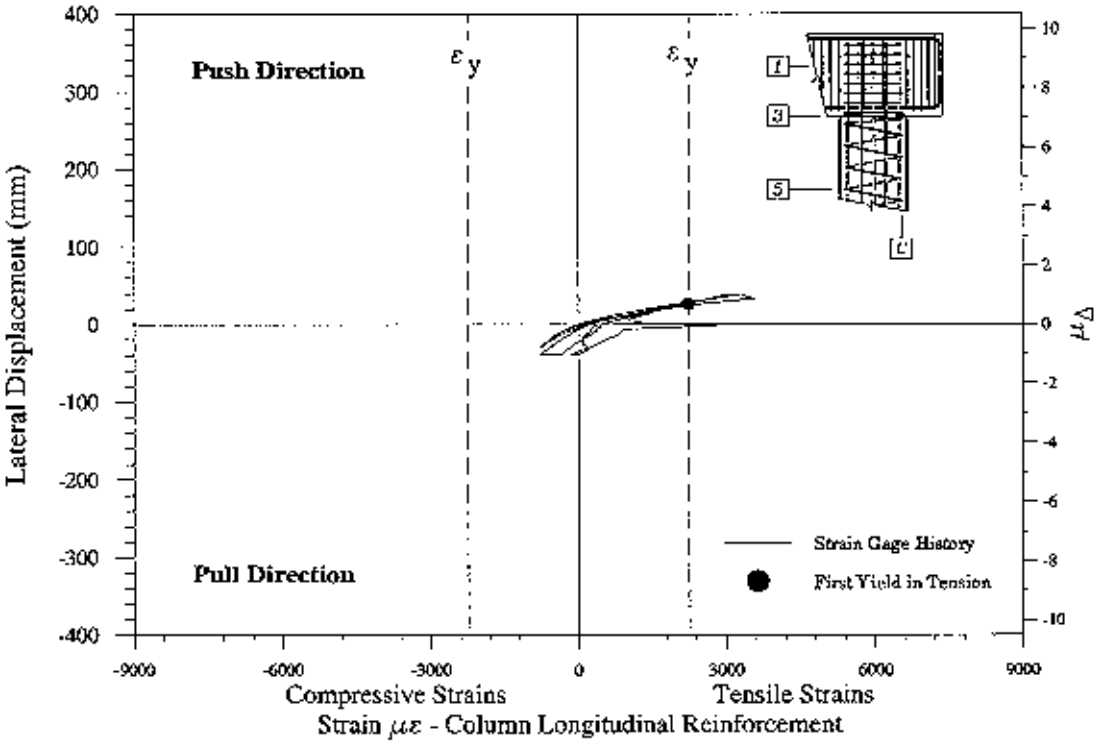

(b) Column EC2 Level C3

Fig.7-37 Column Longitudinal Reinforcement Strain Gages History - Exterior Column *EC2*

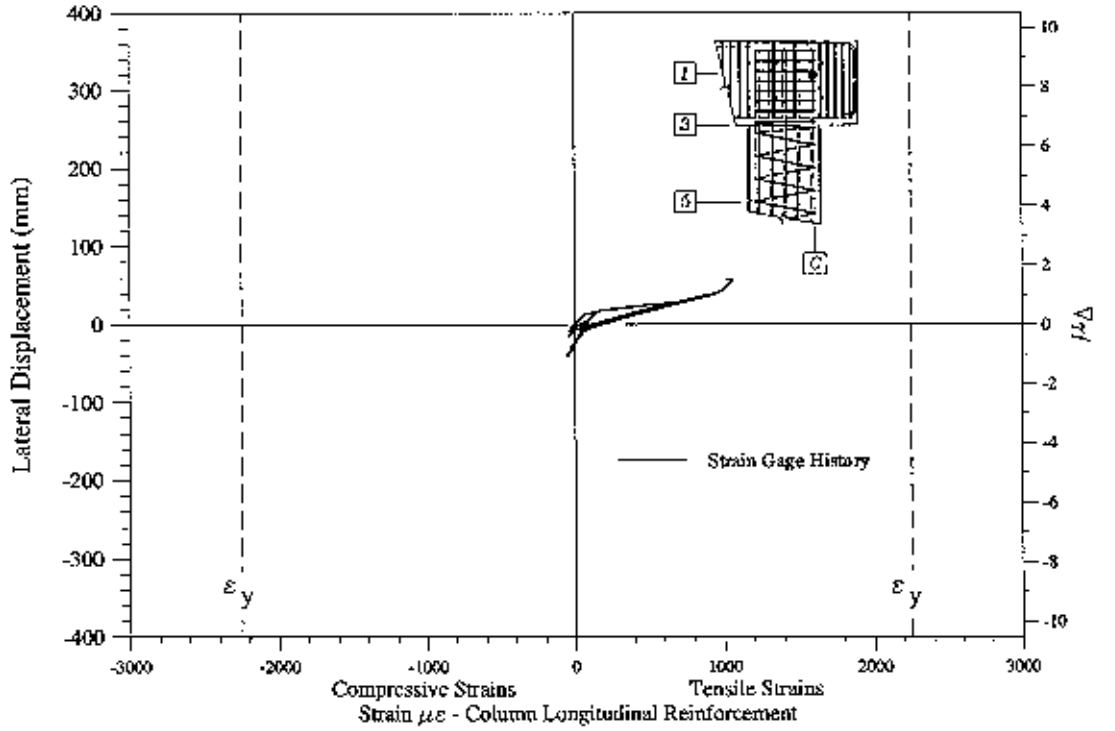

(a) Column EC2 Level C1

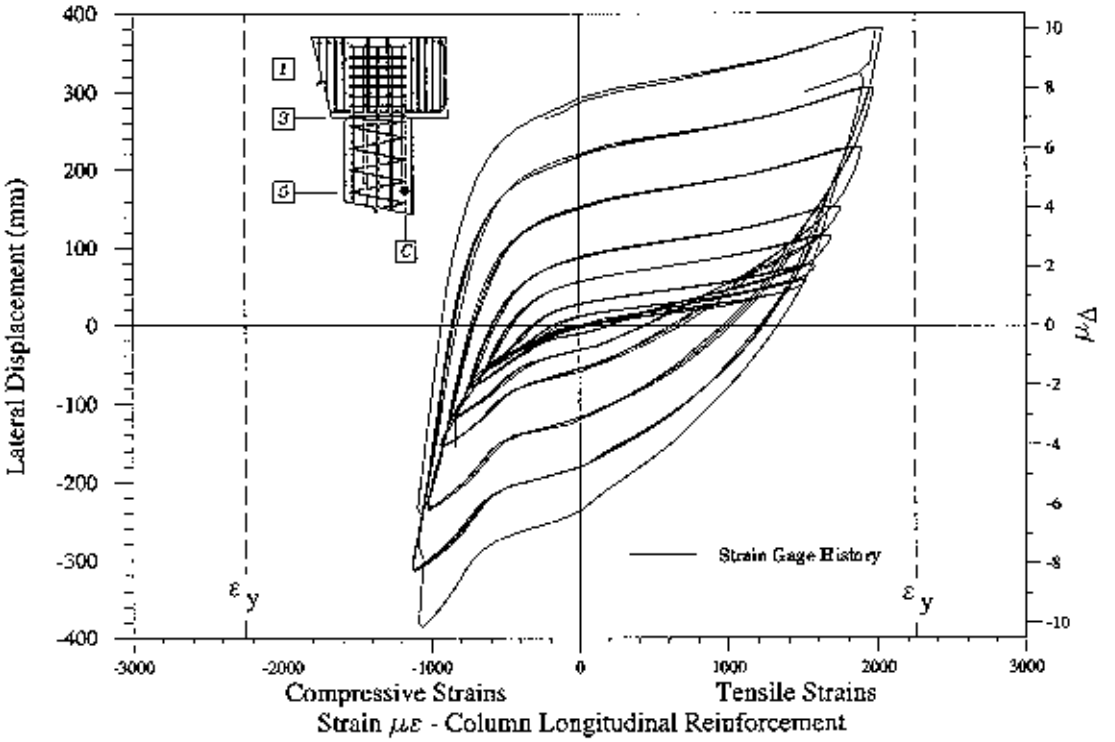

(b) Column EC2 Level C5

Fig.7-38 Column Longitudinal Reinforcement Strain Gages History - Exterior Column *EC2*

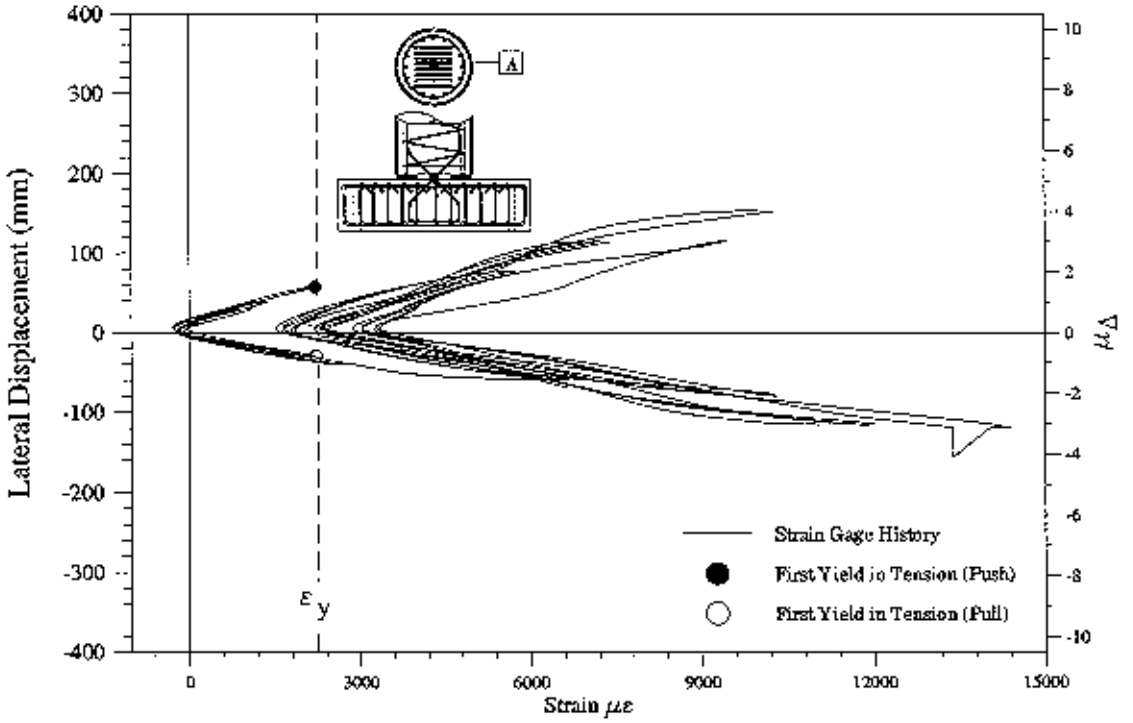

(a) Pin/Column IC Level A

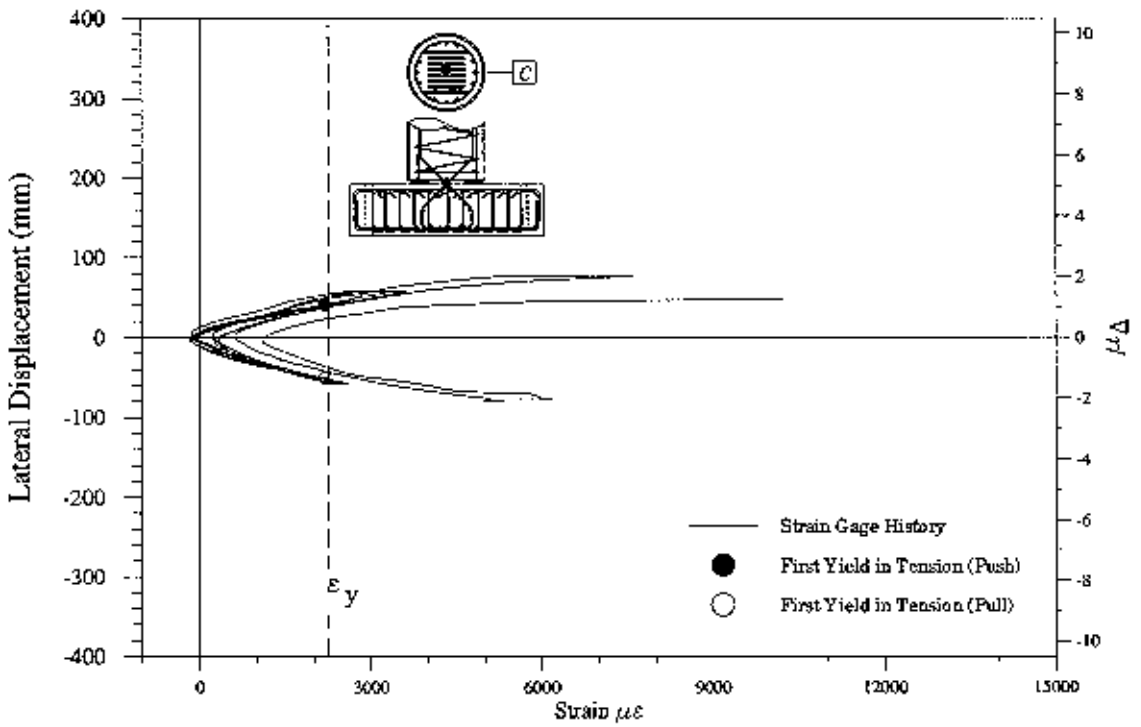

(b) Pin/Column IC Level C

Fig.7-39 Footing Starter Reinforcing Bars Strain Gages History - Interior Column ***IC***

7.5 Vertical Strains from the Steel Shell

Conversion of vertical and hoop strains into stresses when in the inelastic range requires the use of techniques based on an incremental theory of plasticity. However, because the vertical and hoop strains in the steel shell were rather small yielding of the steel shell was determined based on a strain ≐1500 $\mu\varepsilon$.

In this section and future sections the values shown in the strain profile plots are those corresponding to the first cycle peak values. Steel shell vertical strain profiles along vertical line *A* are presented in **Fig.7-40**, and steel shell horizontal strain profiles at level *5* are presented in **Fig.7-41**. Referring to **Fig.7-40**, strains at level ***5***, are higher than at the upper level ***4*** in both loading directions. Depicted in **Fig.7-40** and **Fig.7-41** are also the corresponding vertical strain profiles for the column longitudinal bar *A* at the displacement ductility μ_1, which indicate higher strains in the column reinforcing bars than in the steel shell vertical gages at any stage of testing. A comparison between the steel shell and column bar strains show that only a partial composite action was developed in the instrumented height of the column with a significant contribution from the column bars.

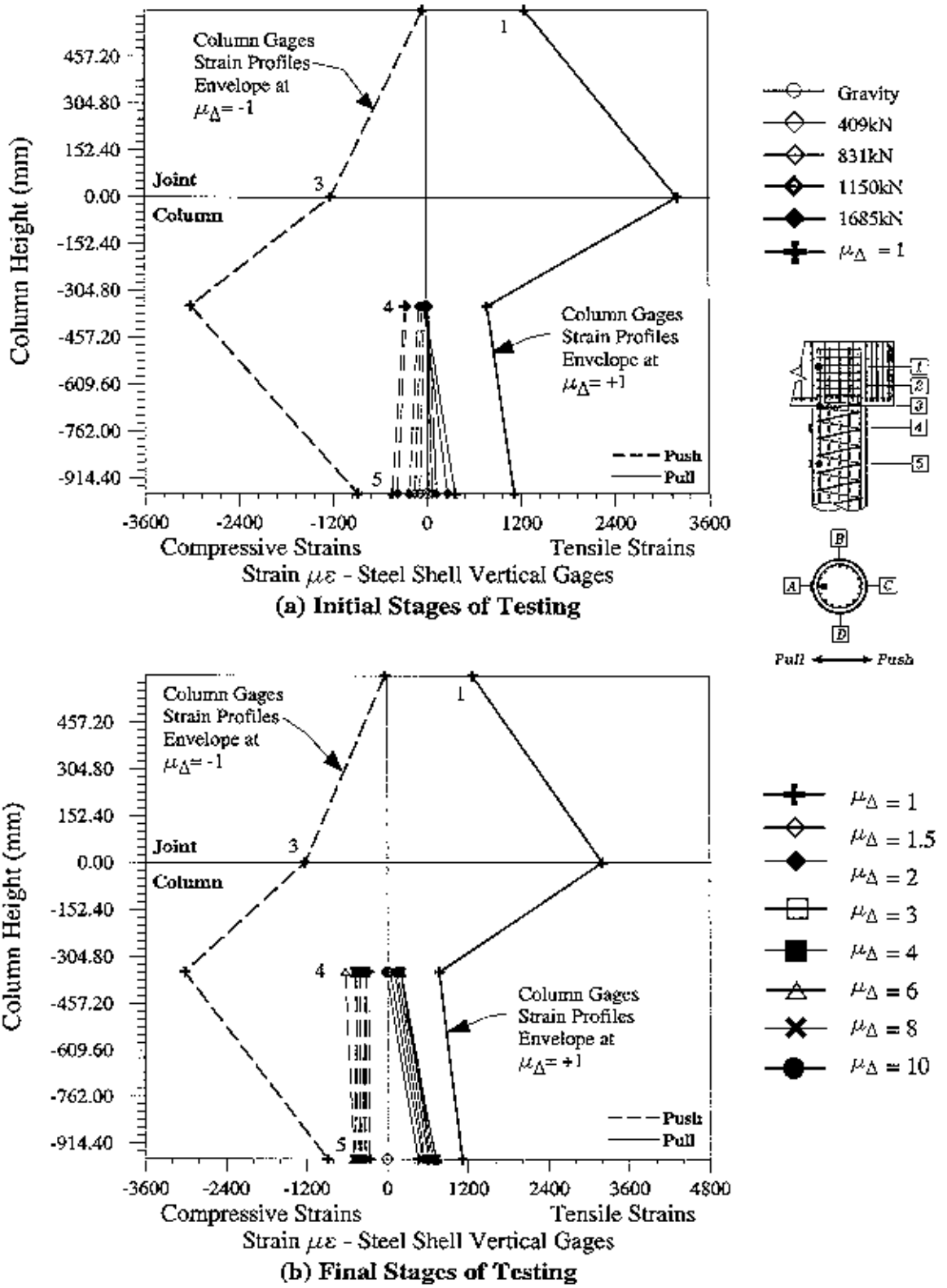

Fig.7-40 Steel Shell Vertical Gages Strain History - Exterior Column *EC2*

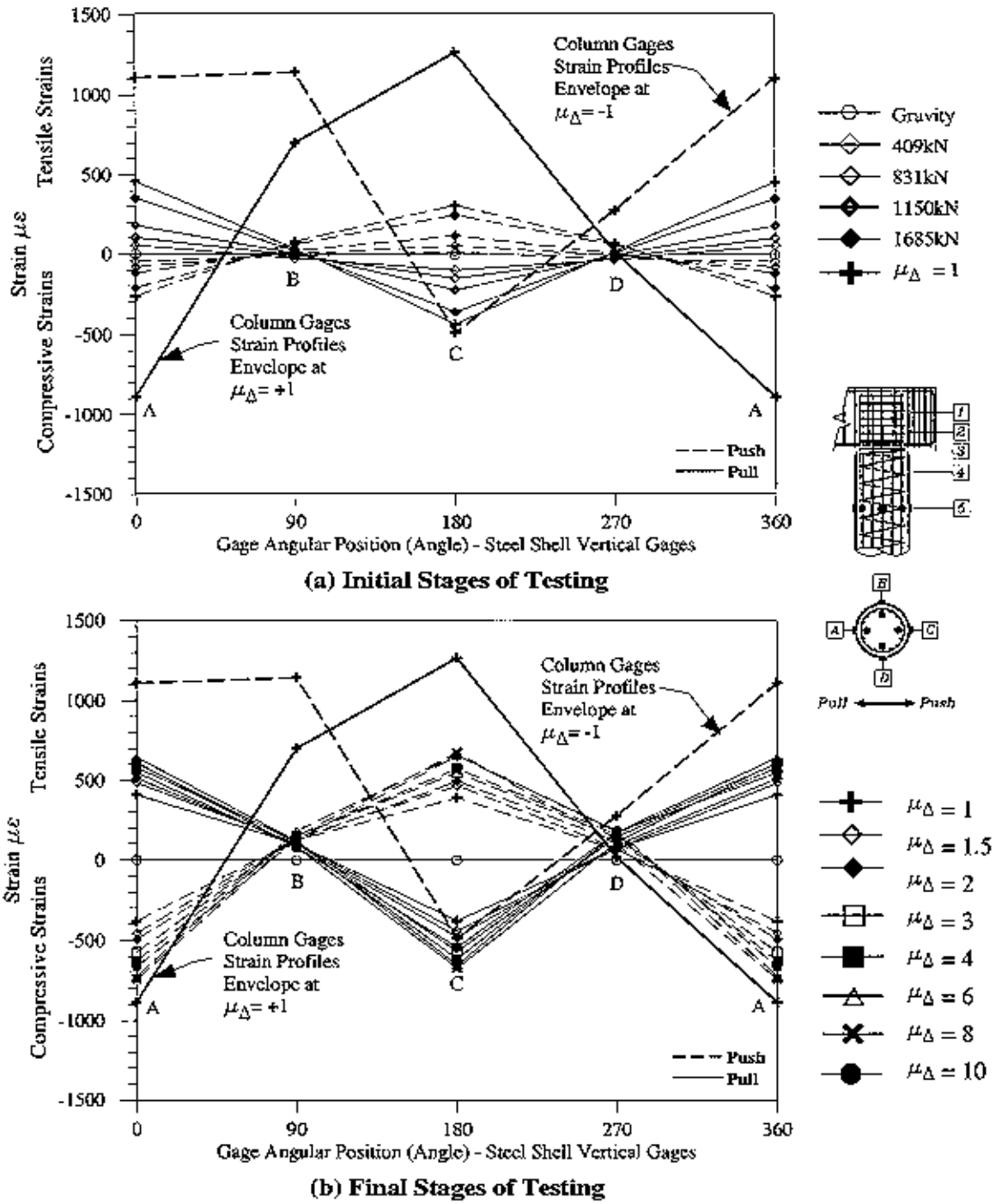

Fig.7-41 Steel Shell Vertical Gages Strain History - Exterior Column ***EC2***

7.6 Column/Joint Transverse Reinforcement Strain

Strains were also recorded in the column transverse reinforcement and in the joint horizontal hoops as shown in the instrumentation layout shown in **Fig.5-25**. As previously described, steel coupons from the column and joint spirals and hoops did not have clearly defined yield points. As a result, yield strains plotted in **Fig.7-42** and **Fig.7-43** were estimated at ±2250 $\mu\varepsilon$. Strain histories of the columns transverse reinforcement gages are presented in **Fig.7-42** and **Fig.7-43**.

Fig.7-42(a) and **Fig.7-42(c)** depict the strain histories of two gages from exterior joint ***KJ2*** transverse reinforcement along lines ***A*** and ***C*** just above the cap beam interface (i.e. level *4*). And **Fig.7-42(b)** and **Fig.7-42(d)** depict the strain histories for exterior column ***EC2*** transverse reinforcement gages along lines ***A*** and ***C*** below the cap beam interface (i.e. level *5*). Strains that develop along lines ***A*** and ***C*** indicate the confinement strain demand in the hinge region, as a result of the applied axial load and lateral deformations. Referring to **Fig.7-42**, the low level of confinement strains in the plastic hinge regions is due to the fact that steel shell provided necessary confinement to the concrete.

Spiral strains along vertical lines ***B*** and/or ***D*** are shown in **Fig.7-43**. Along these lines there is a higher participation of shear to the induced strains. In **Fig.7-43(a)** a sudden strain increase at the lateral load of V=1685kN, V'_p, and level *3* corresponds to the onset of diagonal shear cracking in the joint regions, as described in **Section 7.1.2**. As it should be expected, the demand on the column spirals are low because of the participation of the steel shell in the shear resisting mechanism, and there is an active participation of the joint hoops. However, it should be noted that joint hoop strains indicate that the yield strength was never reached and the amount of hoops provided in the joints was adequate.

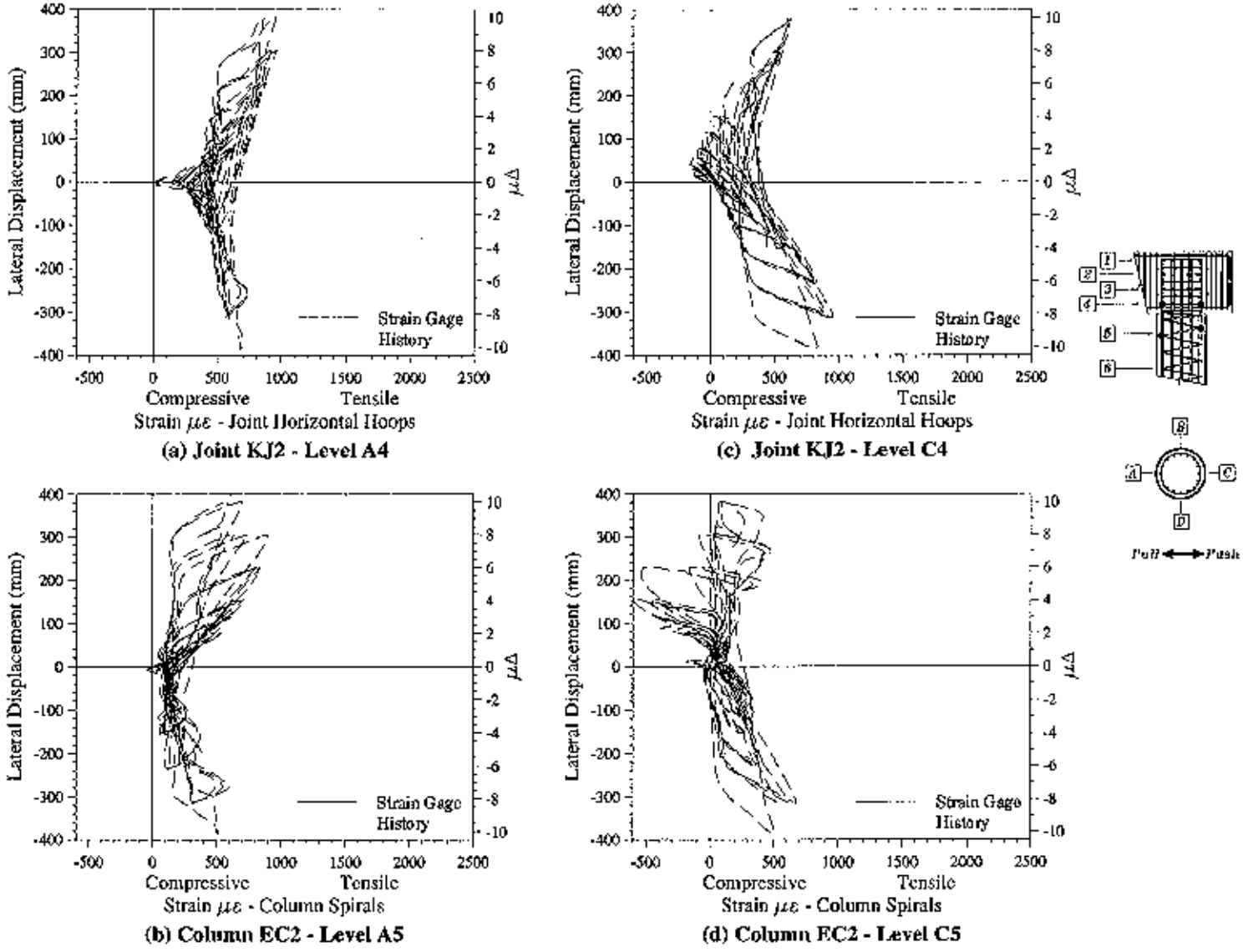

Fig.7-42 Column Transverse Reinforcement Strain History - Exterior Column ***EC2***

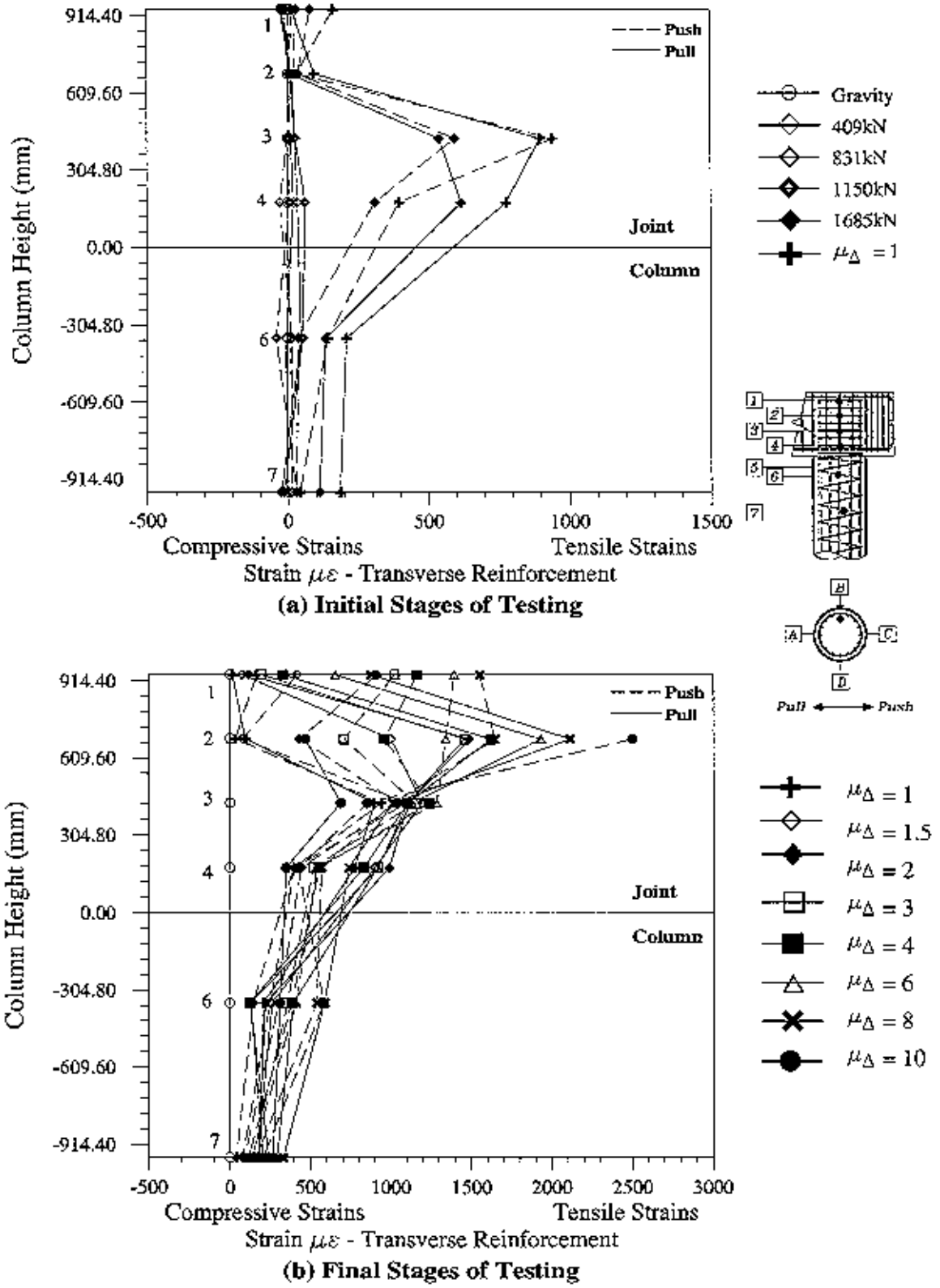

Fig.7-43 Column Transverse Reinforcement Strain History - Exterior Column *EC2*

7.7 Horizontal Strains from the Steel Shell

As previously described, yielding of the steel shell was defined at ±1500 $\mu\varepsilon$ based on a yield strength of 276 MPa. Steel shell horizontal strain profiles along vertical line ***A*** are presented in **Fig.7-44**. Also included in this figure are the corresponding strain profiles for the column transverse reinforcement along line ***A***. As it would be expected, comparable strains in the column transverse reinforcement and in the steel shell horizontal gages were obtained, which indicate the steel shell was adequate in providing additional confinement to the columns. Recorded strains in the steel shell confirms that the thickness of the steel shell was adequate to provide necessary confinement to the concrete infill.

The horizontal steel shell horizontal strain profiles along vertical line ***B*** are presented in **Fig.7-45(a)** and **Fig.7-45(a)**. As in **Fig.7-44**, in **Fig.7-45(a)** are also shown the corresponding vertical strain profiles for the column transverse reinforcement along line ***B*** at the displacement ductility μ_1, and in **Fig.7-45(b)** are depicted the corresponding vertical strain profiles for the column transverse reinforcement along line ***B*** but at the displacement ductility μ_8, which indicate that hoop strains in the steel shell were below the expected yield strains. These strains develop as a result of the input shear force and are small, which indicate that the section exhibits sufficient reserved capacity.

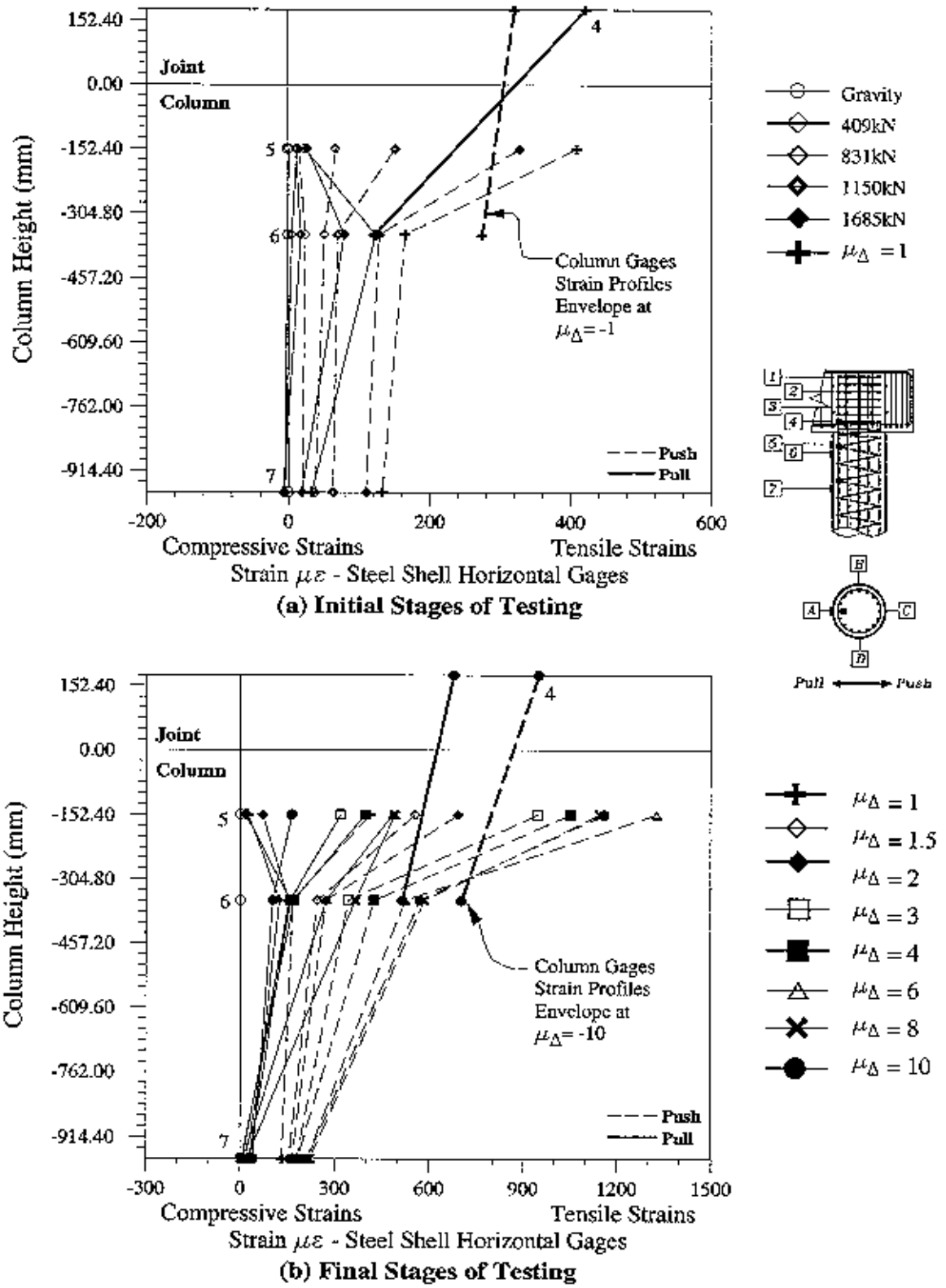

Fig.7-44 Steel Shell Horizontal Gages Strain History - Exterior Column ***EC2***

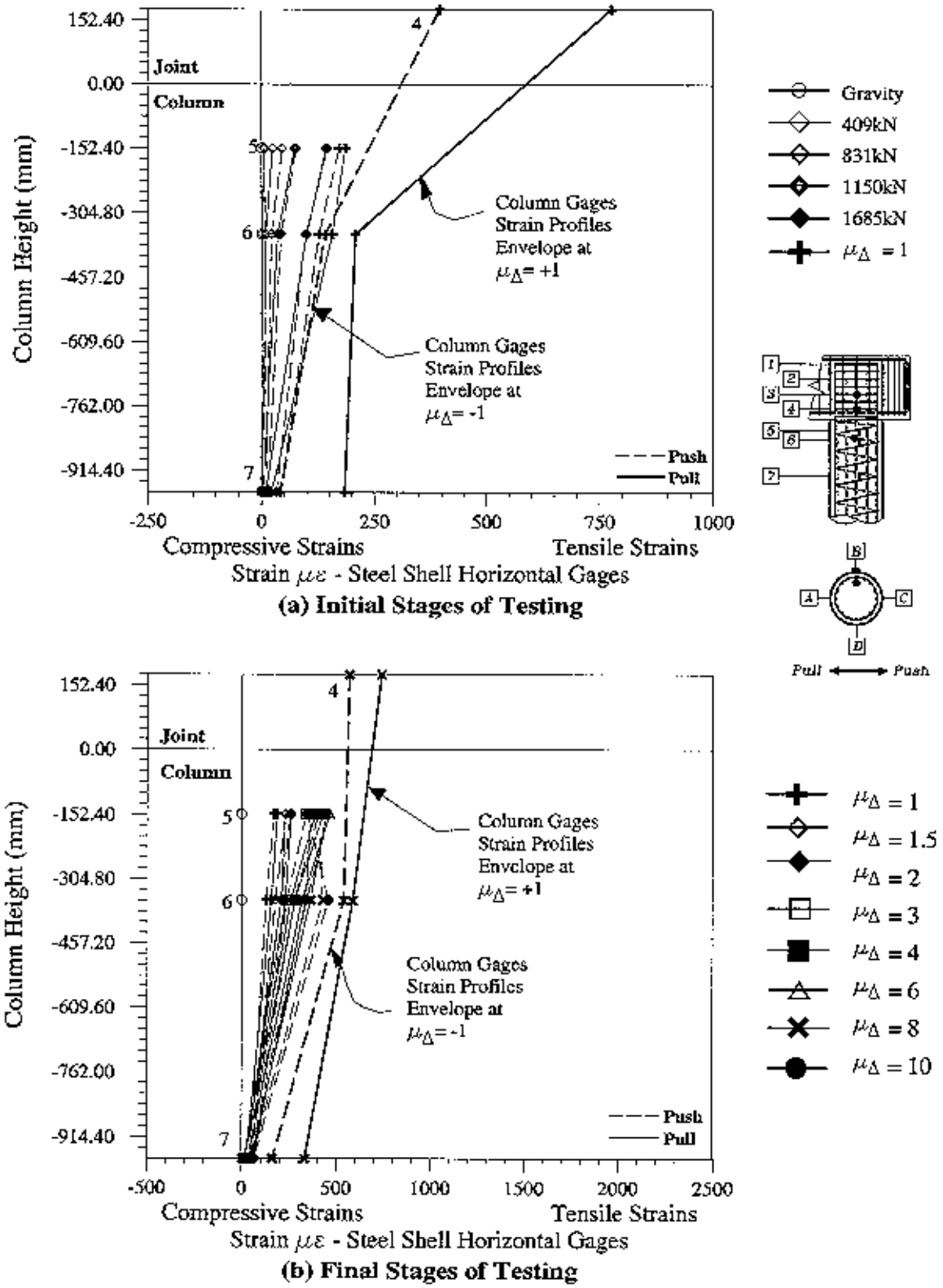

Fig.7-45 Steel Shell Horizontal Gages Strain History - Exterior Column ***EC2***

7.8 Cap Beam Top and Bottom Longitudinal Reinforcement Strains

Instrumentation of the test unit included strain gages along the top and bottom longitudinal reinforcement of the cap beam, as illustrated in **Chapter 3.** In this section strain profiles developed for the cap beam top and bottom reinforcement are presented.

Fig.7-46 and **Fig.7-47** show the strain profiles of the top longitudinal reinforcement along the cap beam and in the vicinity of exterior column ***EC2***, respectively. Strain profiles depicted in **Fig.7-46** and **Fig.7-47** indicate that the yield strength was never developed in the top longitudinal reinforcement during testing. The strain gage labeled ***8*** in **Fig.7-47** was located beyond the outer column bar bend. Large strains were recorded at position 6 at the column face, but a significant strain drop from ***6*** to ***8*** can be clearly seen. This implies that no significant deterioration of bond strength occurred in the stub region,

Bottom longitudinal reinforcement strain profiles along the cap beam and in the vicinity of exterior column ***EC2***, are presented in **Fig.7-48** and **Fig.7-49**, respectively. Strain profiles depicted in these figures show the bottom longitudinal reinforcement response was below yielding during the test, except at position ***5***, as identified in **Fig.7-49**. A maximum tensile strain of +4800 $\mu\varepsilon$ at the displacement ductility of μ_δ was recorded at this location. This is believed to be due to localized cracks and should not be of a concern, because strains at similar locations in other joints were below yield strains. As in the top beam reinforcement, small strains were recorded at position ***8*** in **Fig.7-49**. However, significant strains were induced at position ***7*** outside of the column, which is believed to be due to joint force transfer mechanism.

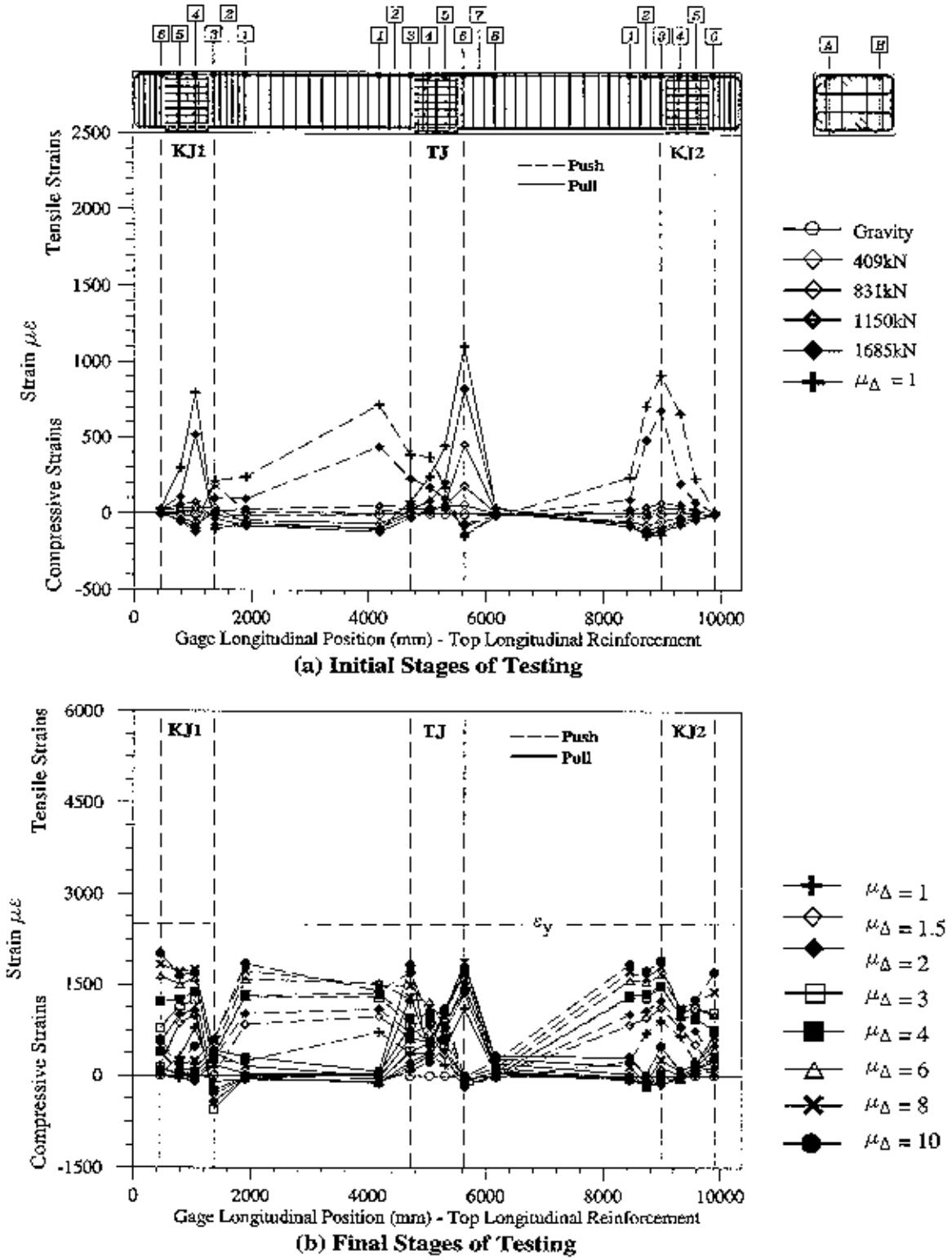

Fig.7-46 Cap Beam Top Longitudinal Reinforcement Strain Profiles

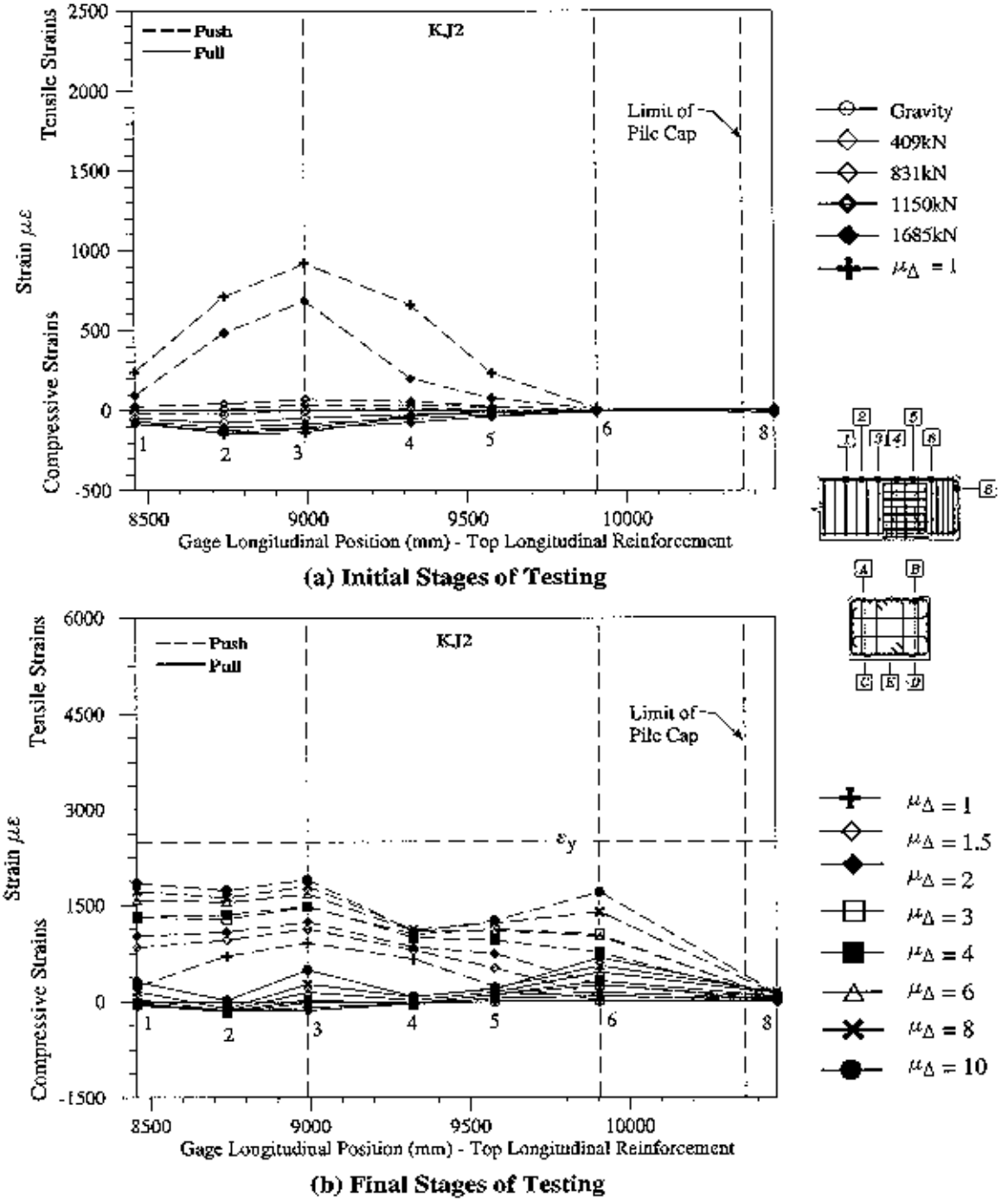

Fig.7-47 Cap Beam Top Longitudinal Reinforcement Strain Profiles- Exterior Column ***EC2***

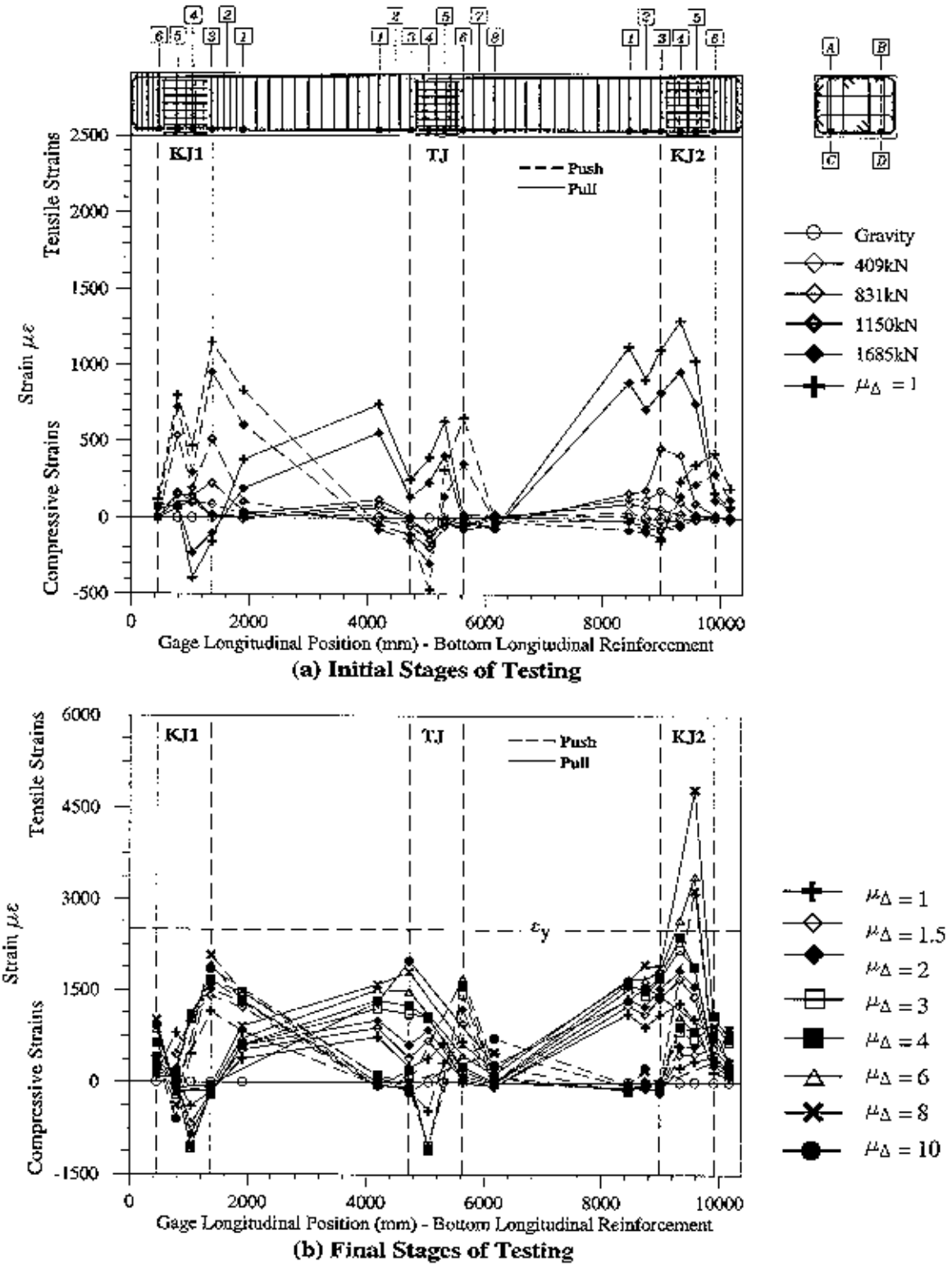

(a) Initial Stages of Testing

(b) Final Stages of Testing

Fig.7-48 Cap Beam Bottom Longitudinal Reinforcement Strain Profiles

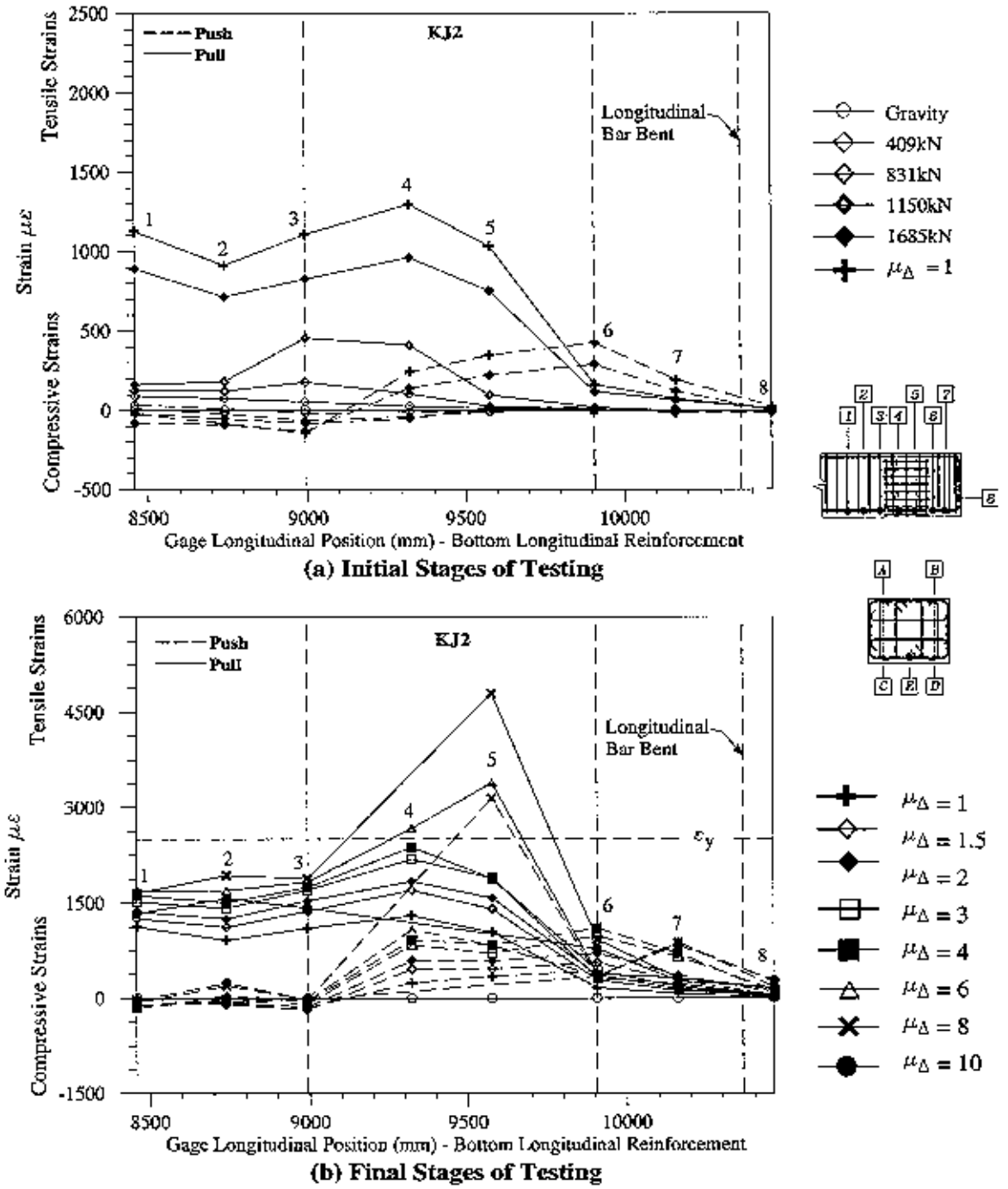

Fig.7-49 Cap Beam Bottom Long. Reinforcement Strain Profiles- Exterior Column ***EC2***

7.9 Cap Beam and Joint Vertical Stirrup Strain

Cap beam and joint vertical stirrups strain profiles and four strain histories obtained from the interior joint stirrup gages, in the vicinity of interior column ***IC***, are presented in **Fig.7-50** and **Fig.7-51**, respectively. Strain levels recorded in this reinforcement can be taken as an indication of joint performance. Consistent with test observations at first joint cracking, a sudden increase in demand in the joint region is seen in the ductility range of $\mu_{1.0}$ to $\mu_{1.5}$. Furthermore, the strains in the reinforcement remained generally below yield up to the displacement ductility level μ_6, but exceeded the yield strains at larger ductility levels. Although, such high strains were not expected, development of strains up to 0.02 at large ductility levels are not detrimental to the structure [5], as confirmed by the recorded force displacement response of the test unit and fracture of the column bars indicating that the ultimate capacity of the column was achieved..

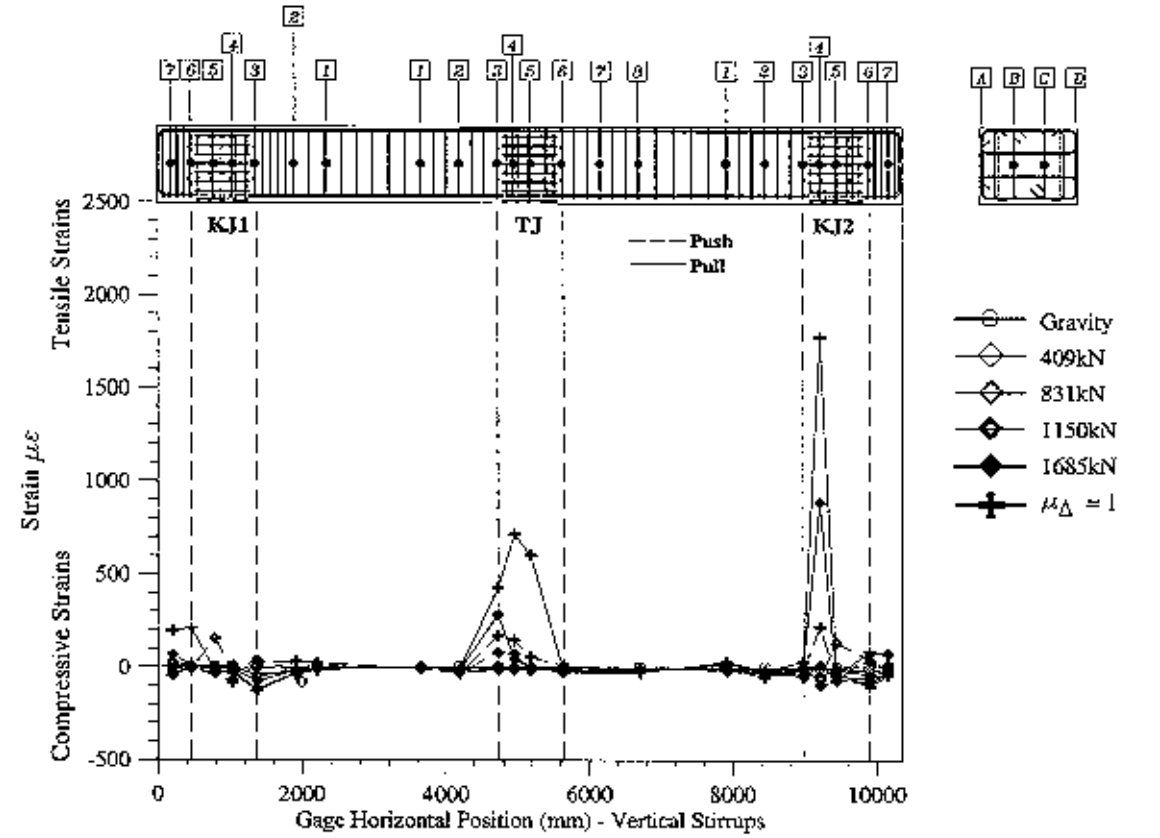

(a) Initial Stages of Testing

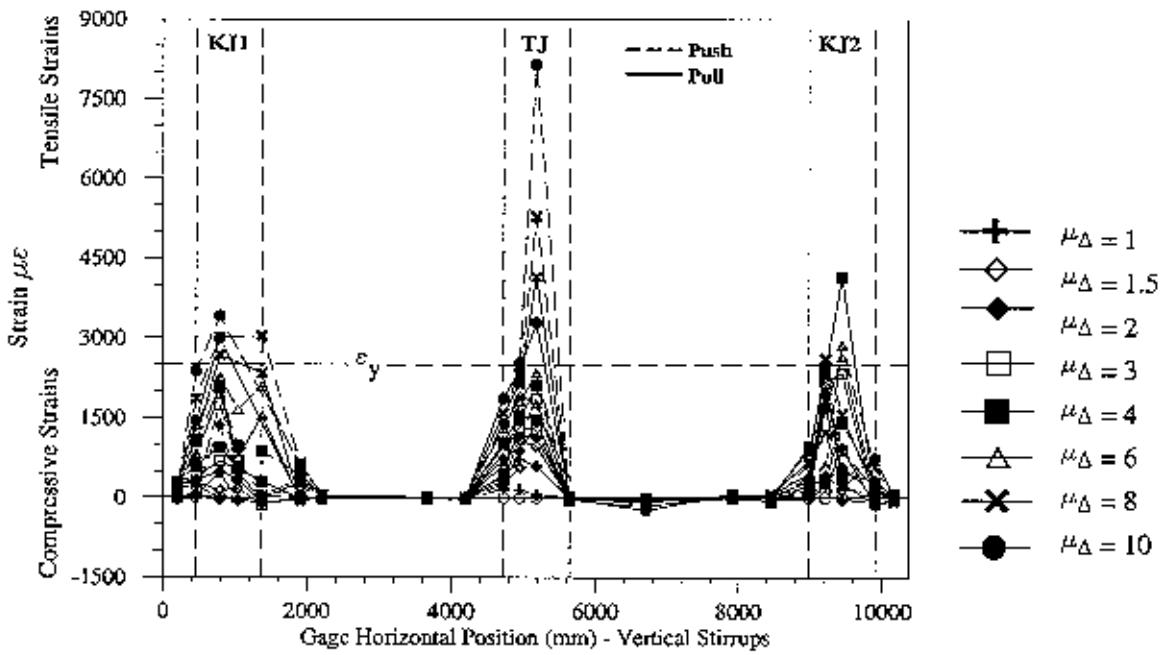

(b) Final Stages of Testing

Fig.7-50 Cap Beam Vertical Stirrups Strain Profiles

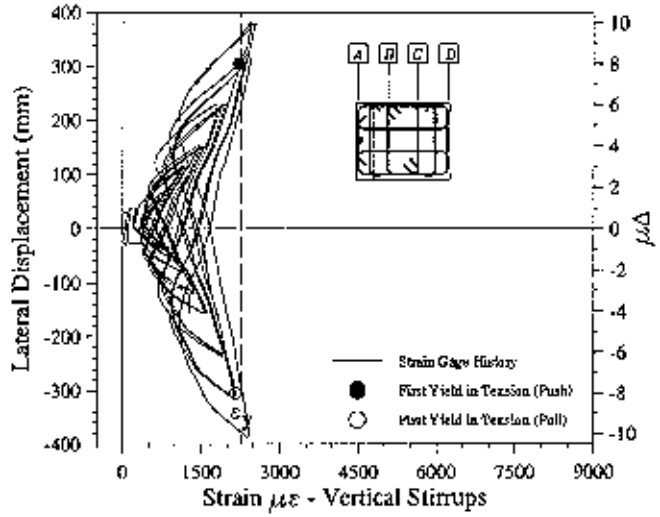

(a) Joint TJ Level 5A

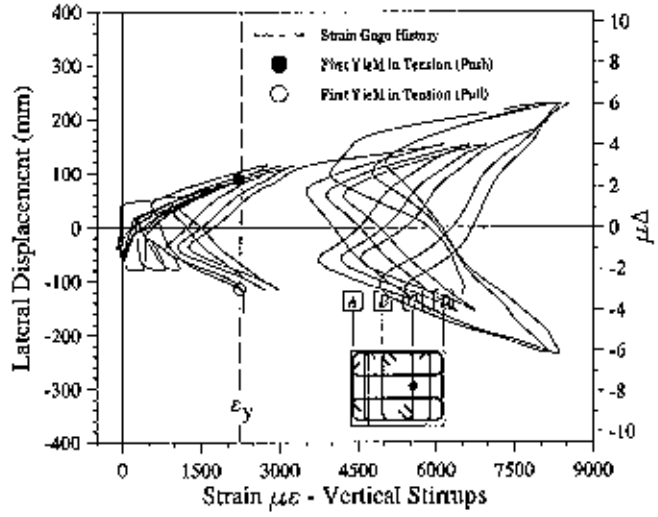

(c) Joint TJ Level 5C

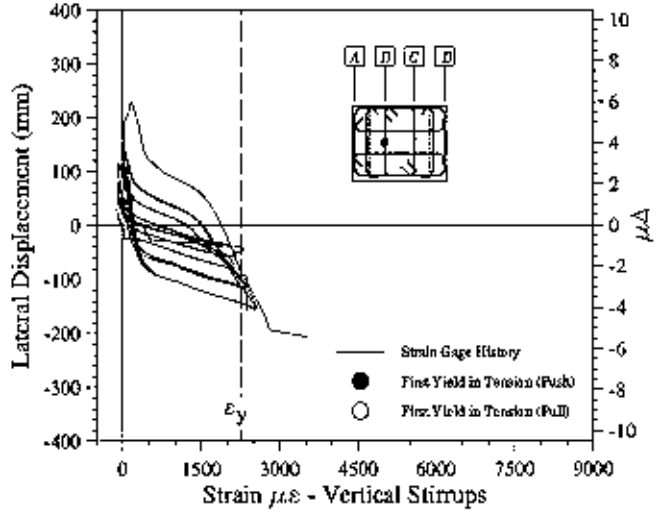

(b) Joint TJ Level 5B

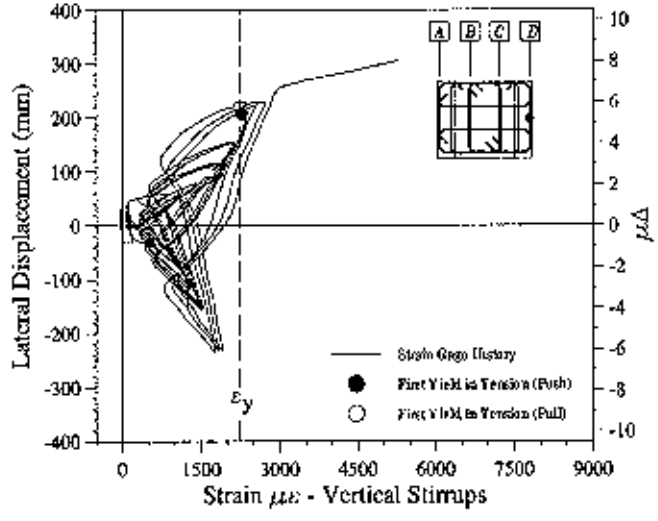

(d) Joint TJ Level 5D

Fig.7-51 Cap Beam Vertical Stirrups Strain Profiles- Interior Column *IC*

7.10 Cap Beam Horizontal Joint J-Hooks Strain

Strain gages were also installed in some of the horizontal J-Hooks located in the joints, and strain histories for these gages are presented in **Fig.7-52**. Gage readings indicate that none of the J-Hooks developed its yield strength, with the maximum recorded strains reaching 60% of ε_y. However, such large strains confirm that the horizontal J-Hooks took part in the force transfer across the joints.

7.11 Strain Measurements in the Cap Beam End Horizontal U-Bars

In order to prevent the bend at the end of the cap beam longitudinal bars from straightening, horizontal U-bars were installed at the ends of the cap beam, as shown in **Fig. 2-9**. In **Fig.7-53** is shown strain history for these horizontal U-pins at the cap beam ends. Strain histories obtained from some of these U-bars are shown in **Fig.7-53**. In all cases low strains were recorded, which should be expected since no spalling occurred to the cap beam end cover concrete. However, it is not advised that such reinforcement be eliminated unless continuity is ensured between the top and the bottom beam longitudinal reinforcement **[4]**. If U-bars are not provided, any damage to the cap beam end cover concrete is likely to trigger a joint failure, which should not be permitted in any circumstances. A further investigation examining anchorage of the external strut in the stub of the exterior joint with discontinuous top and bottom beam longitudinal reinforcement as in the test unit is appropriate.

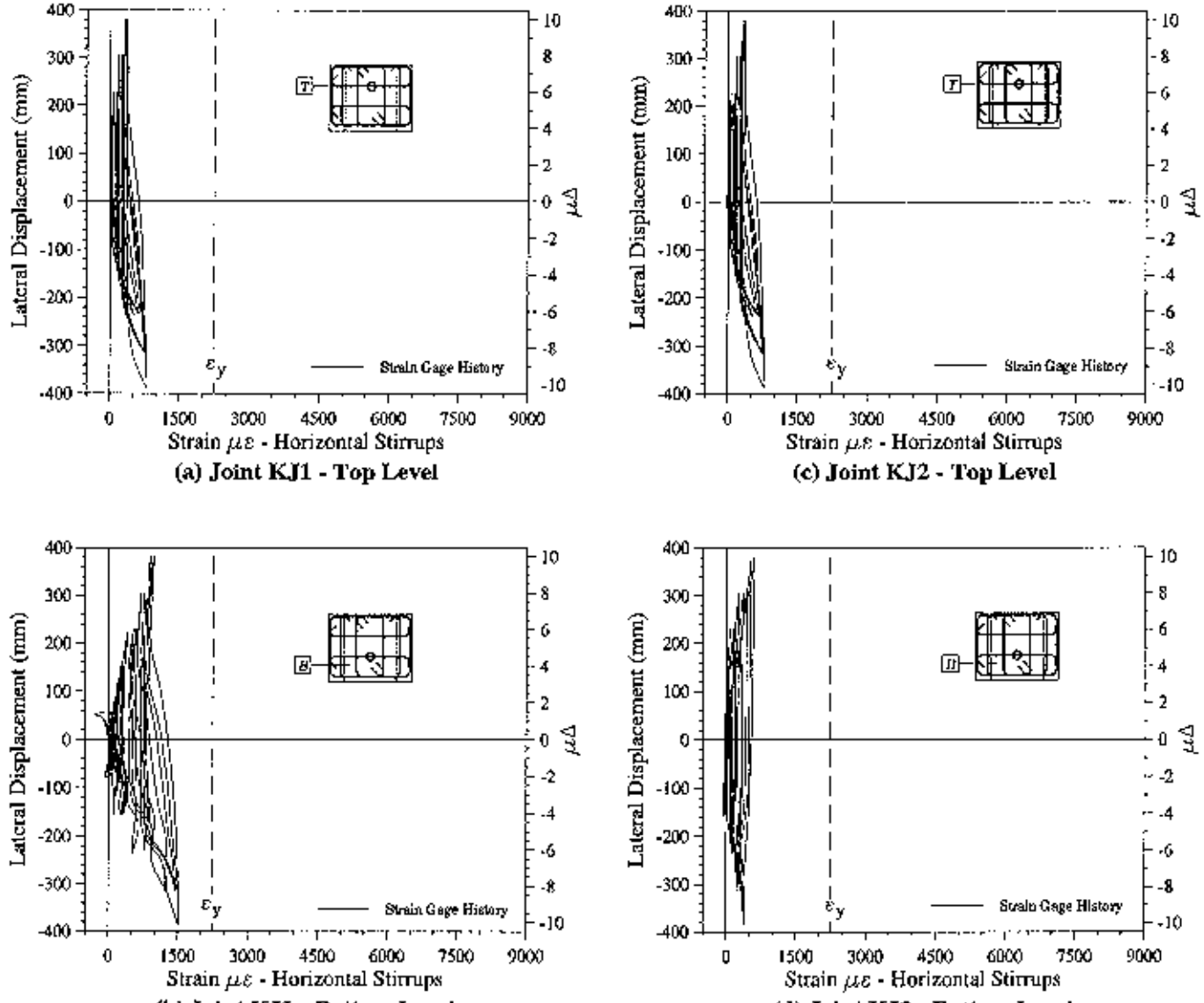

Fig.7-52 Horizontal Joint J-Hooks Strain History

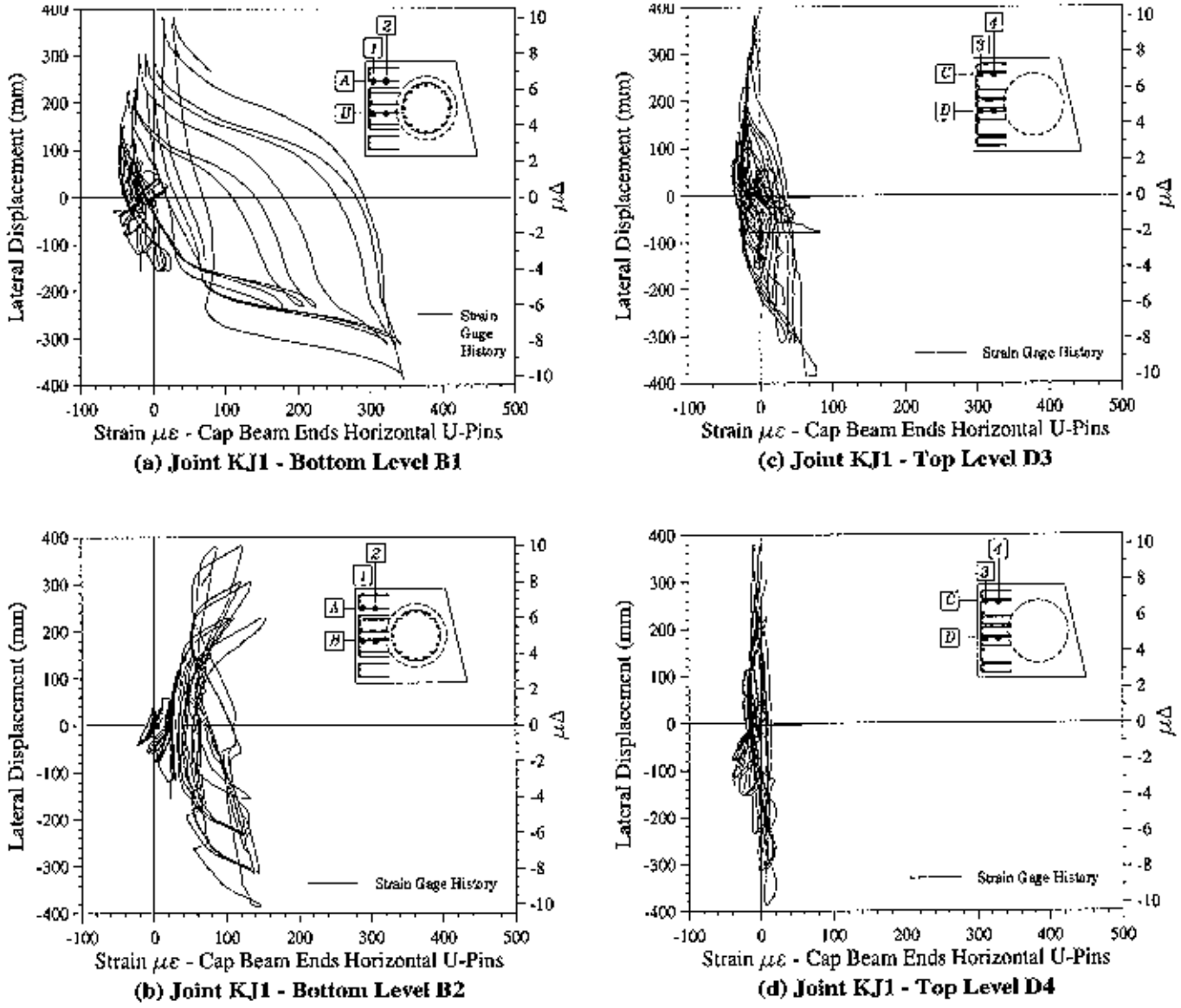

Fig.7-53 Cap Beam End Horizontal *U-Bars* Strain History - Exterior Joint ***KJ1***

8 CONCLUSIONS AND DESIGN RECOMMENDATIONS

8.1 Overview

The full-scale proof test of a bridge bent having three cast-in-place steel shell columns was presented in this report. Overall dimensions of the test structure were chosen based on typical dimensions found in multiple column bridge bents which have been designed and built by the Alaska DOT. The columns in the test unit were modeled from the bottom of the bent cap to the inflection point, as described in **Section 2.1**. The behavior of in-ground hinges, which develop in multiple column bents with continuous pile shaft/column system, was not investigated in this project. In the test unit, steel shells of the columns were terminated below the cap beam to avoid premature damage in the beam by the steel shell during lateral load response. A cap beam width of **1.5D**, where D is the column diameter, was used in the test unit consistent with current seismic design practice **[14]**.

The design of the test unit was performed in accordance with the capacity design philosophy utilizing research findings from previous studies at UCSD **[1][4][5]**. The locations of plastic hinges were selected at the top of the columns and the cap beam was protected from any significant inelastic actions by capacity design. When designing the column/cap beam joints, emphasis was placed in minimizing reinforcement quantities so that constructable joint details were obtained. Anchorage of the column longitudinal reinforcement into the cap beam was achieved with straight bar ends since J-hooks or tails at bar ends can also create congestion of reinforcement in the joint zones.

When subjected to an in-plane simulated seismic loading, the test unit exhibited excellent response with progressive damage occurring in the predetermined column plastic hinge regions as intended in the design. Conclusions drawn from this research study and recommendations for seismic design of multi-column bents suitable for the State of Alaska and other regions of high seismicity are given below.

8.2 Conclusions

Considering the design procedure adopted for the three column bent test unit, its seismic performance, and processed experimental data, the following conclusions can be drawn:

(i) The column longitudinal reinforcement of 2.5% adopted in the test unit, and column plastic hinge confinement and shear requirements were adequate to develop dependable inelastic seismic response for the cast-in-place steel shell three column bent.

(ii) A maximum system ductility of 8 was obtained for the test unit without any significant degradation to its lateral load resisting ability. At this displacement ductility, the columns were subjected to a drift of 7%, which is about 50% higher that expected in design level earthquakes.

(iii) Terminating the column shells 51 mm below the cap beam soffit avoided any damage occurring to the cap beam as a result of large inelastic actions developing in the column hinges during seismic response.

(iv) The UCSD three component shear model ensured adequate strength in the columns and cap beam, which avoided any undesirable brittle shear failure developing in these members.

(v) A minimum embedment length based on a uniform bond stress of $1.17\sqrt{f_c'}$ *[MPa]* was provided for the column bars into the cap beam. Development of column moment capacities in the plastic hinges confirmed that the anchorage details of the column bars were adequate.

(vi) Behavior of the cap beam was satisfactory. As intended in the design, the beam response was essentially elastic with damage limited to evenly distributed cracking. Consequently, the cap beam would not require any repair when the structure is subjected to design level earthquakes.

(vii) The joint design based on a rational force transfer method significantly reduced the amount of reinforcement within the joint. However, the reinforcement provided in the joints was sufficient to ensure desirable response for the multi-column bent under seismic loading.

(viii) The analytical procedure adopted for predicting seismic behavior of the test structure was satisfactory. The theoretical curve underestimated the force resistance of the test unit by up to 8% in the ductility range from 2 to 6, which was a consequence of delayed spalling of cover concrete in the column plastic hinge regions due to the presence of steel shells.

8.3 Seismic Design Recommendations for Bridge Multiple Column Bents

Based on the design and performance of the multi-column bent test unit and other recently completed UCSD research studies relevant to the current investigation **[1][4][5]**, the following design recommendations are made for seismic design of multi-column bridge bents with circular CISS-columns. It is assumed that multi-column bents are designed using the capacity design philosophy with hinges forming at the column ends. The live load contribution was ignored in the laboratory test described in this report. An appropriate level of live load shall be included when determining the design forces when its contribution is expected to be critical.

8.3.1 Column Design

(i) An appropriate level of column longitudinal reinforcement shall be provided based on the design moments calculated for the columns. However, to avoid practical difficulties in placing and confining large steel quantities, it is recommended that the column longitudinal steel ratio be limited to $0.005 \leq \rho_l \leq 0.04$ **[1]**.

(ii) In order to ensure sufficient displacement ductility capacity of multi-column bents, a minimum confinement to the plastic hinge region in accordance with equation **(4.7)** shall be provided. The necessary confinement can be provided in the form of spiral reinforcement or by the column steel shell as was done in the test unit.

(iii) To avoid undesirable shear failure in the columns, adequate transverse reinforcement shall be ensured using the three component shear model **[12]** with the modification for axial load contribution as discussed in **Section 4.1.1**. Consistent with this model, the required amount of spiral reinforcement shall be obtained from equations **(4.5)** and **(4.6)** assuming flexural-shear cracking at $\theta = 35°$. Based on test results, when steel shell column/ pile shaft, are used special shear reinforcement will not generally be required.

8.3.2 Cap Beam Design

(i) Design of cap beam shall be performed using the typical strength reduction factor $\varphi_f = 0.9$.

(ii) When joints are designed using rational force transfer models, it is recommended that the cap beam shall be designed to remain elastic by accounting for strain hardening of the reinforcement and material uncertainties in the columns.

(iii) When a multi-column bent is designed with a wider cap beam, it is appropriate to distribute a portion of the longitudinal reinforcement along the sides as in the test unit while ensuring 75% of the bottom beam reinforcement passes through the column reinforcement cages.

(iv) For bent caps integral with bridge deck, the contribution of deck and soffit reinforcement to the cap beam moment resistance can be accounted for in accordance with current design practice.

8.3.3 Reinforced Concrete Joint Design

In order to reduce the joint reinforcement and improve constructability, the cap beam/column joints of multiple column bridge bents shall be designed using the procedure discussed below. The joint detailing is based on the modified external strut force transfer model **[5]** with the principal tensile stress (see equation **(4.19)** for estimating p_t) as the initial design parameter. In deriving the joint design procedure, the required angles for various struts were obtained assuming the cap beam depth is between **D** and **D+155** (mm), where D is the column diameter. If the depth of the cap beam is outside the above range, the required joint reinforcement shall be evaluated using the procedure described in reference **[5]**.

(i) When $p_t > 0.42\sqrt{f_c'}\ [MPa]$, joint reinforcement is obtained assuming that about $\mathbf{0.5T_c}$ is anchored by the clamping mechanism with the assistance of an external joint strut while the remaining tension force is supported by the splice transfer mechanism (see **Section 4.3.3**).

(ii) Accordingly, ***a bridge tee joint*** is detailed with the following reinforcement:

(a) Additional external vertical stirrups in the cap beam with a total area equal to:

$$A_{jv} = 0.125\ \lambda_o\ A_{sc}\frac{f_{y,c}}{f_{y,v}} \tag{8.1}$$

where λ_o is the overstrength factor of the column longitudinal reinforcement, A_{sc} is the total area of longitudinal column reinforcement, f_{yc} is the yield strength of column longitudinal reinforcement, and f_{yv} is the yield strength of vertical stirrups. The external stirrups shall be provided in the cap beam over a distance h_b from the joint interface as addition to the beam shear requirement, where h_b is the cap beam depth.

(b) Internal vertical joint stirrup reinforcement amounting to:

$$A_{jv} = 0.095\ \lambda_o\ A_{sc}\frac{f_{y,c}}{f_{y,v}} \tag{8.2}$$

(c) Volumetric ratio of the joint horizontal reinforcement (hoops) equivalent to the greater of:

$$\rho_s = \frac{0.30\ \lambda_o\ A_{sc}}{l_a^2}\frac{f_{y,c}}{f_{y,h}} \tag{8.3}$$

or

$$\rho_s \geq 0.29\ \frac{\sqrt{f_c'}}{f_{yh}}\ [MPa] \tag{8.4}$$

where l_a is the anchorage length of the column bars into the joint and f_{yh} is the yield strength of the joint hoop reinforcement. The reinforcement requirement of equation **(8.3)** is to resist a tension force $0.25T_c$ within the joint while the requirement of equation. **(8.4)** is to ensure some tensile resistance when cracking occurs in the joint. Derivations of the above equations may be found in reference **[1]**. It is suggested that the required horizontal spiral reinforcement be distributed over the entire embedment length of the column reinforcement. To simplify construction procedure, this reinforcement may be provided as lap welded hoops rather than continuous spirals.

(d) Area of additional top beam longitudinal reinforcement amounting to:

$$\Delta A_{tb} = 0.17 \lambda_o A_{sc} \frac{f_{y,c}}{f_{y,b}} \quad (8.5)$$

where $\mathbf{f_{yb}}$ is the yield strength of the beam longitudinal reinforcement.

(e) Area of additional bottom beam longitudinal reinforcement equal to:

$$\Delta A_{bb} = 0.15 \lambda_o A_{sc} \frac{f_{y,c}}{f_{y,b}} \quad (8.6)$$

In the above equations, the material properties may be approximated to:

1. $\lambda_o = \mathbf{1.4}$ with an assumption of $\mathbf{f_{yc} = f_{yv} = f_{yh} = f_{yb}}$, or

2. $\lambda_o = \mathbf{1.3}$ with actual measured values of $\mathbf{f_{yc}}$, $\mathbf{f_{yv}}$, $\mathbf{f_{yh}}$ and $\mathbf{f_{yb}}$

(iii) ***A bridge knee joint subjected to opening moments*** is detailed using the procedure described for the tee joint except that no additional beam top reinforcement given by equation **(8.5)** is required. Furthermore, beam longitudinal reinforcement shall be provided as continuous reinforcement through the joint or an alternative detail as adopted in the test unit ensuring anchorage of the joint strut resulting from the splice mechanism (i.e., at node **F** in **Fig. 4.8(a)**).

(iv) No special reinforcement is required for ***a bridge knee joint subjected to closing moments*** when it is designed for opening moments as recommended above. However, it is suggested that the vertical portion of the continuous beam longitudinal reinforcement shall be located approximately at $\mathbf{h_c/2}$ from the outer face of the exterior column.

(v) If the beam longitudinal reinforcement is *not* provided as continuous reinforcement, then the knee joint shall be detailed with additional top beam reinforcement equal to the amount given by equation **(8.5)** to ensure satisfactory joint force transfer under closing moments.

(vi) When $p_t \leq 0.29 \sqrt{f_c'}$ *[MPa]*, joint reinforcement is reduced to nominal requirements with no additional steel in the cap beam. Nominal joint reinforcement shall satisfy the following details [1]:

(a) Vertical joint reinforcement amounting to

$$A_{jv} = 0.0625\lambda_o A_{sc}\frac{f_{y,c}}{f_{y,v}} \quad (8.7)$$

(b) Volumetric ratio of the joint horizontal reinforcement as required by equation **(8.4)**.

(vii) When $0.29\sqrt{f_c'} \le p_t \le 0.42\sqrt{f_c'}$ *[MPa]*, a linear interpolation of the reinforcement required for the two principal tensile stress limits can be used.

(viii) In all cases, column bars shall be extended as close to the top beam longitudinal reinforcement as possible with a minimum embedment length into the joint as given by:

$$l_a \ge 0.3\, d_b \frac{f_y^o}{\sqrt{f_c'}} \quad (8.8)$$

(ix) All the vertical stirrups in the joint region shall be provided as closed ties with appropriate number of crossties in accordance with recommendations in current design practice (e.g.,reference **[14]**)

(x) When the column framing into a joint is detailed with longitudinal reinforcement ratio $\rho_l > 3\%$, a minimum joint concrete strength of 35 MPa shall be specified **[4]**.

(xi) Termination of the connection reinforcement below the cap beam shall be based on an average bond strength of 0.80 MPa, which is consistent with values found in reference **[11]**. The connection reinforcement lap length shall be computed based on the development length of the steel shell or the subgrade moment profile, given by:

$$l_{lap} = \frac{f_{yl}\, t_j}{\mu_{ave}} \quad or \quad l_{lap} = 75\%\, L_{eff} \quad (8.9)$$

where l_{lap} is the distance from the cap beam interface to termination of the connection reinforcement, and L_{eff} is the distance to the point of inflection A, as depicted in **Fig. 8–1**.

(xii) In order to avoid local buckling of the steel shell the concrete infill shall extend beyond the subgrade hinge to a depth where the moment demand is less than 50% of steel shell yield moment, as depicted in **Fig. 8–1**.

Further specialized studies, as illustrated by studies performed by Budek et al.[7], examining termination of the connection reinforcement and concrete infill below the cap beam interface shall provide additional data to substantiate these recommendations.

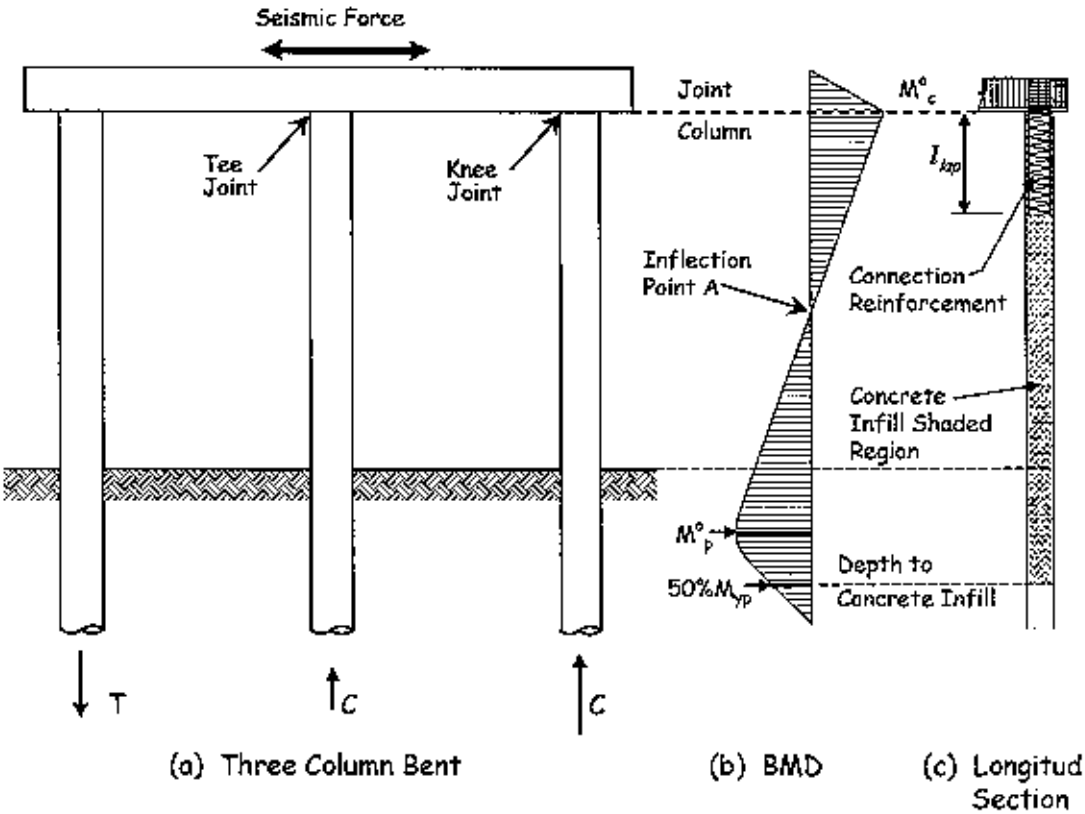

Fig. 8-1 Multiple Column Bridge Bent

(xiii) A displacement ductility of $\mu_\Delta = 4$ shall be set as the maximum limiting ductility capacity for the design of these steel shell column/pile shafts multiple column bents.

When a multiple column bridge bent is designed based on the above recommendations, a ductile seismic response can be expected up to the design drift limit state.

References

[1] Priestley, M. J. N., Seible, F., Calvi, M., *" Seismic Design and Retrofit of Bridges, "* John Wiley & Sons, Inc. , New York, September 1995, 672 pages.

[2] Silva, P. F., Sritharan, S., Seible, F., Priestley, M. J. N., Design Assessment prepared for the State of Alaska Department of Transportation and Public Facilities, Department of AMES - Division of Structural Engineering, University of California San Diego, La Jolla, California, June 1997.

[3] Sritharan, S., Priestley, M. J. N., Seible, F., *"Seismic Response of Column/Cap Beam Tee Connections with Cap Beam Prestressing "*, Department of AMES - Division of Structural Engineering , University of California San Diego, La Jolla, California, 1996, Report # SSRP-96/09.

[4] Sritharan, S., Priestley, M. J. N., Seible, F., *"Seismic Design and Performance of Concrete Multi-Column Bents for Bridges"*, Department of AMES - Division of Structural Engineering , University of California San Diego, La Jolla, California, June 1997, Report # SSRP-97/03.

[5] Sritharan, S., *"Analysis of Concrete Bridge Joints Subjected to Seismic Action"*, Doctoral Dissertation, Department of AMES - Division of Structural Engineering, University of California San Diego, La Jolla, California.

[6] Silva, P. F., Seible, F., Priestley, M. J. N., *"Response of Standard Caltrans Pile-to-Pile Cap Connections Under Simulated Seismic Loads"*, Department of AMES , University of California San Diego, La Jolla, California, November 1997, Report # SSRP-97/09.

[7] Priestley, M. J. N., Budek, A., Benzoni, G., *" An Analytical Study of the Inelastic Seismic Response of Reinforced Concrete Pile-Columns in Conhesionless Soil, "* Department of AMES , University of California San Diego, La Jolla, California, March 1995.

[8] Silva, P. F., Seible, F., Priestley, M. J. N., *"Computer Programs for Section Analysis"*, Department of AMES , University of California San Diego, La Jolla, California, (in preparation).

[9] Seible, F., Kurkchubasche, A., Mazzoni, S., *"CALSD Instructional Computer Programs for Structural Engineering, "*, Department of AMES - Division of Structural Engineering, University of California San Diego, California, January 1991.

[10] Mander, J.B., Priestley, M.J.N., Park, R., " *Theoretical Stress-Strain Model for Confining Concrete*," Journal of Structural Engineering, ASCE, V. 114, No. 8, Aug. 1988, pp. 1804-1826.

[11] Chai, H. Y., Priestley, M. J. N., Seible, F., " *Seismic Retrofit of Circular Bridge Columns for Enhanced Flexural Performance*, "ACI Journal, Proceedings V. 88, No.5, Sept. - Oct. 1991, pp. 572-584.

[12] Kowalsky, M.J., Priestley, M.J.N., and Seible, Frieder, *"Shear Behavior of Lightweight Concrete Columns Under Seismic Conditions,"* Department of AMES , UCSD, La Jolla, CA, July 1995.

[13] Zelinski, R., *"Seismic Design Memo: Various Topics - Preliminary Guidelines,"* Seismic Technology Section, California Department of Transportation, Sacramento, 1995.

[14] American Concrete Institute, *Building Code Requirements for Structural Concrete"* ACI318-95, October 1995.

[15] Priestley, M. J. N., *" Assessment and Design of Joints for Single-Level Bridges with Circular Columns,"* Department of AMES - Division of Structural Engineering, University of California San Diego, La Jolla, California, March 1995, Report # SSRP-93/02, February 1993.

[16] Paulay, T., Priestley, M. J. N., *" Seismic Design of Reinforced Concrete and Masonry Buildings, "* John Wiley & Sons, Inc., New York, 1992, 744 pages.